UNIVERSIDADE DE LISBOA
FACULDADE DE MEDICINA VETERINÁRIA

ANALYSIS OF TIM2 DEFICIENCY IN THE MOUSE RETINA

ANDREIA BARBOSA VALENÇA

Orientador: Professor Doutor Jesús Ruberte París
Co-orientador: Professora Doutora Maria Luísa Mendes Jorge

Tese especialmente elaborada para obtenção do grau de Doutor em Ciências Veterinárias na Especialidade de Ciências Biológicas e Biomédicas

2019

UNIVERSIDADE DE LISBOA
FACULDADE DE MEDICINA VETERINÁRIA

ANALYSIS OF TIM2 DEFICIENCY IN THE MOUSE RETINA

ANDREIA BARBOSA VALENÇA

Orientador: Professor Doutor Jesús Ruberte París
Co-orientador: Professora Doutora Maria Luísa Mendes Jorge

Tese especialmente elaborada para obtenção do grau de Doutor em Ciências Veterinárias na Especialidade de Ciências Biológicas e Biomédicas

Júri:
Presidente: Professor Doutor Luís Filipe Lopes da Costa
Vogais:

- Professor Doutor Jesús Ruberte París
- Professora Doutora Graça Maria Alexandre Pires Lopes de Melo
- Professor Doutor António José de Freitas Duarte
- Doutor António Francisco Rosa Gomes Ambrósio
- Professora Doutora Gabriela Araújo da Silva

2019

À minha Mãe

“Sê todo em cada coisa. Põe quanto és no mínimo que fazes.”
Ricardo Reis

“Success is stumbling from failure to failure with no loss of enthusiasm”
Wiston S. Churchill

ACKNOWLEDGEMENTS

O privilégio de chegar à reta final de uma das fases mais importantes da minha vida apenas foi possível com o trabalho e dedicação de várias pessoas. Desafio quase tão grande quanto escrever esta tese foi encontrar palavras para agradecer a todas essas pessoas que, de alguma forma, percorreram este caminho comigo porque uma tese nunca é trabalho de uma só pessoa...

En primer lugar, quisiera dar las gracias a mi director, Profesor Doctor Jesús Ruberte, por formarme como investigadora, por creer en mi y darme la oportunidad de participar en este proyecto, por su paciencia, inestimable ayuda y enseñanzas y también por contagiarme su energía y pasión por la ciencia cada día.

À Professora Doutora Luísa Mendes Jorge, gostaria de agradecer, de forma muito especial, o privilégio da sua amizade e orientação ao longo de muitos anos, por ter sempre acreditado em mim e nas minhas capacidades, pela sua disponibilidade e dedicação permanente, pela partilha dos seus valiosos conhecimentos, por todo o entusiasmo e motivação com que me guiou e pelos seus conselhos. Sou uma pessoa mais rica, pessoal e profissionalmente, devido ao seu exemplo e ensinamentos. Muito obrigada.

Gostaria de agradecer a todos os membros da Faculdade de Medicina Veterinária e do Centro de Investigação Interdisciplinar em Sanidade Animal (CIISA) que, de algum modo, contribuíram para a realização deste trabalho. Nomeadamente, os Professores Doutores Graça Dias, Graça Pires, Luís Tavares, Luís Costa, Conceição Peleteiro e por último à Doutora Belmira Carrapiço por toda a amizade e apoio. Um obrigado especial à Virgínia Pires, Maria João Soares, Daniel Murta, Samuel Francisco, Teresa Inácio, Margarida Simões, Ana Amaral e Mariana Batista, dentro e fora do Doutoramento.

Gracias también a la Profesora Doctora Fàtima Bosch por darme la oportunidad de trabajar en las excelentes instalaciones del Centre de Biotecnologia Animal i Teràpia Gènica (CBATEG).

A todos los compañeros del CBATEG, especialmente Alba, Ivet, Tura, Anna y Miquel, muchas gracias por dedicarme su tiempo y sus conocimientos, que tanto ayudaran a la realización de esta tesis doctoral. A los Serveis de Microscòpia y Anàlisi Química y al Laboratori de Luminescència i Espectroscòpia de Biomolècules de la Universitat Autònoma de Barcelona, por el apoyo prestado. En particular, gracias a Salva por su buena energía y disponibilidad para mil dudas y por facilitarnos tantísimo los experimentos con todos sus aparatos geniales. Gracias a Eduard Cunilleras por su apoyo y conocimientos.

Quiero dar también las gracias a los componentes de nuestro grupo Profesora Doctora Ana Carretero, Profesor Doctor Víctor Nacher y Profesor Marc Navarro, por sus valiosos conocimientos, apoyo y inestimable ayuda. A mis compañeros de laboratorio, agradecer mucho por todo lo que he aprendido, por todo lo que vivimos dentro y fuera del lab, por estar siempre ahí y hacerme reír cada día de este largo camino. A Ángel, gracias por su alegría y energía positiva con sus temazos reggaetoneros, siempre dándole todo. A David, muchas gracias por compartir conmigo su genialidad de super pos-doc, por las muchas horas de confocal y por todas sus enseñanzas y apoyo, pero sobretodo por su amistad y buen humor y porque sin sus transtornitos nada seria igual. A Aina, gracias por su ilusión contagiosa en los últimos meses y por darme tanto gusto en ser su “mentora”. A Vero, gracias por sus historias y viajes y por la amistad que llevo. A Lore, gracias por su cariño, amistad y comprensión y estar literalmente a mi lado cada día. À Joana, um obrigada especial, por tudo o que já vivemos, por tudo o que nos ajudámos, por tudo o que ainda vem. ¡Con vosotros este camino fue más ligero y feliz y, más que una tesis, me os llevo a vosotros en el corazón, aunque no os de besos y abrazos a menudo!

Porque os amigos são a família que escolhemos, quero deixar um agradecimento a cada um deles. A mis amigos de Barcelona, Nicole, Nadia, Julian, Raul, João et. al., agradecer por ser mi segunda casa. Aos meus amigos, Bianca, Marta, Margarida, Josie, Nanda, Edgar, Ricardo, Miguel, Jota, André, Gi et al., um agradecimento especial pela presença, mesmo à distância, apoio e incentivo ao longo deste caminho.

Um último, mas não menos importante, agradecimento à minha família. Aos meus avós, os melhores do mundo, ao meu pai e à minha irmã obrigada pelo apoio e carinho. À minha mãe, com todo o meu coração, pelo amor incondicional, apoio e paciência inesgotáveis, por acreditar sempre em mim e nos meus feitos e por me dar sempre força para ir mais além e seguir os meus sonhos. Obrigada!

This work was funded by Fundação para a Ciência e Tecnologia (FCT) through the doctoral scholarship SFRH/BD/95330/2013.

Funding was also given from research projects UID/CVT/00276/2013 and PTDC/SAU-ORG/110856/2009 (CIISA, Faculdade de Medicina Veterinária, Universidade de Lisboa), supported by FCT - Portugal, and PI16/00719 (CBATEG, Universitat Autònoma de Barcelona), supported by Instituto de Salud Carlos III – Spain.

ABSTRACT

Analysis of TIM2 deficiency in the mouse retina

Careful control of iron availability in the retina is central to maintenance of iron homeostasis, as its imbalance is associated with oxidative stress and progress of several retinopathies, such as diabetic retinopathy. Ferritin, known for its role in iron storage and detoxification, has also been proposed as an iron-transporter and can be regarded as a potential deliverer of a considerable large amount of iron to the retina compared to transferrin, the classical iron-carrier protein. Ferritin can bind to scavenger receptor class A member 5 (Scara5) and T-cell immunoglobulin and mucin-domain 2 (TIM2) receptors and is likely endocytosed. In this study, the presence of TIM2, which remained unknown in the retina, was investigated. Although no human ortholog for mouse TIM2 has been identified, human TIM1 and mouse TIM2 have similar functions.

Our results revealed for the first time the presence of TIM2 receptors in the mouse retina, mainly expressed in Müller cells, unveiling new aspects of retinal iron metabolism regarding the putative role of TIM2 in this tissue. A knockout mouse for this membrane receptor was generated in order to better understand TIM2 functions in the retina. TIM2 deficiency affected retinal iron metabolism. Iron-loaded ferritin accumulation, probably due to increased ferritin uptake mediated by Scara5, and increased iron uptake by transferrin receptor 1 (TfR1)-transferrin binding led to retinal iron overload. Consequently, increased vascular permeability and blood-retinal barrier (BRB) breakdown were observed, inducing edema of the central retina. Paracellular and transcellular transports were impaired with tight junction integrity loss and increased caveolae number. Two mechanisms seem to be involved in this process: association of iron and ferritin overload with vascular endothelial growth factor (VEGF) overexpression and oxidative stress triggered by reactive oxygen species (ROS) overproduction generated by retinal iron overload.

Altogether, these results point to TIM2 as a new key player in iron homeostasis in the mouse retina, possibly modulating cellular iron levels, and a potential target for the treatment of diabetic macular edema.

Keywords: TIM2 receptors, iron metabolism, blood-retinal barrier integrity, edema, retinopathy.

RESUMO

Análise da deficiência de TIM2 na retina de murganho

A retina necessita especificamente de ferro, devido a este ser um co-factor essencial da enzima guanilato ciclase que assegura a síntese de monofosfato de guanosina cíclico, segundo mensageiro na cascata de fototransdução. Para além disso, a retina é particularmente dependente de ferro devido à contínua necessidade de síntese de membranas, para suprir a constante renovação dos segmentos externos dos fotorrecetores, que requer como co-factor este elemento. Porém, o desequilíbrio da homeostasia do ferro está associado ao dano oxidativo e ao desenvolvimento de várias situações de retinopatia, como por exemplo a retinopatia diabética. A retina é particularmente propensa a stress oxidativo e o excesso de ferro exacerba potencialmente esta situação, devido à participação do ferro na reação de Fenton, que gera a superprodução de espécies reativas de oxigénio que, por sua vez, desencadeiam stress oxidativo. Por conseguinte, a manutenção da homeostasia do ferro é crucial neste tecido. Contudo, mecanismos de regulação do ferro na retina ainda não são completamente conhecidos. A retina obtém ferro a partir da circulação sanguínea. No entanto, a barreira hemato-retiana isola a retina da circulação sanguínea, protegendo-a de potenciais estímulos nocivos. Assim, são necessários mecanismos específicos e rigorosamente regulados de absorção de ferro para atravessar esta barreira e importar a quantidade de ferro estritamente essencial para o normal funcionamento da retina. Classicamente, a transferrina foi estabelecida como a proteína transportadora de ferro na retina, sendo aceite que a transferrina sérica se liga ao seu recetor de membrana, recetor da transferrina 1, na superfície das células endoteliais e do epitélio pigmentar da retina. Após a endocitose deste complexo, o ferro é libertado no parênquima retiniano. Mais recentemente, a ferritina, considerada classicamente como uma proteína de armazenamento de ferro e destoxificação, foi também proposta como uma proteína transportadora deste elemento. A vantagem da ferritina sérica em relação à transferrina no transporte de ferro prende-se na capacidade da ferritina de incorporar ~ 4,500 átomos de ferro, ao passo que a transferrina apenas transporta 2 átomos de ferro, constituindo, assim, a ferritina uma fonte muito eficiente de ferro para os tecidos. A molécula da ferritina é composta por 24 subunidades de dois tipos: cadeia leve (L) e cadeia pesada (H) que se unem aos recetores Scara5 (*scavenger receptor class A member 5*) e TIM2 (*T-cell immunoglobulin and mucin-domain 2*), respetivamente.

O nosso grupo identificou pela primeira vez a presença de recetores Scara5 na retina humana e do murganho. No entanto, até à data, a presença de recetores TIM2 na retina não foi reportada na bibliografia. O TIM2, uma proteína transmembranar do tipo 1, é um membro da família de genes portadores dos domínios mucina e imunoglobulina de células T e, para além de ser um recetor para a ferritina-H, está envolvido na regulação da resposta imunitária.

Apesar de não ter sido identificado um gene ortólogo no humano para o TIM2 do murganho, o TIM1 humano e o TIM2 do murganho partilham uma homologia de 36% e funções similares, tal como a ligação à ferritina-H.

Neste estudo, a presença de recetores TIM2 na retina do murganho, que se expressam principalmente nas células de Müller, é revelada pela primeira vez, abrindo caminho para uma nova abordagem no metabolismo do ferro na retina, tendo em consideração o papel putativo do TIM2 neste tecido. O facto de os recetores TIM2 se expressarem maioritariamente nas células de Müller, as células mais importantes da glia na retina, é também de grande relevância devido ao papel que estas células desempenham na manutenção da homeostasia do ferro, sendo consideradas mediadores importantes no transporte, distribuição e regulação deste elemento na retina.

No sentido de compreender as funções do TIM2 na retina, foi gerado e analisado um modelo de murganho mutante para o recetor TIM2. Os nossos resultados confirmaram a diminuição da expressão dos recetores TIM2 e mostraram um aumento da expressão das principais proteínas envolvidas no metabolismo do ferro, nomeadamente Scara5, recetor da transferrina 1, transferrina, ferritina-L e ferritina-H, nos murganhos com deficiência de recetores TIM2. O aumento da expressão de ferritina observado deve-se provavelmente ao aumento de entrada de ferritina sérica através da sua ligação aos recetores Scara5. Efetivamente, observámos a presença de uma maior densidade de moléculas de ferritina carregadas com ferro, principalmente nas células de Müller, e uma sobrecarga de ferro nas retinas destes murganhos. O aumento da expressão da transferrina e do seu recetor contribuíram também, provavelmente, para o aumento do conteúdo em ferro observado nestas retinas. No estudo das consequências deste excesso de ferro na retina, observámos, *in vivo,* por oftalmoscopia de varrimento laser, a existência de derrames de fluoresceína dos vasos sanguíneos para o parênquima retiniano, o que está descrito como sendo um indicativo de aumento da permeabilidade vascular e rutura da barreira hemato-retiniana. A análise destas retinas por meio de microscopia eletrónica de transmissão revelou a presença de espaços perivasculares a rodear os vasos sanguíneos, aspeto consistente com a acumulação de fluído no espaço extracelular e a formação de edema, sendo este mais pronunciado na parte central da retina. Consequentemente, analisámos as principais proteínas constituintes das junções de oclusão, zonula occludens 1, claudina-5 e ocludina, que estão envolvidas no controlo do transporte paracelular ao longo da barreira hemato-retiniana. Esta análise revelou uma perda de integridade de todas as proteínas juncionais e a alteração do transporte paracelular, conduzindo, assim, ao aumento da permeabilidade vascular. Foi também avaliada a expressão da proteína associada a vesículas do plasmalema, cuja expressão normalmente é baixa ou está ausente em barreiras hemato-retinianas intactas. Foi observado um aumento da expressão desta proteína bem como do número de cavéolas, o que sugeriu um aumento do transporte transcelular, contribuindo para o aumento da permeabilidade vascular. Para

além disso, encontrámos sobreexpressão de VEGF (*vascular endothelial growth factor*), bem como superprodução de espécies reativas de oxigénio e o aumento da expressão de proteínas associadas com dano do DNA e peroxidação lipídica nas retinas destes murganhos. No entanto, apesar de todos estes aspetos serem característicos de uma situação de retinopatia diabética/edema macular diabético, os murganhos com diminuição de recetores TIM2 apresentaram normoglicémia, excluindo, desta forma, um quadro de diabetes.

No conjunto, os nossos resultados mostraram que a deficiência de recetores TIM2 no murganho alterou o metabolismo do ferro na retina, observando-se uma acumulação de ferritina e ferro, sobretudo a nível das células de Müller. Em consequência, a acumulação de ferro deu origem a um aumento da permeabilidade vascular e à rutura da barreira hemato-retiniana, responsáveis pela formação de edema, mais proeminente na retina central. Neste processo podem estar envolvidos dois mecanismos. Por um lado, a associação de excesso de ferro e ferritina com a sobreexpressão de VEGF, levando à fosforilação e degradação das proteínas que constituem as junções de oclusão, bem como o aumento de expressão da proteína associada a vesículas do plasmalema e de cavéolas, responsáveis pela alteração do transporte paracelular e transcelular, respetivamente. Por outro lado, o excesso de ferro desencadeia um estado de stress oxidativo na retina devido à superprodução de espécies reativas de oxigénio, o que por sua vez pode levar também à disrupção das proteínas das junções de oclusão. Para além disto, a sobreexpressão crónica de ferritina, longe de ser neuroprotetora, pode originar um efeito contrário, de modo que o ferro armazenado nas moléculas de ferritina pode, eventualmente, ter um efeito pró-oxidante, contribuindo também para a rutura da barreira hemato-retiniana. A sobreexpressão de Scara5 mostrou que esta proteína poderá ter um papel protetor na manutenção da estrutura da parede vascular, uma vez que inibe a expressão das metaloproteinases de matriz 2 e 9, mediadoras da degradação ou remodelação da matriz extracelular.

No conjunto, os nossos resultados revelaram a presença de um novo recetor de ferritina na retina do murganho, o recetor TIM2, e o seu envolvimento na homeostasia do ferro, possivelmente modulando os níveis deste elemento ao longo da retina neural. Os nossos resultados mostraram ainda que a acumulação de ferro, associada à diminuição de TIM2, em situação de normoglicémia, foi suficiente para provocar a rutura da barreira hemato-retiniana e a formação de edema, características do edema macular diabético, confirmando o papel do ferro no mecanismo de disfunção desta barreira. Por conseguinte, o recetor TIM2 pode vir a ser um alvo terapêutico de interesse nos modelos animais para tratamento do edema macular diabético, sobretudo se atendermos à existência do seu ortólogo TIM1 em pacientes humanos.

Palavras-Chave: recetores TIM2, metabolismo do ferro, integridade da barreira hemato-retiniana, edema, retinopatia.

TABLE OF CONTENTS

LIST OF FIGURES

LIST OF TABLES

LIST OF ABBREVIATIONS

AFP: average fluorescence/pixel
ATP: adenosine triphosphate
BBB: blood-brain barrier
BCA: bicinchoninic acid
BRB: blood-retinal barrier
BSA: bovine serum albumin
CBATEG: Center of Animal Biotechnology and Gene Therapy
cDNA: complementary deoxyribonucleic acid
cGMP: cyclic guanosine monophosphate
CIISA: Centre for Interdisciplinary Research in Animal Health
CNS: central nervous system
DHE: dihydroethidium
DNA: deoxyribonucleic acid
dNTPs: deoxynucleotides
DVP: deep vascular plexus
ECL: enhanced chemiluminescence
EGFP: enhanced green fluorescent protein
ELISA: enzyme-linked immunosorbent assay
ELM: external limiting membrane
EDTA: ethylenediaminetetraacetic acid
EtBr: ethidium bromide
FITC: fluorescein isothiocyanate
FCT: Fundação para a Ciência e a Tecnologia
GAPDH: glyceraldehyde 3-phosphate dehydrogenase
GCL: ganglion cell layer
GFAP: glial fibrillary acidic protein
GS: glutamine synthetase
H-E: hematoxylin and eosin
HRP: horseradish peroxidase
iBRB: inner blood-retinal barrier
IgG: immunoglobulin G
ILM: internal limiting membrane
INL: inner nuclear layer
IPL: inner plexiform layer
IREs: iron responsive elements
IRPs: iron regulatory proteins
IS: inner segments of the photoreceptor cells
IVP: intermediate vascular plexus
JAMs: junctional adhesion molecules
KO: knockout
KOMP: Knockout Mouse Project
LIP: labile iron pool
MOM: mouse on mouse
mRNA: messenger ribonucleic acid
NBF: neutral buffered formalin
NDS: neutral donkey serum
NFL: nerve fiber layer
oBRB: outer blood-retinal barrier

OD: optic disc
ONL: outer nuclear layer
OPL: outer plexiform layer
OS: outer segments of the photoreceptor cells
PAS: periodic acid Schiff
PBI: phosphate buffer Igepal
PBS: phosphate buffered saline
PBST: phosphate buffer saline with Tween 20
PCR: polymerase chain reaction
PVDF: polyvinylidene fluoride
PKCα: protein kinase C alpha
PLVAP: plasmalemma vesicle associated protein
PNA: peanut agglutinin
qRT-PCR: quantitative real-time polymerase chain reaction
RIPA: radioimmunoprecipitation assay
RNA: ribonucleic acid
ROS: reactive oxygen species
RPA2: replication protein A subunit 2
RPE: retinal pigment epithelium
Scara5: scavenger receptor class A member 5
SDS-PAGE: sodium dodecyl sulfate polyacrylamide gel electrophoresis
SEM: standard error of the mean
SLO: scanning laser ophthalmoscopy
SVP: superficial vascular plexus
TAE: Tris-acetate EDTA
TBS: Tris buffered saline
TBST: Tris buffered saline with Tween 20
TEM: transmission electron microscopy
TfR1: transferrin receptor 1
TIBC: total iron binding capacity
TIM1: T-cell immunoglobulin and mucin-domain 1
TIM2: T-cell immunoglobulin and mucin-domain 2
$TIM2^{+/-}$: TIM2 heterozygous
UIBC: unsaturated iron binding capacity
UK: United Kingdom
USA: United States of America
UV: ultraviolet
VEGF: vascular endothelial growth factor
vs.: versus
WB: wash buffer
WT: wild-type
ZO: zonula occludens
ZO-1: zonula occludens-1
4-HNE: 4-hydroxynonenal

LIST OF SYMBOLS AND UNITS OF MEASUREMENT

A.M.: *ante meridiem* (before midday)
AU: arbitrary units
bp: base pairs
CH_3CO_2H: glacial acetic acid
cm: centimeter
CO_2: carbon dioxide
eV: electron volt
Fe^{2+}: ferrous iron
Fe^{3+}: ferric iron
G: gauge
g: gram
H_2O: water
H_2O_2: hydrogen peroxide
HCl: hydrochloric acid
kDa: kilodalton
$K_4Fe(CN)_6$: potassium ferrocyanide
$K_3Fe(CN)_6$: potassium ferricyanide
kV: kilovolt
M: molar
$MgCl_2$: magnesium chloride
mg/dl: milligrams per deciliter
mg/ml: milligrams per milliliter
ml: milliliter
mm: millimeter
mm^2: square millimeter
mM: millimolar
NaCl: sodium chloride
Na_2HPO_4: sodium phosphate dibasic
$Na_2HPO_4.2H_20$: sodium phosphate dibasic dihydrate
$NaH_2PO_4.H_2O$: sodium phosphate monobasic monohydrate
$Na_3(C_6H_5O_7).2H_2O$: sodium citrate tribasic dihydrate
ng: nanogram
ng/µl: nanograms per microliter
ng/ml: nanograms per milliliter
nm: nanometer
nM: nanomolar
O_2: oxygen
O_2•-: superoxide anion
OH^-: hydroxyl ion
HO•: hydroxyl radical
$Pb(NO_3)_2$: lead nitrate
pH: potencial hydrogen
V: volt
µl: microliter
µg: microgram
µg/dl: micrograms per deciliter
µg/ml: micrograms per milliliter
µm: micrometer

μM: micromolar
ºC: degree Celsius
%: percentage

INTRODUCTION

INTRODUCTION

A. The retina and its vascular system

The eye is the sensory organ responsible for visual perception. Positioned within the orbit, the eye is surrounded by bone and soft tissue and is formed by the eyeball and its accessory organs, including the extrinsic muscles of the eyeball, eyelids, conjunctiva, and lacrimal apparatus (Metz, 1868; Ruberte at al., 2016).

A.1. Localization of the retina in the eyeball

The eyeball (*Bulbus oculi*) comprises three concentric tunicae in close apposition: the fibrous layer of the eyeball (*Tunica fibrosa bulbi*), creating the outer wall of the eyeball; the vascular tunic of the eyeball (*Tunica vasculosa bulbi*), a highly vascularized and pigmented medial layer; and the internal layer of the eyeball (*Tunica interna bulbi*), which consists of the retina and its pigmented epithelium, as well as retinal blood vessels (*Vasa sanguinea retinae*) (Schaller, 1992; Smith, 2002; Gartner & Hiatt, 2007).

The fibrous layer of the eyeball is formed by the sclera (*Sclera*) and cornea (*Cornea*) (Figure 1). The sclera is a white protective layer covering the posterior portion of the eye and consists of dense fibrous connective tissue rich in type I collagen and elastic fibers (Schaller, 1992; Smith, 2002; Gonçalves & Bairos, 2006). This resistant fibroelastic coat protects the eyeball and is the point of insertion for the extrinsic muscles of the eyeball (Gartner & Hiatt, 2007). The cornea, situated in the anterior portion of the eyeball, is a transparent, avascular, and highly innervated membrane responsible for the refraction of the light (Schaller, 1992; Gartner & Hiatt, 2007). The transition between the cornea and the sclera is called the limbus. In the mouse limbus, it is possible to observe a circumferential vascular ring (Ruberte et al., 2016).

The vascular tunic of the eyeball, also named uvea, consists of the choroid (*Choroidea*) in its posterior portion, and the ciliary body (*Corpus ciliare*) and the iris (*Iris*) in the anterior portion (Figure 1) (Ruberte et al., 2016). The choroid is a pigmented and well-vascularized tissue loosely attached to the sclera and separated from the retina by the Bruch's membrane (*Lamina basalis*) (Schaller, 1992; Gartner & Hiatt, 2007). The vast network of blood capillaries of the choroid ensures the metabolic needs of the outer layers of the retina of both human and mouse

(Gartner & Hiatt, 2007; Ruberte et al., 2016). In addition, due to its high pigmentation, the choroid is responsible for the absorption of light, preventing reflections through the retina. Unlike other nocturnal species, the mouse has no *tapetum lucidum*, an avascular area of the choroid that reflects light and enhances nocturnal vision (Wise, Dollery & Henkind, 1971; Ruberte et al., 2016).

The ciliary body is a thick annular structure located between the iris and the vitreous chamber, projecting towards the lens. The ciliary processes (*Processus ciliares*) lay in its inner surface and consist of radially arranged fibroelastic ridges responsible for the secretion of aqueous humor, together with the ciliary crown (*Corona ciliaris*) (Schaller, 1992; Esperança-Pina, 2000). In the outermost portion of the ciliary body, closest to the sclera, resides the ciliary muscle (*Musculus ciliaris*), responsible for the accommodation of the lens (Esperança-Pina, 2000; Cook & Peiffer, 2001). In the mouse, the ciliary muscle is not well developed, causing the lack of accommodation of the lens (Ruberte et al., 2016).

The iris is the most anterior part of the vascular tunic and separates the anterior and posterior chambers of the eyeball. This structure acts as a contractile diaphragm with a central opening (*Pupilla*) that regulates the amount of light admitted into the fundus of the eye through the modification of the size and shape of the pupil (Cook & Peiffer, 2001; Gartner & Hiatt, 2007).

The internal tunica of the eyeball consists of the retina (*Retina*) (Figure 1) (Schaller, 1992; Gartner & Hiatt, 2007). The retina is the neurosensory part of the eye and lines the inner surface of the eyeball (Smith, 2002). During embryogenesis, the retina develops from the optic cup, an outgrowth of the diencephalon, which is composed of two neuroepithelial layers: the inner layer that develops into the neural retina; and the outer layer, which becomes the retinal pigment epithelium (RPE) (Carlson, 1999; Rossant & Tam, 2002; Willoughby et al., 2010). The optic disc (*Discus nervi optici*) is the point from which retinal fibers converge into the optic nerve, and also where the central retinal artery and vein emerge (Wise et al., 1971; Hildebrand & Fielder, 2011). In the mouse, the optic disc is situated in the central axis of the eye (Ruberte et al., 2016).

The interior of the eyeball contains the lens (*Lens*) and three chambers of fluid, including the anterior (*Camera anterior bulbi*) and posterior chambers (*Camera posterior bulbi*) filled with the aqueous humor, and the vitreous chamber (*Camera vitrea bulbi*) filled with a more viscous fluid, the vitreous humor (Figure 1) (Ruberte et al., 2016).

The lens, located between the posterior portion of the iris and the vitreous body, is a transparent, biconvex, flexible, and avascular structure that focuses the light on the retina. In comparison to the human eye, the mouse lens is much larger and rounder, occupying 75% of the intraocular space (Ruberte et al., 2016). The aqueous humor (*Humor aquosus*), a

colourless fluid continuously secreted by the ciliary processes, provides nutrients to the surrounding avascular structures, mainly the lens and the cornea, and helps maintaining hydrostatic pressure. The vitreous humor (*Corpus vitreum*), in close apposition to the retina, is a transparent gel mainly composed of glycosaminoglycans, hyaluronic acid, and water. The main function of the vitreous humor is to ensure structural support to the eyeball, as well as to provide a transparent path for light to reach the retina. In the mouse, as the eyeball is mostly occupied by the lens, the vitreous chamber is proportionally smaller compared to that of the human eyeball (Smith, 2002).

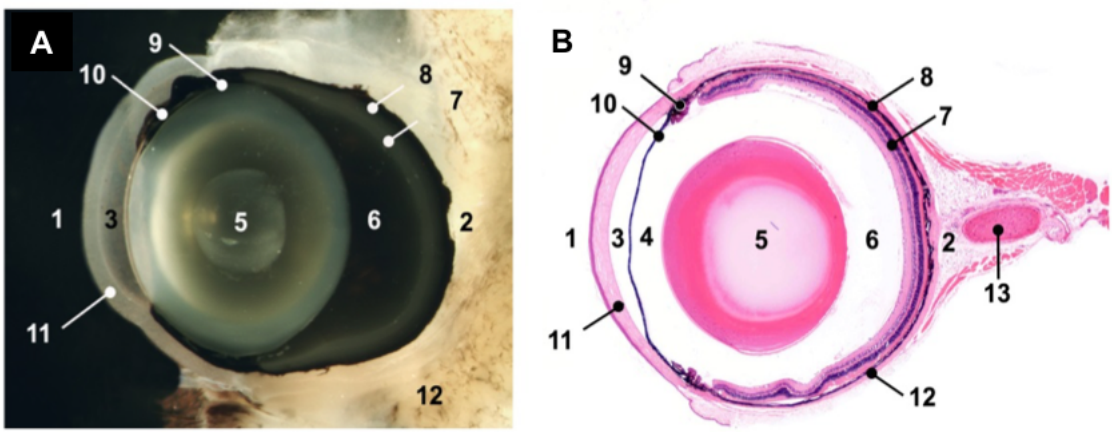

Figure 1. The mouse eyeball. Topographical (**A**) and histological (**B**) sections of the mouse eyeball. 1, anterior pole; 2, posterior pole; 3, anterior chamber of the eyeball; 4, posterior chamber of the eyeball; 5, lens; 6, vitreous chamber of the eyeball; 7, retina; 8, choroid; 9, ciliary body; 10, iris; 11, cornea; 12, sclera; 13, optic nerve. Images from Ruberte et al., 2016.

A.2. Retinal organization and function

The retina is the most complex substructure of the eye and is organized in several layers (Figure 2), from the innermost (adjacent to vitreous chamber) to the outermost (related to the choroid) (Smith, 2002; Hildebrand & Fielder, 2011; Ruberte et al., 2016):

- Internal limiting membrane (*Stratum limitans internum*): adjacent to the vitreous chamber, this layer is the basal lamina of the inner retina and is formed by the footplates of Müller cells.
- Nerve fiber layer (*Stratum neurofibrarum*): composed of unmyelinated axons of ganglion cells that converge towards the optic disc. Axons are surrounded by astrocytes and Müller cell processes.
- Ganglion cell layer (*Stratum ganglionicum*): contains numerous retinal ganglion cells characterized by large vesicular nuclei with prominent nucleoli. Displaced amacrine cells and

astrocytes have also been found in this layer.

- Inner plexiform layer (*Stratum plexiforme internum*): matrix in which synapses between ganglion, bipolar, and amacrine cells occur. Occasionally, displaced cells from adjacent layers, such as astrocytes, can also be found.

- Inner nuclear layer (*Stratum nucleare internum*): harbors the nuclei of bipolar, horizontal, amacrine, and Müller cells.

- Outer plexiform layer (*Stratum plexiforme externum*): consists of a thin layer of synapses between photoreceptor axons and dendrites of bipolar and horizontal cells.

- Outer nuclear layer (*Stratum nucleare externum*): contains the nuclei of photoreceptor cells, cones and rods.

- External limiting membrane (Stratum limitans externum): this is not considered a true membrane, but rather an outer limit created by apical processes of Müller cells that relate to the inner segments of photoreceptor cells.

- Inner and outer segments of photoreceptors (*Stratum neuroepitheliale)*: rods and cones are tightly stacked together into a single layer of photoreceptor cells, which contains inner segments and outer segments. This is the only light-sensitive part of the neuroretina, and all other layers collectively serve to process and transmit these nerve signals between cells.

- Retinal pigment epithelium (*Stratum pigmentosum*): consists of a monolayer of retinal pigment epithelial (RPE) cells containing numerous melanosomes. It is the pigmented outermost layer of the retina, adjacent to the choroid, which covers most of the inside of the eyeball.

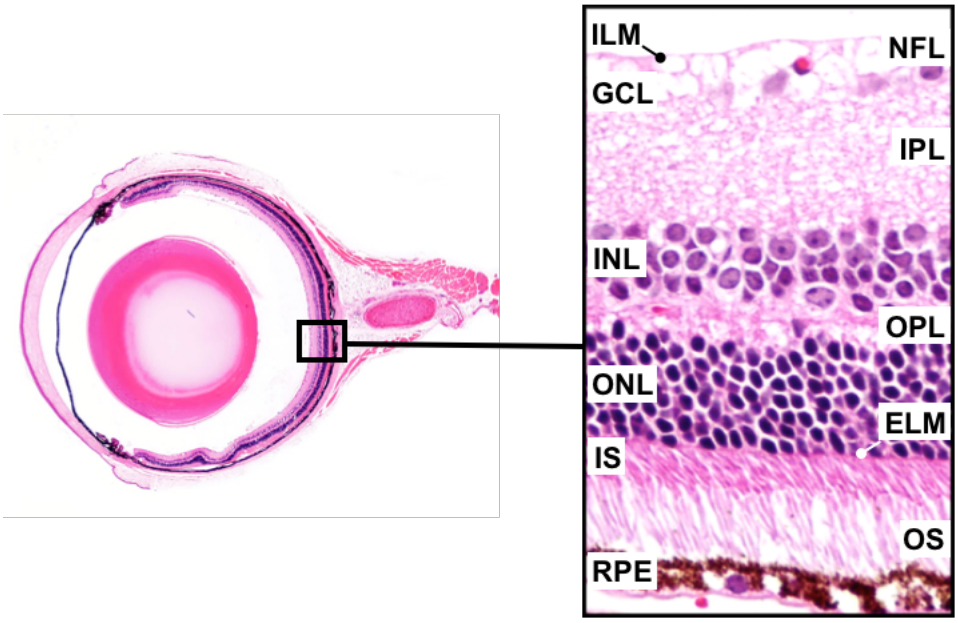

Figure 2. Structure of the retina. Hematoxylin-eosin stained paraffin section of the retina showing the different layers and cells of the retina. NFL, nerve fiber layer; GCL, ganglion cell layer; IPL, inner plexiform layer; INL, inner nuclear layer; OPL, outer plexiform layer; ONL, outer nuclear layer; IS, inner segments of the photoreceptor cells; OS, outer segments of the photoreceptor cells; RPE, retinal pigment epithelium. Images from Ruberte et al., 2016.

The main function of the retina is to capture and transform light into an electrical signal, which is transmitted to the brain (Willoughby et al., 2010). Neural signals, generated when light interacts with photoreceptors, are directly conducted by synaptic transmission along the vertical pathway of excitatory neurotransmission to bipolar and ganglion cells (Figure 3) (Maureen, McCall & Gregg, 2008; McCall & Gregg, 2008b). Then, the visual information is conducted through the axons of ganglion cells that converge into the optic nerve to reach the visual cortex (Maureen et al., 2008; McCall & Gregg, 2008a). In addition, lateral inhibitory pathways, mediated by horizontal and amacrine cells, modulate the nervous impulses. As a result, the normal visual functioning requires a finely tuned interrelationship and functional integration of all cell populations that include neuronal, glial, vascular, and retinal epithelial cells.

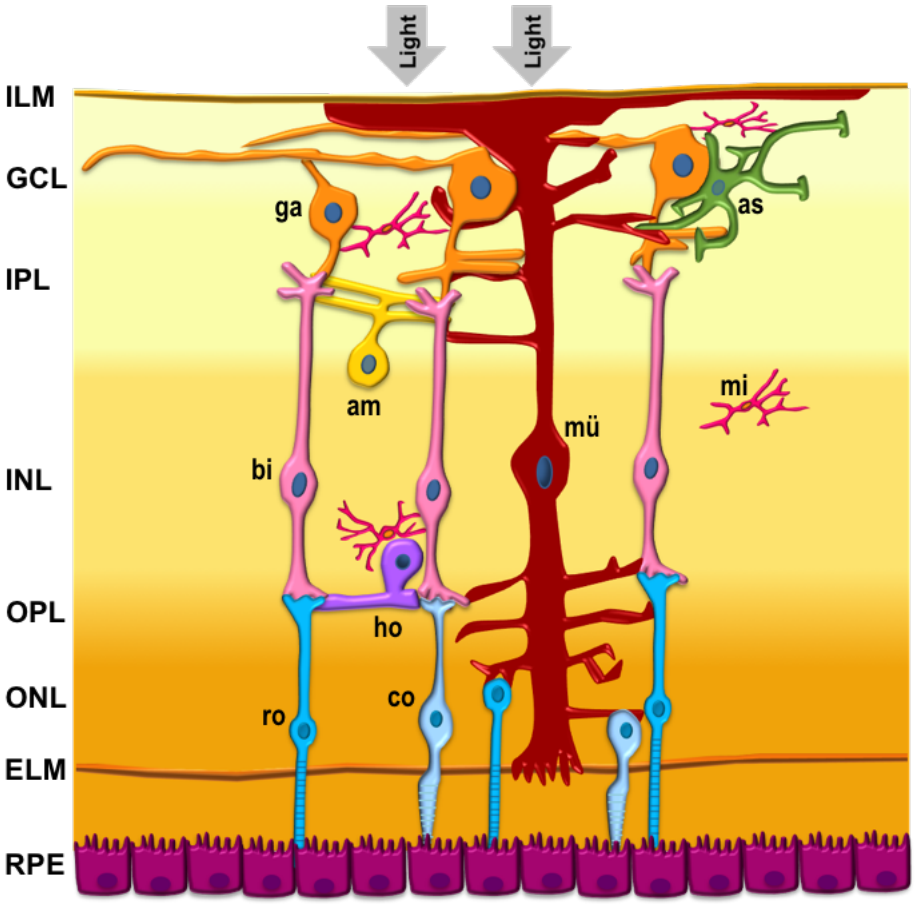

Figure 3. Schematic representation of the retinal circuitry. In the vertebrate retina, neurotransmission along the vertical pathway comprises photoreceptors, rods (ro) and cones (co), transducing light energy into a neural signal that is relayed via bipolar cells (bi) to retinal ganglion cells (ga). Visual signals are shaped by a lateral pathway mediated by horizontal (ho) and amacrine cells (am). Glial cells, Müller cells (mü) and astrocytes, fulfill supportive functions in the retina. Microglial cells (mi) are the resident macrophages of the retina. ILM, internal limiting membrane; GCL, ganglion cell layer; IPL, inner plexiform layer; INL, inner nuclear layer; OPL, outer plexiform layer; ONL, outer nuclear layer; ELM, external limiting membrane; IS/OS, inner and outer segments of the photoreceptor cells; RPE, retinal pigment epithelium.

A.2.1. Retinal neuronal cells

Several neuronal types can be found within the retinal parenchyma: photoreceptors, bipolar, ganglion, horizontal, and amacrine cells (Figure 3).

Photoreceptor cells are a specialized type of sensory neurons able to interact with light, thus generating a nervous impulse that is conducted through the retinal neuronal path to the optic nerve to reach the visual cortex. The photoreceptor layer is formed by two basic cell types, rods and cones, which are responsible for scotopic and photopic vision, respectively (Jeon et al., 1998; Ebrey & Koutalos, 2001). According to this, rods are specialized in the perception of changes in intensity of dim light and have very low spatial resolution. In the mouse, a nocturnal species, rods represent 95% of photoreceptors (Jeon et al., 1998; Smith, 2002). Cones, on the contrary, have very high spatial resolution, are specialized for acuity, and perceive bright light and colors.

Beyond the outer limiting membrane are located the inner and outer segments of the photoreceptors. The inner segments contain the machinery, such as many mitochondria and abundance of glycogen and ribosomes, needed to meet the high metabolic demands associated with phototransduction. The outer segments are endowed with visual pigments and their plasma membrane is stacked into hundreds of membranous laded flat discs. The outer segments are renewed in a highly dynamic fashion, with assembly of new discs at the base, and the shedding and phagocytosis by the RPE at the distal part (Young & Bok, 1969; Wolf, 2004).

Bipolar cells, the most abundant cells in the inner nuclear layer, receive signals from photoreceptors and transmit them to ganglion cells. Their unique axons synapse with ganglion cells and also with amacrine cells (Jeon et al., 1998; Masland, 2011).

Ganglion cells, the last step in the retinal visual pathway, contribute to the formation of the ganglion cell layer. The long axons of ganglion cells form the nerve fiber layer and converge radially in the surface of the retina towards the optic disc (Masland, 2011).

In the vertebrate retina, the visual signal is shaped by feedback and feedforward inhibition by interneurons (Diamond, 2017). Horizontal cells, constituting around 3% of inner nuclear layer cells, mediate interactions between photoreceptor cells and bipolar cells, regulating and adapting responses. Horizontal cells are also responsible for providing feedback signals that modulate the gain of the visual pathway (Jeon et al., 1998; Forrester et al., 2002). Amacrine cells constitute up to 40% of inner nuclear layer cells and establish synapses with bipolar and ganglion cells. In this regard, amacrine cells are responsible for shaping both spatial and temporal characteristics of visual signals (Jeon et al., 1998; Masland, 2011; Diamond, 2017).

A.2.2. Retinal glia and microglia

Glial cells fulfill supportive functions in the retina, as they do in the rest of the central nervous system (CNS). In general, the mammalian retina is populated by two types of macroglial cells: Müller cells and astrocytes (Figure 3).

Müller cells are the most predominant glial elements and are the only cells spanning the entire thickness of the neurosensory retina, from the vitreous chamber to the external limiting membrane, filling all retinal space unoccupied by neurons and helping maintain retinal structural integrity (Kolb et al., 2011; Vecino et al., 2016). Müller cells have a range of functions vital to neuron survival, including metabolic support, clearance of neural waste products, synthesis and recycling of neurotransmitters, phagocytosis of neuronal debris, and regulation of extracellular ionic balance (Kolb et al., 2011). Moreover, Müller cells play an important role in vessel integrity, regulation of blood flow, and neuronal activity, so as to maintain a strictly regulated retinal environment (Newman & Reichenbach, 1996; Gardner et al., 2002; Bringmann et al., 2006; Kur, Newman & Chan-Ling, 2012). Müller cells processes communicate with blood vessels and neurons, forming the so-called neurovascular unit (Hollander et al., 1991; Gardner et al., 2002). Due to this specific disposition, Müller cells are ideally situated to regulate blood flow and match neuronal metabolic needs (Newman, 2003).

Astrocytes are confined to the vascularized areas of the retina where their processes surround blood vessels and unmyelinated axons (Hollander et al., 1991; Gardner et al., 2002). Astrocytes, as Müller cells, perform support functions for neuronal homeostasis, such as provision of metabolites, regulation of ionic concentrations, and recycling of neurotransmitters (Hollander et al., 1991). These cells also contribute to the retina architectural support (Zhang & Stone, 1997), as well as to the functional hyperemia and vascular regulation.

Glial cells, and specially Müller cells, respond to any retinal damage by becoming “reactive”. This reaction is called gliosis and in early, acute phases, is characterized by the secretion of neuroprotective and antioxidant molecules with the aim of protecting the tissue (Bringmann et al., 2006).

Microglial cells, the resident macrophages of the retina, are located in the superficial layers of the retina (Figure 3). Generally, microglial cells remain quiescent, but under certain stimuli may become activated, contributing to the defense against pathogens, phagocytosis, immunoregulation, and tissue repair (Roitt, Brostoff & Male, 2001; Chen, Yang & Kijlstra, 2002; Gardner et al., 2002).

A.3. Retinal vascular system

Light must cross the entire retinal parenchyma to reach the photoreceptors (Figure 3). However, blood vessels deflect incoming light. To overcome this situation, the retinal vascular system shows unique features and adaptations to supply sufficient oxygen and nutrients to the tissue while minimizing the interference of retinal blood vessels with the passage of light to photoreceptor cells (Funk, 1997; Puro, 2012; Ramos et al., 2013). Thus, the retina is characterized by sparse and thin capillaries, which represent only 5% of total retinal mass (Gartner & Hiatt, 2007; Ramos et al., 2013), leaving large vessel-free spaces (Figure 4) (Funk, 1997; Delaey & Van De Voorde, 2000; Wangsa-Wirawan & Linsenmeier, 2003). However, the extremely active retinal metabolism entails a high level of blood oxygen extraction (Delaey & Van De Voorde, 2000), and this specific vascular distribution leaves little functional reserve for adjusting the relatively low blood flow to meet retinal needs, making this tissue very susceptible to hypoxia (Alm & Bill, 1973; Bristow et al., 2002; Wangsa-Wirawan & Linsenmeier, 2003; Ramos et al., 2013). Hence, retinal vasculature must strictly couple blood flow to local needs (Funk, 1997; Delaey & Van De Voorde, 2000; Pournaras et al., 2008).

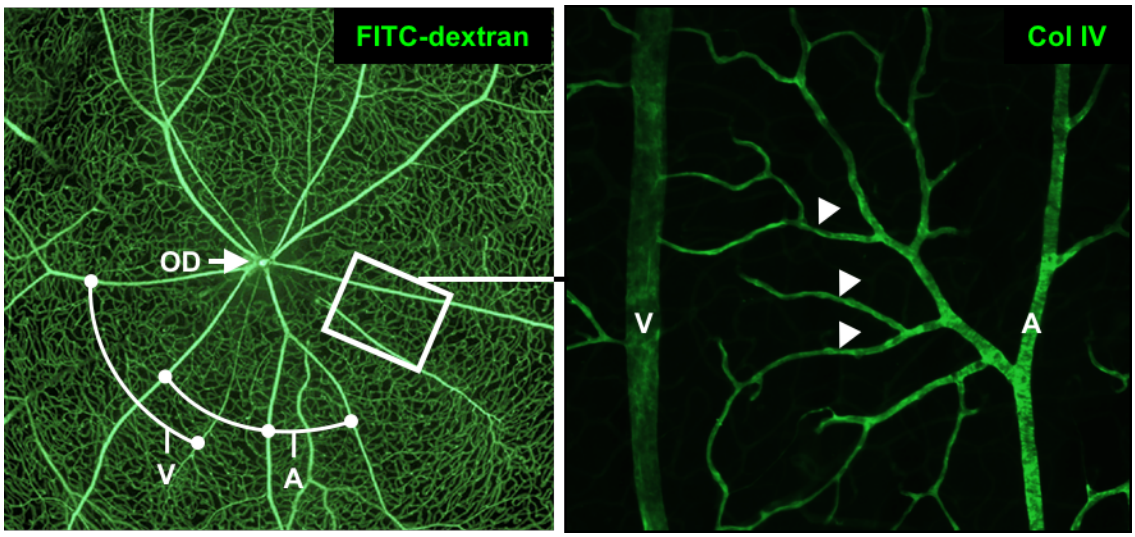

Figure 4. Retinal vascular system. The retina is characterized by sparse and thin capillaries (arrowheads). A, arterioles; Col IV, collagen IV; FITC, fluorescein isothiocyanate; OD, optic disc; V, venules. Images from Ramos et al., 2013.

A.3.1. Retinal vascular pattern

Vertebrates show a wide variety of retinal vascular patterns, ranging from the anangiotic pattern, found in avian retinas and some rodents, and characterized by completely avascular retinas, to the holoangiotic pattern, which is found in most mammals, including mouse and man, where retinas are completely vascularized by a complex network of blood vessels (Figures 4 and 5), including arteries, veins, and capillaries (Wise et al., 1971; De Schaepdrijver, 1989; Dreher, Robinson & Distler, 1992; Germer et al., 1998; Ramos et al., 2013).

Holangiotic retinas are nourished by a dual circulation: retinal vessels supply blood to the inner portion of the retina, from the internal limiting membrane to the inner nuclear layer; while choroidal vessels irrigate the remaining outer retinal layers (Anderson & McIntosh, 1967; Wise et al., 1971; Ramos et al., 2013; Catita et al., 2015).

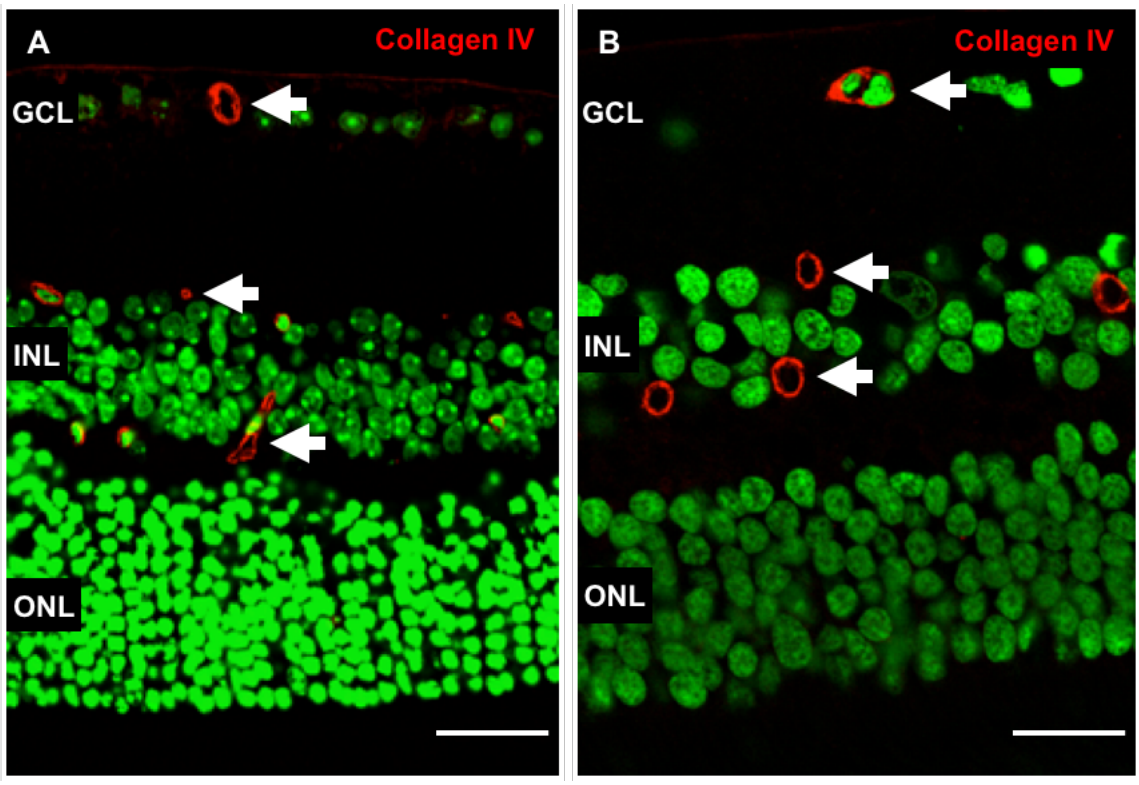

Figure 5. Retinal vascular pattern. Paraffin sections of mouse (**A**) and human (**B**) retinas immunohistochemically labelled with anti-collagen IV antibody (red). Nuclei were counterstained with sytox green (green). GCL, ganglion cell layer; INL, inner nuclear layer; ONL, outer nuclear layer. Arrows: blood vessels. Scale bars: A = 16.92 µm; B = 13.73 µm. Images from Ruberte et al., 2016.

A.3.2. Three-dimensional spatial distribution of blood vessels

In mouse and human, the retinal vasculature is organized in a three-dimensional network, creating three vascular plexi (Paques et al., 2003): the superficial, the intermediate, and the deep vascular plexi (Figure 6).

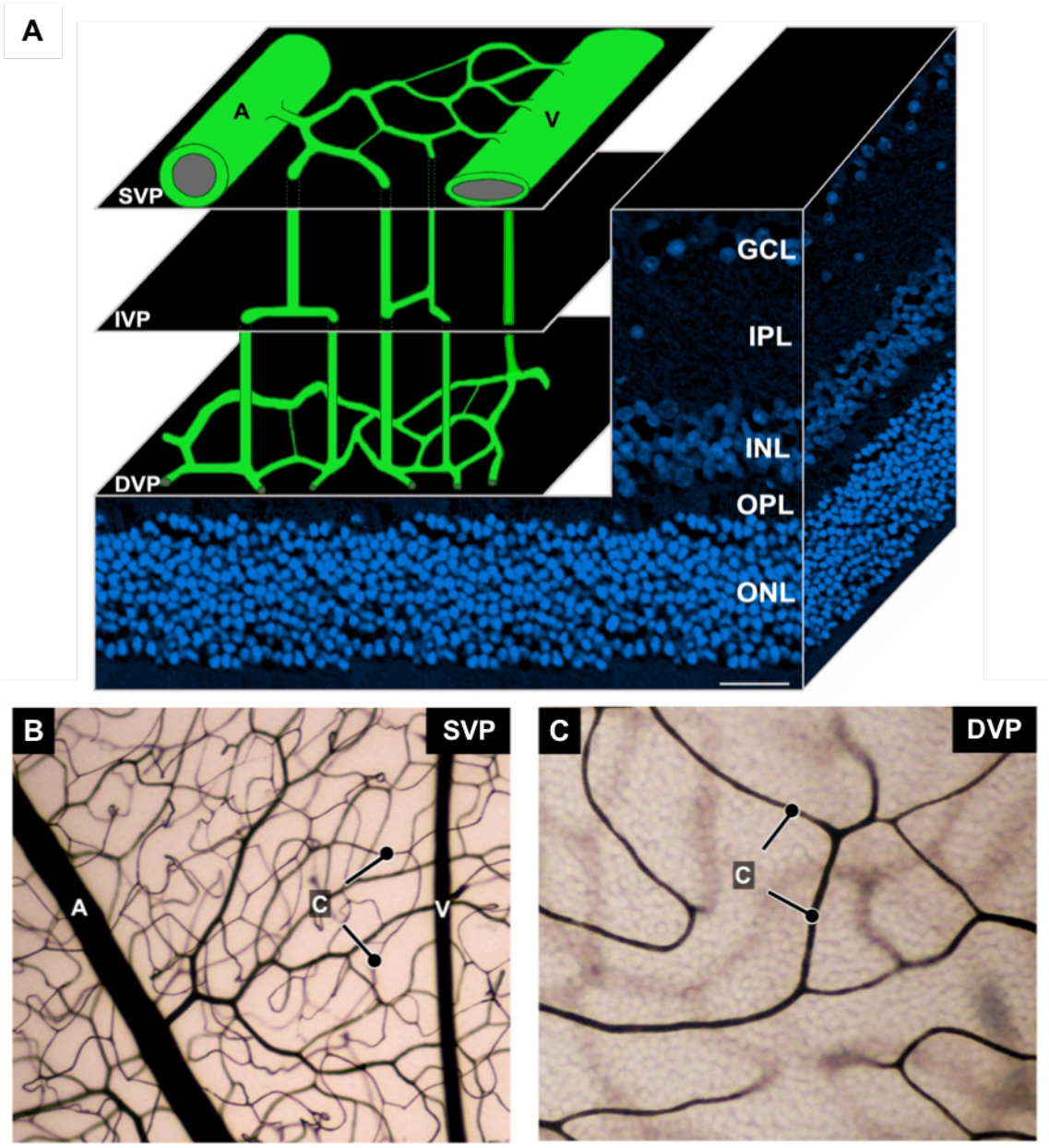

Figure 6. Retinal vascular plexi. A. Schematic representation of the distribution of blood vessels thorough the retinal parenchyma. Nuclei were counterstained with ToPro3 (blue). The localization of the retinal blood vessels in the superficial (**B**) and deep (**C**) vascular plexi was evidenced using Indian ink injection (black). A, arteriole; C, capillaries; DVP, deep vascular plexus; GCL, ganglion cell layer; SVP, superficial vascular plexus; IVP, intermediate vascular plexus; V, venule; INL, inner nuclear layer; IPL, inner plexiform layer; ONL, outer nuclear layer; OPL, outer plexiform layer. Scale bar = 20.36 µm. Images from Ruberte et al., 2016.

The superficial vascular plexus (SVP) is located at the level of the ganglion cell layer and contains large arterioles and venules, as well as a capillary network that connects them.

The intermediate vascular plexus (IVP), located at the inner plexiform layer, is filled with short capillary segments that run towards the deep layers (Paques et al., 2003; Smith, 1950).

Lastly, the deep vascular plexus (DVP), in the outer plexiform layer, consists predominantly of an anastomotic network of capillaries (Paques et al., 2003; Kur et al., 2012).

In the mouse, the central retinal artery (*A. centralis retinae*) emerges at the optic disc where it divides into four to eight retinal arterioles, a variable number depending on the strain and even on the individual (McLenachan et al., 2015; Ruberte et al., 2016). Recently, McLenachan and our laboratory (2015) proposed a classification for categorizing the types of arteriolar bifurcation patterns (Figure 7): Type A1 arterioles undergo major bifurcation at the peripheral retina, while Type A2 and Type A3 arterioles bifurcate at the central retina, either proximal to the optic disc or at the optic disc, respectively. Main retinal arterioles extend radially towards the retinal periphery, while dividing by both dichotomous and side-arm branching into pre-capillary arterioles, spreading across the superficial retina (Anderson & McIntosh, 1967; Wise et al., 1971; Kur et al., 2012). As retinal arterioles divide into pre-capillary arterioles, their walls become thinner and the vascular lumen decreases until they branch into numerous retinal capillaries (Wise et al., 1971; Watson et al., 2012; McLenachan et al., 2015). Some pre-capillary arterioles from the superficial plexus run almost vertically into the deep layers of the retina (Smith, 1950).

The deep retinal capillary bed is drained by post-capillary venules that converge into larger retinal venules located in the superficial vascular layer (Pournaras et al., 2008; McLenachan et al., 2015). The mouse retina possesses between five to six retinal venules. Interestingly, venules may be classified into two types (McLenachan et al., 2015) (Figure 7): Type V1 venules extend to the retinal margins and form an incomplete circumferential vein that drains peripheral regions of the capillary bed, while Type V2 venules end in a more central region of the retina to connect with the deep vascular plexus. As retinal venules approach the optic disc, their caliber and wall thickness increase, and leave the eye through the central retinal vein (*V. centralis retinae*), which drains hypoxic blood directly or via the ophthalmic vein (*V. ophthalmica*) into the cavernous sinus (Anderson & McIntosh, 1967; Sobotta & Becher, 1974; Pournaras et al., 2008).

In man, the central retinal artery branches into four main retinal arterioles as it enters through the optic disc: superonasal and inferonasal arteries (*Arteriolae nasalis retinae superior et inferior*), and superotemporal and inferotemporal arteries (*Arteriolae temporalis retinae superior et inferior*) (Sobotta & Becher, 1974). The venous system of humans is supplied by

four main branches of the central retinal vein, which run parallel to the arterioles: superonasal and inferonasal venules (*V. nasalis retinae superior et inferior*), and superotemporal and inferotemporal venules (*V. temporalis retinae superior et inferior*) (Sobotta & Becher, 1974).

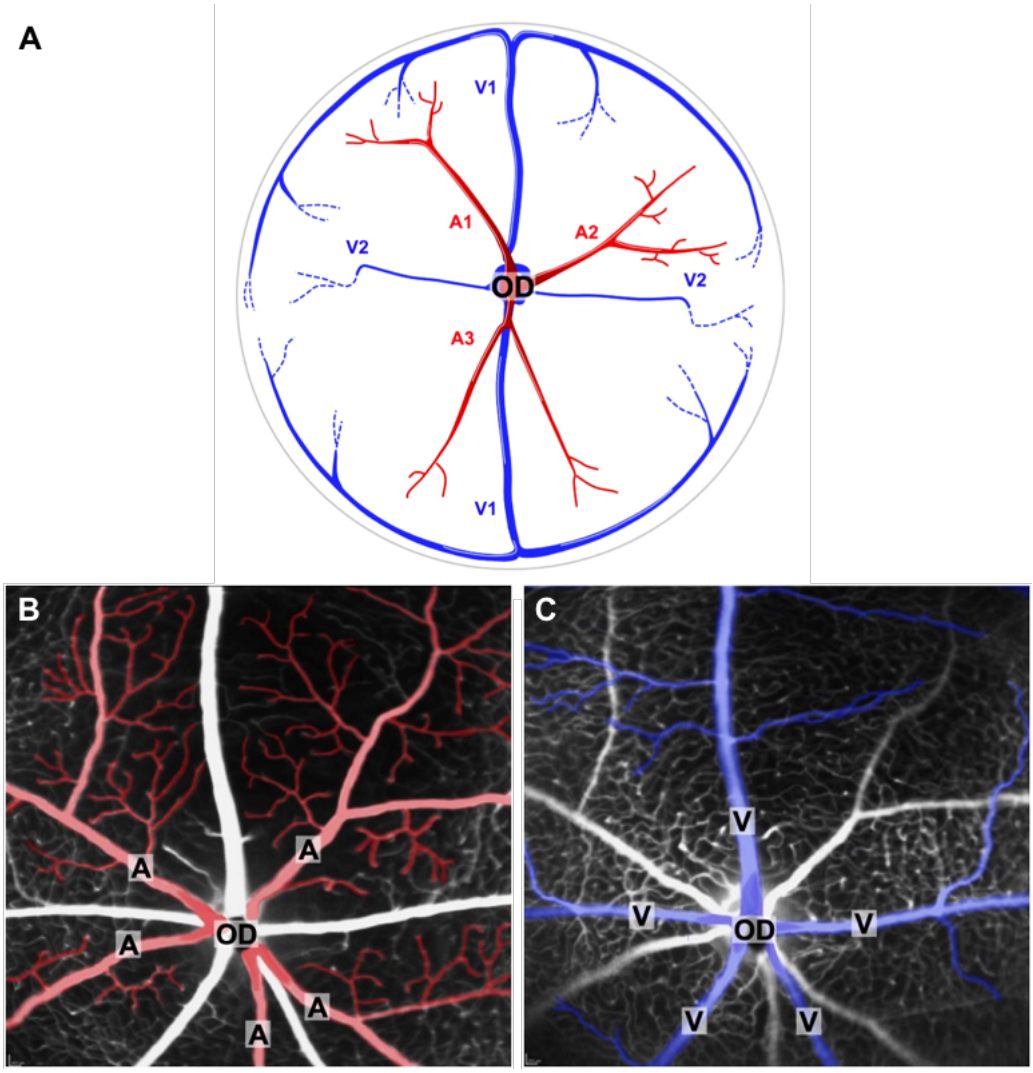

Figure 7. Vascularization of the retina. A. Schematic representation of arteriolar and venular retinal pattern distribution in the mouse - A1, A2, A3: types of arterioles; V1, V2: types of venules. **B** and **C**. Fundus fluorescein angiograms of the mouse retina showing retinal arterioles (red) and retinal venules (blue). A, arterioles; OD, optic disc; V, venules. Images from McLenachan et al., 2015.

In addition, the human retina has an avascular area near the central part of the retina known as the macula (*Macula lutea*). In the center of the macula resides the fovea (*Fovea centralis*) (Wise et al., 1971). The fovea, that is the area of maximal visual acuity, is characterized by the lack of vessels and flattened retinal layers to confer the most transparency to this region (Gartner & Hiatt, 2007). The mouse, unlike man, has no fovea and the central axis of the eye coincides with the optic disc (Smith et al., 2002; Ruberte et al., 2016).

A.3.3. Choroidal vascularization and the retina

Choroidal blood vessels nourish the avascular layers of the outer retina via diffusion processes through the RPE (Figure 8) (Saint-Geniez, Maldonado & D'Amore, 2006; Kur et al., 2012). Unlike the retinal vasculature, choriocapillaries are highly fenestrated and very permeable to plasma proteins (Bill, Törnquist & Alm, 1980; Federman, 1982).

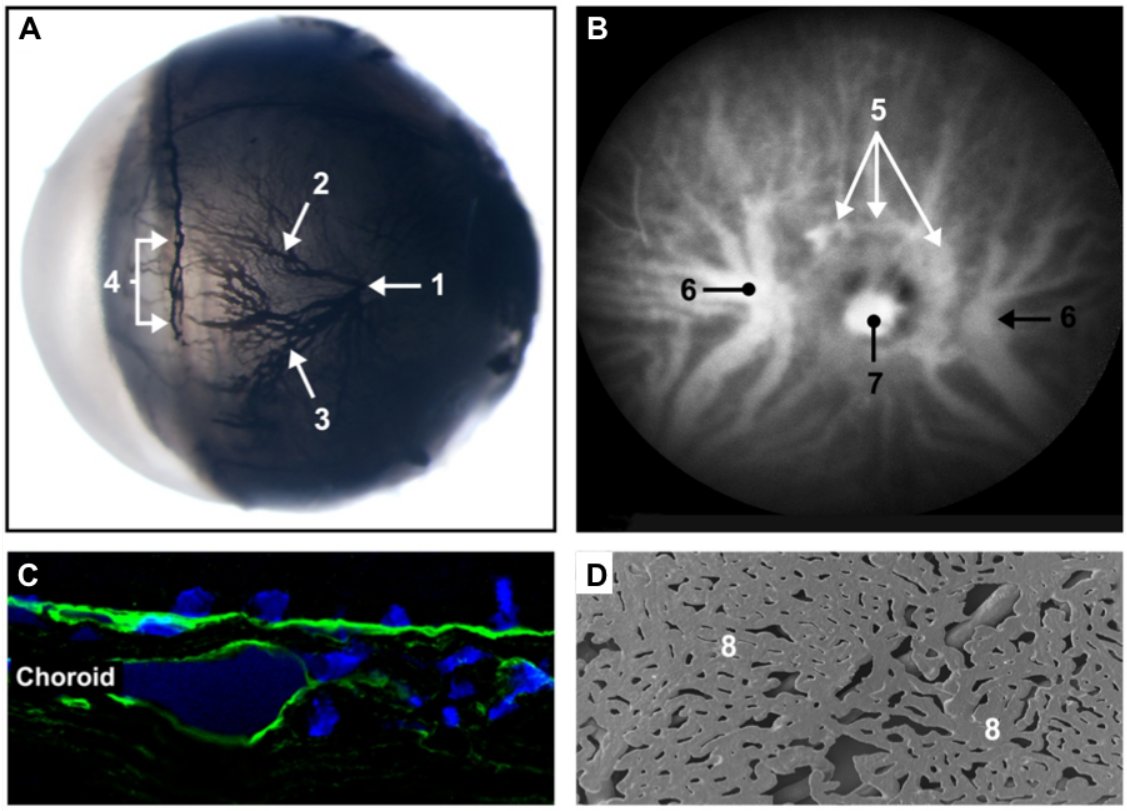

Figure 8. Choroidal vasculature. A. Arterial injection with Indian ink. **B.** Indocyanine green angiography. **C.** Confocal laser microscopy image of immunodetection against collagen IV (green). Nuclei were counterstained with ToPro3 (blue). **D.** Scanning electron microscopy image of vascular corrosion cast (Mercox). 1, long posterior ciliary artery; 2, dorsal branch; 3, ventral branch; 4, major circulus arteriosus of iris; 5, vascular circulus of optic nerve; 6, short posterior ciliary artery; 7, central retinal artery; 8, lamina choriocapillaris. Images from Ruberte et al., 2016.

A.3.4. Structure of blood vessels

The structural conformation of the vessel wall is essential to control vascular diameter, regulate blood flow, and maintain vascular permeability (Martinez-Lemus, 2012). The blood vessel wall comprises three layers or tunicae: the *tunica intima*, the innermost layer, formed by a

monolayer of endothelial cells; the *tunica media*, where smooth muscle cells and/or pericytes are found, depending on vessel type; and the *tunica adventitia*, the most external layer, consisting of connective tissue (Wise et al., 1971; Saint-Geniez & D'Amore, 2004).

The *tunica intima* of retinal arterioles consists of a single layer of endothelial cells oriented longitudinally along the vessel axis (Figure 9). Endothelial cells within this layer remain attached to a subendothelial layer of connective tissue, which is continuous to the basement membrane of the *tunica media*. The *tunica media* of arterioles contains a well-developed coat of smooth muscle cells circularly oriented to the vessel axis, each being surrounded by its basement membrane. As vessels branch into smaller pre-capillary arterioles, the number of smooth muscle cells decreases, giving rise to a discontinuous layer of sparse cells. The external layer, *tunica adventitia*, mainly consists of collagen fibers surrounding all the components of the arteriolar wall (Wise et al., 1971; Kur et al., 2012; Pournaras et al., 2008). Retinal venules, as retinal arterioles, are composed of the *tunica intima*, the *tunica media*, and the *tunica adventitia*. The *tunica intima* of retinal venules, similar to the *tunica intima* of arterioles, consists of a single layer of endothelial cells (Figure 9). In comparison to arterioles, the subendothelial layer of venules is thinner. Moreover, the *tunica media* contains widely spaced pericytes and smooth muscle cells, yet small caliber venules are reduced to only one layer of pericytes (Wise et al., 1971; Kur et al., 2012). The basement membrane of retinal venules is mainly composed of loosely arranged collagen fibers.

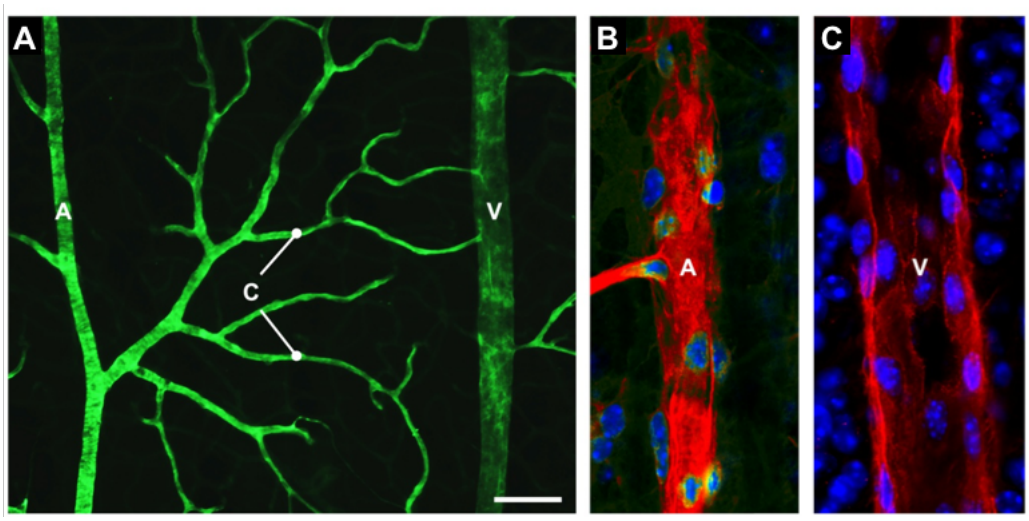

Figure 9. Retinal arterioles and venules. **A.** Immunohistochemistry with collagen IV (green) showing the distribution of the retinal vessels. Confocal microscopy image of an arteriole (**B**) and a venule (**C**) labelled with the lectin from *Lycopersicon sculentum* (red). Nuclei were counterstained with ToPro3 (blue). A, arteriole; C, capillaries; V, venule. Scale bar = 111.09 µm. Images from Ruberte et al., 2016.

Retinal capillaries consist of a continuous layer of endothelial cells and discontinuous layer of pericytes, which extend parallel to the vessel axis and share a common basement membrane (Figure 10) (Hughes & Chan-Ling, 2004; Kur et al., 2012). Capillaries may be classified into three groups, based on blood flow direction: pre-capillaries, mid-capillaries, and post-capillaries (Nehls & Drenckhahn, 1991).

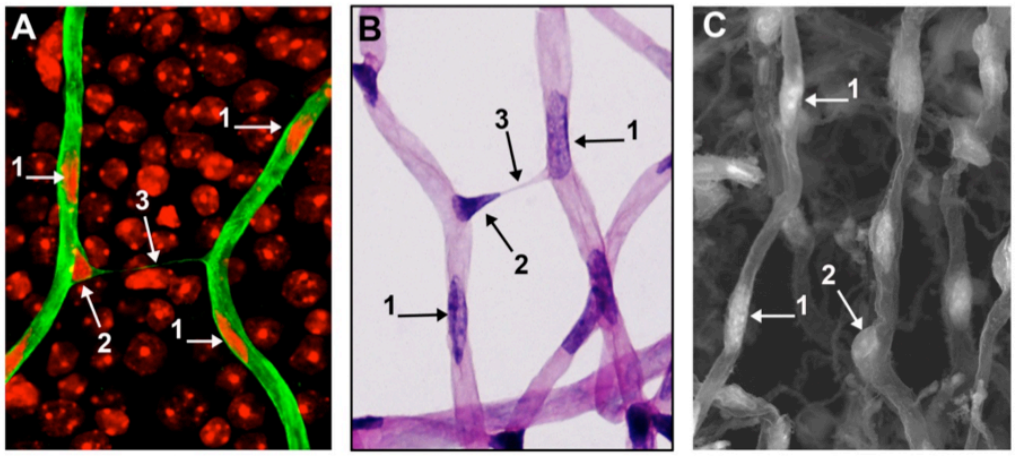

Figure 10. Retinal capillaries. A. Confocal laser microscopy images of retinal capillaries immunostained with collagen IV (green). Nuclei were counterstained with propidium iodide (red). **B.** Digested retinal capillaries stained with PAS-Hematoxylin evidencing intervascular bridges (3), which are fibrous strands that connect neighboring capillaries. **C.** Scanning electron microscopy image of a partially corroded retina. 1, endothelial cell; 2, pericyte; 3, intervascular bridge. Images from Ruberte et al., 2016.

A.3.4.1 Vascular wall components

The vascular wall components, endothelial cells, smooth muscle cells, pericytes, and basement membrane, are dynamically interconnected and have characteristic features according to the blood vessel type, tissue type or even between neighboring cells of the same organ and vessel type (Nehls & Dreckhahn, 1991; Worth et al., 2001; Aird, 2012).

A.3.4.1.1. Endothelial cells

Endothelial cells are elongated cells with flattened cytoplasm and long elliptical nuclei, which protrude into the lumen, and line the inside of the vessel (Figure 11) (Arribas et al., 2007; Bharadwaj et al., 2013). Ultrastructurally, endothelial cells show nuclei with highly condensed heterochromatin along the nuclear membrane, abundant mitochondria and ribosomes, as well

as vesicular components, such as caveolae, which are implicated in cellular endocytosis and transcytosis (Ishikawa, 1963; Wise et al., 1971; Bharadwaj et al., 2013; Catita et al., 2015). One distinctive morphological feature of retinal endothelial cells is the presence of tight junctional complexes along the opposing surfaces of adjacent cells. In the retina, arteriolar endothelial cells are elongated and spindle-shaped in comparison to the more polygonal shape in venules, or to an irregularly shape in capillaries (Yu et al., 1997; Aird, 2007; Yu et al., 2010).

Endothelial cells play a wide variety of functions in blood vessels. The endothelium is necessary to maintain vascular functional integrity and acts as a semi-permeable barrier to control the transfer of small and large molecules (Cunha-Vaz, 1976; Pournaras et al., 1998; Sumpio, Riley & Dardik, 2002; Michiels, 2003; Aird, 2007). In fact, the retinal endothelium is considered one of the main components of the blood-retinal barrier (BRB) mainly due to its elaborate network of tight junctions (Pournaras et al., 1998). Endothelial cells are also involved in the regulation of vascular tone, blood flow, hemostasis, and inflammatory and immunologic responses, as well as in angiogenesis and vasculogenesis (Thorin & Shreeve, 1998; Michiels, 2003; Aird, 2007).

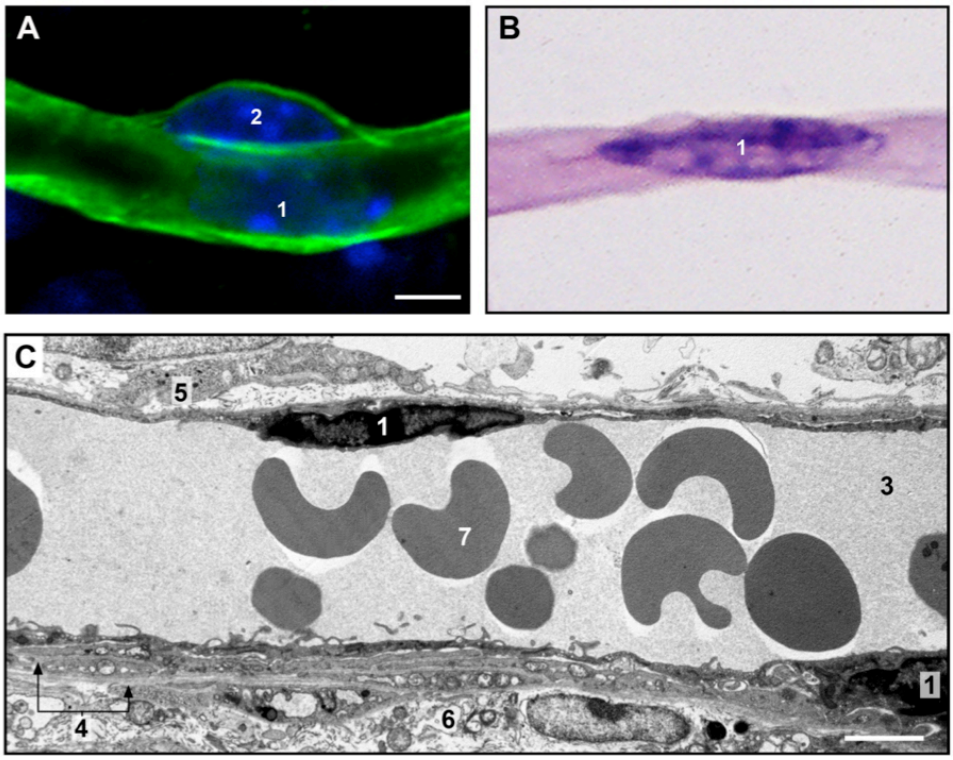

Figure 11. Endothelial cells. A. Confocal laser microscopy images of retinal capillaries immunostained with collagen IV (green). Nuclei were counterstained with ToPro3 (blue). **B.** Retinal trypsin digestion stained with PAS-Hematoxylin. **C.** Transmission electron microscopy image of a retinal vessel. 1, endothelial cell; 2, pericyte; 3, vascular lumen; 4, basement membrane; 5, Müller cell; 6, astrocyte; 7, erythrocyte. Scale bars: A = 3.2 µm; C = 2.07 µm. Images from Ruberte et al., 2016.

A.3.4.1.2. Smooth muscle cells

In general, vascular smooth muscle cells display a spindle-shaped morphology with variable size and arrangement based on the vessel type (Figure 12) (Absher et al., 1989). Ultrastructurally, the nucleus of these cells is flattened and elongated and there is an accumulation of mitochondria, Golgi apparatus, and sarcoplasmic reticulum close to nuclear poles. Vesicles and caveolae are particularly frequent on the abluminal side of the cell (Komuro, Desaki & Uehara 1982). Numerous myofilaments run along the cytoplasm of these cells, including thick filaments, actin filaments, and intermediate filaments (Komuro et al., 1982; Tang, 2008). In the retina, arteriolar smooth muscle cells show a more irregular or flattened shape with few cytoplasmic processes, whereas in pre-capillary arterioles the cell bodies are distinctly protruding and their cytoplasmic processes are arranged circularly, surrounding the vessel (Komuro et al., 1982; Armulik, Genové & Betsholtz, 2011; Kur et al., 2012). In contrast, venular smooth muscle cells are bigger and stellate-shaped with several branching processes (Armulik et al., 2011).

Vascular smooth muscle cells are responsible for the regulation of blood vessel tone, blood pressure, and blood flow distribution (Owens, Kumar & Wamhoff, 2004; Hughes & Chan-Ling, 2004). Vascular smooth muscle cells also have the ability to synthesize large amounts of extracellular matrix to promote vascular repair, as well as migrate and proliferate in response to growth factors and cytokines, and initiate inflammatory signals (Worth et al., 2001; Wynne, Chiao & Webb, 2009; Lacolley et al., 2012).

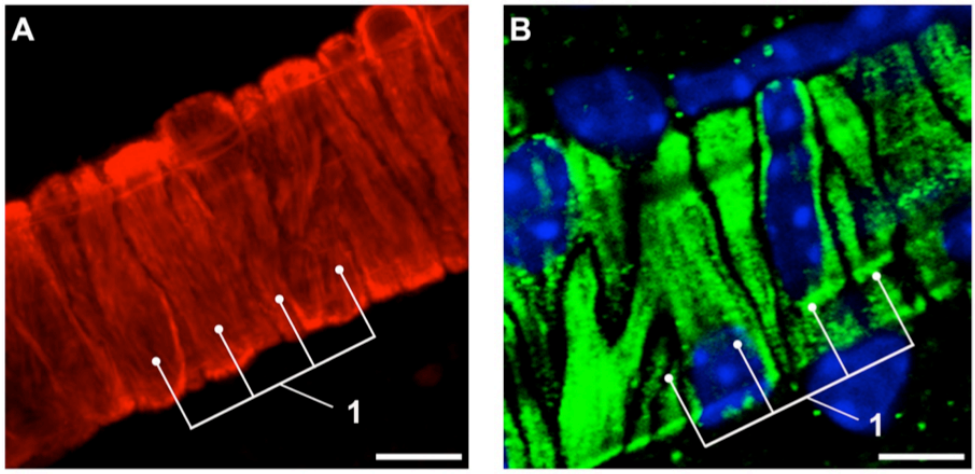

Figure 12. Smooth muscle cells. A. F-actin stained with *Phalloidin* (red). **B.** α-smooth muscle actin (green) evidenced by immunohistochemistry. Both images were acquired from whole-mount retinas with a confocal microscope. Nuclei were counterstained with ToPro3 (blue). 1, smooth muscle cells. Scale bars: A = 7.69 μm; B = 8.51 μm. Images from Ruberte et al., 2016.

A.3.4.1.3. Pericytes

Pericytes, together with smooth muscle cells, represent the contractile cell population of blood vessels. Pericytes are embedded within the vascular basement membrane and surround endothelial cells (Figure 13) (Sims, 1986; Armulik et al., 2011). There is great morphological heterogeneity within pericytes, with regard to their origin, distribution, phenotype, and function (Nehls & Drenckhahn, 1991; Pfister et al., 2008).

In addition to regulating blood flow at capillary level, pericytes have the ability to control endothelial proliferation and are involved in processes such as angiogenesis and neovascularization (Enge et al., 2002; Pfister et al., 2008; Pournaras et al., 2008). It has also been proposed that pericytes aid in the maintenance and structural rigidity of the microvessel wall and stabilize developing microvessels by depositing extracellular matrix (Herman & D'Amore, 1985; Sims, 1986; Armulik et al., 2011). Moreover, the BRB is further strengthened by pericytes (Yao et al., 2014).

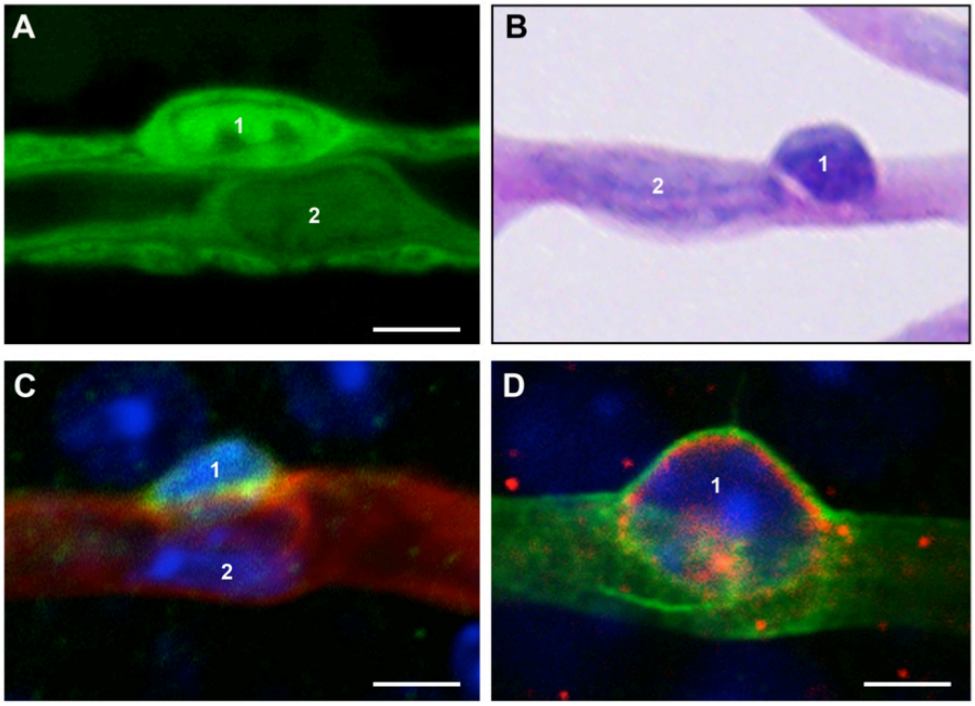

Figure 13. Pericytes. A. EGFP detection in a capillary of a β-actin EGFP transgenic mouse. **B.** Trypsin digestion of the retina stained with PAS-Hematoxylin. **C** and **D.** Double immunohistochemistry using two well-known pericyte biomarkers, neuron glial 2 chondroitin sulfate (C, green) and platelet-derived growth factor receptor-β (D, red). Nuclei were counterstained with ToPro3 (blue). 1, pericyte; 2, endothelial cell. Scale bars: A = 3.2 μm; C = 3.5 μm; D = 3.44 μm. Images from Ruberte et al., 2016.

A.3.4.1.4. Basement membrane of blood vessels

The blood vessel basement membrane forms a connective sheath surrounding endothelial cells, pericytes, and smooth muscle cells. Basement membranes are continuous self-assembled layers of proteins, glycoproteins, and proteoglycans (Baluk et al., 2003; Catita et al., 2015). The primary function of the basement membrane is to provide strength, support, and integrity to the vessel wall, acting as a framework for vascular cells and anchoring the vessel to the surrounding tissue (Baluk et al., 2003; Hayden, Sowers & Tyagi, 2005; Catita et al., 2015). At the same time, the basement membrane regulates endothelial cell proliferation and migration, and tissue repair (Forrester & Knott, 1997; Pöschl et al., 2004), and is a fundamental component of the BRB, acting as an important selective barrier, regulating the pass of blood-borne molecules to retinal parenchyma (Pournaras et al., 2008).

A.4. The blood-retinal barrier

The retina is gifted with a complex and restrictive system of physical barriers, the BRB, which maintains an appropriate environment for the neural tissue by regulating the permeability, ion concentrations, and the delivery of nutrients, while protecting from the action of harmful stimuli (Figure 14) (Cunha-Vaz, 1976; Bradbury & Lightman, 1990; Törnquist, Alm & Bill, 1990; Pournaras et al., 2008; Cunha-Vaz, Bernardes & Lobo, 2011; Campbell & Humphries, 2012; Kur et al., 2012). Considered as a special part of the blood-brain barrier (BBB), the BRB shares many properties, structurally and functionally, with the BBB. Both barriers are formed by a complex architecture of cell-to-cell junctions between barrier-forming cells and a paucity of vesicles within those cells (Vinores, 1995). However, in contrast with the BBB, the BRB consists of both an inner BRB (iBRB), that comprises retinal endothelial cells, and an outer BRB (oBRB), that consists of RPE cells and Bruch's membrane (Figure 15) (Campbell & Humphries, 2012).

Alterations and loss of function of the BRB play a crucial role in the development of retinal diseases and vision loss (Cunha-Vaz, 1976). The most relevant retinal diseases with BRB alterations and/or breakdown are diabetic retinopathy and age-related macular degeneration (Cunha-Vaz et al., 2011). Although it is now accepted that dynamic adaptations of endothelial cells and other cell types involved in the BRB underlie vascular leakage in retinal disease, there is still a fundamental lack of understanding of the cellular mechanisms underlying both the function of the BRB in physiological conditions as well as its dysfunction in pathological conditions.

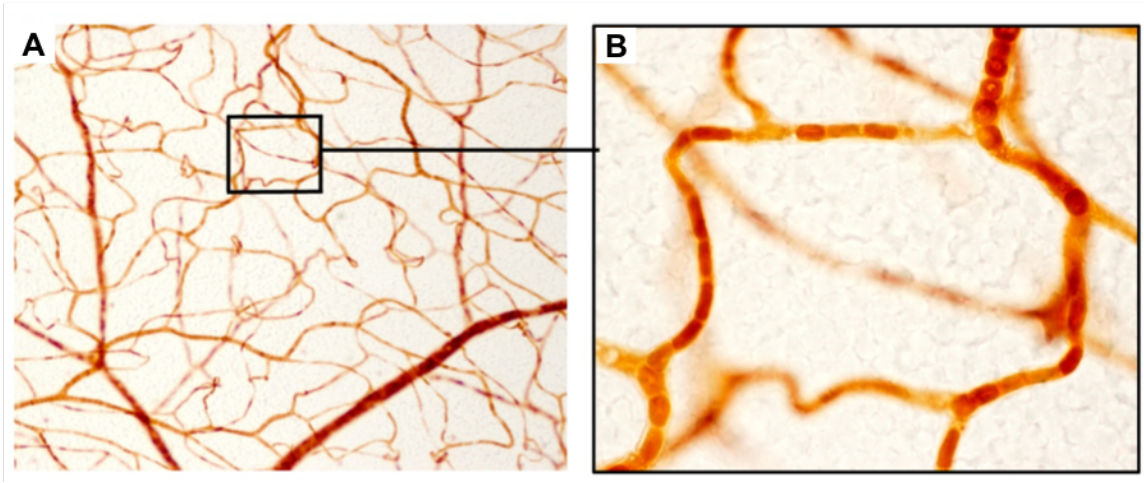

Figure 14. Blood-retinal barrier. Intact BRB integrity showed by intravascular confinement of horseradish peroxidase (HRP) injected intravenously and developed with 3,3'-diaminobenzidine substrate (brown). Images from Ruberte et al., 2016.

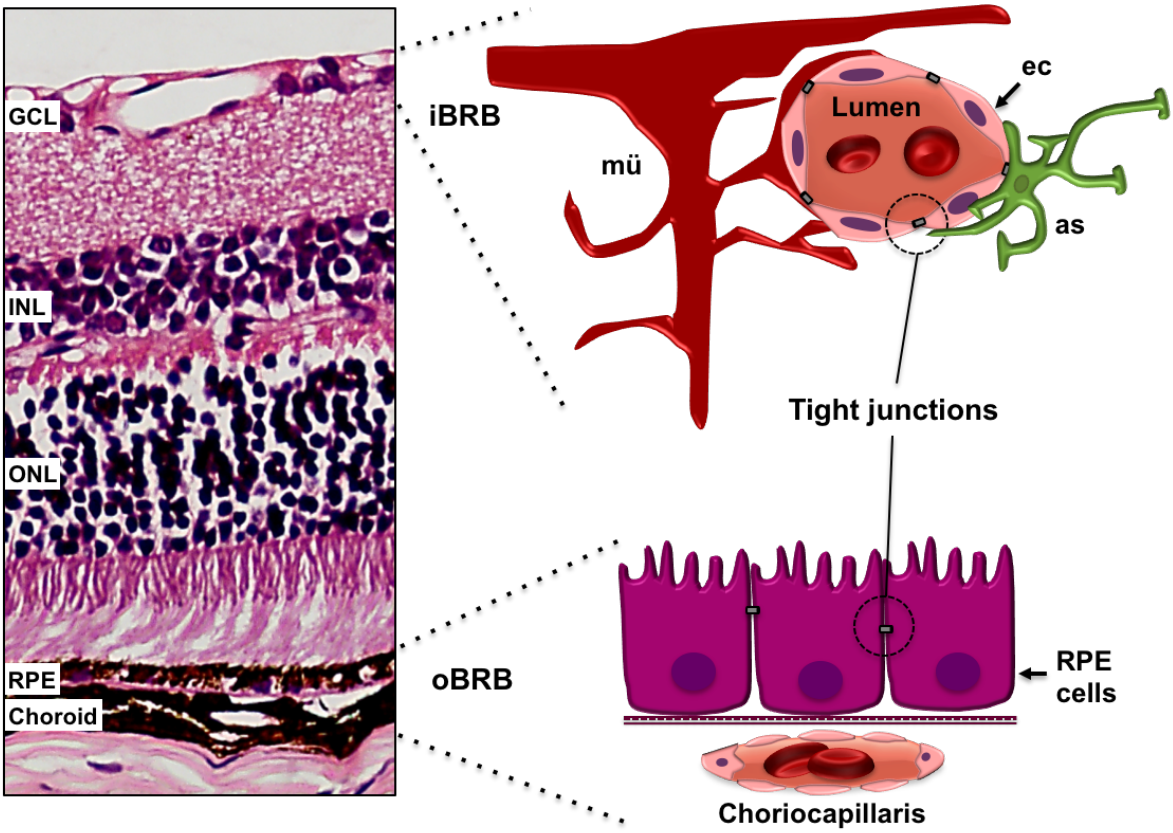

Figure 15. Schematic representation of the blood-retinal barrier. Structurally, the BRB is composed of two distinct barriers that regulate the permeability between blood and retinal parenchyma. The iBRB, located in the inner retinal microvasculature, is formed by tight junctions between retinal endothelial cells. The oBRB consists of tight junctions between retinal pigment epithelial cells, at the choroid-epithelial interface. as, astrocyte; ec, endothelial cell; GCL, ganglion cell layer; iBRB, inner blood-retinal barrier; INL, inner nuclear layer; L, lumen; mü, Müller cell; oBRB, outer blood-retinal barrier; ONL, outer nuclear layer; RPE, retinal pigment epithelium.

A.4.1. The inner blood-retinal barrier

The iBRB plays a major role in controlling fluid entry into the neural retina and is mainly maintained by retinal endothelial cells, which are characterized, similarly to endothelial cells in the brain, by having the highest number of tight junction strands of the organism, lack of fenestrations, and low pinocytic activity. In addition to the vascular endothelium, there are other elements that contribute to this barrier, such as glial cells, pericytes, and the basement membrane (Cunha-Vaz, 1976; Abbott, Rönnbäck & Hansson, 2006; Armulik et al., 2010; Klaassen, Van Noorden & Schlingemann, 2013). In this regard, a neuro-glio-vascular cross-talk involving astrocytes and Müller cells, as well as interactions of endothelial cells with pericytes and smooth muscle cells, dynamically regulates tight junctions (Fruttiger, 2007; Cunha-Vaz, 2009; Campbell & Humphries, 2012; Klaassen et al., 2013; Sorrentino et al., 2016). Moreover, it is known that glial cells closely invest all retinal vessels, creating the glial limiting membrane (*Glia limitans*) that separates vessels from the retinal parenchyma and delimits the perivascular space (Wise et al., 1971; Gardner et al., 2002). Thus, glial cells play a critical role in the formation, modulation, and maintenance of the iBRB, in the uptake of nutrients, and in the disposal of waste products under normal conditions (Tout et al., 1993; Distler & Dreher, 1996; Abbott et al., 2006; Reichenbach et al., 2007; Yao et al., 2014). In fact, astrocytes, Müller cells, and pericytes are able to transmit regulatory signals to endothelial cells to influence their and iBRB activity to adapt to changes in the microenvironment of the retinal neuronal circuitry (Cunha-Vaz at al., 2011).

Pericytes have also been described to maintain the integrity and permeability of the BRB, due to their close interaction with endothelial cells (Herman & D'Amore, 1985; Sims, 1986; Vinores, 1995; Gardner et al., 2002). Lastly, the basement membrane is part of the iBRB, providing structural support and a physical barrier to restrict the diffusion of particles from the cell into the blood (Wang et al., 2006).

A.4.2. The outer blood-retinal barrier

To complete the protective environment created by the iBRB, the oBRB is formed by tight junctions between neighboring RPE cells, which rest on the underlying Bruch's membrane, and separates the neural retina from the fenestrated choriocapillaries. Therefore, this barrier functions to regulate the access of solutes and nutrients from the choroid to the photoreceptors, as well as to eliminate waste products and to maintain retinal adhesion, preserving homeostasis of the outer third of the retina. The metabolic relationship of the RPE apical villi and photoreceptors is considered to be critical for the maintenance of visual function (Wallez & Huber, 2008; Cunha-Vaz et al., 2011; Campbell & Humphries, 2012).

A.4.3 Tight junctions

Tight junctions, also known as zonula occludens, are specialized polymeric adhesion complexes, which act to seal the intercellular space of neighboring cells, and, thereby, generate a permeability barrier required for transport processes and limit the diffusion of molecules through this barrier (Figure 16) (Farquhar & Palade, 1963; Hogan, Alvarado & Weddell, 1971; Balda & Matter, 1998; Ghassemifar, Lai & Rakoczy, 2006; Günzel & Yu, 2013). In addition, tight junctions function as a cell signaling coordination center that affects differentiation, proliferation, and polarity of cells (Klaassen et al., 2013).

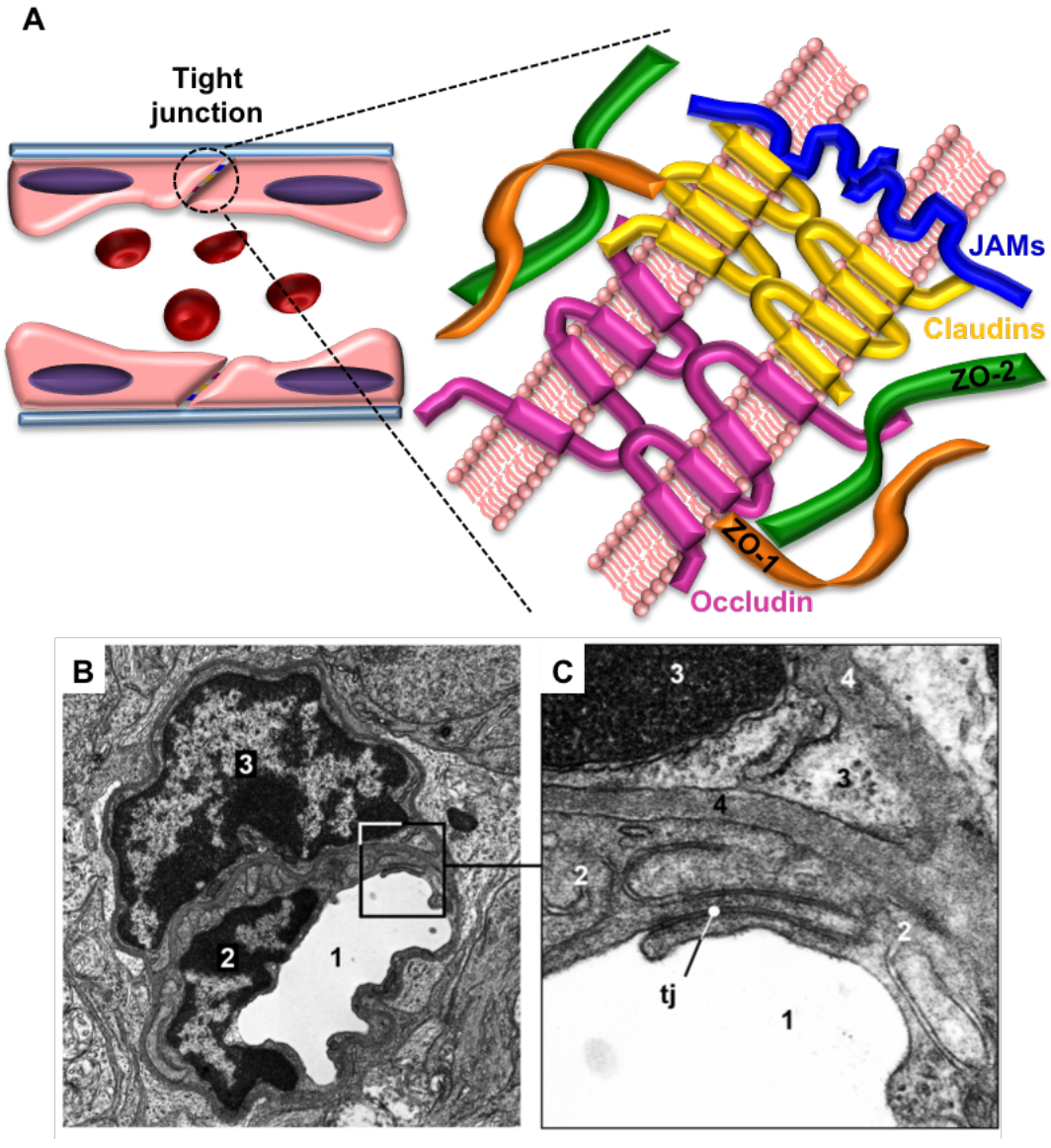

Figure 16. Tight junctions. A. Schematic representation of tight junctions in retinal endothelial cells. Transmembrane proteins include occludin, claudins, and junctional adhesion molecules (JAMs). Integral membrane proteins, such as zonula occludens (ZO) 1 and 2, couple the transmembrane proteins to the actin cytoskeleton. **B** and **C.** Transmission electron microscopy micrograph of a tight junction. 1, lumen; 2, endothelial cell; 3, pericyte; 4, basement membrane; tj, tight junction. B and C images from Ruberte et al., 2016.

Several types of transmembrane, scaffolding, and signaling proteins interact to form the tight junctional complex. Transmembrane proteins include occludin, claudins, and junctional adhesion molecules (JAMs). These proteins extend to the paracellular space creating the characteristic seal. In addition, there are also integral membrane proteins forming tight junctions: zonula occludens (ZO) and cingulin (Fanning, Mitic & Anderson, 1999).

Occludin and claudins, the main components of tight junctions, span the plasma membrane, have four transmembrane domains, and are able to interact homotypically and heterotypically (Furuse et al., 1993, 1998; Phillips et al., 2008; Peng et al., 2011). Occludin was the first transmembrane protein to be isolated (Furuse et al., 1993) and it has been suggested that, although not crucial for tight junction formation, may have key regulatory roles (Antonetti et al., 1998). In the mammalian eye, occludin immunoreactivity was detected along the borders of endothelial and RPE cells (Morcos et al., 2001).

Claudins constitute a large family of transmembrane proteins believed to form the backbone of tight junctions (Tsukita, Furuse & Itoh, 2001). It seems to exist a tissue- and cell-specificity in claudins expression. In this regard, claudin-5 has been found to be expressed in endothelial, but not epithelial, tight junctions of different tissues, including the brain, confirming the specific confinement of this protein to vascular beds (Morita et al., 1999). The analysis of brain blood vessels from mice lacking claudin-5 expression revealed tight junctions of normal appearance (Nitta el al., 2003). However, an increase of the BBB permeability mainly to small size solutes was observed. These observations suggest that different types of claudins may confer different barrier properties to cells that express them. In endothelial cells of retinal vessels, claudin-1 and claudin-5 have been observed (Morcos et al., 2001; Barber & Antonetti, 2003; Koto el al., 2007).

Other transmembrane proteins include JAMs, a family of proteins belonging to the immunoglobulin superfamily, which seem to associate laterally to the claudin-based backbone of tight junction strands (Martin-Padura et al., 1998; Tsukita et al., 2001; Ebnet et al., 2004; Cunha-Vaz et al., 2011).

The ZO family of proteins comprises ZO-1, ZO-2, and ZO-3. These peripheral cytoplasmic proteins, found ubiquitously within tight junctions of epithelial and endothelial cells (Harhaj & Antonetti, 2004), function to anchor the transmembrane proteins to the actin cytoskeleton through multiple protein-protein interaction domains, and are crucial for the distinct organization and initial formation of tight junctions (Stevenson et al., 1986; Konari et al., 1995; Campbell & Humphries, 2012). In fact, the lack of expression of all three ZO family members in a cell line caused the abolition of tight junction formation and failure of claudin molecules polymerization (Umeda et al., 2006). The expression of ZO-1 protein has been observed in the barrier-forming cells of the retina (Tserentsoodol et al., 1998). Moreover, retinal ZO-1

phosphorylation has been associated with the disruption of the BRB (Antonetti et al., 1999), suggesting that ZO-1 could be a key regulator of retinal permeability.

Tight junctions are frequently entangled with adherens junctions, mainly formed by VE-cadherin, and gap junctions, composed of connexins. Accordingly, the presence of adherens junctions stimulates the formation of tight junctions (Taddei et al., 2008), while gap junction proteins facilitate the assembly of adherens and tight junctions (Klaassen et al., 2013). In fact, as the tighter regulation of permeability is required, the more complex this system is structured.

A.4.4. Selective transport across the blood-retinal barrier

The BRB is not an absolute barrier but a highly selective barrier that regulates the movement of ions, water, solutes, and cells across the vascular bed and epithelia. The net movement over time across the BRB is described by permeability and depends on two routes: the paracellular and the transcellular transports (Figure 17) (Díaz-Coránguez, Ramos & Antonetti, 2017).

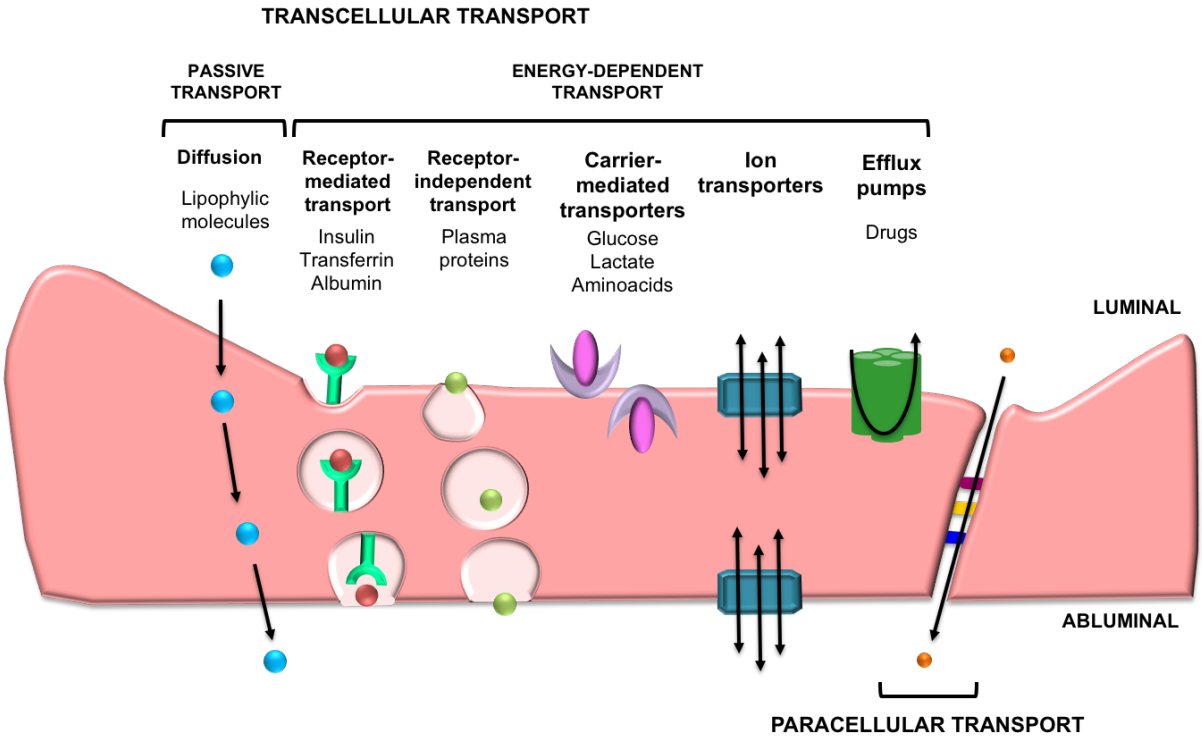

Figure 17. Mechanisms of transport across the blood-retinal barrier. Schematic overview of transcellular mechanisms of the BRB: lipid-soluble molecules cross the BRB by passive transport; other transport mechanism are energy-dependent processes and comprise receptor-mediated or receptor-independent transport through caveolae, carrier-mediated transporters, ion transporters, and efflux pumps. Paracellular transport allows the movement of small molecules from the blood (luminal) into the retinal (abluminal) side via the paracellular space regulated by tight junctions.

A.4.4.1. Paracellular transport

The paracellular pathway is regulated by the dynamic opening and closing of tight junctions (Figures 16 and 17) and restricts passage of solutes larger than 3 nm in radius across epithelia and endothelia, while water and small water-soluble compounds pass preferentially through this route (Pappenheimer, Renkin & Borrero, 1951; Klaassen et al., 2013).

Claudins and occludins are the main tight junction components involved in paracellular permeability. The extracellular loops of claudins have been proposed to create charge-selective paracellular aqueous pores that permit the passive diffusion of ions between cells. Thus, the claudin composition of a tight junction determines the ion selectivity of the paracellular pathway, because changes in claudin expression correlate with alterations in conductivity for specific ions (Van Itallie & Anderson, 2006; Krause et al., 2008). On the other hand, occludin has been linked to the formation of the intramembrane diffusion barrier and regulates the paracellular diffusion of small hydrophilic molecules and the transepithelial migration of neutrophils (Antonetti et al., 1998; Aijaz, Balda & Matter, 2006). Furthermore, JAMs have been reported to regulate the paracellular transmigration of leukocytes across the endothelium.

A.4.4.2. Transcellular transport

Transcellular transport, the movement of solutes across a cell layer through the cells, is necessary for the regulation of retinal homeostasis. In general, there are a variety of routes that conform the transcellular route. More concretely, transport across the endothelium and the RPE cells is highly selective and regulated by membrane transporters and by vesicular mechanisms (Figure 17).

For a wide range of lipid-soluble molecules passive transport across the BRB is possible (Hosoya et al., 2010; Toda et al., 2011). All other types of transcellular transport for larger lipophilic molecules and hydrophilic molecules are energy-dependent and involve: transport through caveolae with or without binding to cargo-specific receptors; carrier-mediated transport mechanisms; specific transporters, such as ion and amino acid transporters; and active efflux pumps, such as multidrug resistance pumps (Zlokovic, 2008; Klaassen et al., 2013).

The transport of molecules depends on their size, charge, and chemistry, and also on the structural-functional properties of the endothelium/epithelium and, in particular, the caveolae that actively carry the cargo across the barrier by receptor-mediated and receptor-independent

transcytosis, generally bypassing the lysosomes. Some plasma proteins follow dual pathways, endocytosis and transcytosis. The endocytosed plasma proteins and the molecules that they carry or their metabolites are used by cells themselves, whereas the transcytosed proteins are made available to the adjacent tissues. For a given molecule, the endocytosis/transcytosis ratio may vary with the pathophysiological state of the vascular bed involved (Simionescu & Simionescu, 1991; Simionescu, Gafencu & Antohe, 2002; Simionescu, Popov & Sima, 2009).

Caveolae-mediated transcytosis involves the migration of plasma membrane vesicles from one side of the cell to the other, and/or a channel resulting from vesicular fusion (Simionescu, 1979). Caveolae, a special type of lipid raft, are cell-surface plasma membrane invaginations (Figure 18) (Palade, 1953; Yamada, 1955), and, besides transcellular transport, are also associated with endocytosis (Anderson, 1993), regulation of cholesterol levels (Rothberg et al., 1990), sensing of flow (Milovanova et al., 2008), and signal transduction (Lisanti et al., 1994). Caveolin-1, the major protein component of caveolae, is expressed in developing and mature retinal vessels and choroidal vasculature (Gu et al., 2014).

The transcellular pathway, facilitated by caveolae and receptor-mediated transport mechanisms, is the preferred route for active transport of macromolecules, allowing albumin, transferrin, insulin, lipoproteins, and possibly immunoglobulins to penetrate from the circulation into tissues (Predescu, Vogel & Malik, 2004; Red-Horse & Ferrara, 2007; Anderson, 2008).

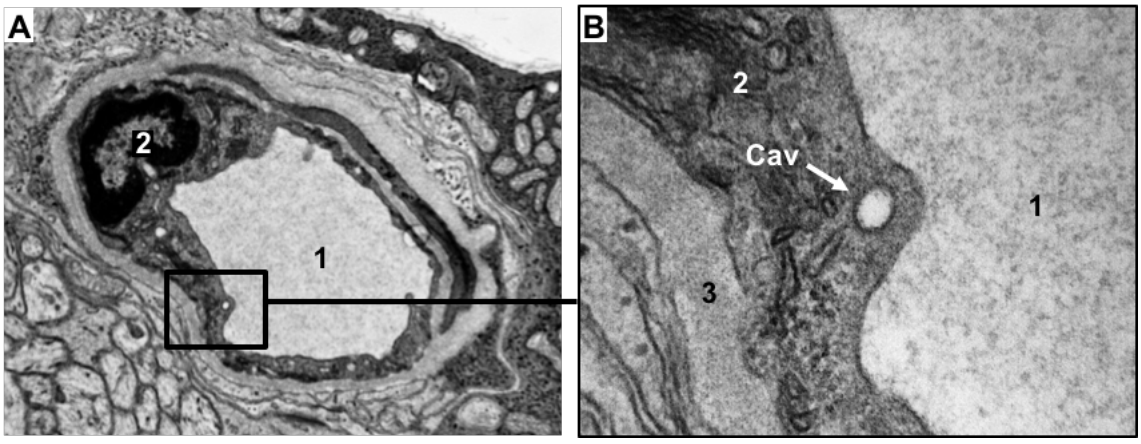

Figure 18. Caveolae. Transmission electron microscopy micrograph of a caveola. 1, lumen; 2, endothelial cell; 3, basement membrane; Cav, caveola.

Brain and retinal endothelia are characterized by a relative low number of caveolae, with a preferential location at the abluminal cell surface, suggesting a preferential direction of transcytosis from tissue to blood. In contrast, non-barrier endothelium typically has more

caveolae at the luminal surface (Sagaties et al., 1987; Hofman et al., 2000, 2001). Interestingly, transcytosis is altered during retinal pathological conditions. In fact, it has been shown that vascular endothelial growth factor (VEGF) induces increased permeability through an increase vesicular transport (Hofman et al., 2000). Moreover, transcytosis rate is also increased in streptozotocin-induced diabetic rats (Gardiner, Stitt & Archer, 1995).

B. Iron

Iron is the fourth most abundant element in the Earth's crust and is essential for most life on the planet (Frey & Reed 2012). Mammalian cells require sufficient amounts of iron to satisfy metabolic needs or to accomplish specialized functions, such as oxygen transport, adenosine triphosphate (ATP) production, myelin synthesis and maintenance, and neurotransmitters synthesis (Yefimova et al., 2000; Wang & Pantopoulos, 2011; Duck & Connor, 2016). Furthermore, enzymes of the citric acid cycle, succinate dehydrogenase, and aconitase, are iron dependent. Iron is also a crucial component of cytochromes a, b, and c, cytochrome oxidase, and the iron-sulfur complexes of the electron transport chain, making iron essential for ATP production (Wigglesworth & Baum, 1988; Poss & Tonegawa, 1997). Iron is also required by the ribonucleotide reductase, which is the rate-limiting enzyme of the first metabolic reaction in deoxyribonucleic acid (DNA) synthesis (Wigglesworth & Baum, 1988). In the CNS, oligodendrocytes require iron for myelin synthesis and maintenance (LeVine & Macklin, 1990; Morris et al., 1992). Iron is also an essential cofactor for synthesis of neurotransmitters, including dopamine, norepinephrine, and serotonin (Youdim, 1990; He et al., 2007). Moreover, iron plays an important role in xenobiotic metabolism, cell growth, apoptosis, gene regulation, and inflammation (Cairo & Recalcati, 2007; He et al., 2007; Outten & Theil, 2009; Zhang & Enns, 2009; Wang & Pantopoulos, 2011). Therefore, cells must maintain a sufficient amount of iron.

B.1. Iron homeostasis

In physiological conditions, iron can exist in two different oxidation states, the reduced ferrous (Fe^{2+}) and the oxidized ferric (Fe^{3+}) iron forms (Figure 19). In fact, the biological importance of iron relays in its properties as a transition metal, namely its ability to readily undergo one-electron redox reactions between the Fe^{2+} and Fe^{3+} states. Both of these forms have different reactivity and different chemical properties. Although being the most stable form, Fe^{3+} is largely insoluble and therefore plants and animals poorly absorb it. Thus, acidification of the

environment is necessary to promote its reduction to Fe^{2+}, which will be transported across the plasma membrane (Miller & Berner, 1989; García-Castiñeiras, 2010; Ganz & Nemeth, 2015).

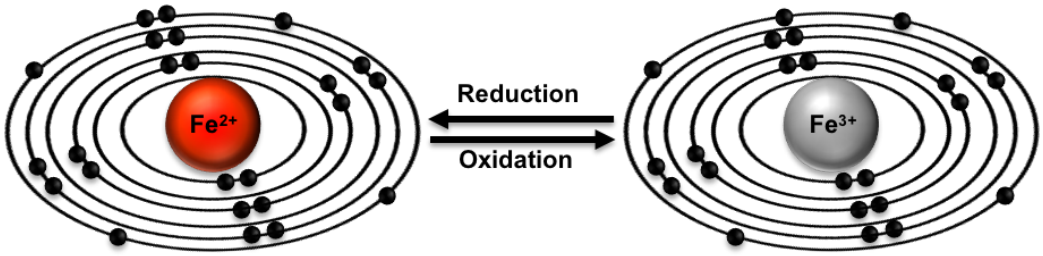

Figure 19. Iron oxidation states. Iron is a transition metal and readily undergoes one-electron reaction between the reduced ferrous iron form (Fe^{2+}) and the oxidized ferric form (Fe^{3+}).

While the redox reactivity of iron makes it extremely useful, iron in excess becomes toxic because of its propensity to generate free radical. Free Fe^{2+} participates in the Fenton reaction by catalyzing the conversion of hydrogen peroxide to the hydroxyl radical, the most reactive of reactive oxygen species (ROS) (Halliwell & Gutteridge, 1984; Udipi, Ghugre & Gokhale, 2012). Moreover, as disposal of excess iron is usually a slow process, there is a tendency to iron accumulation with aging (Cook & Yu, 1998; Kohgo et al., 2008; Xu et al., 2008; Gozzelino & Arosio, 2016). Thus, iron homeostasis must be tightly controlled at both systemic and cellular levels to maintain the delicate balance between iron essentiality and toxicity (Figure 20). Due to this dual nature, there are elegant and elaborate control mechanisms to maintain iron homeostasis by coordinately regulating iron absorption, iron recycling, and mobilization of stored iron. In this regard, a set of iron-binding and transport proteins (iron-handling proteins) are involved in iron import (transferrin, transferrin receptor 1 (TfR1), and divalent metal transporter-1), storage (ferritin), and export (ceruloplasmin, hephaestin, ferroportin, and hepcidin) (Burdo & Connor, 2003; Wang & Pantopoulos, 2011). More recently, ferritin has also been proposed as an iron transport protein (Ponka, Beaumont & Richardson, 1998; Fisher et al., 2007) that can specifically bind to scavenger receptor class A member 5 (Scara5) (Li et al., 2009) and T-cell immunoglobulin and mucin-domain 2 (TIM2) (Chen et al., 2005).

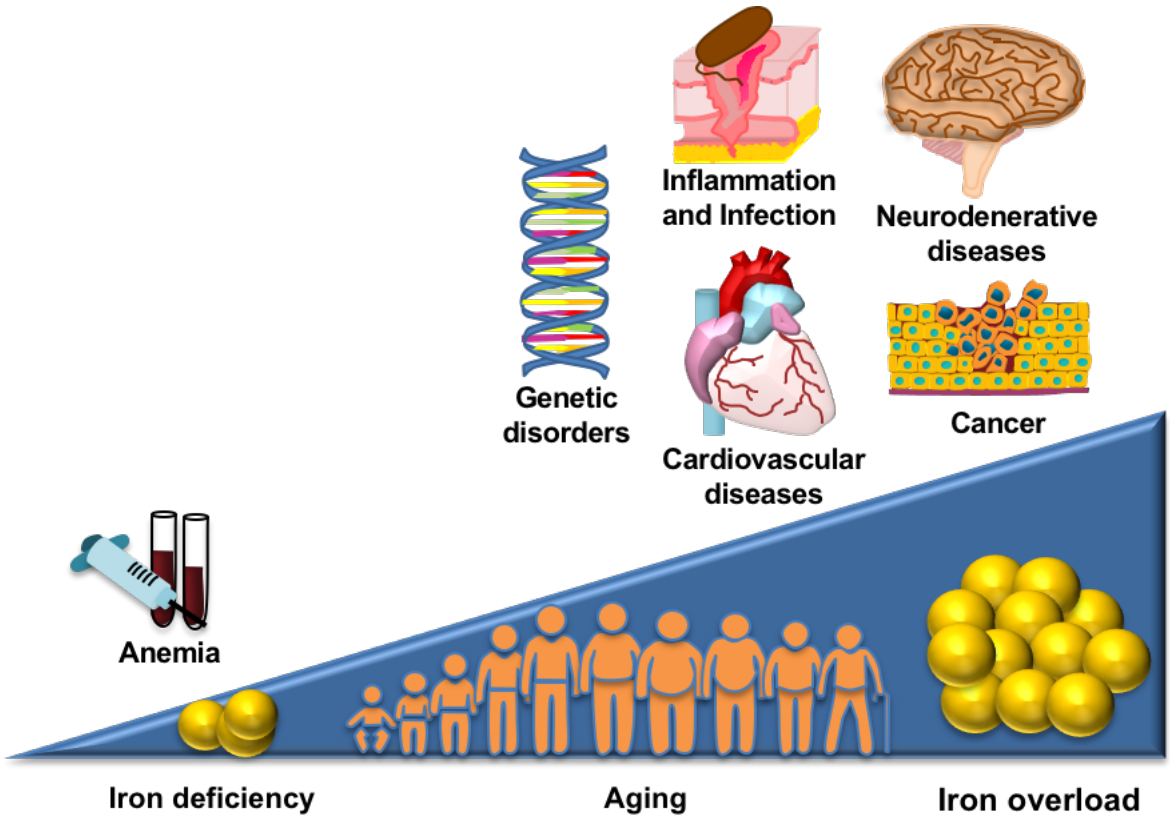

Figure 20. Iron in pathophysiologic conditions. Although essential to ensure survival, disruption of iron homeostasis has been shown to be involved in several pathophysiological conditions.

B.1.1. Classical pathway of iron import into the tissue

In general, iron is taken up by most tissues through a transferrin mediated mechanism (Figure 21). Under physiological conditions, non-heme iron in the circulation is bound to apo-transferrin as Fe^{3+}, which limits the generation of toxic radicals. Apo-transferrin can bind two atoms of Fe^{3+} at the same time (Baker & Morgan, 1994). At the cell surface, iron-loaded holo-transferrin binds with high affinity to the TfR1. Then, this complex is internalized via clathrin-coated pits into endosomes (Yefimova et al., 2000; He et al., 2007; Song & Dunaief, 2013). A proton pump promotes acidification of the endosome to lower the pH to about 5.5, triggering the release of Fe^{3+} from transferrin that remains bound to TfR1 (Sipe & Murphy, 1991). An endosomal ferrireductase, such as STEAP3, reduces Fe^{3+} to Fe^{2+}, which is transported across the endosomal membrane by the divalent metal transport 1 (Gunshin et al., 1997; Burdo et al., 2001; Song & Dunaief, 2013). The apo-transferrin-TfR1 complex is then recycled to the cell surface, where apo-transferrin is released to capture plasma Fe^{3+} (Hunt & Davis, 1992).
Although iron import through ferritin was established, the exact mechanism of ferritin uptake by cells is still not completely understood (Ponka et al., 1998; Fisher et al., 2007).

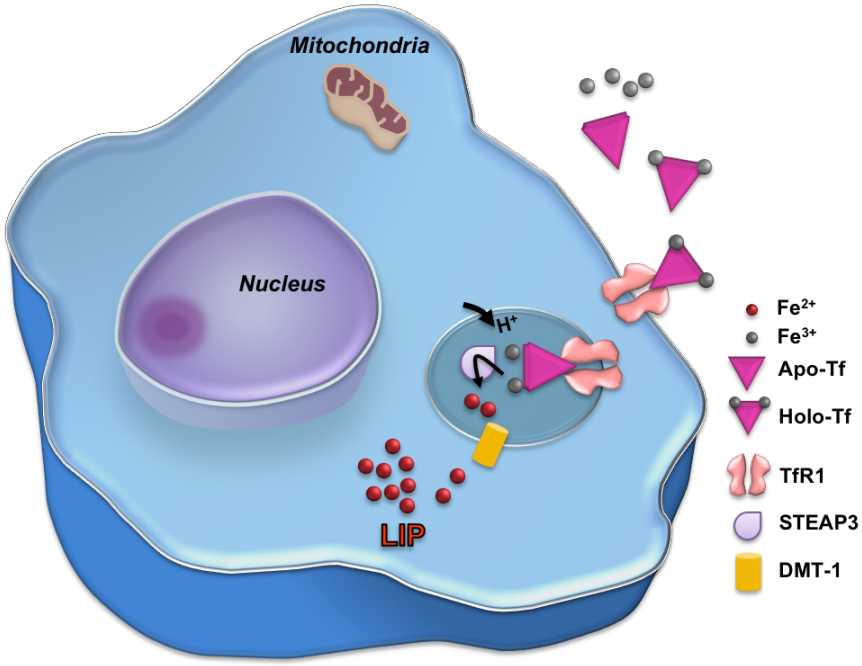

Figure 21. Schematic representation of the classical pathway of iron import into tissues. Iron-loaded transferrin (Holo-Tf) binds with high affinity to the transferrin receptor 1 (TfR1) at the cell surface. This complex is then internalized into an endosome, where the release of Fe^{3+} is triggered under acidification. Fe^{3+} is reduced by STEAP3 to Fe^{2+}, which is transported across the endosomal membrane by the divalent metal transport 1 (DMT-1) and becomes part of the labile iron pool (LIP) in the cytosol. Apo-Tf, apo-transferrin; Fe^{2+}, ferrous iron; Fe^{3+}, ferric iron.

B.1.2. Intracellular iron utilization

The iron released from the endosome becomes part of the labile iron pool (LIP) in the cytosol where remains bound to small organic chelators, such as citrate or adenosine phosphate, carboxylate, and polypeptides (Figure 22) (Richardson & Ponka, 1997; Kohgo et al., 2008; Jiang et al., 2009; Hentze et al., 2010). LIP is an important source of iron for numerous cytosolic and nuclear iron proteins, as well as being a source for cellular organelles, such as mitochondria which process most of the metabolically active iron in the cell (Rouault & Cooperman, 2006; He et al., 2007). Although LIP is biologically active in intracellular metabolism, it is toxic if present in excess. Thus, maintenance of appropriate LIP levels is critical for homeostasis (Mackenzie, Iwasaki & Tsuji, 2008).

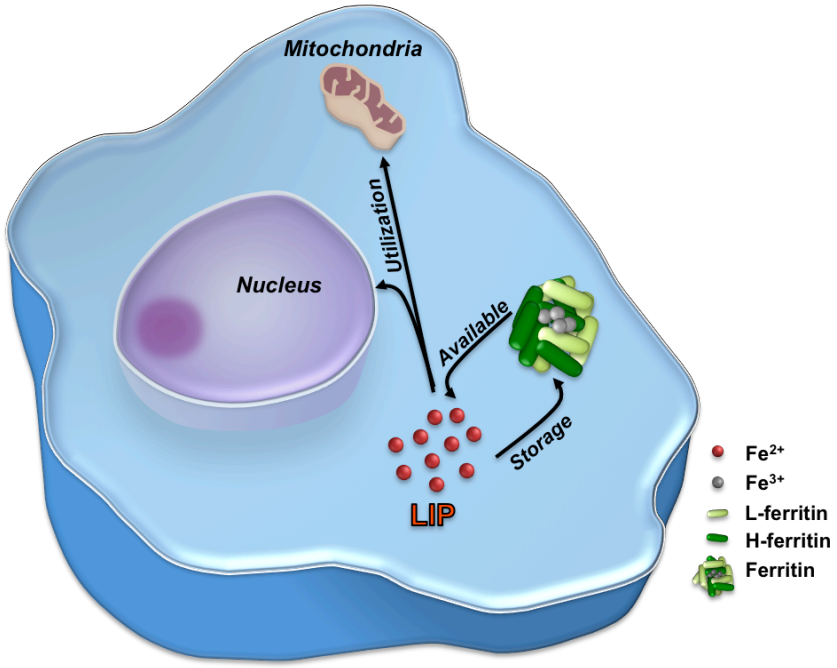

Figure 22. Schematic representation of the utilization and storage of intracellular iron. Iron in the labile iron pool (LIP) is an important source for numerous cytosolic and nuclear iron-dependent proteins, as well as being a source for cellular organelles, such as mitochondria. Intracellular iron can also be safely incorporated into ferritin, which can be then released to satisfy possible intracellular demands. Fe^{2+}, ferrous iron; Fe^{3+}, ferric iron; H-ferritin, heavy ferritin; L-ferritin, light ferritin.

B.1.3. Intracellular iron storage

In non-erythroid cells, the majority (70-80%) of intracellular iron is safely incorporated into ferritin (Figure 22) (Aisen, Enns & Wessling-Resnik, 2001; Arosio & Levi, 2010), an iron-handling protein ubiquitously distributed, classically known for its role in iron storage and detoxification (Arosio, Ingrassia & Cavadini, 2009). Ferritin forms a hollow sphere capable of storing ~ 4,500 iron atoms which can be released to satisfy possible intracellular demands (Levi et al., 1992; Aisen et al., 2001). Lysosome- and proteasome-mediated degradation mechanisms are thought to be involved in iron release from ferritin, which is then used in the cytosol for further cellular metabolic purposes (Kurz et al., 2004; Mehlhase et al., 2005).

Ferritin is composed of 24 subunits of heavy (H) or light (L) type, each with a specific function, with variable stoichiometry of the two ferritin subunits in different tissues. Fe^{2+} entering ferritin is oxidized to Fe^{3+} by the ferroxidase activity of H-ferritin in an oxygen-dependent manner. Subsequently, Fe^{3+} is transported to the protein cavity, where core formation commences. L-ferritin is 50% identical to H-ferritin at the amino acid level but lacks ferroxidase activity, thus storing iron at a low rate compared with the H subunit (Harrison & Arosio, 1996; Levi et al., 1992, 1994; Aisen et al., 2001; He et al., 2007). This enclosure and sequestration of iron is

vital, as it prevents toxic redox reactions from occurring, reducing oxidative stress (Harrison & Arosio, 1996; Chasteen & Harrison, 1999; Arosio & Levi, 2010).

Inside the cell, iron levels are also tightly controlled by an elegant machinery involving the iron regulatory proteins (IRPs) that bind to the iron responsive elements (IREs) on the messenger ribonucleic acid (mRNA) of iron-handling proteins (Mackenzie et al., 2008; Wang & Pantopoulos, 2011; Anderson et al., 2012). This regulation allows individual cells to regulate iron uptake, sequestration, and export depending on their iron status. Under conditions of iron starvation, IRPs are activated for high affinity binding to IREs in the 3'-untranslated region of *TfR1* mRNA and to a single IRE in the 5'-untranslated region of the mRNAs encoding both H- and L-ferritin chains. This stabilizes *TfR1* mRNA (Binder et al., 1994) and inhibits *ferritin* mRNA translation (Muckenthaler, Gray & Hentze, 1998). Conversely, failure of IRPs to bind to cognate IREs in iron-replete cells leads to degradation of *TfR1* mRNA and synthesis of ferritin.

B.1.4. Cellular iron export

Iron that is not utilized or stored by the cell may be exported. Ferroportin is a transmembrane iron transporter that cooperates with ferroxidases, such as ceruloplasmin and hephaestin, to export intracellular Fe^{2+} and oxidize it to the Fe^{3+} (Osaki, Johnson & Frieden, 1966; Vulpe et al., 1999; Abboud & Haile, 2000; Donovan et al., 2000; McKie et al., 2000). These enzymes are crucial for iron export and, when disrupted, result in cellular iron accumulation and cellular degeneration (Song & Dunaief, 2013). Ferroportin is regulated by trans-acting factors, including the peptide hormone hepcidin. Hepcidin binds to ferroportin, triggering its internalization and degradation (Nemeth et al., 2004; Knutson et al., 2005).

B.2. Iron in the retina

In the retina, iron is particularly important for the visual phototransduction cascade as iron is an essential cofactor for the enzyme guanylate cyclase, which synthesizes cyclic guanosine monophosphate (cGMP), the second messenger in this cascade (Yau & Baylor, 1989). Additionally, RPE65, the isomerohydrolase found in the microsomal membrane of the RPE and responsible for catalyzing the conversion of all-trans-retinyl ester to 11-cis-retinol in the visual cycle, is an iron-containing protein that is also dependent on iron for its isomerohydrolase activity (Moiseyev et al., 2005). Additionally, photoreceptor cells are constantly shedding and synthesizing their outer segments containing disc membranes. Thus, photoreceptors depend highly on iron-containing enzymes, including fatty acid desaturase, for synthesis of lipids used in disc membrane replacement (Schichi, 1969).

B.2.1. Iron import into the retina

As previously discussed, the retina is isolated from the bloodstream by the BRB. Tight junctions of the neuroretinal vasculature and RPE cells prevent intercellular diffusion, thereby protecting both sides of the retina from potentially harmful substances that circulate in the blood. A consequence of such a blockade, however, is that transport mechanisms must be designed for the many trophic substances that are required for normal retinal function (Cunha-Vaz, 1976; Cunha-Vaz et al., 2011).

According to the classical pathway of iron import, iron-loaded holo-transferrin is endocytosed by cells following binding to the TfR1 found in the cell surface. Transferrin and TfR1 have been found in the retinal parenchyma. Immunohistochemistry has revealed the presence of transferrin in the inner retina, inner and outer segments of photoreceptors, and RPE, while immunolabeling of TfR1 has been observed in the ganglion cell layer, inner nuclear layer, outer plexiform layer, inner segments of photoreceptors, and RPE (Yefimova et al., 2000). Thus, transferrin has been established as the classical iron transporter protein in the retina, being widely accepted that serum transferrin binds to its receptor on the surface of vascular endothelial cells and RPE and, in this way, iron is delivered to the retina (Hunt, Dewey & Davis, 1989; Burdo et al., 2003; Burdo & Connor, 2003; García-Castiñeiras, 2010).

B.2.2. New pathway of iron import into the retina

Recently, serum ferritin has also been proposed as a new iron carrier protein in the retina through L-ferritin binding to Scara5 (Mendes-Jorge et al., 2014). L-ferritin binds specifically and saturably to Scara5 (Li et al., 2009), and is likely to undergo endocytosis and be transcytosed across the BRB (Ponka et al., 1998; Fisher et al., 2007). The advantage of serum ferritin as an iron carrier, compared to serum transferrin, is that ferritin can sequester 2000-fold more iron than transferrin (Fisher et al., 2007), constituting a very efficient non-transferrin source of iron to tissues. Nevertheless, little is known about the role of these receptors in the retina and despite its importance, iron influx and cell type involved in iron accumulation and storage mechanisms in the retina are still not completely understood.

TIM2 membrane receptor can also function as an iron uptake pathway by binding to its ligand H-ferritin, which leads to the endocytosis of extracellular H-ferritin (Chen et al., 2005; Han et al., 2011). TIM2 expression has been described in spleen, mainly on germinal center B cells, bile duct epithelial cells and hepatocytes, renal distal tubule cells, as well as in oligodendrocytes (Chen et al., 2005; Watanabe et al., 2007; Todorich et al., 2008). However, the presence of TIM2 in the retina still remains unknown.

TIM2, a type 1 transmembrane protein, is a member of the T cell immunoglobulin and mucin domain containing protein family. The TIM family is comprised of three members in humans (TIM1, TIM3, and TIM4) and eight in mice (TIM1-8), and it is known by its involvement in the regulation of immune responses (McIntire et al., 2001; McIntire, Umetsu & DeKruyff, 2004). TIM2 has been shown to participate in T-cell activation upon binding to Semaphorin 4A, thereby exerting its effects on the immune system (Kumanogoh et al., 2002; Rodriguez-Manzanet et al., 2009). Although no human ortholog for mouse TIM2 has been identified, human TIM1 and mouse TIM2 share a homology of 36% with each other and similar functions, specifically binding to H-ferritin and Semaphorin 4A (Chiou et al., 2018).

B.3. Deleterious effects of iron

Although an essential micronutrient for the normal function of the organism, iron can be toxic if its level and/or distribution are not carefully regulated. It is well known that iron is a potentially harmful pro-oxidant when accumulated excessively in tissues, triggering the production of ROS. Toxicity associated with iron overload in the retina is developed through the overproduction of ROS that overwhelms inherent antioxidant mechanisms of neurons, vascular, and glial cells, leading to a cascade of oxidative stress that contributes to retinal damage (Wong et al., 2007; Galaris & Pantopoulos, 2008; Goralska et al., 2009; Kell, 2009; Loh, Hadziahmetovic & Dunaief, 2009; Gammella, Recalcati & Cairo, 2016).

ROS, a collection of partially reduced oxygen-containing molecules, including peroxides (H_2O_2 and ROOH), superoxide anion (O_2•-), and free radicals, are formed during normal cellular metabolism. In fact, physiological concentrations of ROS are essential for life as these molecules are necessary to support redox signaling events that are involved in important physiological functions and adaptive cell responses, such as chemotaxis, hormone synthesis, immune response, cytoskeletal remodeling, and calcium homeostasis (Dröge, 2002; Trachootham et al., 2008; Ray, Huang & Tsuji, 2012). Moreover, the production of O_2•- and H_2O_2 is an inevitable consequence of aerobic metabolism. O_2•- is generated continuously by the mitochondrial electron transport system as well as during several cellular oxidase catalyzed reactions. H_2O_2 is generated as a result of enzymatic (superoxide dismutase) and non-enzymatic destruction of O_2•-.

These molecules are not particularly reactive by themselves. However, the interaction of these partially reduced forms of oxygen with transition elements, including iron, lead to the production of highly damaging radicals (Halliwell & Gutteridge, 1984, 1990; Harwell, 2007; Kell, 2009; Udipi et al., 2012; Gammella et al., 2016). The most important reaction of H_2O_2 with free or

poorly liganded Fe^{2+} is the Fenton reaction (Figure 23). In this reaction, Fe^{2+} is oxidized to Fe^{3+}, generating a hydroxyl ion (OH^-) and a hydroxyl radical (HO•). HO• is exceptionally damaging and reacts with all kind of biological molecules, including nucleic acids, carbohydrates, proteins, and lipids, and may irreversibly destroy or alter the function of the target molecule, affecting cellular function (Halliwell & Gutteridge, 1984, 1990; Wardman & Candeias, 1996; Meneghini, 1997; Dröge, 2002; Harwell, 2007; Kell, 2009; Udipi et al., 2012). O2•- can also react with Fe^{3+} in the Haber-Weiss reaction to produce Fe^{2+} again thereby effecting redox cycling (Figure 23) (Kehrer, 2000).

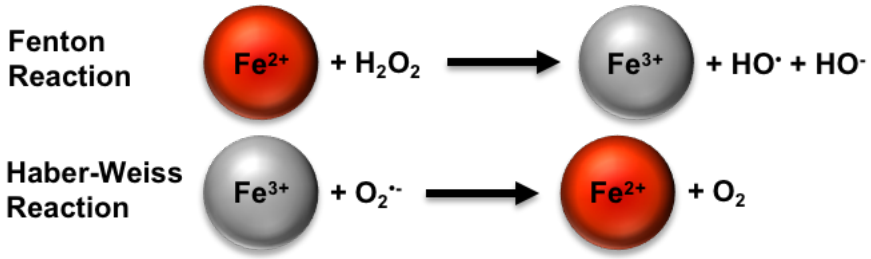

Figure 23. Reactive oxygen species and iron redox cycling. In the Fenton reaction, ferrous iron (Fe^{2+}) is oxidized to ferric iron (Fe^{3+}) through the reaction with hydrogen peroxide (H_2O_2), leading to the generation of hydroxyl radical (HO•) and hydroxyl ion (OH^-). Ferric iron (Fe^{3+}) is again reduced to ferrous iron (Fe^{2+}) by one-electron transfer from superoxide anion (O_2•-) to give oxygen (O_2) in the Haber-Weiss reaction, thereby effecting redox cycling.

Oxidative stress, induced by increased iron-mediated ROS generation, causes DNA damage, lipid peroxidation, and aberrant posttranslational modifications of proteins, thus leading to injury, cell death, and disease (Figure 24) (Halliwell & Gutteridge, 1984, 1990; Dröge, 2002; Galaris & Pantopoulos, 2008; Kell, 2009; Ray et al., 2012; Udipi et al., 2012; Gammella et al., 2016). In the nucleus, HO• causes DNA damage, especially double strand breaks as well as chemical changes in deoxyribose, purines, and pyrimidines. HO• can be added onto C-8 of guanine leading to guanine modification. Many of the damaged proteins are enzymes, hence critical cellular functions, including ATP generation, are adversely affected. Lipid peroxidation increases membrane fragility of cell organelles, such as mitochondria, lysosomes, and endoplasmic reticulum, leading to impaired cell function (Fardy & Silverman, 1995; Casanueva & Viteri, 2003; de La Rosa, Moshage & Nieto, 2008; Kell, 2009).

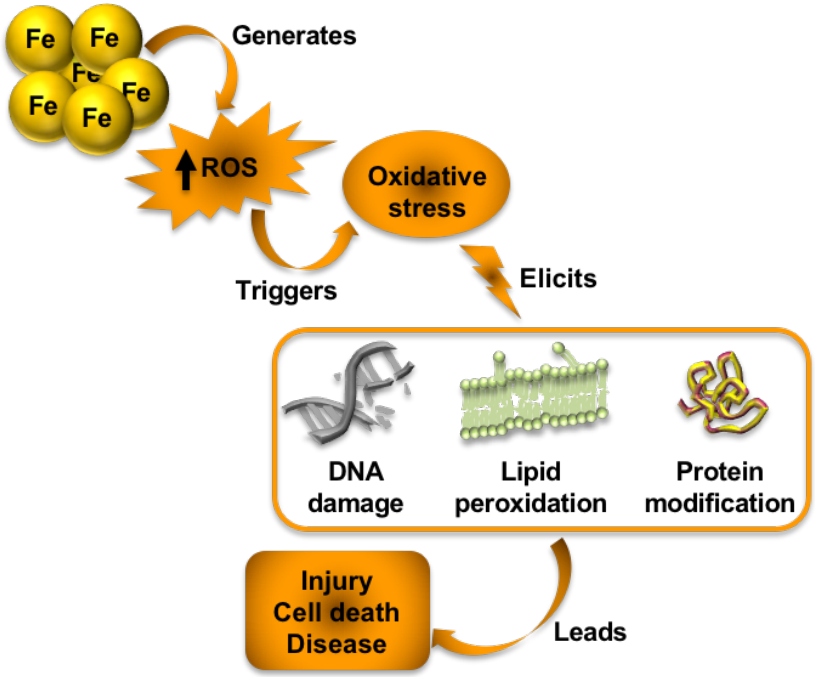

Figure 24. Oxidative stress cascade. Iron in excess, through the participation in the Fenton reaction, generates the overproduction of ROS, which triggers oxidative stress. In turn, oxidative stress elicits DNA damage, lipid peroxidation, and aberrant protein modifications that ultimately lead to injury, cell death, and disease.

Conversely, oxidative stress itself influences iron metabolism and iron proteins, which may in turn propagate a vicious cycle of oxidative stress and iron accumulation (Deb et al., 2009; Hadziahmetovic et al., 2011b). Thus, maintaining the cellular LIP as low as possible is crucial for redox biology and for the regulation of metabolism and other cellular functions by ROS.

The retina, due to the constant exposure to light, oxygen-rich environment, high oxygen tension, high metabolic rate, and high concentration of polyunsaturated fatty acids, combined with high requirements of iron, is particularly prone to oxidative stress (Berman, 1991; He et al., 2007; Loh et al., 2009; García-Castiñeira, 2010; Gnana-Prakasam et al., 2010; Song & Dunaief, 2013). Therefore, regulation of iron homeostasis is crucial in the retina, where the slightest iron imbalance would automatically exacerbate any possible situation of oxidative stress (Halliwell & Gutteridge, 1990; Sies, 1991; Ray et al., 2012).

Iron overload, accompanied by cellular damage and oxidative stress, has been implicated in neurodegenerative diseases affecting the brain, including Parkinson's and Alzheimer's diseases (Lhermitte, Kraus & McAlpine, 1924; Connor et al., 1992; Greenough, Camakaris & Bush, 2013; Ayton et al., 2014; Gozzalino & Arosio, 2016), and in the pathogenesis of retinal diseases, such as age-related macular degeneration (Dunaief, 2006; Wong et al., 2007) and diabetic retinopathy (Feng et al., 2007; Ciudin, Hernández & Simó, 2010; Chaudhary et al., 2018).

B.3.1. Diabetic retinopathy

Diabetes mellitus is a chronic metabolic disease that affects 415 million adults worldwide and its prevalence is expected to reach 642 million by 2040 (Sabanayagam et al., 2016). The epidemic of diabetes and its complications poses a major global health and economic threat with a substantial economic burden at both patients and health systems levels. Therefore, there is an urgent need to develop and implement new therapies to cure diabetes mellitus and to delay its progression to complications.

Diabetic retinopathy is the most common microvascular complication in diabetic patients that can progress to the loss of vision, affecting approximately 35% of the diabetic population (Congdon, Friedman & Lietman, 2003; Hammes, 2018). Diabetic retinopathy is characterized by inflammation, neurodegeneration, and microvascular alterations in the retina (Barber et al., 1998; Antonetti et al., 2006; Tang & Kern, 2011). The progress of diabetic retinopathy can be divided in non-proliferative and proliferative phases. Non-proliferative diabetic retinopathy is characterized by vasodegenerative changes, including pericyte loss, thickening of blood vessel basement membrane, acellular capillaries, capillary closure, and increased vascular permeability. These vascular abnormalities cause diabetic macular edema and ischemia (Barber et al., 2005; Kaur, Foulds & Ling, 2008). Retinal ischemia, in turn, triggers the upregulation of angiogenic factors leading to the neovascularization that occurs during the proliferative phase of the disease. Diabetic macular edema is a complex pathological process caused by multiple factors, including BRB breakdown and oxidative stress (Madsen-Bouterse & Kowluru, 2008; Zhang et al., 2014), and represents the most common cause of vision loss in patients with diabetic retinopathy (Duh, Sun & Stitt, 2017).

Intracellular retinal iron accumulation has been associated to the development and exacerbation of diabetic retinopathy (Feng et al., 2007; Ciudin et al., 2010; Chaudhary et al., 2018). However, implications of retinal iron imbalance in this pathology are still not completely elucidated. During diabetic retinopathy, the retinal microenvironment may accumulate iron by various mechanisms. Hyperglycemia has been reported to cause breakdown of heme containing molecules releasing free iron (Cussimanio et al., 2003). Intraretinal and intravitreal hemorrhages associated with diabetic retinopathy also result in additional iron overload. Additionally, inflammation can alter the expression of iron-regulatory gene hepcidin leading to iron accumulation (Gnana-Prakasam et al., 2008; Wessling-Resnik, 2010). Furthermore, retinal iron overload affects BRB integrity and accelerates retinal cell loss by enhancing oxidative stress (Ciudin et al., 2010; Chaudhary et al., 2018).

OBJECTIVES

OJECTIVES

RATIONALE

Background:

1. Iron overload is implicated in diabetic retinopathy.
2. Ferritin, a known marker of iron status, is increased in the retina during diabetes.
3. Ferritin, a classical iron storage protein, was recently proposed as a new iron transporter protein.
4. Scara5 and TIM2 are specific receptors for ferritin import to tissues.
5. Our laboratory described, for the first time, ferritin uptake into the retina via L-ferritin specific binding to Scara5.
6. TIM2 has not been reported yet in the retina.

Hypothesis:

The expression of TIM2, the main receptor for H-ferritin, could be a mechanism for influencing the entry of ferritin into the retina and modulate iron levels during diabetic retinopathy.

MAIN OBJECTIVE

To prove that a decrease of TIM2 expression affects iron import into the retina. In order to achieve this, a TIM2 knockout mice model will be generated and analyzed.

Specific objectives:

- To characterize TIM2 expression in the mouse retina.
- To analyze the consequences of retinal TIM2 deficiency in iron import.

MATERIAL AND METHODS

MATERIAL AND METHODS

A. Material

A.1. Mice

In the present study, 4- to 6-month-old TIM2 heterozygous (+/-) mice and wild-type (WT) littermates were used. Mice were genotyped by standard polymerase chain reaction (PCR) of tail genomic DNA (B.1).

All mice were fed ad libitum with a standard diet (2018S TEKLAD Global, Harlan Teklad, Madison, WI, USA) and maintained under conditions of controlled temperature and light (12-hour light/dark cycles, light on at 8:00 A.M.).

Animals were euthanized by means of anesthetics inhalation (IsoFlo®, Esteve, Barcelona, Spain). Animal care and experimental procedures were approved by the ethics committee in animal and human experimentation of the Universitat Autònoma de Barcelona.

A.1.1. Generation of TIM2 knockout mice

Embryonic stem cell clones C57BL/6N-A/a carrying the *Timd2* knockout (KO) with conditional potential ($Timd2^{tm1a(KOMP)Wtsi}$) were obtained from KOMP (Knockout Mouse Project) Repository. TIM2 KO mice were generated after injection of the clone EPD0604_4_C03 into C57BL/6JOlaHsd blastocysts. Chimeric offspring were mated with C57BL/6JOlaHsd mice. Germline transmission of the mutant allele was confirmed by PCR analysis of genomic DNA from tails of mice.

A.2. Equipment

The instruments and material used during this work were facilitated by CIISA (Faculty of Veterinary Medicine, Universidade de Lisboa), CBATEG (Universitat Autònoma de Barcelona), Anatomy and Embryology Unit (Veterinary School, Universitat Autònoma de Barcelona), and Microscopy and Chemistry Analysis Facilities and Luminescence and Spectroscopy

Biomolecules Laboratory (Faculty of Science, Universitat Autònoma de Barcelona). The following equipment was employed:

- **Microscopes**:
  - Epifluorescence microscope: Nikon Eclipse E-800 (Nikon Corp., Tokyo, Japan)
  - Stereoscopic microscopes: Nikon SMZ-800 and Nikon SMZ-1000 (Nikon)
  - Confocal laser microscopes: Leica TCS-SP2 AOBS and Leica TCS-SP5 X confocal microscope (Leica Microsystems GmbH, Heidelberg, Germany)
  - Transmission electron microscope: Jeol JEM-1400 (Jeol Ltd., Tokyo, Japan)
  - Transmission electron microscope: Jeol JEM-2011 (Jeol)
- **Digital cameras**:
  - Nikon digital camera DXM 1200F (Nikon)
  - Soft Imaging System CC-12 (Olympus Soft Imaging Solutions Gmbh, Münster, Germany)
- **Ophthalmoscope**:
  - Heidelberg Retina Angiography 2 (HRA2) Imaging Instrument (Heidelberg Engineering, Germany)
- **Spectrometer**:
  - Agilent 7500ce (Agilent, Santa Clara, CA, USA)
- **Spectrophotometer**:
  - NanoDrop ND-2000c (Thermo Fisher Scientific, Willmington, DE, USA)
- **Microtomes**:
  - Microtome Shandon Retraction AS325 (Rankin Biomedical Corporation, Holly, MI, USA)
  - Ultramicrotome Leica EM UC6 (Leica Microsystems)
- **Imaging detection system:**
  - Molecular Imager ChemiDoc XRS System (Bio-Rad Laboratories, Hercules, CA, USA)
- **Thermal cyclers:**
  - T100 Thermal cycler (Bio-Rad)
  - CFX384 Thermal cycler (Bio-Rad)
- **Microplate reader:**
  - iEMS Reader/Dispenser MF (Labsystems Oy, Helsinki, Finland)
  - PowerWave HT (BioTek, Winooski, VT, USA)
- **Biochemistry analyzer:**
  - Olympus AU400 Autoanalyzer (Olympus, Hamburg, Germany)
  - Glucometer Elite (Bayer, Leverkusen, Germany)

- **General laboratory equipment:**
  - Centrifuge 5702R (Eppendorf, Hamburg, Germany)
  - Shaker UNIMAX -1010, incubator INKUBATOR-1000 and vortex REAX-top (Heidolph instruments, Schwabach, Germany)
  - Modular inclusion center AP280: cryo-console AP280-1 and dispensing console AP280-2 (Especialidades médicas Myr SL, Tarragona, Spain)
  - pH meter PHM210 Standard (Radiometer analytical SAS, Villeurbanne Cedex, France)
  - Vacuum oven Fisher Bioblock Scientific (Fisher, Strasbourg, France)
  - Electric homogenizer Ultra-turrax T8 (IKA-Werke, Staufen, Germany)
  - Water bath Grant GD100 (Grant Instruments, Cambridge, UK)
  - Dry Thermostat block Tembloc-P (JP Selecta S.A., Barcelona, Spain)

B. Methods

B.1. Genotyping

Genotyping is the process of determining the genetic variants of an individual by examining the individual's DNA, thus enabling to proper identify and confirm the genotype of genetically modified animals. Genotyping protocols are frequently based on reliable methods, such as PCR and Southern blotting (Picazo & García-Olmo, 2015). In this study, standard PCR analysis was used for routine genotyping during maintenance of the genetically modified mice colony.

B.1.1. DNA extraction from mouse tail

High-quality genomic DNA may be isolated from various biological tissues. Tail biopsy is considered the most common tissue sampling method for genotyping mice (Picazo & García-Olmo, 2015). The protocol used for isolating a highly purified DNA preparation from mouse tail is described as follows:

1. Sample: 0.5-1 cm of mouse tail was cut into a sterile eppendorf tube.
2. Lysis: 700 µl of lysis buffer TESNA[1] containing 10% proteinase K (Roche, Basel, Switzerland) was added per tail and incubated, in a water bath with gentle shaking, overnight at 57°C.

[1] TESNA: 5 ml Tris-HCl 2M (pH 8) + 1 ml EDTA + 0.2 g sodium dodecyl sulfate + 1.17 g NaCl in 100 ml milliQ water.

3. Centrifugation: samples were centrifuged at 8,000 *g* for 15 minutes and the supernatant was transferred to a new sterile tube.
4. DNA precipitation: 700 µl of isopropanol (Panreac Química SLU, Castellar del Vallés, Spain) was added to each tube and shaken, and mixed vigorously.
5. Centrifugation: samples were centrifuged at 8,000 *g* for 10 minutes to remove and discard the supernatant.
6. DNA purification: 400 µl of 70% ethanol was added to each tube.
7. Centrifugation: samples were centrifuged at 8,000 *g* for 10 minutes to remove and discard the supernatant.
8. Remove ethanol: to eliminate residual ethanol, the samples were air dried at 37ºC for 10 minutes.
9. DNA elution: 1 ml of milliQ water was added to each tube and incubated for 1 hour at 65ºC, while shaking to resuspend DNA. (Total yield was approximately 50-100 ng/µl DNA). DNA samples were stored at 4ºC until further analysis.

B.1.2. PCR amplification

PCR amplification is based on temperature cycling on a DNA template to be amplified and generate numerous identical copies that can be readily analyzed. Initially, high temperature is used to separate double-strands of DNA and then temperature is lowered to let primers anneal to the template. Primers are specific sequences of oligonucleotides that determine the targeted genomic DNA fragment (Table 1). A final temperature of around 72°C is required for optimal DNA polymerase activity to extend the two primers by incorporating deoxynucleotides (dNTPs). DNA fragments are then separated by size of base pairs (bp) with agarose gel electrophoresis (Picazo & García-Olmo, 2015). The PCR-based genotyping from mouse tail genomic DNA protocol used was the following:

1. DNA amplification: GoTaq® G2 Flexi DNA Polymerase Kit (Promega, Madison, WI, USA) was used to amplify mouse tail DNA in a thermal cycler. The 30 µl PCR reaction mixture contained 6 µl of 5x Green GoTaq Flexi Buffer, 2.4 µl $MgCl_2$ (2 mM), 0.6 µl of dNTP mix solution (each 0.2 mM), 0.99 µl of each primer (0.3 µM), 0.3 µl of GoTaq® G2 Flexi DNA Polymerase (1.5 units), and 2 µl of genomic DNA as template. The cycling program used begins with an initial denaturation at 94°C for 3 minutes, followed by 35 cycles of DNA denaturation at 94°C for 30 seconds, optimized annealing reaction at 60°C for 30 seconds, extension at 72ºC for 30 seconds and a final step of 72ºC for 2 minutes. No template samples were used as negative controls.

2. Agarose gel: to visualize DNA amplification, 20 µl of PCR products were separated on 1% agarose gel made with TAE[2] buffer using standard electrophoresis methods (80-120 V).
3. Staining: agarose gels were stained with ethidium bromide (EtBr, Sigma-Aldrich, St. Louis, MI, USA) diluted in milliQ water (10 mg/ml).
4. Visualization: DNA amplified bands were imaged under UV light using a ChemiDoc XRS System with QuantityOne software version 4.5 (Bio-Rad).

Table 1. Oligonucleotide primers for genotyping mouse tail DNA.

Mice	Direction	Sequence (5' to 3')
WT	Forward	AGG AGT CAG GTG GGA GGA TTA
WT	Reverse	CGT GTG CAT GTT TGT TTT CC
TIM2$^{+/-}$	Reverse	GGT ATC GTT ATG CGC CTT CT

B.2. Morphological studies

B.2.1. Tissue processing

Taking into account that different methods may require different preparation of tissue samples, retinas used in this study were processed depending on the method envisioned.

B.2.1.1. Whole-mounts

The use of tissue whole-mounts, where an entire tissue is directly placed onto a slide, is a widely accepted tool in the fields of retinal neurobiology. The main advantage of using retinal whole-mounts is adequate preservation of cell morphology. This approach allows visualization of the entire retinal parenchyma and preservation of the vascular network structure, while minimizing tissue damage during dissection (Hashimoto, Ishikawa & Kusakabe, 1999; McMenamin, 2000). Mouse eyes were processed as follows:

1. Eye dissection: eyeballs were enucleated from euthanized mice and immersed in cold phosphate buffered saline (PBS)[3] on a dissection plate provided with a latex pad.
2. Retinal dissection: each eye was anchored to the latex pad with two insect pins: one pin fixed in the cornea and the other in the posterior pole of the eyeball. To access the anterior chamber of the eye, an incision was made along the corneo-scleral groove. After removing

[2] TAE 50x (pH 8): 24.2 g Tris base + 5.71 ml of CH_3CO_2H + 3.72 g EDTA.$2H_2O$ + 100 ml milliQ water; TAE 1x: 20ml TAE 50x + 980 ml milliQ water.
[3] PBS: 1.5 g $Na_2HPO_4.2H_2O$ + 0.28 g $NaH_2PO_4.H_2O$ + 8.1 g NaCl + 1000 ml distilled water.

the lens, the retina was separated from the choroid and isolated by cutting the optic nerve. Usually, the retinal pigment epithelium remained adhered to the choroid.

3. Fixation: After flattening the retinas by anchoring 4-5 insect pins to the latex pad plate, the samples were embedded in 10% neutral buffered formalin (NBF)[4] for 2 hours at room temperature.
4. Washing: several washes (at least 5) in phosphate buffer Igepal (PBI)[5] were performed to remove the fixative solution.

B.2.1.2. Paraffin embedded sections

The advantages of using paraffin sections of retina are the preservation of the structural relationships between cells and extracellular components useful for fluorescence and confocal microscopy, as well as long-term storage, and the possibility of using several techniques in the same sample. Paraffin sections of mouse eyes were obtained as follows:

1. Eye dissection: eyeballs were enucleated from euthanized mice.
2. Fixation: eye samples were immersed and fixed in 10% NBF for 24 hours at room temperature.
3. Washing: fixative solution was removed by washing 15-20 minutes in PBS (at least 4 washes), under constant agitation in a shaker.
4. Dehydration: eye samples were dehydrated through a series of graded ethanol baths to displace the water:
   - 70% ethanol, 2 washes of 1 hour each.
   - 80% ethanol, 2 washes of 1 hour each.
   - 96% ethanol, 2 washes of 1 hour each.
   - 100% ethanol, 2 washes of 1 hour each.
5. Transparency: to render the tissue transparent, eye samples were immersed in xylene (Panreac Química) for 1 hour.
6. Paraffin infiltration: samples were placed in a paraffin bath for 24 hours at 57ºC in a vacuum oven. Paraffin wax was changed once during this period. The infiltrated tissues were then embedded into paraffin blocks.
7. Eye sections: paraffin blocks were sectioned using a microtome. Sagittal 3-4 µm thick sections of the eye were obtained and mounted in glass slides previously covered with Silane (Sigma-Aldrich).

[4] NBF: 100 ml of 37% formaldehyde + 4 g $NaH_2PO_4.H_2O$ + 6.5 g Na_2HPO_4 in 900 ml distilled water.
[5] PBI: 1000 µl Igepal + 1000 ml PBS.

B.2.2. Conventional histologic hematoxylin-eosin stain

Hematoxylin and eosin (H-E) stains are commonly used to demonstrate a wide range of normal and abnormal structures or functional components in various tissues (Fischer et al., 2008; Titford 2009). Hematoxylin stains nucleic acids, while eosin stains proteins nonspecifically so that in a typical tissue, nuclei are stained blue, whereas the cytoplasm and extracellular matrix have different degrees of pink staining (Fischer et al., 2008). The following protocol describes H-E stain of retinal paraffin sections:

1. Deparaffinization and rehydration:
   - Xylene: 2 washes of 5 minutes each.
   - 100% ethanol, 2 washes of 5 minutes each.
   - 96% ethanol, 2 washes of 5 minutes each.
   - 80% ethanol, 1 wash of 5 minutes.
   - 70% ethanol, 1 wash of 5 minutes.
   - Distilled water, 1 wash of 5 minutes.
2. Washing: samples were washed in running water for 5 minutes.
3. Harris' Hematoxylin: sample slides were immersed in Harris' Hematoxylin solution (Sigma-Aldrich) for 5-10 minutes.
4. Washing: samples were washed in running water for 5 minutes.
5. Differentiating: quick immersion in a solution of 0.25% HCl diluted in 70% ethanol.
6. Eosin: sample slides were immersed in Eosin solution (Merck Millipore, Billerica, MA, USA) from 30 seconds to 1 minute.
7. Dehydration: sample slides were dehydrated by 2 quick immersions in 96% ethanol and 1 in 100% ethanol.
8. Transparency: sample slides were immersed in xylene for 5 minutes.
9. Mounting: sample slides were mounted with DPX Mountant (Sigma-Aldrich) and covered with a coverslip.
10. Visualization: the analysis of the samples was performed by means of an optical epifluorescence microscope (Nikon Eclipse E-800). Images were acquired with a digital camera (Nikon DXM 1200F).

B.2.3. Immunohistochemistry

Immunohistochemistry is a widely used method to identify proteins within a tissue by the interaction of target antigens with specific antibodies (Presnell & Schreibman, 1997). The site

of antigen-antibody binding is then visualized with an appropriate chromogen or fluorochrome labeled to a secondary antibody directed against the specific primary antibody.

This technique was used to analyze the distribution and localization of specific cellular components within tissue context. Double immunohistochemistry was accomplished using two primary antibodies on the same sample, each labeled with a different chromogen, to analyze topographic relationships between two proteins or to identify two different cells. To avoid non-specific bindings, primary antibodies were always incubated in a solution containing 10% of normal serum from the host of the secondary antibody. When the secondary antibody was produced in goat, albumin from bovine serum (BSA, Sigma-Aldrich) was not used. When primary antibodies employed were produced in mouse a blocking mouse on mouse commercial kit was used following the suggested protocol (KIT MOM™, Vector Laboratories, USA). Negative controls were always carried out by omitting the primary antibody. Antibodies and fluorochromes, as well as dilutions employed and commercial suppliers, are summarized in tables 2, 3, and 4.

Table 2. Primary antibodies used for immunohistochemistry.

Primary antibody	Antigen retrieval	Dilution	Commercial supplier
Goat anti-TIM2	Citrate	1:100	R&D Systems
Rabbit anti-Scara5	Citrate	1:200	LSBio
Rat anti-transferrin receptor 1	EDTA	1:100	Abcam
Rabbit anti-transferrin	Citrate	1:100	Abcam
Rabbit anti-ferritin heavy chain	Citrate	1:100	Abcam
Rabbit anti-ferritin light chain	Citrate	1:100	Abcam
Rabbit anti-parvalbumin	Citrate	1:100	Abcam
Rabbit anti-calbindin	Citrate	1:100	Swant
Mouse anti-PKCα	Citrate	1:100	Sigma-Aldrich
Rabbit anti-GS	Citrate	1:500	Sigma-Aldrich
Rabbit anti-GFAP	Citrate	1:1000	Dako
Rabbit anti-laminin	Citrate	1:100	Dako
Rabbit anti-4HNE	Citrate	1:100	Abcam
Lectin PNA	Citrate	1:50	Sigma-Aldrich
Goat anti-collagen IV	Citrate	1:20	Merck Millipore
Mouse anti-Brn3a	Citrate	1:100	Santa Cruz Biotechnology
Rabbit anti-ZO-1	-	1:50	Thermo Fisher Scientific
Rabbit anti-claudin-5	-	1:50	Thermo Fisher Scientific
Rabbit anti-occludin	-	1:50	Thermo Fisher Scientific

Table 3. Secondary antibodies used for immunohistochemistry.

Secondary antibody	Dilution	Commercial supplier
Anti-rat IgG-biotin	1:100	Abcam
Anti-goat-biotin	1:100	Santa Cruz Biotechnology
Anti-rabbit IgG-alexa 568	1:100	Invitrogen
Anti-rabbit IgG-alexa 488	1:100	Abcam
Anti-goat IgG-alexa 568	1:100	Invitrogen
Anti-goat IgG-alexa 488	1.100	Life Technologies

Table 4. Fluorochromes used for immunohistochemistry.

Fluorochrome	Dilution	Commercial supplier
Streptavidin Alexa Fluor 488	1:100	Molecular Probes
Streptavidin Alexa Fluor 568	1:100	Molecular Probes

When required, to ensure a better penetration of fixative, thoracic aortas of mice were cannulated cranially (25G catheter) and injected with 1 ml of PBS followed by 1 ml of 10% NBF. This procedure was performed after euthanasia with isoflurane overdose on mice previously injected intraperitoneally with 0.1 ml of 5% heparin (Hospira Productos Farmacéuticos y Hospitalarios S.L., Spain).

B.2.3.1. Whole-mount retinas

After mice retinas were processed, as previously described (B.2.1.1.), the following protocol was used:

1. Permeabilization: samples were immersed in a solution of 0.1% Triton X-100 (Sigma-Aldrich) in PBS for 2 hours at room temperature or overnight at 4ºC.
2. Washing: 4 washes in PBI under constant agitation for 10 minutes each were performed.
3. Blocking: samples were immersed in wash buffer (WB)[6] under constant agitation for 10 minutes at room temperature.
4. Primary antibody: samples were incubated with primary antibody under constant agitation for 30 minutes at room temperature and then overnight at 4ºC.
5. Washing: 4 washes in PBI for 10 minutes each, and 1 wash in WB for 10 minutes were performed.

[6] WB: 3 g BSA + 1 ml Igepal in 1000 ml PBS.

6. Secondary antibody: samples were incubated with secondary antibody under constant agitation for 3 hours at room temperature or overnight at 4ºC.
7. Washing: 5 washes in PBI for 10 minutes each were performed.
8. Fluorochrome (if biotinylated secondary antibody): samples were incubated with fluorochrome under constant agitation for 1 hour at room temperature.
9. Washing: 5 washes in PBI for 10 minutes each were performed.
10. Counterstain: nuclei counterstaining was performed using Hoechst (Sigma-Aldrich) or To-Pro-3 iodide (Molecular probes, Eugene, OR, USA), both diluted in PBS 1:100 and incubated under constant agitation for 10 minutes at room temperature.
11. Washing: samples were rinsed in 5 washes of PBI for 1 hour.
12. Mounting: retinas were flattened over a slide with the retinal internal face directed to the coverslip. Fluoromount (Sigma-Aldrich) was used as anti-fading mounting media. Finally, slides were sealed with nail lacquer.
13. Visualization: images were taken with a Leica TCS SP2 or TCS-SP5 confocal laser scanning microscope with Leica LAS AF Lite imaging software (Leica).

B.2.3.2. Paraffin embedded retinal sections

Once paraffin embedded retinal sections were processed as detailed in section B.2.1.2., the following protocol was performed:

1. Deparaffinization and rehydration:
   - Xylene: 2 washes of 5 minutes each.
   - 100% ethanol, 2 washes of 5 minutes each.
   - 96% ethanol, 2 washes of 5 minutes each.
   - 80% ethanol, 1 wash of 5 minutes.
   - 70% ethanol, 1 wash of 5 minutes.
   - Distilled water, 1 wash of 5 minutes.
2. Antigen retrieval (optional): to expose the antigenic site after formalin fixation in order to allow antibodies to bind, the slides were incubated in different antigen retrieval solutions:
   - Heat-induced: samples were incubated in sodium citrate retrieval solution[7] or ethylenediaminetetraacetic acid (EDTA) solution[8] for 4 minutes at boiling temperature using a pressure cooker, and rest for 30 minutes.
3. Washing: samples were washed in PBI for 5 minutes
4. Blocking: samples were immersed in WB for 5 minutes.

[7] Sodium citrate solution (pH 6): 0.283 g citric acid + 1.8 g sodium citrate in 750 ml distilled water.
[8] EDTA solution (pH 9): 0.372 g EDTA 1mM in 1000 ml distilled water.

5. Primary antibody: samples were incubated with primary antibody overnight at 4ºC.
6. Washing: 3 washes in PBI for 5 minutes each, and 1 wash in WB for 5 minutes were performed.
7. Secondary antibody: samples were incubated with secondary antibody for 3 hours at room temperature.
8. Washing: 3 washes in PBI for 5 minutes each were performed.
9. Fluorochrome (if biotinylated secondary antibody): samples were incubated with fluorochrome for 1 hour at room temperature.
10. Counterstain: nuclei counterstaining was performed using Hoechst or To-Pro-3 iodide, both diluted in PBS 1:100 and incubated for 5 minutes at room temperature.
11. Washing: 3 washes in PBI for 5 minutes each were performed.
12. Mounting: Fluoromount was used as anti-fading mounting media. The slides were sealed with nail lacquer.
13. Visualization: images were taken with a Leica TCS SP2 or TCS-SP5 confocal laser scanning microscope with Leica LAS AF Lite imaging software (Leica).

B.2.4. Transmission electron microscopy

Transmission electron microscopy (TEM) is a microscopy technique that entails imaging of stained thin sections of tissues by using a beam of electrons that passes through the sample to be absorbed and scattered, producing an image of different contrasts (Winey et al., 2014). For TEM studies, mouse eyes were processed following the protocol described below:

1. Dissection: fresh eye samples were preserved at 4ºC. The cornea and lens were removed by making an incision around the outside of the cornea, where the cornea meets the sclera. Next, the lens was discarded.
2. Retinal sections: retinal fragments (approximately 1 mm^2) were dissected from the retina.
3. Fixation: samples were immersed in fixative solution containing 2.5% glutaraldehyde and 2% paraformaldehyde for 2 hours.
4. Post-fixation: samples were rinsed in PBI and post-fixed for 2 hours with 1% osmium tetroxide.
5. Washing: samples were repeatedly washed in distilled water.
6. Dehydration and infiltration: samples were immersed in a series of increasing acetone solutions (Panreac Química). Spurr resin (Sigma-Aldrich) was also added gradually as follows:
   - 70% acetone, overnight.
   - 80% acetone, 2 washes of 10 minutes each.

- 90% acetone, 2 washes of 10 minutes each.
- 96% acetone, 3 washes of 10 minutes each.
- 100% acetone, 3 washes of 10 minutes each.
- Acetone-Spurr resin 3:1, 5 hours.
- Acetone-Spurr resin 1:1, overnight.
- Acetone-Spurr resin 1:3, 8 hours.
- 100% Spurr resin for 2 days.

7. Polymerization: Spurr resin blocks were polymerized at 60ºC for at least 48 hours.
8. Semithin sections: 1 µm sections were made from resin blocks using an ultramicrotome.
9. Staining: semithin sections were stained with 0.5% toluidine blue (Panreac Química).
10. Ultrathin sections: semithin sections were observed with a stereoscopic microscope to select retinal regions of interest. Ultrathin sections (60-80 nm) were cut from the selected regions.
11. Contrast: ultrathin sections were contrasted with lead citrate[9] and 2% aqueous uranyl acetate.
12. Visualization: retinal samples were analyzed with a transmission electron microscope Jeol JEM-1400 (Jeol).

B.2.4.1. Inverted transmission electron micrographs

Staining with lead citrate and uranyl acetate confers electron-density to all structures allowing the visualization by TEM (Winey et al., 2014). Ultrathin sections of 12 samples were left unstained in order to enable the visualization of metal-charged structures with a transmission electron microscope (Iancu & Manov, 2017). Images selected for their electron-dense content were inverted to obtain inverted micrographs.

B.2.5. Scanning laser ophthalmoscopy

Scanning laser ophthalmoscopy (SLO) produces dynamic fundus images based on a laser beam that enters the eye through the pupil while the reflected light is detected by a photomultiplier (Paques et al., 2006). This fundus imaging technique is of great interest for diagnostic imaging of retinal diseases in humans as well as in experimental mice models (Staurenghi et al., 2005; Paques et al., 2006). The protocol used for *in vivo* fluorescein angiographies of mice is described below:

[9] Lead citrate: 1.33 g $Pb(NO_3)_2$ + 1.76 g $Na_3(C_6H_5O_7).2H_2O$ in 30 ml distilled water.

1. Anesthesia: 10 to 40 units of anesthetic solution[10] were injected intraperitoneally into each mouse. After induction of anesthesia, a drop of Tropicamide (Alcon, Barcelona, Spain) and Collyrium anesthetic (Alcon) was applied on each eye to dilate the pupils and relax the lens. To prevent dry eyes, a drop of Viscofresh sterile ophthalmic solution (Allergan, Ireland) was applied on each eye and a custom-made mouse contact lens was placed on the cornea. Application of eye drops was repeated as necessary during the procedure.
2. Fluorescent dye: to stain blood vessels, 5 units of 5% sodium fluorescein (Sigma-Aldrich) were injected subcutaneously in each mouse.
3. Angiography: retinal images were acquired for both eyes with HRA2 Imaging Instrument and the Heidelberg Eye Explorer software (Heidelberg Engineering) focusing on the different vascular plexus. After angiography procedures, mice were transferred to a warm cage to recover under close observation.

B.2.6. Detection of LacZ expression: X-gal staining

The TIM2 gene trap contains the LacZ reporter gene, which encodes the β-galactosidase enzyme. X-gal staining is a rapid and convenient histochemical technique used to detect the LacZ reporter gene expression. Briefly, β-galactosidase cleaves X-gal, into galactose and 5-bromo-4-chloro-3-hydroxyindole; this second compound is then oxidized into a final product that is blue in color (5,5'-dibromo-4,4'-dichloro-indigo).

X-gal staining provides a visual assay of LacZ activity (Burn, 2012; Shen et al., 2017) and the blue stain can be used as a marker of our gene of interest in various tissues of the $TIM2^{+/-}$ mouse. WT littermate controls were processed to identify patterns of non-specific staining due to endogenous galactosidase and resident bacterial enzyme activity. The following protocol was used:

1. Organ harvesting: following perfusion with PBS, organs were harvested and washed in PBS.
2. Fixation: samples were immersed and fixed in 4% paraformaldehyde for 2 hours at room temperature.
3. Washing: fixative solution was removed by washing 10 minutes in PBS (at least 3 washes), under constant agitation in a shaker.
4. X-gal incubation: samples were immersed overnight in x-gal solution[11] under gentle agitation in a shaker at 37ºC covered from light.

[10] Anesthetic solution: 0.5 ml xilacine 2% + 2 ml ketamine 50% + 7.5 ml physiological saline serum.
[11] X-gal solution: 20 µl $K_4Fe(CN)_6$ + 20 µl $K_3Fe(CN)_6$ + 2 µl $MgCl_2$ + 10 µl X-gal stock solution (40 mg/ml) + 948 µl PBS.

5. Washing: x-gal solution was removed by washing 10 minutes in PBS (at least 3 washes), under constant agitation in a shaker.
6. Visualization: the analysis of the samples was performed using a stereoscopic microscope and images were acquired with a digital camera (Nikon DXM 1200F).
7. Inclusion: samples were stored in 10% NBF at 4ºC covered from light until being processed for paraffin embedding.

B.3. Analytical, morphometrical, and biochemical studies

B.3.1. Analyses of iron metabolism parameters in blood

Blood samples were obtained after anesthesia by inhalation with an overdose of isoflurane, either by decapitation or intracardiac sampling. Blood was immediately collected for analyses of iron metabolism parameters. Once centrifuged, samples were kept frozen at -80ºC. Serum iron concentration and unsaturated iron binding capacity (UIBC) were determined using an automated biochemistry analyzer (Chemistry Analyzer AU400, Olympus) and manufacturer's reagents (Olympus System Reagent, Beckman Coulter, Galway, Ireland). Total iron binding capacity (TIBC) was calculated by adding serum iron and UIBC. In turn, transferrin saturation was inferred by the ratio between serum iron and TIBC. Serum ferritin levels were determined using a highly sensitive two-site enzyme-linked immunosorbent assay (ELISA) for measuring ferritin in mouse biological samples (Mouse Ferritin ELISA kit, Abcam) and standard microplate ELISA methodology (iEMS Reader/Dispenser MF, Labsystems Oy).

B.3.2. Energy dispersive X-ray spectroscopy

Energy dispersive X-ray spectroscopy is a technique that enables to detect and measure chemical components in samples. The microscope's electron beam is focused on a minute area of the sample, and the relative abundance of all detectable elements in the irradiated region are determined rapidly by measuring the intensities of characteristic X-rays emitted by their atoms (Whallon, Flegler & Klomparens, 1989). For the analysis of iron by energy dispersive X-ray spectroscopy, 160 nm thick retinal unstained ultrathin sections of 12 samples were observed in a transmission electron microscope Jeol JEM-2011 (Jeol) equipped with an X-ray detector Oxford INCA (Oxford Instruments, Abingdon, UK) using an accelerating voltage at 200 kV. Acquired spectra were analyzed with the Oxford INCA software (Oxford Instruments).

B.3.3. Inductively coupled plasma mass spectrometry

Inductively coupled plasma mass spectroscopy is one of the most powerful and sensitive methods for qualitative and quantitative trace element detection. It features a multielemental capability, good precision, a long linear dynamic range, low detection limits, and the ability to do rapid isotopic analysis. Inductively coupled plasma mass spectroscopy has been widely used for the analysis of metallic, inorganic as well as organic, and biological samples. Briefly, atomic elements are led through a plasma source where they become ionized. Then, these ions are sorted on account of their mass (Pröfrock & Prange, 2012). For retinal iron content studies, mouse eyes were processed following the protocol described below:

1. Dissection: fresh enucleated eyes were placed on a dissection plate with PBS on ice to quickly dissect the retina. Both retinas from each animal were collected in individual vials.
2. Sample digestion: samples were treated with concentrated nitric acid in a dry block at 120ºC for 30 minutes in order to achieve complete retinal digestion.
3. Metal determination: retinal iron content was determined using an inductively coupled plasma mass spectrometer Agilent 7500ce and referenced to the total retinal iron content per animal (µg iron/animal). PBS was also analyzed to normalize values.

B.3.4. Quantification of iron by colorimetric analysis

Retinal iron content as well as Fe^{2+} and Fe^{3+} contents were measured by colorimetric analysis using a commercial iron assay kit (Abcam), according to manufacturer's instructions:

1. Dissection: fresh enucleated eyes were placed on a dissection plate with PBS on ice to quickly dissect the retina.
2. Homogenization: a pool of 10 retinas from each group of animals was homogenized in 500 µl iron assay buffer using a Dounce homogenizer sitting on ice in order to obtain sufficient amount of sample to perform duplicate reading of total iron and Fe^{2+}.
3. Centrifugation: samples were centrifuged at 8,000 *g* at 4°C for 10 minutes in order to aspirate the supernatant.
4. Standard curve: a set of standard dilutions was prepared using 1 mM iron standard.
5. Microplate preparation: 100 µl of each sample and standard dilution were set up in duplicate in a microplate. Samples assigned to Fe^{2+} determination were incubated with 5 µl iron assay buffer while standards and samples assigned to total iron determination were incubated with 5 µl iron reducer for 30 minutes at 25ºC. Followed this, all samples

and standards were incubated with 100 µl iron probe for 60 minutes at 25ºC protected from light.

6. Iron determination: the optical density of each well was measured at 593 nm using a colorimetric microplate reader (PowerWave HT, BioTek). Total iron and Fe^{2+} contents were extrapolated directly from the standard curve obtained. Fe^{3+} content was obtained by calculating the difference between total iron and Fe^{2+} contents.

B.3.5. Quantitative analysis of vascular tortuosity

Tortuosity of the retinal vasculature was quantified using fundus fluorescein angiograms acquired by SLO, as described by Mohsenin, Mohsenin & Adelman (2013). Tortuosity index was calculated by dividing the vessel length (arc length) by the linear distance between two crossing points of the vessel (chord length):

$$\textbf{Tortuosity} = \frac{\text{Arc length}}{\text{Chord length}}$$

ImageJ software (National Institutes of Health, Bethesda, MD, USA) was used to draw a concentric circle centered on the optic disc to limit the area of interest. A straight line was drawn from the center of the circle (optic disc) to the crossing point of the circumference (Chord length). Individual measurements of major arterioles and venules were obtained drawing the vascular path starting from the optic disc to the crossing point of the circle (arc length). Finally, tortuosity indices were compared by statistical analysis.

B.3.6. Quantitative analysis of retinal thickness

Measurement of thickness of retinal layers offers a comprehensive assessment of retinal anatomy that can potentially identify retinal alterations (Shinoda et al., 2008; Wanek et al., 2016). Two paraffin sections close to the optic nerve were collected for each eye followed by H-E staining. The measurements were taken on the total thickness of the retina over a 100, 500, and 1000 µm distances on both sides of the optic nerve. All measurements were performed on each retinal section with a Nikon Eclipse E-800 microscope (Nikon) equipped with Soft Imaging System CC-12 (Olympus) and the analySIS image-analytical software (Olympus). Finally, retinal morphology of $TIM2^{+/-}$ and WT based on mean thickness of total retina for 100, 500, and 1000 µm apart of the optic nerve were compared by statistical analysis.

B.3.7. Glycemia

Mouse tail vein blood glucose levels were determined using a glucometer (Bayer).

B.3.8. Detection of labile iron

Labile Fe^{2+} in whole-mount retinas was detected using FeRhoNox-1 fluorescent imaging probe (Goryo Chemical, Inc., Sapporo, Japan), according to manufacturer's instructions. FeRhoNox-1 is an activatable fluorescent probe that specifically detects labile Fe^{2+} ions via red fluorescence. FeRhoNox-1 was dissolved in dimethyl sulfoxide to produce a 1mM solution, which was further diluted with PBS to a final concentration of 5 μM. Whole-mount retinas were washed in PBS and then incubated with the diluted solution for 60 minutes at 37ºC, 5% CO_2, protected from light. After rinsing with PBS, nuclei were counterstained with Hoechst. Images were taken with a Leica TCS SP2 or TCS-SP5 confocal microscope with Leica LAS AF Lite imaging software (Leica).

B.3.9. Evaluation of oxidative stress

Dihydroethidium (DHE) fluorescence has been extensively used to detect ROS production. DHE specifically reacts with intracellular superoxide anion and is converted to the red fluorescent compound ethidium, which intercalates with the cell's DNA (Zhao et al., 2003; Robinson et al., 2006; Zielonka, Vasquez-Vivar & Kalyanaraman, 2008, Sasaki et al., 2010). To evaluate retinal oxidative stress levels, ROS generation was detected by DHE (Invitrogen, Carlsbad, CA, USA). Retinal paraffin sections were incubated with 50 μM DHE for 30 minutes at 37°C in dimethyl sulfoxide, protected from light, and nuclei counterstaining was performed using Hoechst. Images were taken with a Leica TCS SP2 or TCS-SP5 confocal microscope with Leica LAS AF Lite imaging software (Leica). Values of mean fluorescence intensity measured with the same software were compared by statistical analysis.

B.3.10. Quantitative analysis of fluorescence microscopy images

Quantitative analysis of fluorescence microscopy images is both a sensitive and specific method that can provide a quantitative analysis of protein expression in specific regions (Ntziachristos, 2006; Hamilton, 2009). Mean fluorescence intensity was measured with Leica LAS AF Lite imaging software according to the equation:

$$\mathbf{AFP} = \frac{\sum i(p)}{n(p)} \quad \text{(Intensity units/pixel)}$$

Where i(p) is the intensity of a pixel within the confocal plane of the cell, and n(p) is the total number of pixels of the plane. The results are reported in arbitrary units (AU).

B.4. Western blotting

In molecular biology, western blotting is a technique used to identify specific proteins from whole-tissue or cells. Briefly, this technique involves the separation of proteins by electrophoresis into a polyacrylamide gel according to their molecular weight, followed by their transfer to a more solid surface, such as a high binding affinity membrane, producing a replica of the original gel. Finally, the target protein is identified by the specificity of the antibody-antigen interaction (Mahmood & Yang, 2012).

B.4.1. Sample processing

For western blot analysis of retinal tissue, the samples were processed as follows:

1. Dissection: fresh enucleated eyes were placed on a dissection plate with PBS or Tris buffered saline (TBS)[12], on ice to prevent degradation by proteases. The cornea and lens were removed by making an incision around the limbus, where the cornea meets the sclera.
2. Sample lysis: a pool of 12 retinas from each group of animals was processed in order to obtain sufficient amount of protein sample to perform all the experiments. Retinas were placed in 600 µl lysis solution (radioimmunoprecipitation assay buffer, RIPA)[13] containing a protease inhibitor cocktail (Roche). Next, samples were manually macerated using scalpel, electric homogenizer, and vortex homogenization, and kept on ice for 30 minutes.
3. Centrifugation: samples were centrifuged at 8,000 *g* at 4°C for 10 minutes in order to aspirate the supernatant lysate.
4. Protein quantification: total protein concentration was determined using Pierce BCA Protein Assay kit (Sigma-Aldrich) according to manufacturer's instructions to ensure equal loading of samples. Protein samples were stored at -20ºC until further analysis.

[12] TBS (pH 7.6): 6 g Tris base + 8 g NaCl + 0.2 g KCl in 1000 milliQ water.
[13] RIPA buffer: 0.88 g NaCl + 1 g Triton X-100 + 1 g sodium deoxycholate + 0.1 g sodium dodecyl sulfate + 2.5 ml Tris-HCl 1M (pH 7.6) in 100 ml milliQ water.

B.4.2. Gel electrophoresis, transfer, antibody probing, and detection

Retinal pools of western blot samples were used following the protocol:

1. Protein denaturation: retinal lysates were resuspended in Laemmli sample buffer[14] and heated at 95°C for 5 minutes.
2. Protein separation and transfer: equal amounts of protein samples were separated in a 12% pre-cast SDS-PAGE gel (Bio-Rad) and transferred to an Immobilon-P polyvinylidene fluoride (PVDF) membrane (Merck Millipore) for antibody probing.
3. Washing: 3 washes of 0.05% Tween 20 (Sigma-Aldrich) in TBS (TBST) or PBS (PBST) under constant agitation for 10 minutes each were performed.
4. Blocking: the membrane was incubated in blocking buffer[15] for 1 hour at room temperature under constant agitation.
5. Antibody probing: the membrane was incubated with the recommended dilution of primary antibodies in blocking buffer overnight at 4ºC and after washing with TBST or PBST, membranes were incubated with HRP-conjugated secondary antibody in blocking buffer for 30 minutes at room temperature. A summary of antibodies employed is described in Table 5.
6. Washing: 3 washes of 0.05% TBST or in PBST under constant agitation for 10 minutes each were performed.
7. Signal detection: enhanced chemiluminescence (ECL) was performed by using Luminata Crescendo HRP substrate (Merck Millipore) or Westar ηC Ultra 2.0 (Cyanagen, Bologna, Italy) following the kit manufacturer's recommendations.
8. Visualization: digital images of chemiluminescent westerns were acquired using Molecular Imager ChemiDoc XRS System with QuantityOne software version 4.5 (Bio-Rad).
9. Densitometric quantification: the signal of each protein was determined using ImageJ software (National Institutes of Health) after verifying that the band signal was not saturated with QuantityOne software (Bio-Rad). To correlate the antibody staining intensity with density of the bands, background signal was subtracted, and total protein expression levels were estimated using Plot lane tool of ImageJ software (National Institutes of Health), after normalizing blot loading to the levels of α-tubulin primary antibody (Abcam). Densitometry results are the means of relative expression values (normalized to WT) from 3 repetitions of western blot experiments using the same samples.

[14] Laemmli buffer (2x): 2.4 ml Tris-HCl 1M (pH 6.8) + 4 ml glycerol + 0.01% bromophenol blue + 0.8 g sodium dodecyl sulfate + 1 ml 2-β-mercaptoethanol + 2.8 ml milliQ water.
[15] Blocking buffer: 5% non-fat dry milk or 3% BSA in TBST or PBST.

Table 5. Primary and secondary antibodies used for western blotting.

Antibody		Dilution	Commercial supplier
Primary	Rabbit anti-α-tubulin	1:500000	Abcam
	Rat anti-TIM2	1:1000	Abcam
	Rabbit anti-Scara5	1:1000	Abcam
	Rabbit anti-transferrin receptor 1	1:200	Abcam
	Rabbit anti-transferrin	1:5000	Acris
	Rabbit anti-ferritin light chain	1:500	Abcam
	Rabbit anti-ferritin heavy chain	1:300	Abcam
	Rat anti-PLVAP	1:500	Abcam
	Rabbit anti-ZO-1	1:100	Thermo Fisher Scientific
	Rabbit anti-claudin-5	1:100	Thermo Fisher Scientific
	Rabbit anti-occludin	1:100	Thermo Fisher Scientific
	Rabbit anti-RPA2	1:25000	Abcam
	Rabbit anti-γ-H2AX	1:250	Abcam
	Goat anti-VEGF-A	1:100	Santa Cruz Biotechnology
Secondary	Anti-rabbit IgG-HRP	1:25000	Bionova Scientific
	Anti-rat IgG-HRP	1:20000	Abcam
	Anti-goat IgG-HRP	1:10000	Dako

B.5. Quantitative real-time PCR

Quantitative real-time PCR (qRT-PCR) is a method frequently used for the analysis and quantification of gene expression of biological samples, by means of amplification of complementary DNA (cDNA) obtained from reverse transcription of mRNA (Kubista et al., 2006; Nascimento, Suarez & Pinhal, 2010).

B.5.1. RNA isolation and cDNA preparation

Mouse eye samples for PCR analysis were processed as follows:

1. Dissection: fresh enucleated eyes were placed in a dissection plate with sterile RNAse-free cold water solution to quickly dissect the retina.

2. RNA extraction: RNA was purified and treated with DNase using the Maxwell RSC simply RNA tissue Kit (Promega) following the manufacturer's instructions.
3. RNA quantification: total RNA was quantified by measuring the absorbance at 260 nm using a NanoDrop ND-2000c spectrophotometer (Thermo Fisher Scientific), and the purity was assessed by determining the ratio of the absorbance at 260 and 280 nm (NanoDrop), which indicated that all 260/280 nm ratios were >1.9.
4. cDNA transcription: RNA was reverse transcribed into cDNA using iScript cDNA synthesis kit (Bio-Rad). Briefly, each reverse transcription reaction contained 1000 ng of extracted total RNA sample using iScript Reverse Transcriptase according to the manufacturer's instructions, with an RNase inhibitor in a final volume of 20 µl. The transcription program was the following: 25°C for 5 minutes, 42°C for 30 minutes, 85°C for 5 minutes. cDNA aliquots were stored at -20ºC until further analysis.

B.5.2. Analysis of gene expression

Quantification of amplified cDNA was performed with the SYBR green dye (Bio-Rad), which binds to the double strands of cDNA synthesized in each successive cycle, resulting in an increase in fluorescence intensity emitted proportional to the amount of cDNA produced (Storch, 2007). Relative gene expression was determined using housekeeping genes, an accurate and validated normalization factor (Vandesompele et al., 2002). Housekeeping genes are used as endogenous control of gene expression because they are expected to maintain constant expression levels in all cells and conditions (Eisenberg & Levanon, 2013). For this particular study, *36B4* and *GAPDH* genes were chosen as stable and recommended reference genes (Simpson et al., 2000; Zhang et al., 2016).

Gene relative quantification was carried out with SYBR green dye (Bio-Rad) using a T100 or CFX384 Thermal cycler (Bio-Rad) and MicroAmp Optical 96- or 384-well plates (Bio-Rad), respectively. The 10 µl PCR reaction mixtures contained 5 µl of iTaq Universal SYBR Green Supermix (Bio-Rad), 0.5 µl of each primer pair, and 0.25-1 µl of diluted cDNA as template. According to *Mus musculus* gene, validated primers pairs (PrimePCR SYBR Green Assay, Bio-Rad) used are listed in table 6.

Standard cycling conditions were used according to manufacturer's instructions: initial denaturation at 95°C for 5 seconds, followed by 35 cycles of cDNA denaturation at 95ºC for 30 seconds, annealing and extension at 60ºC for 30 seconds, and a final step of melt curve analysis from 65ºC to 95ºC with 0.5ºC increments every 5 seconds. Negative (non-template control) controls were included in each round of PCR amplification. Primer specificity and the formation of primer-dimers were confirmed by melt curve analysis. Measurements of each

sample for each gene were made in triplicate and the relative quantification for each target gene was analyzed by the CFX Maestro software (Bio-Rad) according to the $2^{-\Delta\Delta Ct}$ method for relative quantification in qRT-PCR suggested by Pfaffl (2001, 2002), using a normalization factor, which was the geometric mean of *36B4* and *GAPDH* genes. Relative expression values were compared by statistical analysis.

Table 6. Primers pairs for qRT-PCR.

Target	PrimePCR assay ID	Commercial supplier
H-Ferritin	qMmuCID0009602	Bio-Rad
L-Ferritin	qMmuCED0049569	Bio-Rad
Scara5	qMmuCID0013506	Bio-Rad
TfR1	qMmuCID0039655	Bio-Rad
Tf	qMmuCID0061477	Bio-Rad
36B4	qMmuCED0061738	Bio-Rad
GAPDH	qMmuCED0027497	Bio-Rad

B.6. Functional studies: Assessment of retinal vascular integrity

Serum albumin has been used to show BRB failure (Vinores, 1995; Minshall & Malik, 2006). In order to evaluate retinal vascular integrity, anesthetized mice received tail vein injections of fluorescein isothiocyanate conjugated-BSA (FITC-BSA, 100 mg/kg) (Sigma-Aldrich) in sterile PBS. Eyes were dilated with a drop of Tropicamide and Collyrium anesthetic and the vasculature was visualized by means of SLO. After the last session, mice were sacrificed, and left eyes were removed and fixed in 10% NBF for paraffin embedding. Retinas from right eyes were dissected and fixed in 10% NBF for 2 hours at 4°C. The protocol for immunohistochemistry was used as previously described in B.2.4.1. and B.2.4.2. and images were taken with a Leica TCS SP2 or TCS-SP5 confocal microscope with Leica LAS AF Lite imaging software (Leica).

C. Statistical analysis

Results are shown as mean ± standard error of the mean (SEM). Statistical analyses were performed by unpaired t-test using Prism software version 6 (GraphPad Software, Inc., La Jolla, CA, USA). Significance was accepted at $p<0.05$.

RESULTS

RESULTS

A. Characterization of TIM2 expression in the mouse retina

A.1. TIM2 expression in the mouse retina

In order to demonstrate TIM2 expression in the retina, western blot and immunohistochemistry analyses were performed with specific antibodies. To assure that the target antigen was expressed in the retina and add confidence in the specificity of the antibody labeling, mouse spleen was used as a positive control tissue (Chen et al., 2005).

Western blot analysis of TIM2 protein expression in the spleen and retina showed a specific band with a molecular weight of 33 kDa (Figure 25A), confirming the presence of TIM2 receptors in the retina.

As expected, immunolabeling of spleen paraffin embedded sections against TIM2 showed that this receptor was expressed in the red and white pulp, with stronger expression in the germinal center (Figure 25B). Retinal paraffin embedded sections immunostained with the same antibody revealed that TIM2 was expressed throughout the entire retinal parenchyma, predominantly in the ganglion cell layer, along the internal limiting membrane. Moreover, the subcellular localization of TIM2 in the retina seemed to be predominantly cytoplasmic and the protein expression pattern suggested that TIM2 was mainly expressed in Müller cells (Figure 25B).

These results revealed for the first time the presence of TIM2 in the mouse retina.

A.2. Localization of TIM2 in retinal cells

Once established that TIM2 was present in the mouse retina, we next aimed to characterize the precise cell type expressing TIM2 receptors. Therefore, colocalization analyses were performed in paraffin embedded sections immunolabeled with anti-TIM2 antibody and a variety of specific cellular markers.

Dual immunostaining with anti-glutamine synthetase antibody, a specific marker of Müller cells

(Mizutani, Gerhardinger & Lorenzi, 1998), was performed. As expected, TIM2 and glutamine synthetase revealed a strong colocalization, with higher immunoreactivity in cell processes and endfeet of Müller cells along the internal limiting membrane (Figure 26). On the other hand, dual immunostaning with anti-glial fibrillary acidic protein (GFAP) antibody, a specific marker of astrocytes (Sarthy, Fu & Huang, 1991), revealed no TIM2 expression in these glial cells (Figure 27).

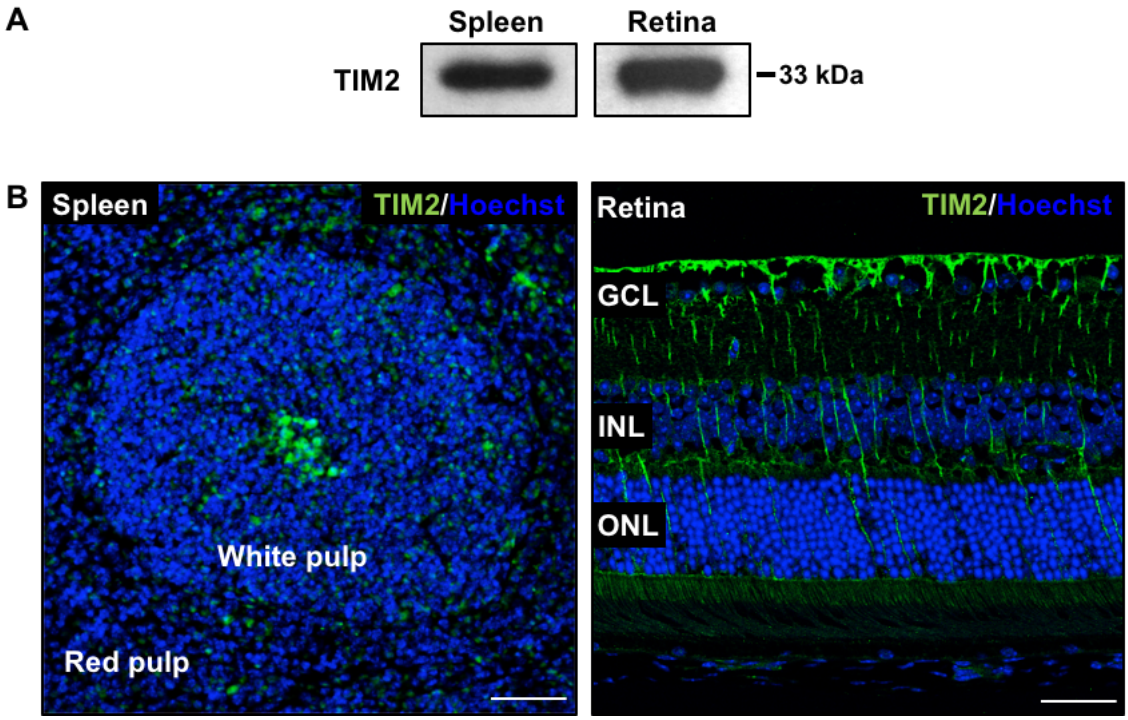

Figure 25. Analysis of TIM2 expression in the mouse spleen and retina. A. Western blot revealed that TIM2 was expressed in the spleen and retina. **B**. Spleen sections immunostained with an anti-TIM2 antibody (green) showed that TIM2 was expressed in the red and white pulp, with stronger expression in the germinal center. Retinal sections immunostained with the same anti-TIM2 antibody (green) showed that TIM2 was expressed throughout the retinal parenchyma, predominantly in the ganglion cell layer. Nuclei were counterstained with Hoechst (blue). GCL, ganglion cell layer; INL, inner nuclear layer; ONL, outer nuclear layer. Scale bars: Spleen = 49.92 µm; Retina = 39.27 µm.

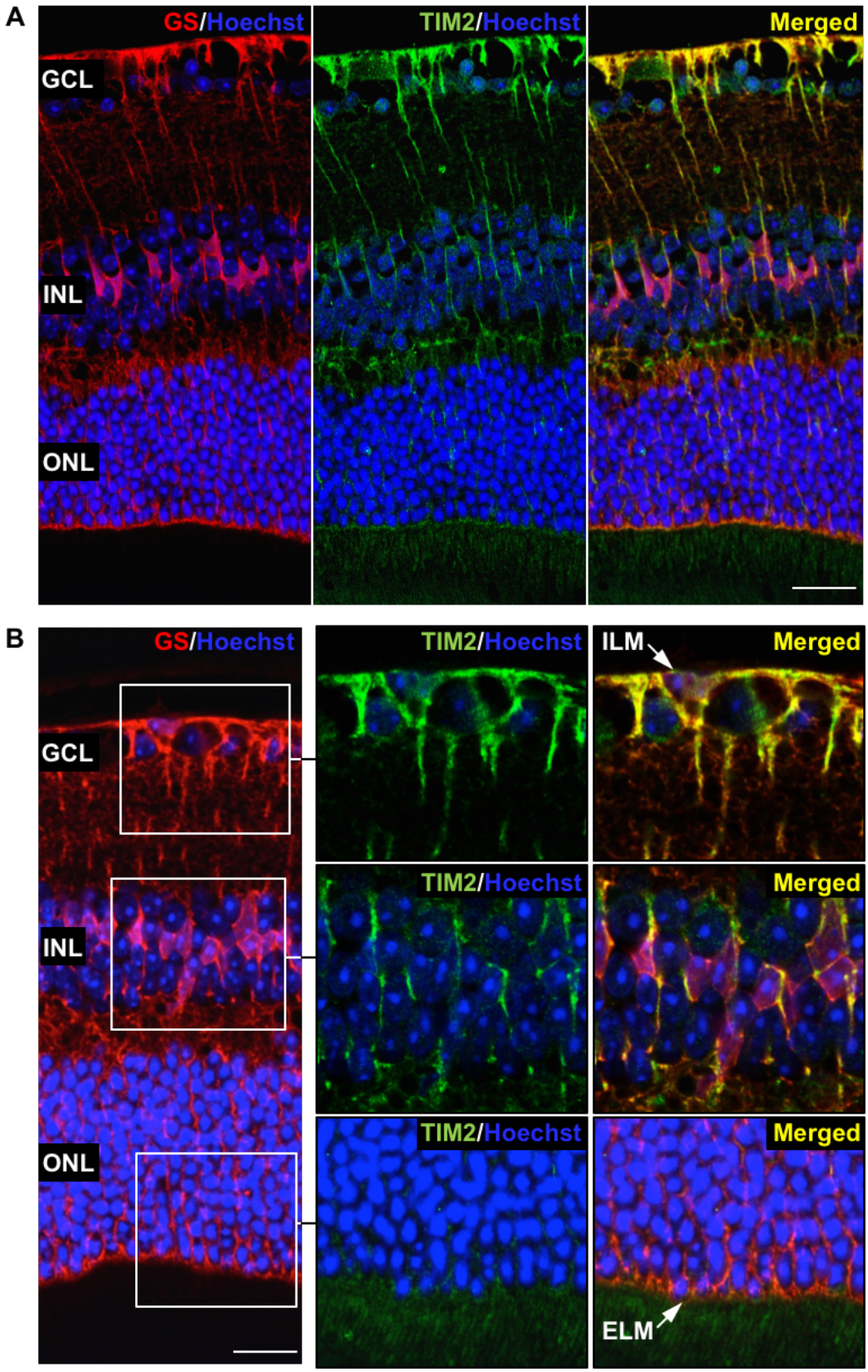

Figure 26. Analysis of TIM2 expression in Müller cells. A. Dual immunostaining with anti-GS antibody (red) and anti-TIM2 antibody (green) revealed a strong colocalization between TIM2 and GS. **B.** TIM2 expression was stronger in cell processes and endfeet along the internal limiting membrane. Nuclei were counterstained with Hoechst (blue). ELM, external limiting membrane; GCL, ganglion cell layer; GS, glutamine synthetase; ILM, internal limiting membrane; INL, inner nuclear layer; ONL, outer nuclear layer. Scale bars: A = 23.9 µm; B = 18.84 µm.

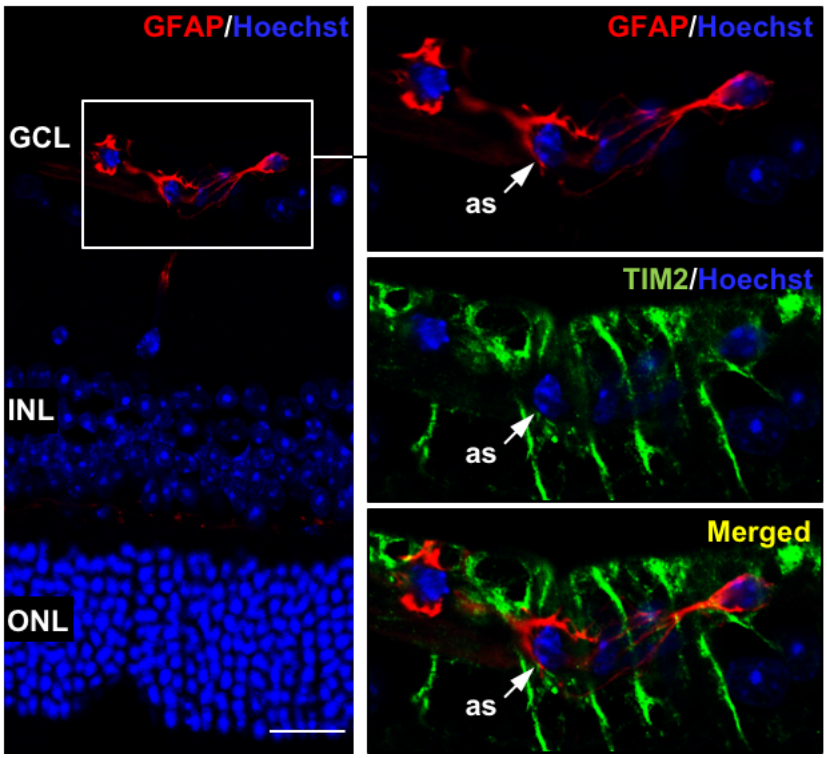

Figure 27. Analysis of TIM2 expression in astrocytes. Dual immunostaining against GFAP (red) and TIM2 (green) revealed no TIM2 expression in astrocytes. Nuclei were counterstained with Hoechst (blue). as, astrocyte; GCL, ganglion cell layer; INL, inner nuclear layer; ONL, outer nuclear layer. Scale bar = 21.76 µm.

Concerning retinal neurons, no TIM2 expression was detected in ganglion cells, identified with Brn3a, a specific marker (Nadal-Nicolás et al., 2009) (Figure 28).

Anti-protein kinase C alpha, parvalbumin, and calbindin antibodies were used to identify bipolar, amacrine, and horizontal cells, respectively (Haverkamp & Wässle, 2000; Koch & Hess, 2011; Morona et al., 2008). Double immunohistochemistry analyses showed a weak expression of TIM2 surrounding the nucleus of all these retinal neuronal cells (Figures 29, 30, and 31). TIM2 expression was also found in some axons of bipolar cells (Figure 29).

The peanut agglutinin is a lectin commonly used to identify cones by its selective binding to the inner segments of these cells. Rods are not stained with this lectin (Ohtoshi et al., 2004). Dual staining with anti-TIM2 antibody and peanut agglutinin lectin showed TIM2 expression in the inner segments of photoreceptors, although no colocalization was observed with peanut agglutinin lectin. This result reveled that TIM2 was not expressed in cones, but it was detected in the inner segments of rods (Figure 32).

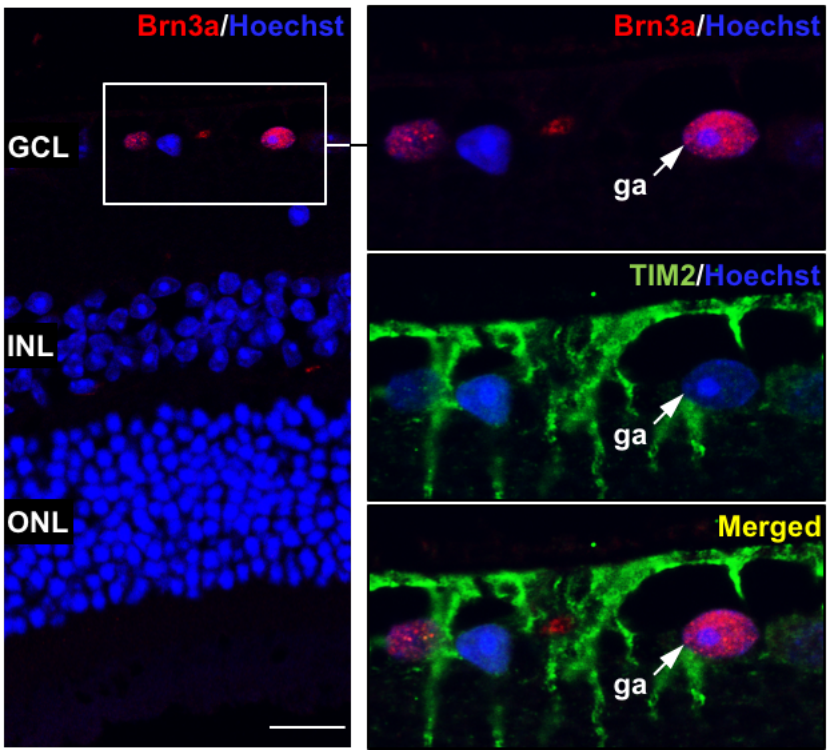

Figure 28. Analysis of TIM2 expression in ganglion cells. The double staining with anti-Brn3a (red) and anti-TIM2 (green) antibodies revealed no TIM2 expression in ganglion cells. Nuclei were counterstained with Hoechst (blue). ga, ganglion cell; GCL, ganglion cell layer; INL, inner nuclear layer; ONL, outer nuclear layer. Scale bar = 18.98 µm.

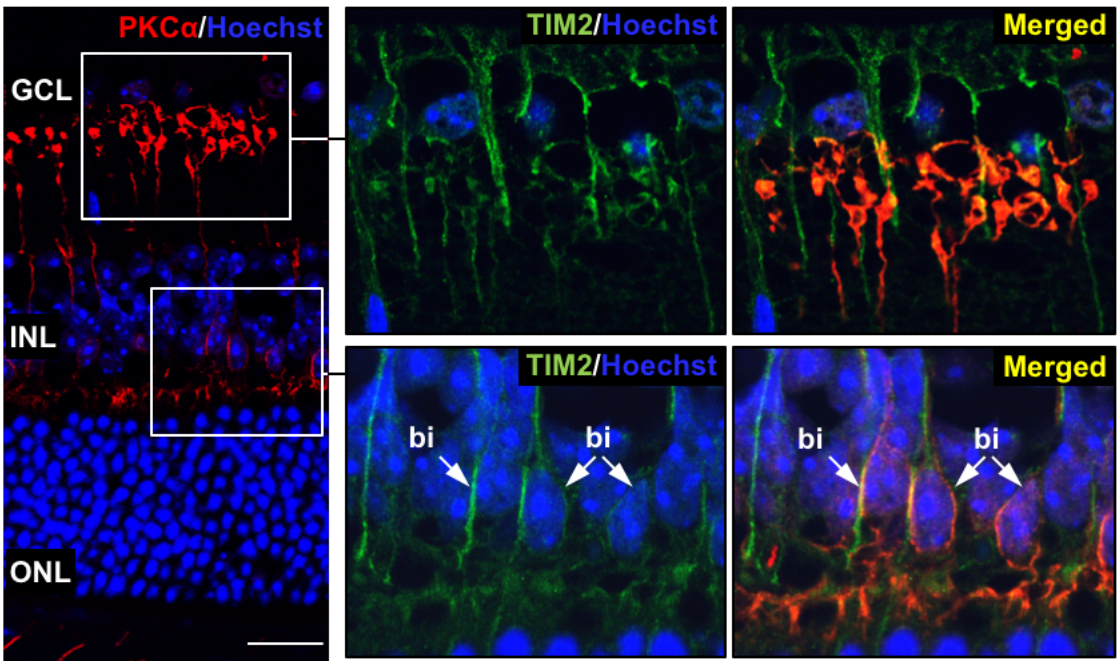

Figure 29. Analysis of TIM2 expression in bipolar cells. PKCα-positive bipolar cells (red) expressed TIM2 (green) in the cytoplasm. Nuclei were counterstained with Hoechst (blue). bi, bipolar cells; GCL, ganglion cell layer; INL, inner nuclear layer; ONL, outer nuclear layer; PKCα, protein kinase C alpha. Scale bar = 21.02 µm.

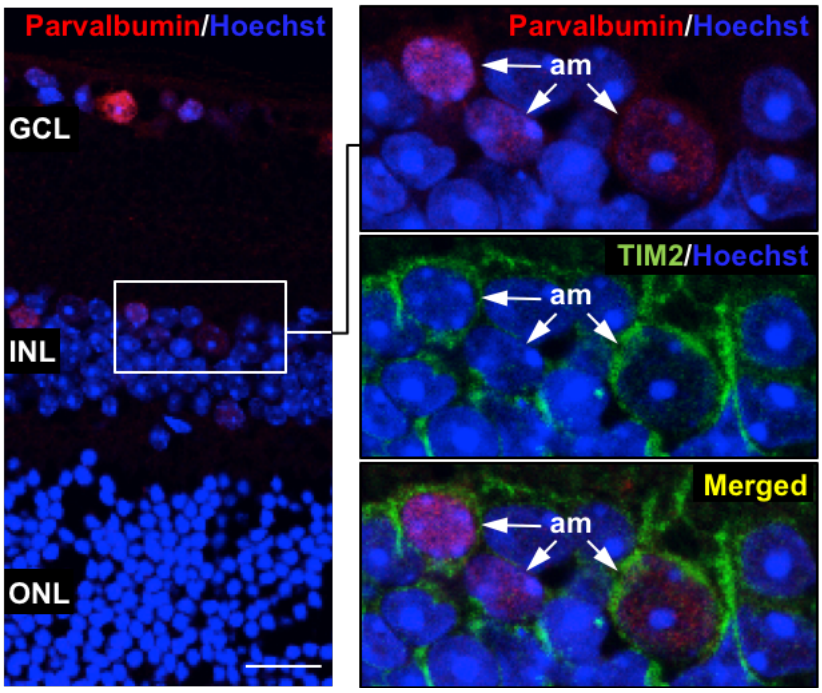

Figure 30. Analysis of TIM2 expression in amacrine cells. Amacrine cells immunolabeled with anti-parvalbumin (red*)* and anti-TIM2 (green) antibodies showed TIM2 expression in their cytoplasm. Nuclei were counterstained with Hoechst (blue). am, amacrine cells; GCL, ganglion cell layer; INL, inner nuclear layer; ONL, outer nuclear layer. Scale bar = 21.17 µm.

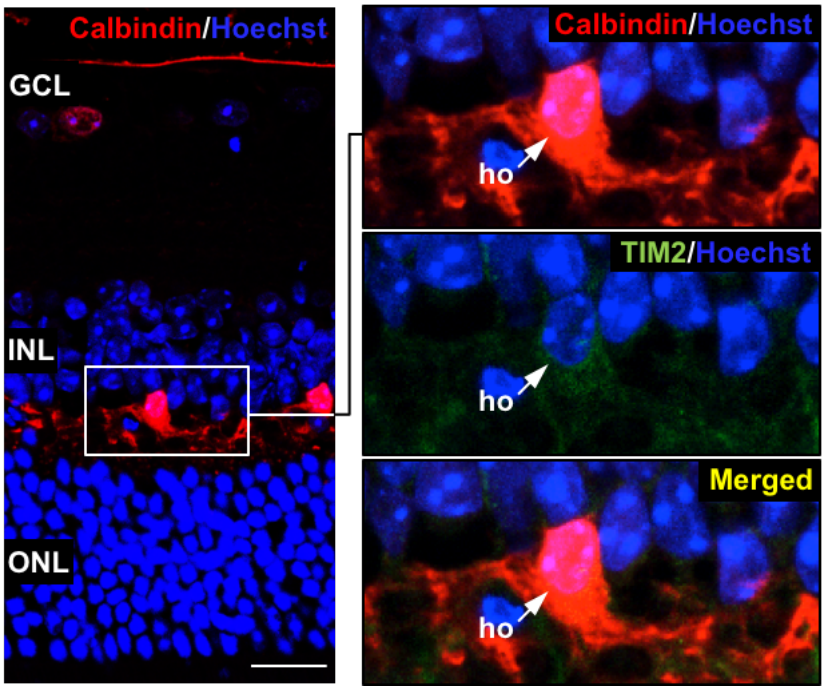

Figure 31. Analysis of TIM2 expression in horizontal cells. Dual immunolabeling with anti-calbindin (red) and anti-TIM2 (green) antibodies detected the expression of TIM2 in horizontal cells. Nuclei were counterstained with Hoechst (blue). GCL, ganglion cell layer; ho, horizontal cell; INL, inner nuclear layer; ONL, outer nuclear layer. Scale bar = 18.8 µm.

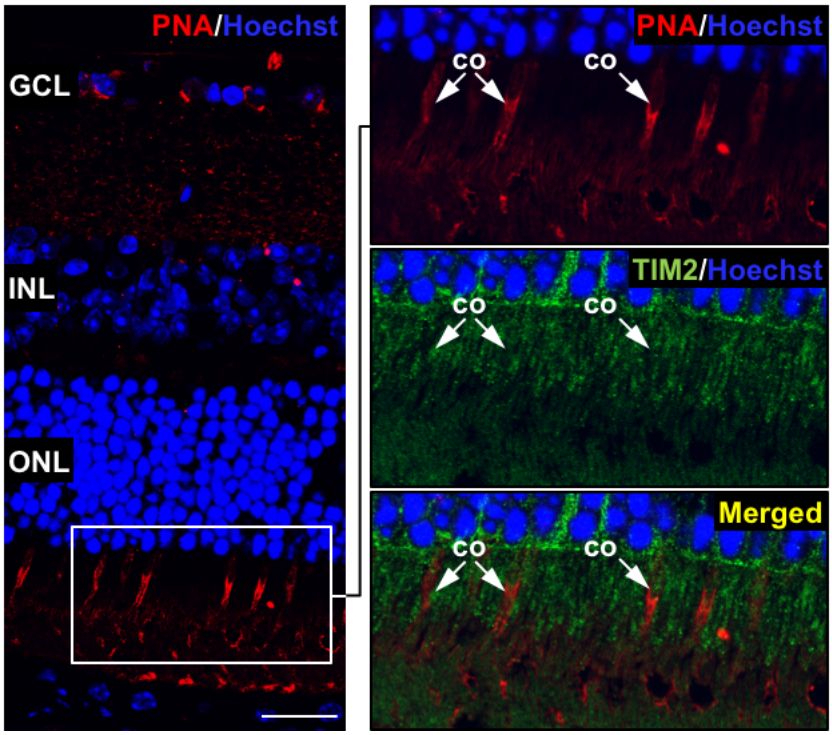

Figure 32. Analysis of TIM2 expression in photoreceptor cells. Dual staining with PNA lectin (red) and anti-TIM2 antibody (green) showed no TIM2 expression in cones (arrow), but rather an expression in the inner segments of rods. Nuclei were counterstained with Hoechst (blue). co, cones; GCL, ganglion cell layer; INL, inner nuclear layer; ONL, outer nuclear layer; PNA, peanut agglutinin. Scale bar = 22.81 µm.

Altogether, our results showed that TIM2 was mainly expressed in Müllers cells. A weak expression could be detected in bipolar, amacrine, and horizontal cells, and at the level of the inner segments of rods. No expression was detected in astrocytes, ganglion cells or cones (Table 7).

Table 7. TIM2 expression in retinal cells.

Retinal cell type	TIM2 expression
Müller cells	+++
Astrocytes	-
Ganglion cells	-
Bipolar cells	+
Amacrine cells	+
Horizontal cells	+
Cones	-
Rods	+

A.3. TIM2 expression in retinal blood vessels

To evaluate the expression of TIM2 in the retinal vascular tree, double immunohistochemistry with antibodies against TIM2 and laminin, to evidence the blood vessel basement membrane (LeBleu, Macdonald & Kalluri, 2007), was performed.

Our results demonstrated that, although TIM2 was found surrounding blood vessels, no TIM2 expression was detected in endothelial cells or any other cellular component of the vessel wall (Figure 33).

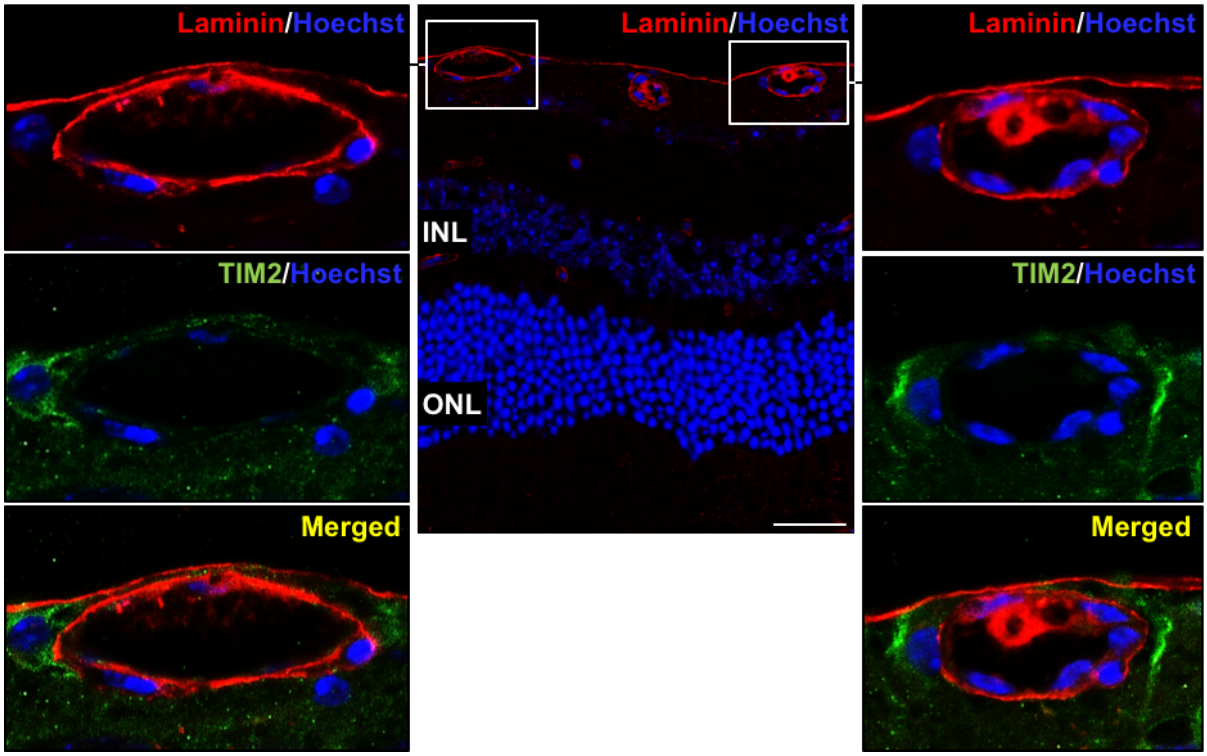

Figure 33. Analysis of TIM2 expression in retinal blood vessels. Double immunohistochemistry with anti-laminin (red) and anti-TIM2 (green) antibodies evidenced that, although TIM2 was found surrounding blood vessels, TIM2 expression was not detected in endothelial cells or any other cellular component of the vessel wall. Nuclei were counterstained with Hoechst (blue). INL, inner nuclear layer; ONL, outer nuclear layer. Left panel: venule; right panel: arteriole. Scale bar = 34.01 μm.

B. Generation and validation of TIM2 knockout mice

B.1. Generation of TIM2 knockout mice

Having confirmed and characterized TIM2 expression in the mouse retina, we proceed to our second objective in this study, the analysis of the consequences of retinal TIM2 deficiency in iron import. In the literature, a TIM2 deficient mouse model had already been generated to study immune response (Rennert el al., 2006). However, the genetic background of the mouse strain used (BALB/c) was not suitable for our purpose due to some abnormalities described in several retinal layers (Huber et al., 2009; Santos et al., 2010; Bell et al., 2012).

For this work, a TIM2 knockout mouse model was generated by disrupting TIM2 gene function through the insertion of a cassette containing the LacZ reporter gene into the intron of the TIM2 gene (Figure 34A). Mice genotyping was performed by PCR analysis of genomic DNA from tails of mice. Only TIM2 heterozygous knockout ($TIM2^{+/-}$) mice were obtained, probably due to embryonic lethality in TIM2 homozygous ($TIM2^{-/-}$) mice (Figure 34B).

For the present work, $TIM2^{+/-}$ mice and their wild-type (WT) littermates were used.

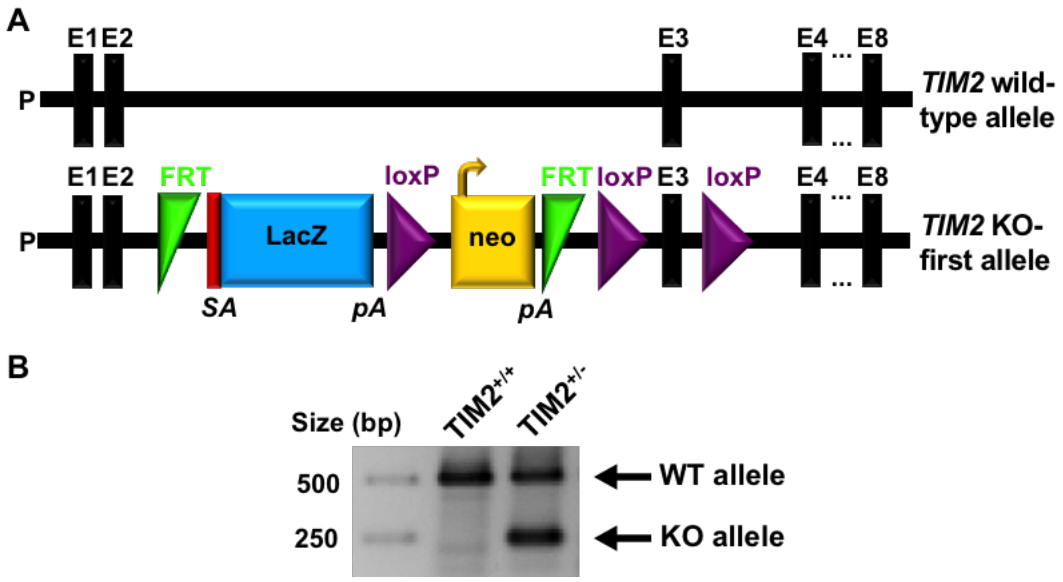

Figure 34. Generation of TIM2 KO mice. A. Schematic diagram of the generation of TIM2 KO mice used to study the TIM2 deficiency in mice. **B.** Genotyping of mice by PCR analysis of genomic DNA from mice tails. $TIM2^{+/-}$ mice were identified by the presence of two size bands (~250 and ~500 bp) equivalent to a KO allele and a WT allele. bp, base pair; E, exon; FRT, flippase recognition target; KO, knockout; LacZ, gene encoding bacterial beta-galactosidase; loxP, locus of crossover in P1; neo, promoter-driven neomycin resistance gene; P, promoter; pA, SV40 polyadenylation signal poly A; SA, splice acceptor element from engrailed-2; WT, wild-type.

B.2. Validation of the generated TIM2 heterozygous knockout mouse

$TIM2^{+/-}$ mice generated should contain the LacZ reporter gene that can be detected by X-gal staining (Burn, 2012; Shen et al., 2017). Taking advantage of this, X-gal staining was performed in spleens of $TIM2^{+/-}$ and WT mice. A blue stain was observed throughout the red and white pulp, with stronger expression in the germinal center of spleens from $TIM2^{+/-}$ mice. No blue stain was observed in spleens of WT mice. Our results demonstrated the presence of the LacZ reporter gene only in $TIM2^{+/-}$ mice (Figure 35A) in a localization consistent with TIM2 expression in WT mice.

H-E staining performed in sections from X-gal stained $TIM2^{+/-}$ spleens confirmed the insertion of LacZ reporter gene throughout the red and white pulp (Figure 35B), and the disruption of TIM2 gene function in this tissue.

Western blot analysis of TIM2 protein expression was also performed, revealing a decrease of TIM2 protein expression in spleens from $TIM2^{+/-}$ mice, consistent with a decrease in the intensity of the 33 kDa band observed. Quantitative densitometry analysis confirmed a decrease in TIM2 protein levels (0.45-fold change) in a pool of 6 $TIM2^{+/-}$ spleens relative to a pool of 6 WT spleens (Figure 35C).

B.3. Evaluation of the effects of TIM2 deficiency on the retinal cellular architecture

Having confirmed the decrease of TIM2 expression in $TIM2^{+/-}$ mice, we then evaluated whether this deficiency influenced the spatial arrangement of retinal cells. To assess retinal cell disposition, paraffin embedded sections were stained with H-E, and comparison between WT and $TIM2^{+/-}$ retinas was made. As shown in Figure 36, the cellular architecture of each layer was maintained in retinas from $TIM2^{+/-}$ mice. All the retinal layers were clearly identifiable and the characteristic cellular organization was maintained, although a separation between some nuclei could be observed.

Retinal layers were also evaluated by TEM. Ultrathin sections of retinas from $TIM2^{+/-}$ mice also showed a normal cellular disposition at the level of the ganglion cell layer (Figure 37A), inner nuclear layer (Figure 37B), and outer nuclear layer (Figure 37C) compared to WT mice.

These results indicated that TIM2 gene deficiency had no apparent effect in the retinal cellular organization, with all retinal layers preserved in $TIM2^{+/-}$ mice.

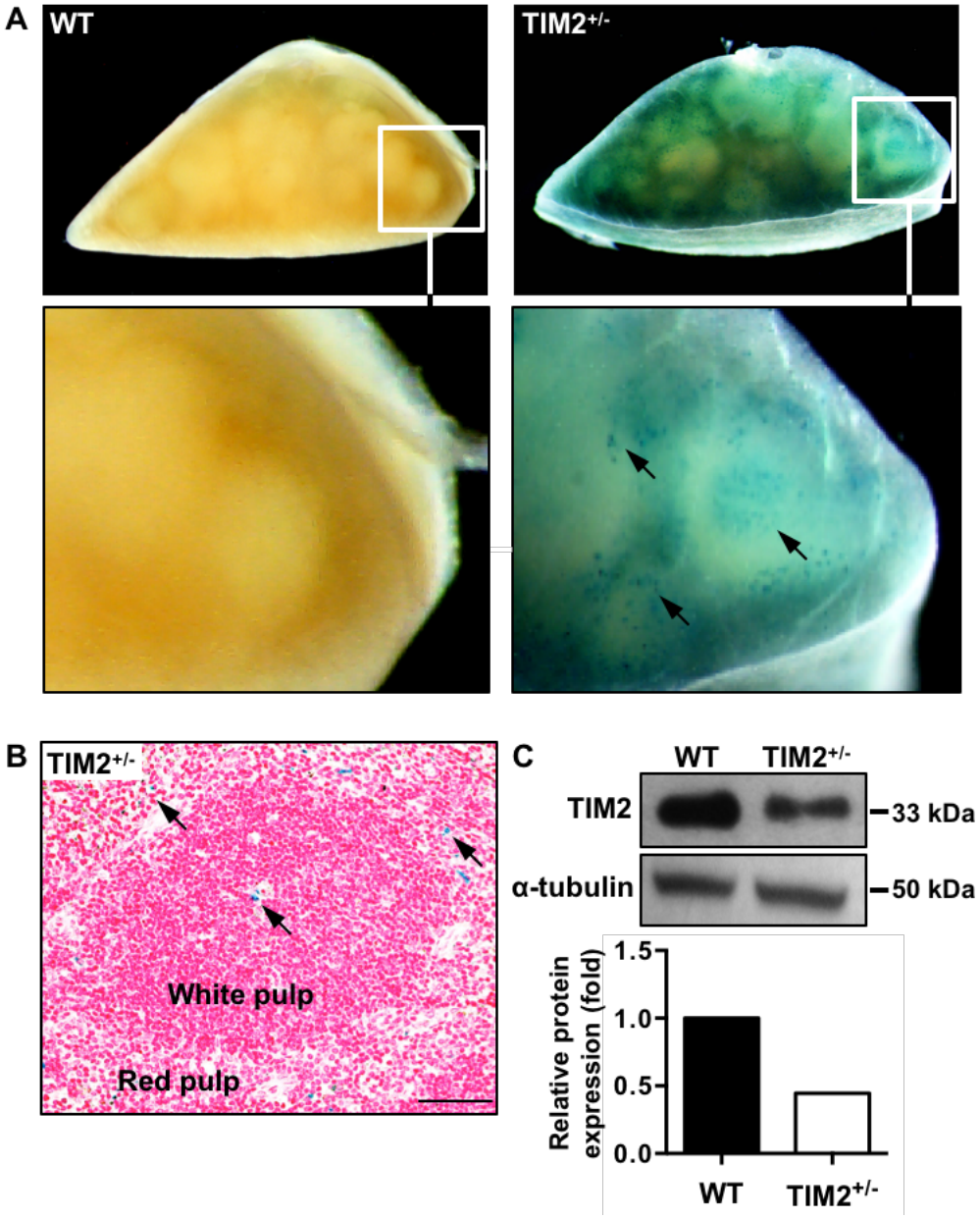

Figure 35. Validation of TIM2 KO mice. Spleen was used as a positive control tissue to validate the reduction of TIM2 expression in TIM2$^{+/-}$ mice vs. WT littermates. **A.** X-gal detection of LacZ activity showed a dark blue stain (arrows) in spleens from TIM2$^{+/-}$ mice, confirming the correct insertion of the cassette containing LacZ in the TIM2 gene. LacZ expression was not detected in spleens from WT littermates. **B.** Paraffin embedded spleen sections stained with H-E from X-gal stained TIM2$^{+/-}$ mice showed a blue pattern (arrows) compatible with that of X-gal staining. **C.** Western blot analysis and quantitative densitometry revealed a decrease of TIM2 protein expression in a pool of 6 TIM2$^{+/-}$ spleens compared to a pool of 6 WT spleens. α-tubulin was used as a loading control. WT, wild-type. Scale bar = 44.77 μm.

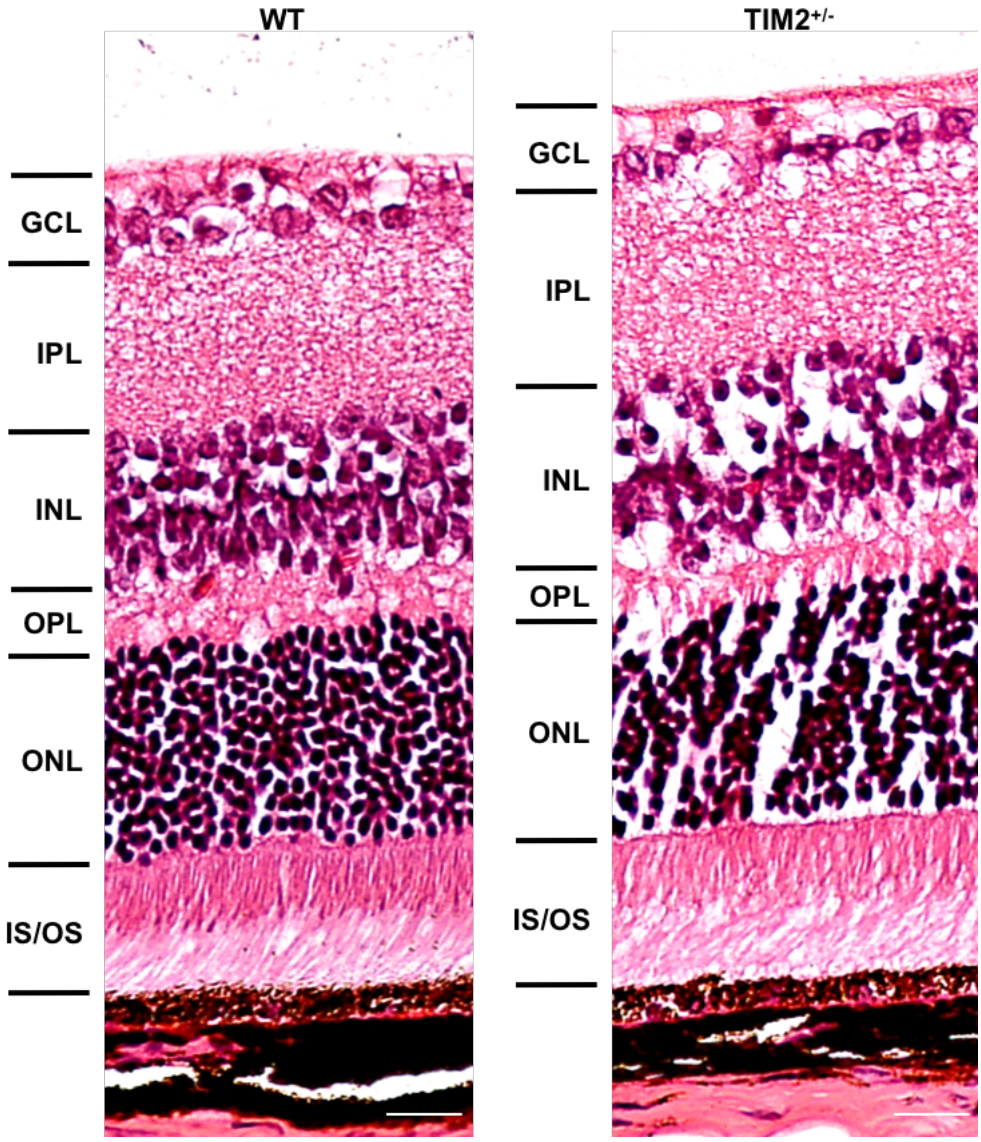

Figure 36. Analysis of retinal morphology. Paraffin embedded retinal sections stained with H-E from WT and TIM2$^{+/-}$ mice revealed a normal architecture of all retinal layers. GCL, ganglion cell layer; IPL, inner plexiform layer; INL, inner nuclear layer; OPL, outer plexiform layer; ONL, outer nuclear layer; IS/OS, inner and outer segments of photoreceptors; WT, wild-type. Scale bars: WT = 14.86 µm; TIM2$^{+/-}$ = 14.83 µm.

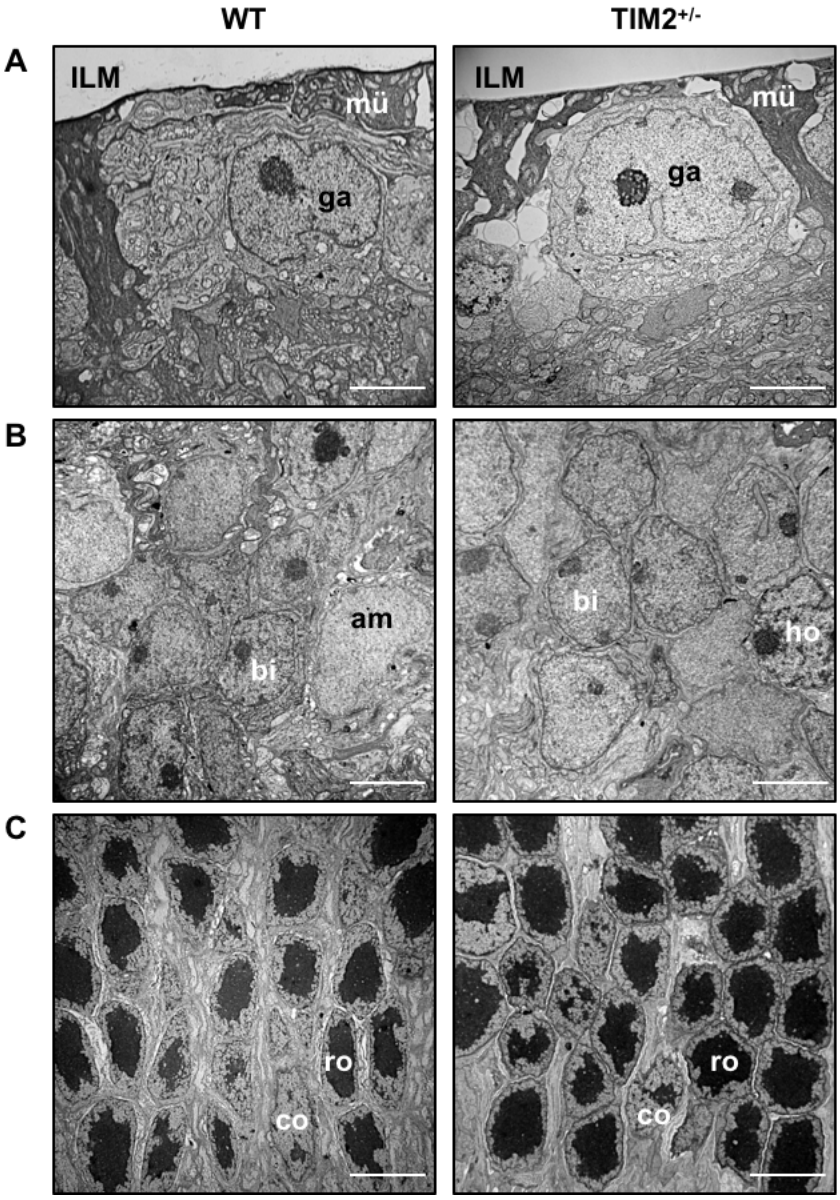

Figure 37. Ultrastructural analysis of retinal morphology. Transmission electron microscopy images from TIM2$^{+/-}$ mice showed normal cellular disposition at the level of the ganglion cell layer **(A)**, inner nuclear layer **(B)**, and outer nuclear layer **(C)** compared to WT mice. am, amacrine cell; bi, bipolar cell; co, cone; ga, ganglion cell; ho, horizontal cell; ILM, internal limiting membrane; mü, Müller cell; ro, rod; WT, wild-type. Scale bars: (A) WT = 3.51 µm; TIM2$^{+/-}$ = 3.51 µm; (B) WT = 4.74 µm; TIM2$^{+/-}$ = 4.74 µm; (C) WT = 4.74 µm; TIM2$^{+/-}$ = 4.74 µm.

B.4. Analysis of TIM2 expression in TIM2$^{+/-}$ mice retinas

We next proceeded to confirm the diminution of TIM2 expression in the retina of TIM2$^{+/-}$ mice by means of western blot and immunohistochemistry analyses.

As expected, western blot analysis showed a decrease of TIM2 protein expression in retinas from TIM2$^{+/-}$ mice, consistent with a decrease in the intensity of the 33 kDa band observed. The quantification by densitometry confirmed a decrease in the protein expression of TIM2 (0.41-fold change) in a pool of 12 retinas from TIM2$^{+/-}$ mice compared to a pool of 12 retinas from WT mice (Figure 38A). Accordingly, immunolabeling with anti-TIM2 antibody also showed a decrease in the intensity of TIM2 expression throughout the retina in TIM2$^{+/-}$ mice (Figure 38B).

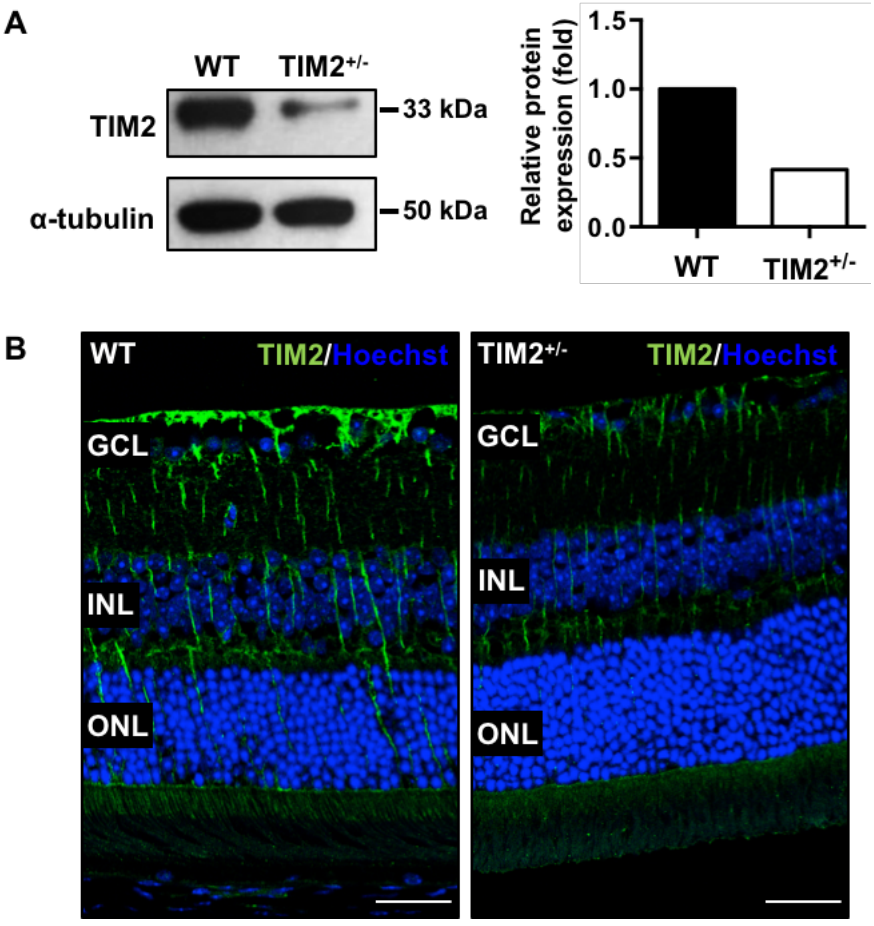

Figure 38. Analysis of TIM2 protein expression in the retina. A. The expression of TIM2 protein assessed by western blot analysis and quantified by means of densitometry showed a decrease of TIM2 protein expression in a pool of 12 TIM2$^{+/-}$ retinas compared to a pool of 12 WT. α-tubulin was used as a loading control. **B.** Retinal sections immunostained with anti-TIM2 antibody (green) showed decreased expression throughout the retinal parenchyma of TIM2$^{+/-}$ mice compared to WT mice. Nuclei were counterstained with Hoechst (blue). GCL, ganglion cell layer; INL, inner nuclear layer; ONL, outer nuclear layer; WT, wild-type. Scale bars: WT = 32.63 µm; TIM2$^{+/-}$ = 32.62 µm.

C. Analysis of the consequences of TIM2 deficiency in retinal iron import

Having achieved our goal in decreasing retinal TIM2 expression, we next studied the effects on iron-handling proteins expression involved in iron import into the retina.

C.1. Effects on ferritin expression

As previously exposed, the ferritin molecule is composed of H- and L-ferritin subunits, specific antibodies for each chain were used to evaluate ferritin expression in the retina (Mendes-Jorge et al., 2014).

Western blotting revealed an increased H-ferritin expression in TIM2$^{+/-}$ retinas, shown by a specific band with higher intensity with a molecular weight of 21 kDa. After normalization, quantitative densitometry analysis of western blot results indicated that H-ferritin protein was overexpressed (1.60-fold change) in a pool of 12 TIM2$^{+/-}$ retinas compared to a pool of 12 WT retinas (Figure 39A). This was paralleled by an increase of intensity of the specific immunolabeling of anti-H-ferritin antibody throughout the retinal parenchyma in TIM2$^{+/-}$ mice evaluated by scanning laser confocal microscopy (Figure 39B). The protein expression of L-ferritin was also increased in retinas from TIM2$^{+/-}$ mice, demonstrated by western blot with a specific band with higher intensity (19 kDa). Quantitative densitometry analysis confirmed L-ferritin overexpression (1.75-fold change) in a pool of 12 retinas from TIM2$^{+/-}$ mice compared to WT (Figure 40A). Immunohistochemistry against L-ferritin showed a similar increase of L-ferritin expression throughout the retina in TIM2$^{+/-}$ mice (Figure 40B).

H- and *L-ferritin* mRNA transcript levels were also analyzed by qRT-PCR and normalized by *36B4* and *GAPDH* housekeeping genes (Simpson et al., 2000; Zhang et al., 2016). This analysis revealed that, although *H-ferritin* mRNA transcript levels were increased 1.15-fold along with a 1.62-fold increase in mRNA transcript levels of *L-ferritin* in retinas from TIM2$^{+/-}$, neither of the mRNA transcript levels was significantly upregulated (p=0.4742 and p=0.0778, respectively; n=6) (Figure 41).

Our results showed that despite the diminution of TIM2 receptors, retinal ferritin expression was increased. Since no significant *L-* and *H-ferritin* upregulation was detected, ferritin import into the retina seemed to be the mechanism responsible for ferritin content accumulation in this tissue.

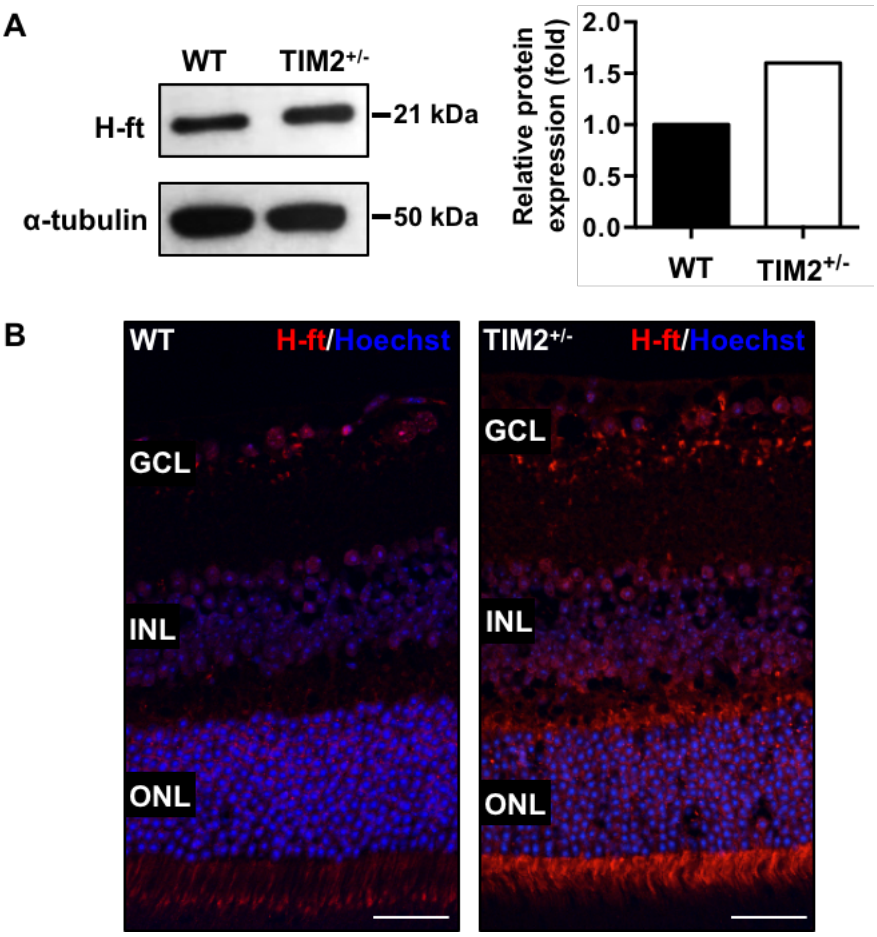

Figure 39. Analysis of H-ferritin protein expression in the retina. A. Western blot analysis and quantitative densitometry revealed that H-ferritin protein expression was increased in a pool of 12 TIM2$^{+/-}$ retinas in comparison to a pool of 12 WT retinas. α-tubulin was used as a loading control. **B.** Retinal sections immunostained with anti-H-ferritin antibody (red) showed increased expression throughout the retinal parenchyma of TIM2$^{+/-}$ mice compared to WT. Nuclei were counterstained with Hoechst (blue). GCL, ganglion cell layer; H-ft, H-ferritin; INL, inner nuclear layer; ONL, outer nuclear layer; WT, wild-type. Scale bars: WT = 31.36 μm; TIM2$^{+/-}$ = 34.55 μm.

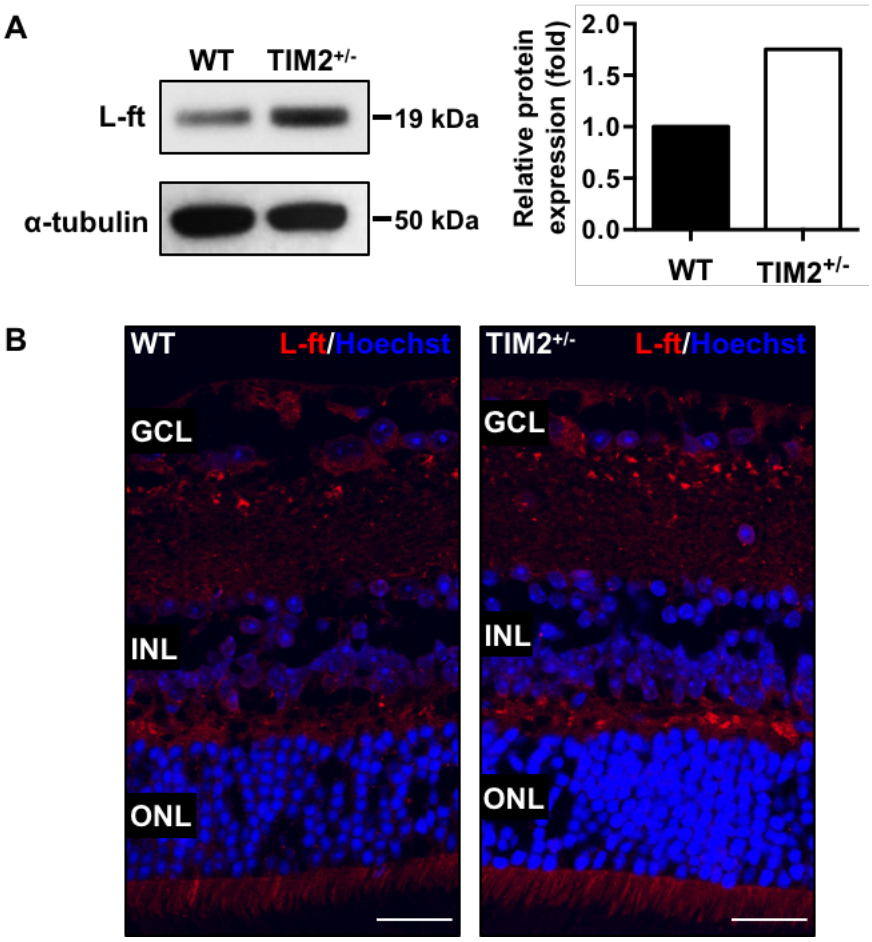

Figure 40. Analysis of L-ferritin protein expression in the retina. A. Western blot analysis and quantitative densitometry revealed that L-ferritin protein expression was increased in a pool of 12 TIM2$^{+/-}$ retinas in comparison to a pool of 12 WT retinas. α-tubulin was used as a loading control. **B.** Retinal sections immunostained with anti-L-ferritin antibody (red) showed increased expression throughout the retinal parenchyma of TIM2$^{+/-}$ mice compared to WT mice. Nuclei were counterstained with Hoechst (blue). GCL, ganglion cell layer; L-ft, L-ferritin; INL, inner nuclear layer; ONL, outer nuclear layer; WT, wild-type. Scale bars: WT = 24.58 µm; TIM2$^{+/-}$ = 24.58 µm.

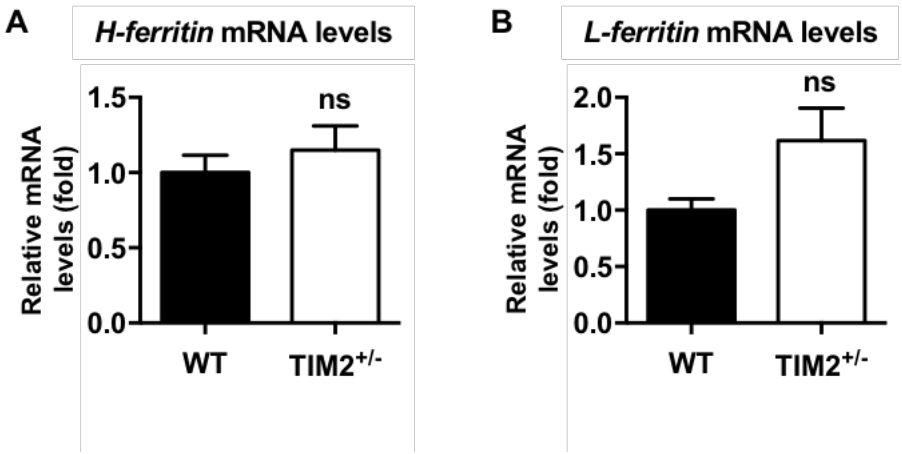

Figure 41. Analysis of *H-* and *L-ferritin* mRNA transcript levels in the retina. A. mRNA transcript levels of *H-ferritin* evaluated by qRT-PCR were not significantly increased in retinas from TIM2$^{+/-}$ mice compared with retinas from WT mice, after normalization with *36B4* and *GAPDH* housekeeping genes. **B.** mRNA transcript levels of *L-ferritin* evaluated by qRT-PCR were not significantly increased in retinas from TIM2$^{+/-}$ mice compared with retinas from WT mice, after normalization with *36B4* housekeeping gene. Data are presented as mean ± SEM (n=6). ns, not significant; WT, wild-type.

For cellular uptake, H-ferritin specifically binds to TIM2 (Chen et al., 2005) while L-ferritin binds to Scara5 membrane receptors (Li et al., 2009). In the light of the increased import of ferritin into the retina, we next evaluated ferritin entry through Scara5 specific binding to L-ferritin subunit.

We found that *Scara5* mRNA transcript levels, normalized by *36B4* and *GAPDH* housekeeping genes, were significantly upregulated (1.78-fold change; p=0.0404; n=6) in retinas from TIM2$^{+/-}$ mice compared to retinas from WT mice (Figure 42A).

Accordingly, Scara5 protein expression measured by western blot was also increased in TIM2$^{+/-}$ retinas, shown by a specific band with higher intensity with a molecular weight of 48 kDa. The quantification by densitometry confirmed Scara5 overexpression (1.60-fold change) in a pool of 12 retinas from TIM2$^{+/-}$ mice compared to a pool of 12 retinas from WT mice (Figure 42B).

Consistent with gene and protein overexpression, Scara5 immunohistochemical analysis also indicated increased expression of this protein in retinas from TIM2$^{+/-}$ mice (Figure 42C).

Our results showed that Scara5 was overexpressed in TIM2$^{+/-}$ retinas, suggesting that the increased ferritin import was mainly mediated by Scara5 receptors.

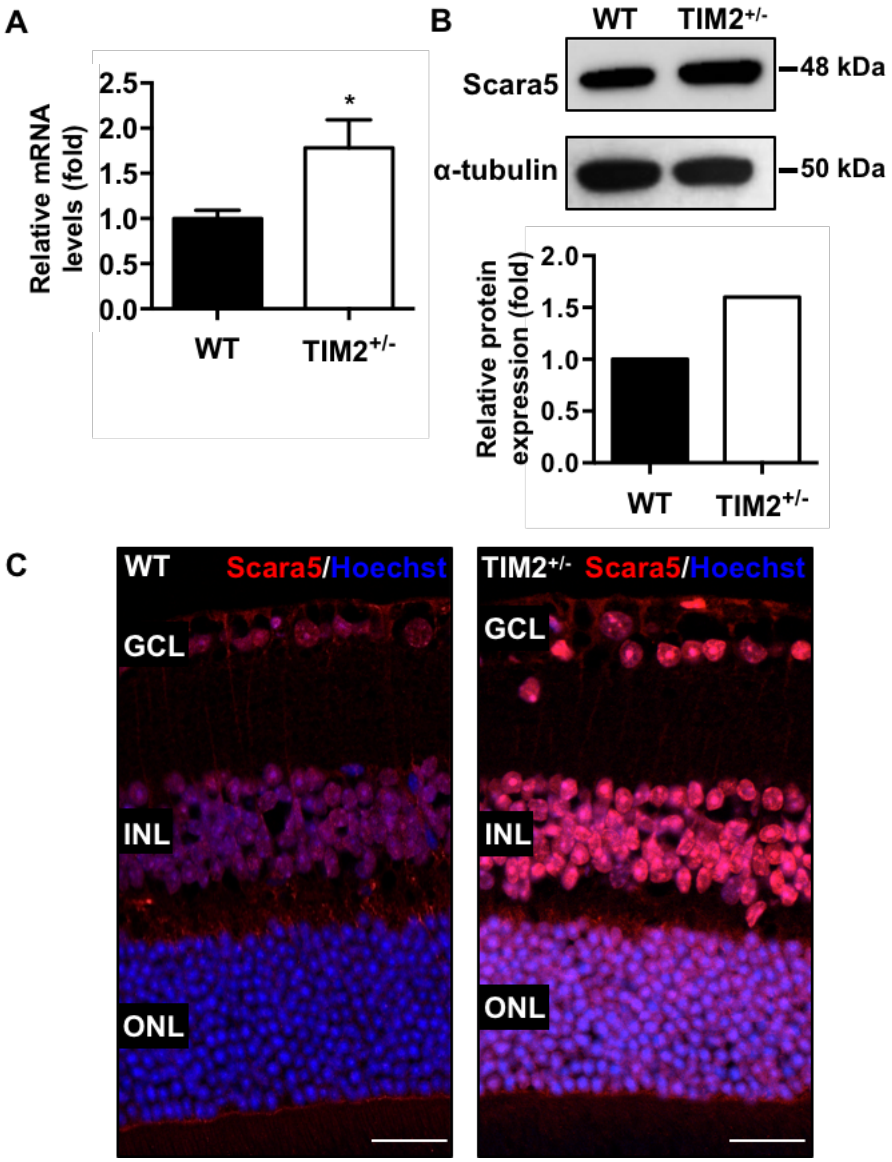

Figure 42. Analysis of Scara5 expression in the retina. A. *Scara5* mRNA transcript levels evaluated by qRT-PCR were significantly upregulated in retinas from TIM2$^{+/-}$ mice compared with retinas from WT mice, after normalization with *36B4* and *GAPDH* housekeeping genes. Data are presented as mean ± SEM (n=6). **B.** Western blot analysis and quantitative densitometry showed that Scara5 was increased in a pool of 12 TIM2$^{+/-}$ retinas in comparison to a pool of 12 WT retinas. α-tubulin was used as a loading control. **C.** Retinal sections immunostained with anti-Scara5 antibody (red) showed increased expression throughout the retinal parenchyma of TIM2$^{+/-}$ mice compared to WT mice. Nuclei were counterstained with Hoechst (blue). GCL, ganglion cell layer; INL, inner nuclear layer; ONL, outer nuclear layer; WT, wild-type. Asterisks indicate statistically significant differences: *p<0.05. Scale bars: WT = 26.35 μm; TIM2$^{+/-}$ = 23.65 μm.

C.2. Effects on transferrin and TfR1 expression

Once established the increased intake of exogenous ferritin through Scara5 receptors in TIM2$^{+/-}$ retinas, we next aimed to investigate the effects of TIM2 deficiency on transferrin and TfR1 expression.

Transferrin mRNA transcript levels, normalized by *36B4* and *GAPDH* housekeeping genes, were significantly upregulated (1.65-fold change; p=0.0449; n=6) in retinas from TIM2$^{+/-}$ mice compared with retinas from WT mice (Figure 43A). Transferrin protein expression measured by western blot and quantified by densitometry was also increased by 1.65-fold in a pool of 12 TIM2$^{+/-}$ retinas compared to a pool of 12 WT retinas (Figure 43B). Transferrin immunohistochemical analysis also indicated increased expression in the retina from TIM2$^{+/-}$ mice (Figure 43C).

TfR1 mRNA transcript levels, normalized by housekeeping genes *36B4* and *GAPDH*, were significantly upregulated (1.77-fold change; p=0.0177; n=6) in retinas from TIM2$^{+/-}$ mice compared with retinas from WT mice (Figure 44A). TfR1 protein expression measured by western blot and quantified by densitometry was also increased by 1.90-fold in a pool of 12 TIM2$^{+/-}$ retinas compared to a pool of 12 WT retinas (Figure 44B). Immunohistochemistry against TfR1 showed an increased in the protein expression in TIM2$^{+/-}$ retinas compared to WT retinas (Figure 44C).

Altogether, our results showed that besides exogenous ferritin accumulation, transferrin-bound iron import was also significantly increased in TIM2$^{+/-}$ retinas (Table 8).

Table 8. Iron-handling protein expression in TIM2$^{+/-}$ retinas vs. WT retinas.

Iron-handling proteins	Gene expression	Protein expression
H-ferritin	ns	+
L-ferritin	ns	++
Scara5	++	+
Transferrin	+	+
TfR1	++	++

ns, not significant; +, >1.5-fold change; ++, ≥1.75-fold change.

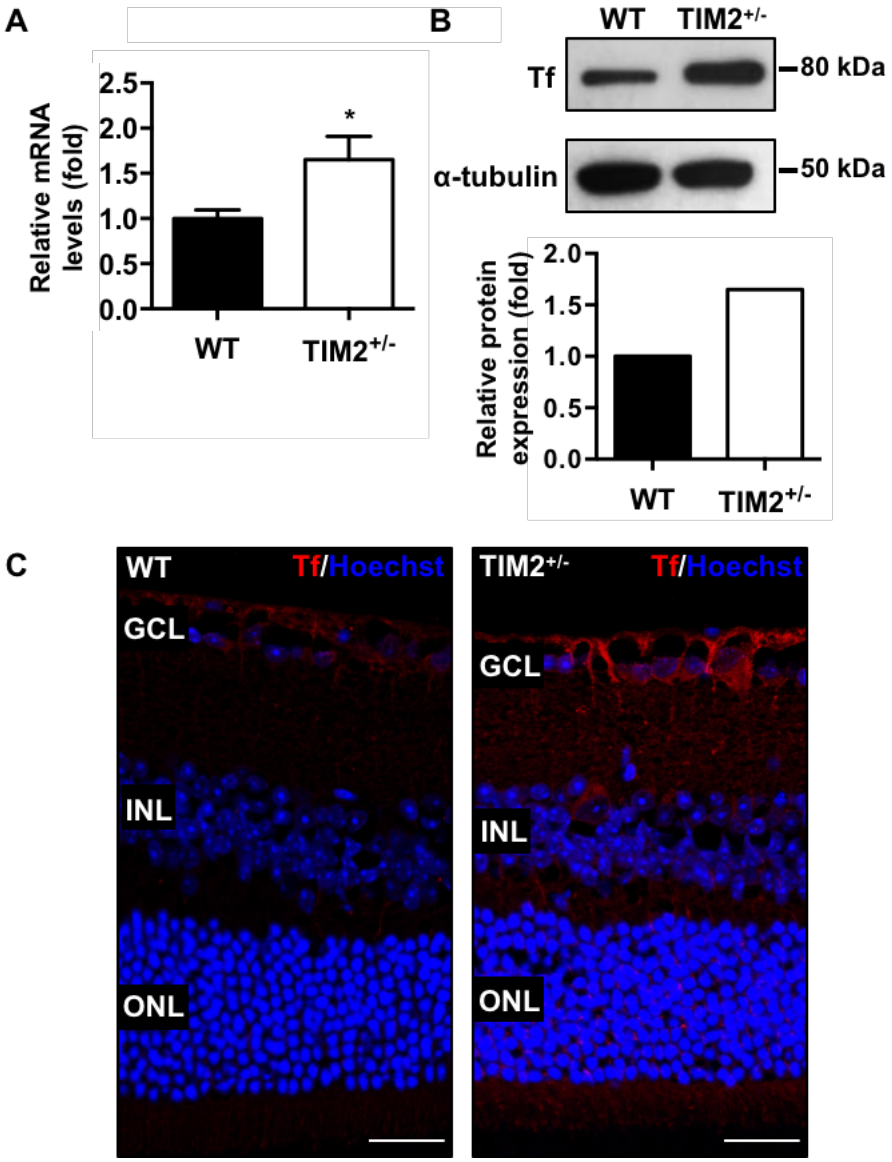

Figure 43. Analysis of transferrin expression in the retina. A. *Transferrin* mRNA transcript levels evaluated by qRT-PCR were significantly upregulated in retinas from TIM2$^{+/-}$ mice compared with retinas from WT mice, after normalization with *36B4* and *GAPDH* housekeeping genes. Data are presented as mean ± SEM (n=6). **B.** Western blot analysis and quantitative densitometry revealed that transferrin was increased in a pool of 12 TIM2$^{+/-}$ retinas in comparison to a pool of 12 WT retinas. α-tubulin was used as a loading control. **C.** Retinal sections immunostained with anti-transferrin antibody (red) showed increased expression throughout the retinal parenchyma of TIM2$^{+/-}$ mice compared to WT mice. Nuclei were counterstained with Hoechst (blue). GCL, ganglion cell layer; INL, inner nuclear layer; ONL, outer nuclear layer; Tf, transferrin; WT, wild-type. Asterisks indicate statistically significant differences: *p<0.05. Scale bars: WT = 26.85 µm; TIM2$^{+/-}$ = 24.58 µm.

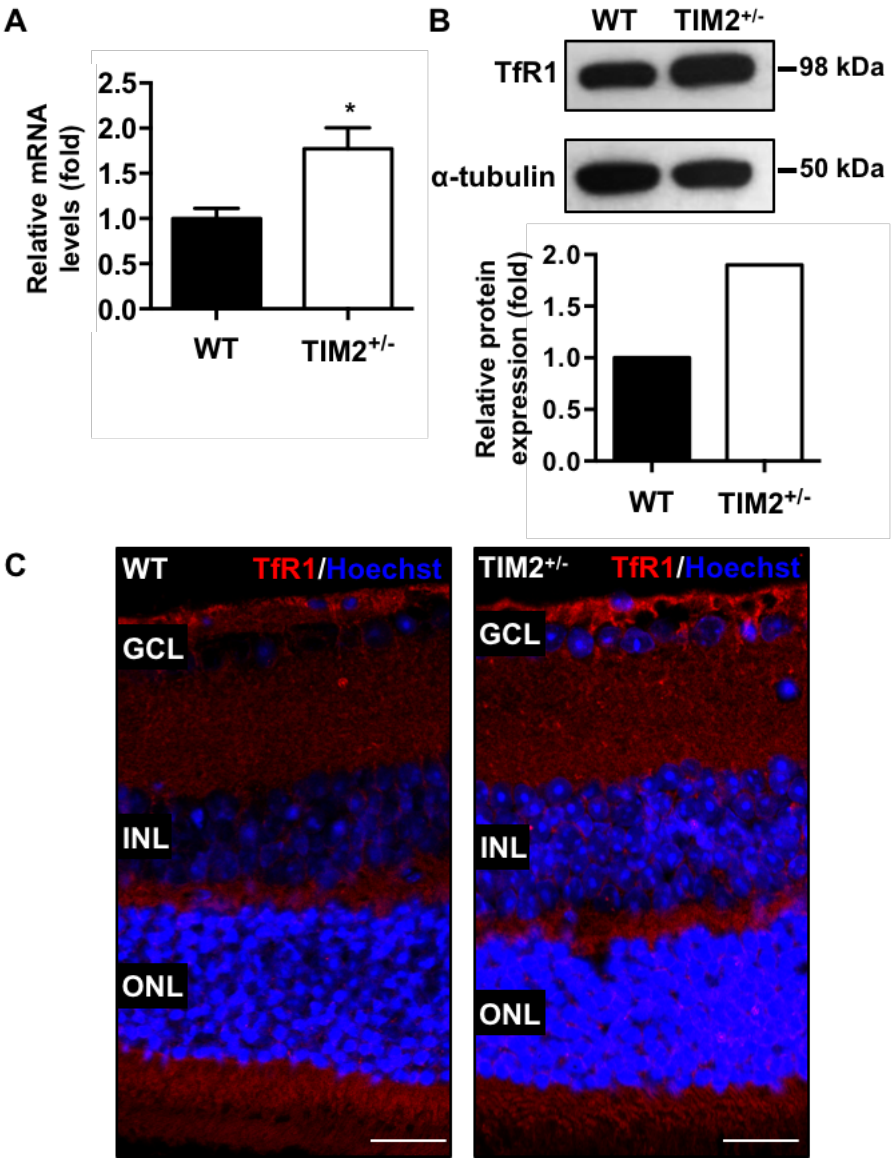

Figure 44. Analysis of TfR1 expression in the retina. A. *TfR1* mRNA transcript levels evaluated by qRT-PCR were significantly upregulated in retinas from TIM2$^{+/-}$ mice compared with retinas from WT mice, after normalization with *36B4* and *GAPDH* housekeeping genes. Data are presented as mean ± SEM (n=6). **B.** Western blot analysis and quantitative densitometry revealed that TfR1 was increased in a pool of 12 TIM2$^{+/-}$ retinas in comparison to a pool of 12 WT retinas. α-tubulin was used as a loading control. **C.** Retinal sections immunostained with anti-TfR1 antibody (red) showed increased expression throughout the retinal parenchyma of TIM2$^{+/-}$ mice compared to WT mice. Nuclei were counterstained with Hoechst (blue). GCL, ganglion cell layer; INL, inner nuclear layer; ONL, outer nuclear layer; WT, wild-type. Asterisks indicate statistically significant differences: *p<0.05. Scale bars: WT = 29.8 μm; TIM2$^{+/-}$ = 26.7 μm.

C.3. Effects on iron status

Having observed that the expression of iron carriers in the retina was increased in TIM2$^{+/-}$ mice, we next aimed to investigate the iron status.

We evaluated serum ferritin status in TIM2$^{+/-}$ mice by means of ELISA and, as expected, we observed a significant increase in serum ferritin levels in TIM2$^{+/-}$ mice compared to WT mice (1485 ± 79.85 vs. 1200 ± 81.09 ng/ml; p=0.0289; n=12) (Figure 45A).

We next assessed serum iron and unsaturated iron binding capacity, by means of standard biochemistry analyses. Serum iron, soluble Fe^{3+} and transferrin-bound Fe^{3+} (Geisser & Burckhardt, 2011), levels were similar between TIM2$^{+/-}$ and WT mice (103.2 ± 6.362 vs. 106.3 ± 6.396 µg/dl; p=0.7569; n=12) (Figure 45B).

Transferrin saturation percentage over 60% is suggestive of iron overload (Santos et al., 2000; Chaudhury et al., 2006). Transferrin saturation percentage in serum, inferred by the ratio between serum iron and total iron binding capacity, did not differ significantly between TIM2$^{+/-}$ and WT mice (33. 24 ± 1.868 % vs. 33.39 ± 2.199 %; p=0.9614; n=12) (Figure 45C), revealing normal serum iron state in TIM2$^{+/-}$ mice.

These results showed that, although in TIM2$^{+/-}$ mice serum iron levels were normal, serum ferritin levels were significantly increased, consistent with ferritin overexpression observed in the retinal parenchyma.

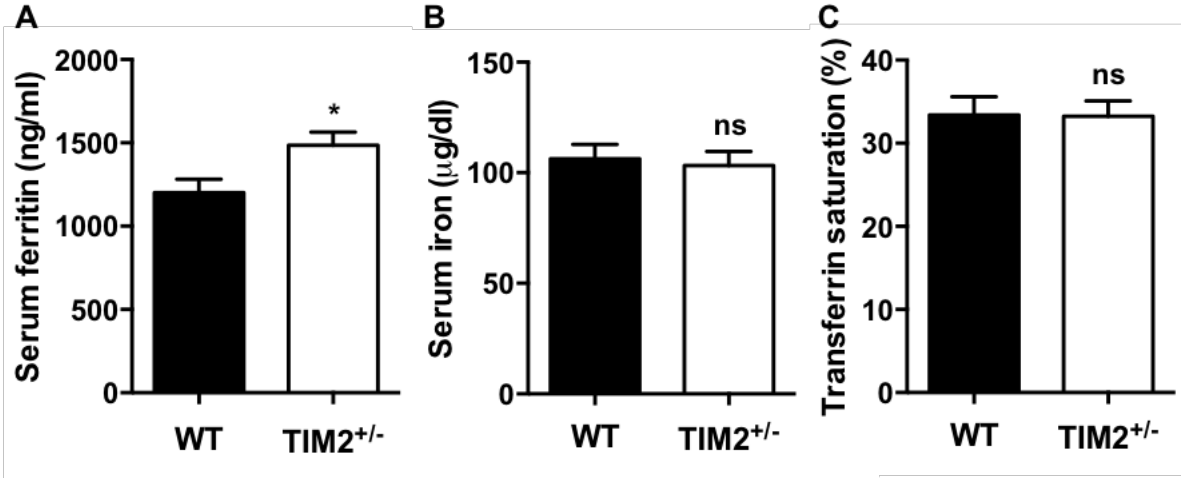

Figure 45. Analysis of iron status. A. Serum ferritin level evaluated by ELISA was significantly increased in TIM2$^{+/-}$ mice compared to WT mice. **B.** The analysis of serum iron showed no significant differences between TIM2$^{+/-}$ and WT mice. **C.** Transferrin saturation percentage in serum was similar between TIM2$^{+/-}$ and WT mice. Data are presented as mean ± SEM (n=12). ns, not significant; WT, wild-type. Asterisks indicate statistically significant differences: *p<0.05.

C.4. Localization of ferritin in the retina

In light of ferritin accumulation in the retina of TIM2$^{+/-}$ mice, we next studied the cellular distribution of this protein. The presence of ferritin molecules can be evidenced from the spherical shape and size (~ 8 nm) of their electron-dense cores in TEM (Massover & Cowley, 1973; Iancu, 1992). Regarding this, the localization of ferritin in TIM2$^{+/-}$ retinas was analyzed by means of TEM, revealing an increase in the number of spherical electron-dense particles, mainly observed in Müller cells, particularly at the level of their inner cytoplasmic prolongations (Figure 46). The size of these spherical electron-dense particles was ~ 8 nm, compatible with that of ferritin (Figure 47), confirming the accumulation of ferritin in TIM2$^{+/-}$ retinas in accordance to previous protein overexpression observed.

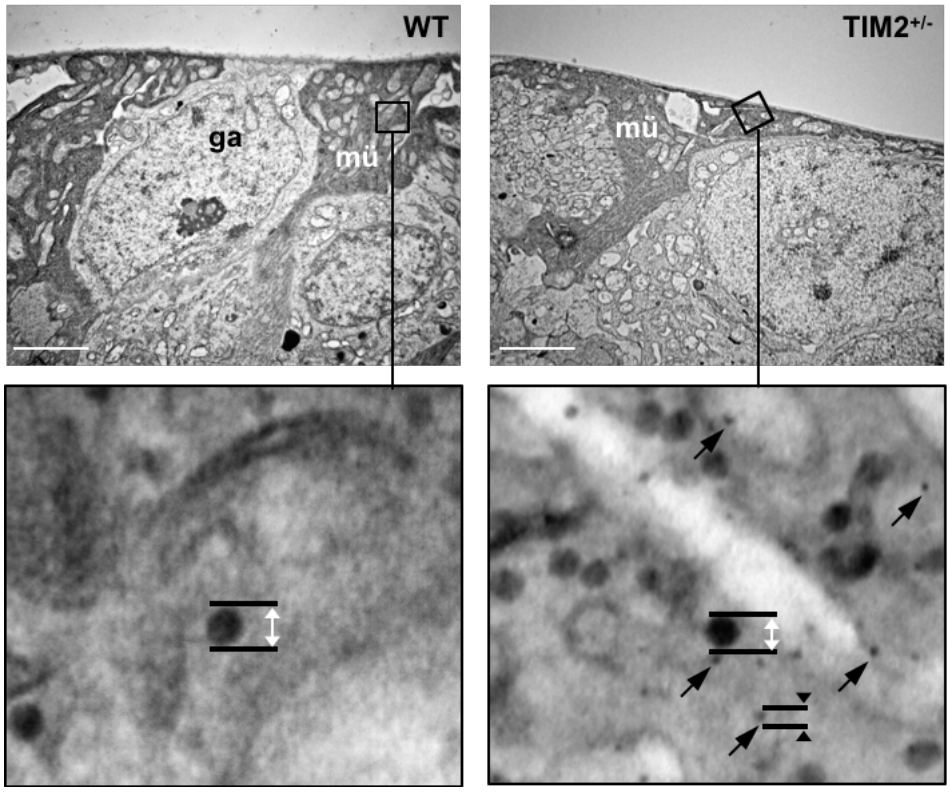

Figure 46. Localization of ferritin in the retina. Transmission electron microscopy analysis of retinas from TIM2$^{+/-}$ mice showed an increase in electron-dense particles (black arrows), mainly localized in Müller cells. The size of the spherical electron-dense particles was ~ 8 nm, compatible with the size of ferritin (arrowheads), while the measured size of larger electron-dense particles was ~ 30 nm, compatible with glycogen (white arrows). ga, ganglion cell; mü, Müller cell; WT, wild-type. Scale bars: WT = 2.96 µm; TIM2$^{+/-}$ = 2.96 µm.

C.5. Evaluation of iron content in retinal ferritin

Considering the accumulation of ferritin electron-dense particles in Müller cells in TIM2$^{+/-}$ retinas, we next investigated their iron content. Under TEM, metal-charged molecules, like iron-loaded ferritin, present a characteristic electron-density in unstained ultrathin sections. However, to be visualized, ferritin must contain at least 1500 atoms of iron (Iancu, 1983; Iancu & Manov, 2017).

TEM images of unstained ultrathin sections of retinas from TIM2$^{+/-}$ mice revealed the presence of ~ 8 nm electro-dense particles in Müller cells, compatible with iron-loaded ferritin (Figure 47A). Digital light inversion of micrographs allowed an easier visualization of these electro-dense structures (Figure 47B). In order to identify its metallic component, we performed energy dispersive X-ray spectroscopy, focusing in ~ 8 nm particles compatible with iron-loaded ferritin (Figure 47C). Our results confirmed the presence of iron in these ~ 8 nm electro-dense particles (4.91 ± 0.43 %), corroborating the presence of iron-loaded ferritin in TIM2$^{+/-}$ mice Müller cells.

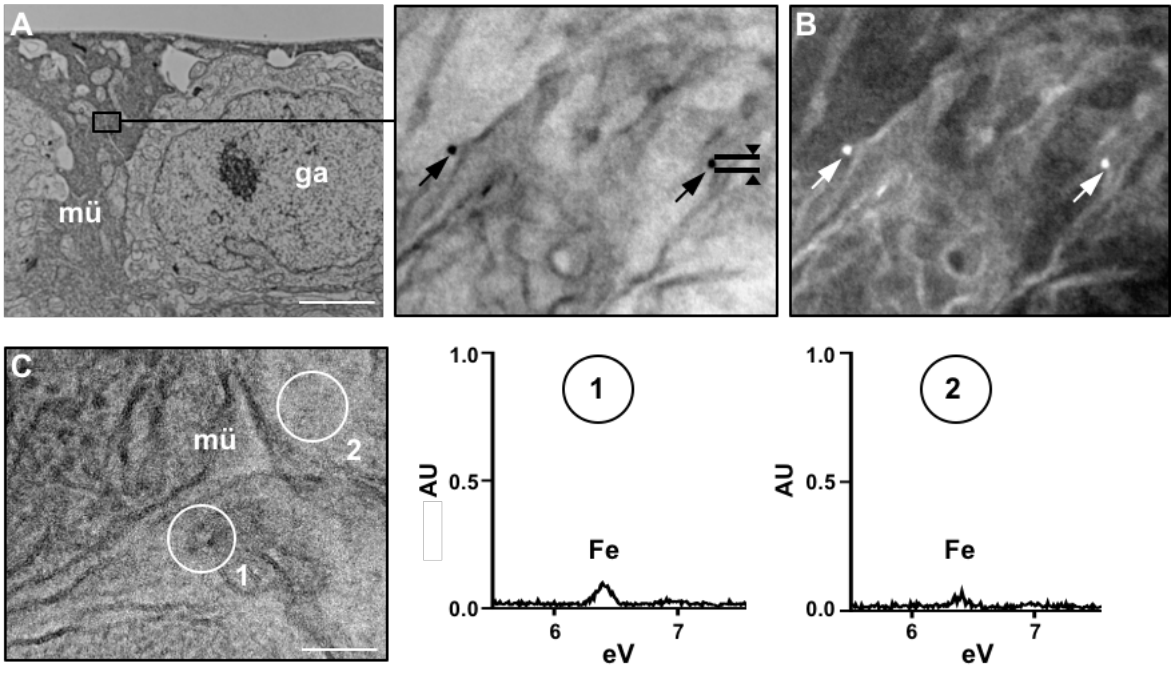

Figure 47. Analysis of iron content in ferritin in the retina. A. Transmission electron microscopy analysis of unstained ultrathin sections of retinas from TIM2$^{+/-}$ mice showed ~ 8 nm size (arrowheads) metal-charged particles, compatible with iron-loaded ferritin (black arrows). **B.** Inverted micrograph emphasizing the same metal-charged particles compatible with iron-loaded ferritin (white arrows). **C.** Energy dispersive X-ray spectroscopy analysis revealed a higher peak corresponding to iron in particles compatible with ferritin (1) in comparison to adjacent areas (2). AU, arbitrary units; eV, electron volts; Fe, iron; ga, ganglion cell; mü, Müller cell. Scale bars: A = 2.7 µm; C = 0.08 µm.

C.6. Evaluation of iron content in the retina

Taking in consideration the increase in iron-loaded ferritin, we next evaluated the total retinal iron content in TIM2$^{+/-}$ mice by means of inductively coupled plasma mass spectrometry and colorimetric analysis.

Inductively coupled plasma mass spectrometry analysis showed a significant increase of iron content in retinas from TIM2$^{+/-}$ mice when compared with retinas from WT mice (0.038 ± 0.002 vs. 0.032 ± 0.0018 µg; p=0.0442; n=10) (Figure 48A).

Consistently, the colorimetric analysis of retinal iron using a commercial iron assay kit revealed that iron was increased in a pool of 10 retinas from TIM2$^{+/-}$ mice compared to a pool of 10 retinas from WT mice (1.2138 vs. 1.1034 µg/ml) (Figure 48B).

Altogether, our results confirmed that retinal iron overload was present in parallel with serum and retinal ferritin accumulation.

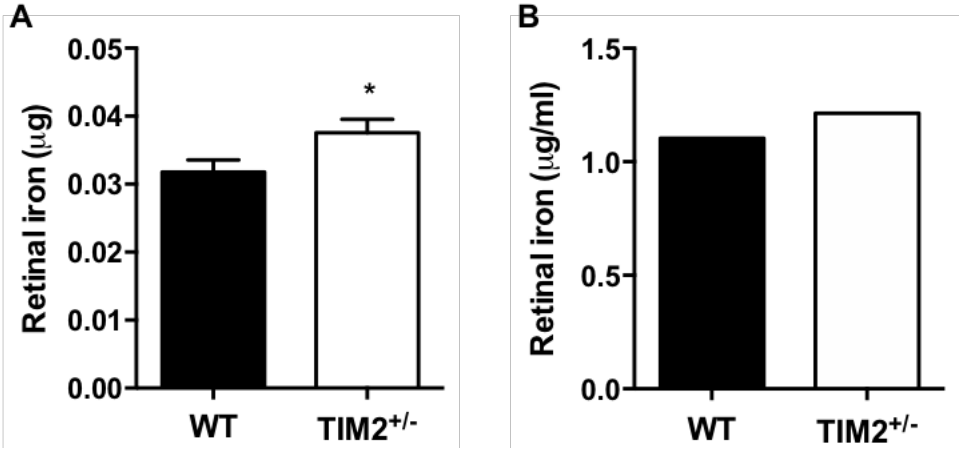

Figure 48. Analysis of iron content in the retina. A. The retinal iron content analyzed by inductively coupled mass spectrometry revealed that iron was significantly increased in retinas from TIM2$^{+/-}$ mice compared with retinas from WT mice. Data are presented as mean ± SEM (n=10). **B.** The analysis of retinal iron by colorimetric assay using a commercial iron assay kit also demonstrated an increase in iron in a pool of 10 retinas from TIM2$^{+/-}$ mice in comparison to a pool of 10 retinas from WT mice. WT, wild-type. Asterisks indicate statistically significant differences: *p<0.05.

D. Assessment of retinal iron overload effects in TIM2$^{+/-}$ mice

D.1. Effects on vascular integrity

Once established a significant iron overload in retinas from TIM2$^{+/-}$ mice, we next examined its consequences in vascular integrity. In order to do this, *in vivo* fluorescein angiography was performed. Retinal vascularization was readily visualized with a scanning laser ophthalmoscope, revealing focal points of vascular leakage in TIM2$^{+/-}$ mice (Figure 49).

This result suggested that iron overload in TIM2$^{+/-}$ retinas was associated with increased permeability.

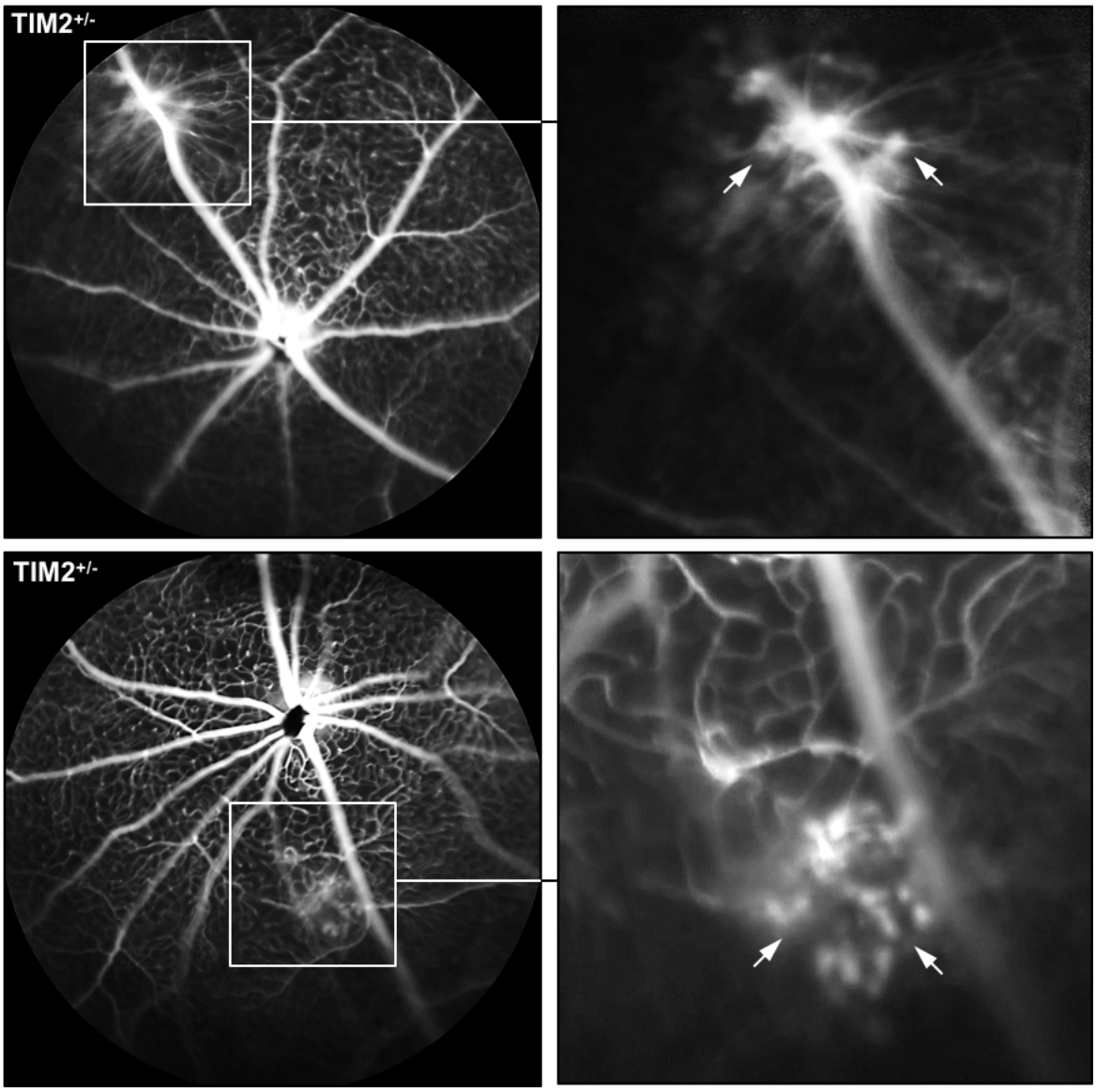

Figure 49. Assessment of vascular integrity in the retina. Fundus fluorescein angiograms acquired *in vivo* by SLO showed retinal vascular leakage (arrows) in TIM2$^{+/-}$ mice.

Serum albumin has been used as a tracer to assess BRB function. The demonstration of extravascular albumin within the neural retina is indicative of BRB failure (Vinores, 1995; Minshall & Malik, 2006). To further assess vascular permeability and BRB integrity, albumin extravasation was studied. For this purpose, FITC-BSA was injected intravenously in 6 TIM2$^{+/-}$ and 6 WT mice. Visualization *in vivo* by means of SLO showed diffuse leakage of FITC-BSA in the retinal parenchyma of retinas from TIM2$^{+/-}$ mice compared to exclusively intravascular FITC-BSA in WT retinas (Figure 50).

Accordingly, confocal microscopy analyses of whole-mount retinas and paraffin embedded retinal sections from mice injected intravenously with FITC-BSA and immunolabeled with anti-collagen IV antibody, for blood vessel basement membrane identification, showed diffuse extravasation of FITC-BSA (Figure 51A), with higher accumulation at BRB breakdown sites in TIM2$^{+/-}$ retinal blood vessels (Figure 51B).

The presence of vascular leakage was an indicative of BRB breakdown, confirming the increased vascular permeability in TIM2$^{+/-}$ mice probably due to vascular integrity loss.

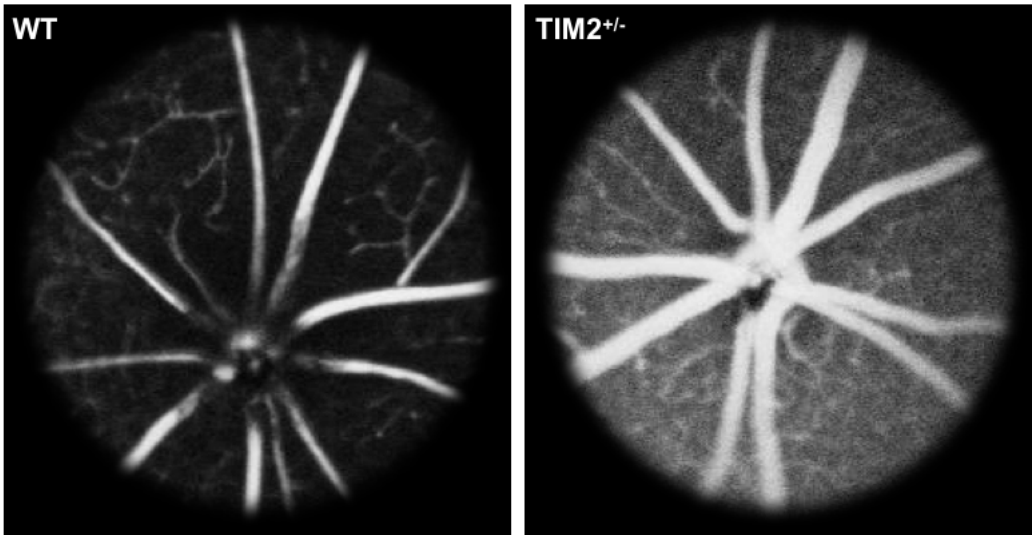

Figure 50. Assessment of vascular permeability in the retina. The permeability of BRB was assessed by intravenous injection of FITC-BSA. Fundus angiograms acquired *in vivo* by SLO showed diffuse leakage of FITC-BSA in the retinal parenchyma of retinas from TIM2$^{+/-}$ mice compared to exclusively intravascular FITC-BSA in WT retinas. WT, wild-type.

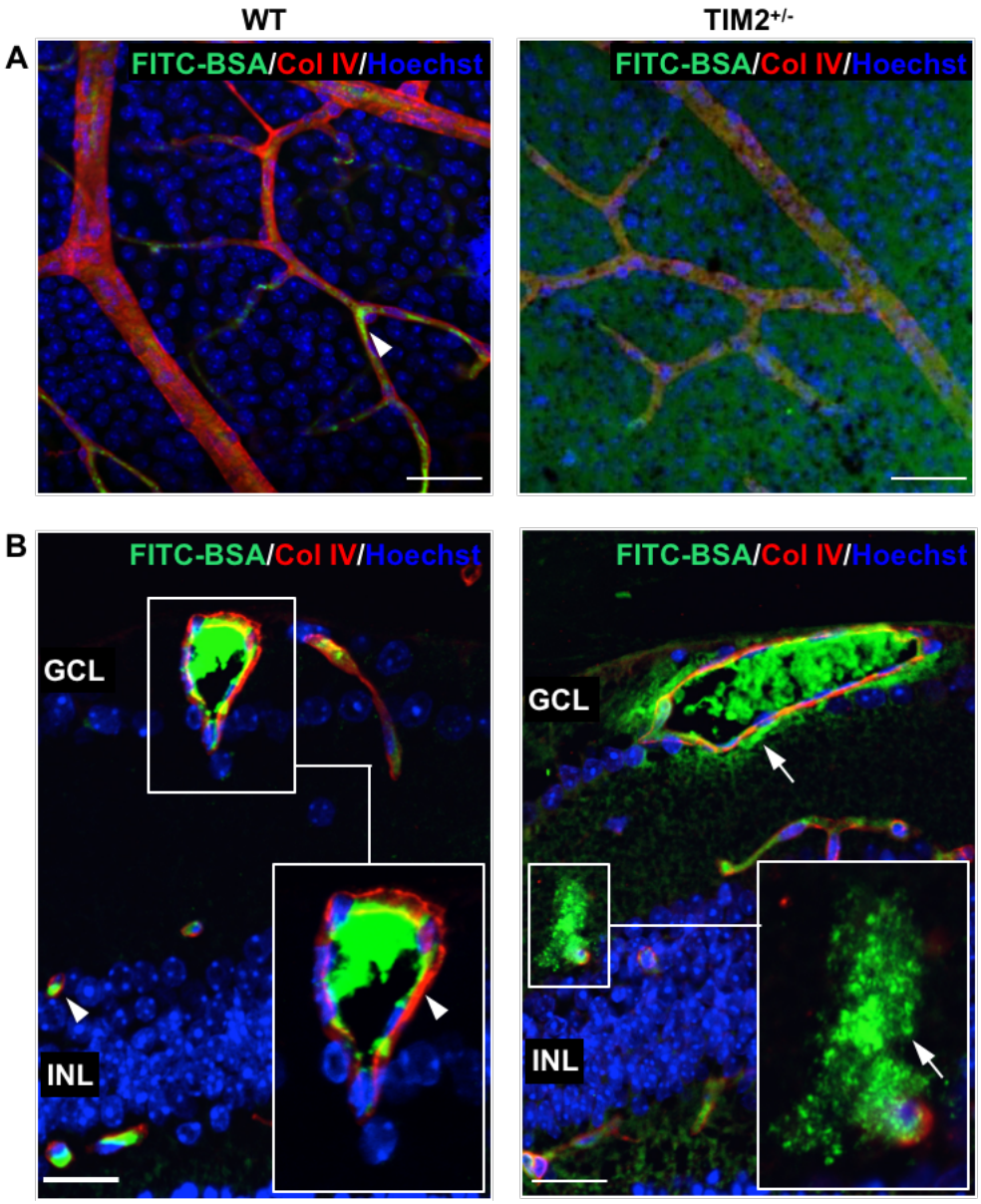

Figure 51. Assessment of blood-retinal barrier integrity. A. Confocal microscopy analysis of whole-mount retinas from mice injected intravenously with FITC-BSA revealed diffuse extravascular FITC-BSA (green) in the parenchyma of retinas from TIM2$^{+/-}$ mice immunostained with anti-collagen IV antibody (red) compared to exclusively intravascular FITC-BSA (arrowhead) observed in WT retinas. **B.** A number of blood vessels in retinal sections from TIM2$^{+/-}$ mice presented extravascular FITC-BSA (green; arrows) in the parenchyma adjacent to the blood basement membrane stained with anti-collagen IV antibody (red) compared to exclusively intravascular FITC-BSA (arrowhead) observed in WT retinas. Nuclei were counterstained with Hoechst (blue). Col IV, collagen IV; FITC-BSA, fluorescein isothiocyanate conjugated-bovine serum albumin; GCL, ganglion cell layer; INL, inner nuclear layer; WT, wild-type. Scale bars: (A) WT = 39.68 µm; TIM2$^{+/-}$ = 39.68 µm; (B) WT = 22.86 µm; TIM2$^{+/-}$ = 26.89 µm.

D.2. Evaluation of edema

A consequence of BRB breakdown is abnormal inflow and accumulation of proteins and fluids into the neuroretinal tissue, which leads to edema formation. Edema is characterized by focal enlargement of the extracellular space and retinal thickening, contributing to vision loss by altering the functional cell relationship (Cunha-Vaz, 1976; Coscas, Cunha-Vaz & Soubrane, 2010; Daruich et al., 2018). Considering the previous result, we proceeded to assess the presence of edema in TIM2$^{+/-}$ retinas.

TEM analysis of retinal blood vessels of TIM2$^{+/-}$ mice revealed perivascular spaces surrounding blood vessels, consistent with the accumulation of fluid in the extracellular space, mainly at the level of ganglion cell layer (Figure 52A).

Quantitative assessment of retinal thickness, widely considered a reliable method to evaluate edema formation (Shahidi et al., 1991; Cunha-Vaz, 2010), was performed in histological sections stained with H-E in a central area, a medial area, and a peripheric area on both sides of the optic disc (Figure 52B). The result showed that TIM2$^{+/-}$ retinas were significantly thicker than WT retinas in all measured areas, with the highest difference observed in that closest to the optic disc (219.6 ± 4.18 vs. 191.0 ± 7.023 µm; p=0.0091) (Figure 52C).

Taken together, our results confirmed that increased vascular permeability and BRB breakdown induced edema in TIM2$^{+/-}$ retinas, which was more pronounced in the central part of the retina.

D.3. Effects on vascular morphology

Since abnormalities in the retinal vascular pattern, such as changes in vessel shape and tortuosity, are often associated with the occurrence of retinopathies (Joshi, 2012; McLenachan et al., 2015), we aimed to assess if the vascular morphology was also affected. Vascular tortuosity was studied in 2D fundus fluorescein images of 10 mice per group (Figure 53A), and its index was defined as the ratio of the vessel length over the linear distance of the same vascular segment (Figure 53B) (Mohsenin et al., 2013).

Quantitative analysis of vascular tortuosity revealed no significant differences between WT and TIM2$^{+/-}$ retinas, either in arterioles (1.048 ± 0.0024 vs. 1.056 ± 0.005 AU; p=0.1299) (Figure 53C) or venules (1.033 ± 0.0017 vs. 1.035 ± 0.0024 AU; p=0.4344) (Figure 53D).

Our results showed a normal vascular pattern in TIM2$^{+/-}$ retinas, excluding vascular tortuosity as a possible cause for the increased permeability observed.

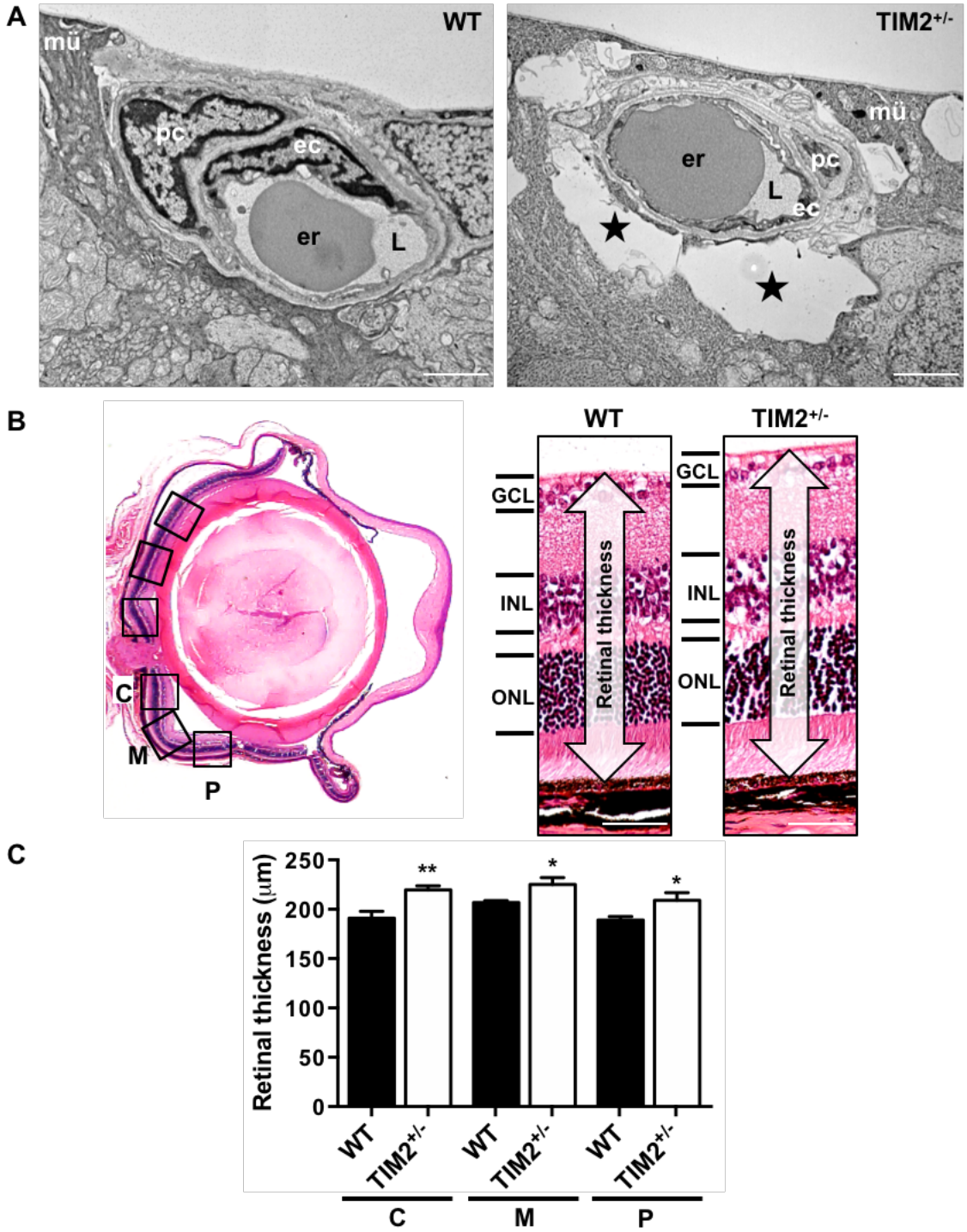

Figure 52. Evaluation of edema formation in the retina. A. Transmission electron microscopy analysis of retinal vessels revealed perivascular spaces (stars) surrounding the blood vessel wall of TIM2$^{+/-}$ mice, consistent with the presence of edema. **B.** Total thickness was assessed in a central area (C), a medial area (M), and a peripheric area (P) on both sides of the optic disc in retinal sections stained with H-E from WT and TIM2$^{+/-}$ mice. **C.** Quantitative analysis of total retinal thickness revealed that retinas from TIM2$^{+/-}$ mice were significantly thicker in all measured areas than retinas from WT mice. Data are presented as mean ± SEM (n=6). Asterisks indicate statistically significant differences: *p<0.05, **p<0.01. ec, endothelial cell; er, erythrocyte; GCL, ganglion cell layer; INL, inner nuclear layer; L, lumen; mü, Müller cell; pc, pericyte; ONL, outer nuclear layer; WT, wild-type. Scale bars: (A) WT = 2.03 µm; TIM2$^{+/-}$ = 1.68 µm; (B) WT = 35.23 µm; TIM2$^{+/-}$ = 35.25 µm.

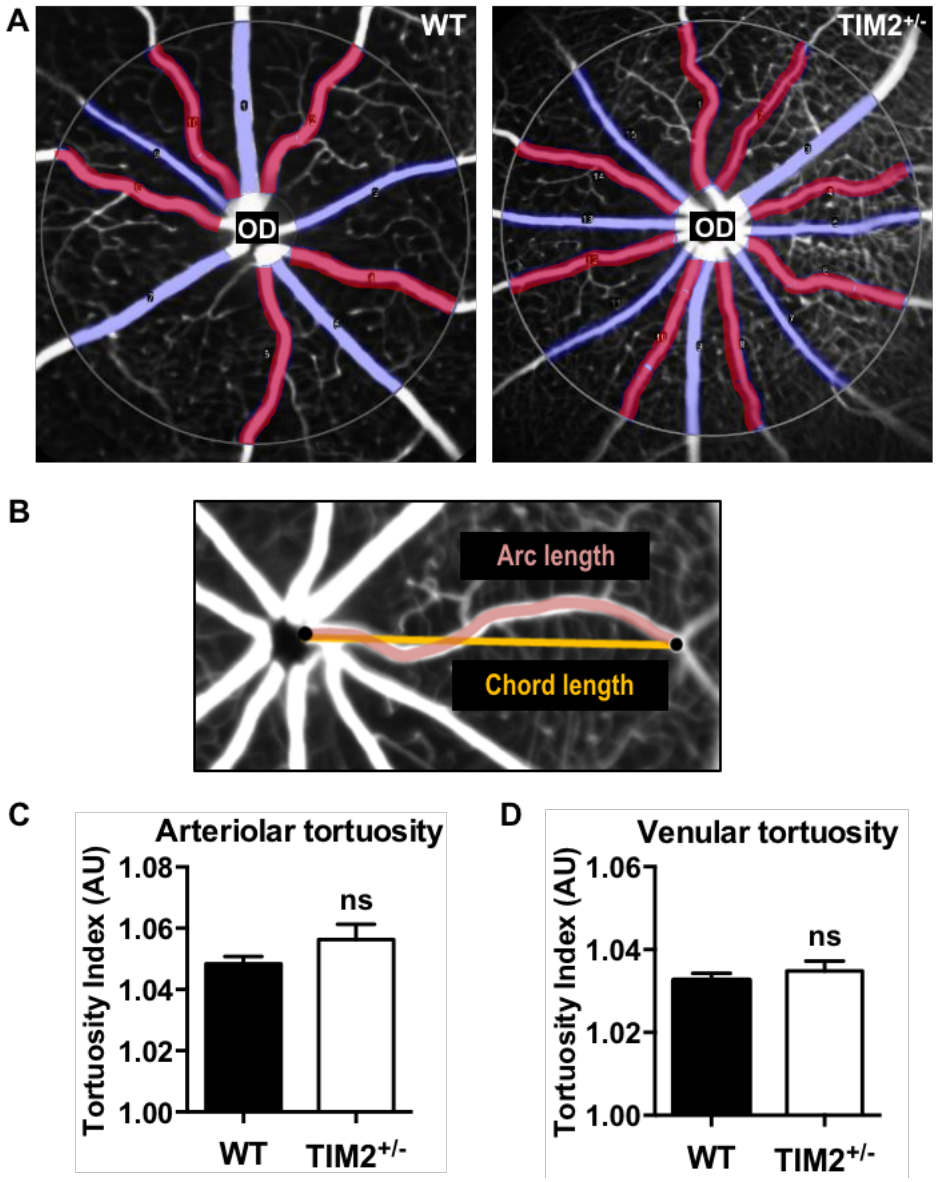

Figure 53. Assessment of vascular tortuosity in the retina. A. Vascular tortuosity was assessed in retinal arterioles (red) and venules (blue) of WT and TIM2$^{+/-}$ mice using 2D images of fundus fluorescein angiograms acquired by SLO. **B.** Tortuosity index was calculated by dividing the arc length by the chord length. Quantitative analysis of vascular tortuosity revealed no significant differences of tortuosity in retinal arterioles (**C**) or retinal venules (**D**) between WT and TIM2$^{+/-}$ mice. Data are presented as mean ± SEM (n=10). AU, arbitrary units; ns, not significant; OD, optic disc; WT, wild-type.

D.4. Effects on paracellular transport

In BBB and BRB, the very tight control of solute and fluid flux across the endothelium is conferred by well-developed tight junctions (Klaassen et al., 2013). As shown above, vascular leakage was evident in TIM2$^{+/-}$ retinas. We next focused in the analysis of tight junction integrity in retinal endothelial cells of TIM2$^{+/-}$ mice, knowing that tight junction disruption leads to BRB breakdown, increased permeability, and paracellular transport alteration.

Ultrathin sections of retinas analyzed by TEM revealed a reduced electron-density of tight junctions and slight separation between adjacent membranes of neighboring endothelial cells in TIM2$^{+/-}$ mice (Figure 54), confirming compromised endothelial cell-cell junctional integrity and altered paracellular transport.

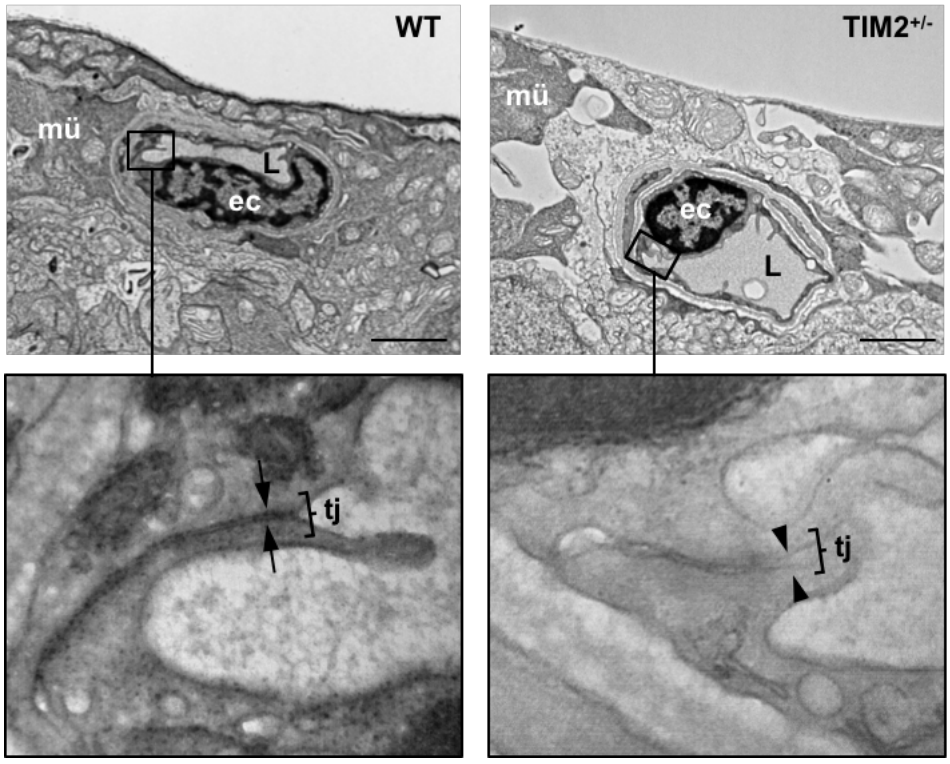

Figure 54. Ultrastructural analysis of tight junctions in the retina. Transmission electron microscopy analysis of retinal blood vessels from TIM2$^{+/-}$ mice revealed reduced electron-density of tight junctions and slight separation (arrowheads) between adjacent membranes of neighboring endothelial cells in comparison to strong electro-dense tight junctions (arrows) in retinal capillaries from WT mice, due to close apposition of transmembrane molecules. ec, endothelial cell; L, lumen; mü, Müller cell; tj, tight junction; WT, wild-type. Scale bars: WT = 1.57 µm; TIM2$^{+/-}$ = 1.56 µm.

Considering the morphological alterations observed, we further analyzed the expression of the main proteins that constitute tight junctions, ZO-1, claudin-5, and occludin, by western blot and immunohistochemistry analyses with specific antibodies (Haurigot et al., 2009).

Western blot analysis revealed a decrease of ZO-1 protein expression, consistent with decreased intensity of the 220 kDa band, in TIM2$^{+/-}$ retinas compared to WT retinas. Quantitative densitometry confirmed reduced ZO-1 protein expression (0.52-fold change) in a pool of 12 retinas from TIM2$^{+/-}$ mice relative to a pool of 12 retinas from WT mice (Figure 55A). Consistently, whole-mount retinas immunolabeled with anti-ZO-1 and anti-collagen IV antibodies showed a disruption in the continuity of ZO-1 staining along endothelial cell borders in blood vessels of TIM2$^{+/-}$ mice, while intact ZO-1 expression along the contour of endothelial cells was observed in retinal blood vessels of WT mice (Figure 55B).

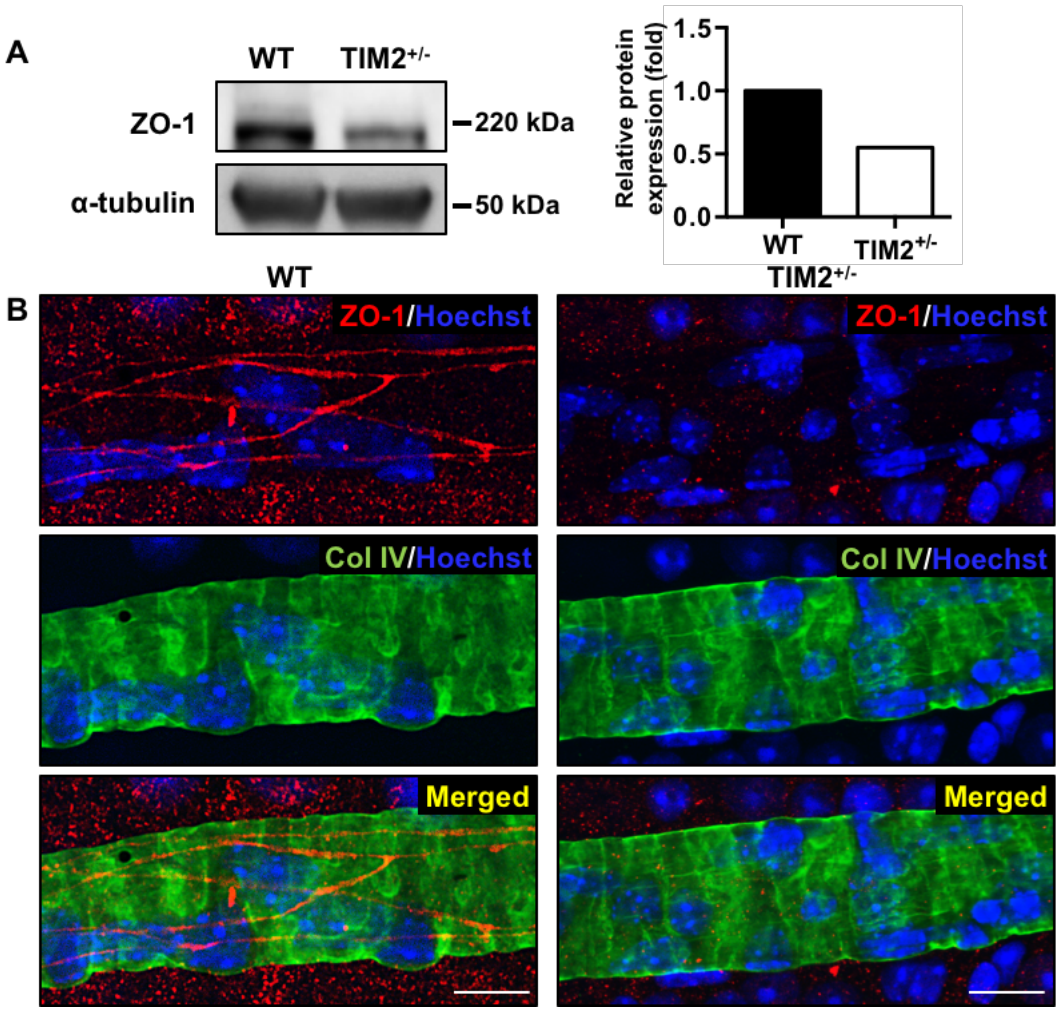

Figure 55. Analysis of ZO-1 expression in the retina. A. Western blot analysis and quantitative densitometry revealed reduced ZO-1 protein expression in a pool of 12 TIM2$^{+/-}$ retinas relative to a pool of 12 WT retinas. α-tubulin was used as a loading control. **B.** Confocal microscopy analysis of whole-mount retinas stained with anti-ZO-1 (red) and anti-collagen IV (green*)* antibodies showed disrupted ZO-1 expression in blood vessels of TIM2$^{+/-}$ mice compared to intact expression in blood vessels of WT mice. Nuclei were counterstained with Hoechst (blue). Col IV, collagen IV; WT, wild-type. Scale bars: WT = 9.02 μm; TIM2$^{+/-}$ = 14.33 μm.

A reduced intensity of the specific band of claudin-5, with a molecular weight of 25 kDa, compatible with a decrease of claudin-5 protein expression, was also observed in TIM2$^{+/-}$ retinas compared to WT retinas. The quantification by densitometry confirmed reduced claudin-5 protein expression (0.70-fold change) in a pool of 12 retinas from TIM2$^{+/-}$ mice relative to a pool of 12 retinas from WT mice (Figure 56A). This was paralleled by a reduced claudin-5 staining in endothelial cell borders in TIM2$^{+/-}$ retinal blood vessels compared to the intact claudin-5 expression in retinal blood vessels of WT mice observed by means of immunohistochemistry analysis (Figure 56B).

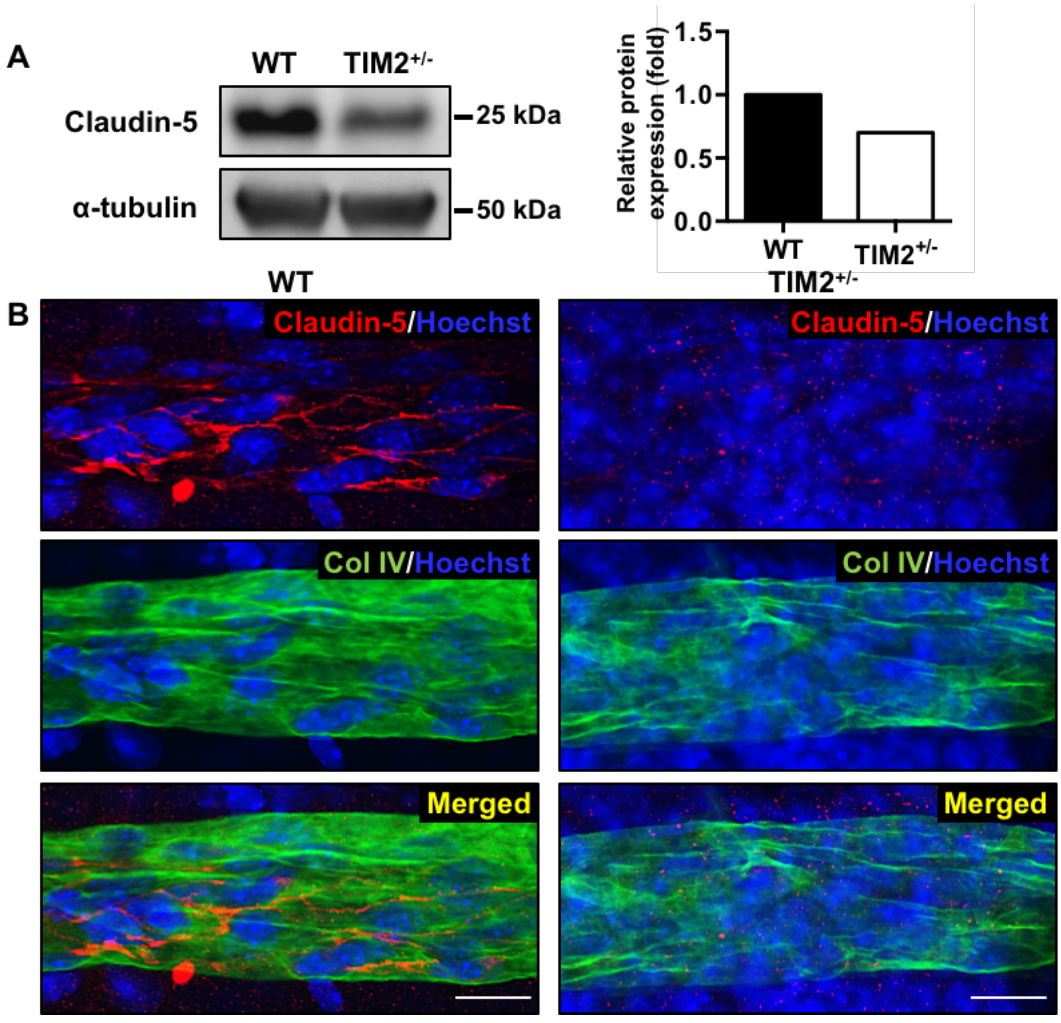

Figure 56. Analysis of claudin-5 expression in the retina. A. Western blot analysis and quantitative densitometry demonstrated a decrease of claudin-5 protein expression in a pool of 12 TIM2$^{+/-}$ retinas in comparison to a pool of 12 WT retinas. α-tubulin was used as a loading control. **B.** Confocal microscopy analysis of whole-mount retinas stained with anti-claudin-5 (red) and anti-collagen IV (green) antibodies showed disrupted expression of claudin-5 in blood vessels of TIM2$^{+/-}$ mice compared to intact expression in blood vessels of WT mice. Nuclei were counterstained with Hoechst (blue). Col IV, collagen IV; WT, wild-type. Scale bars: WT = 13.48 μm; TIM2$^{+/-}$ = 14.51 μm.

The analysis of occludin protein expression by western blot also demonstrated a decrease of occludin protein expression in TIM2$^{+/-}$ retinas compared to WT retinas, consistent with a decrease in the intensity of the 53 kDa band observed. Quantitative densitometry confirmed reduced occludin protein expression (0.60-fold change) in a pool of 12 retinas from TIM2$^{+/-}$ mice relative to a pool of 12 retinas from WT mice (Figure 57A). Similarly, immunohistochemistry against occludin showed a disrupted stain in retinal blood vessels of TIM2$^{+/-}$ mice compared to the intact occludin expression in retinal blood vessels of WT mice (Figure 57B).

Altogether, these results showed a decrease in the levels of ZO-1, claudin-5, and occludin, accounting for tight junction integrity loss in retinas from TIM2$^{+/-}$ mice, which led to paracellular transport alteration, increased permeability, and BRB failure.

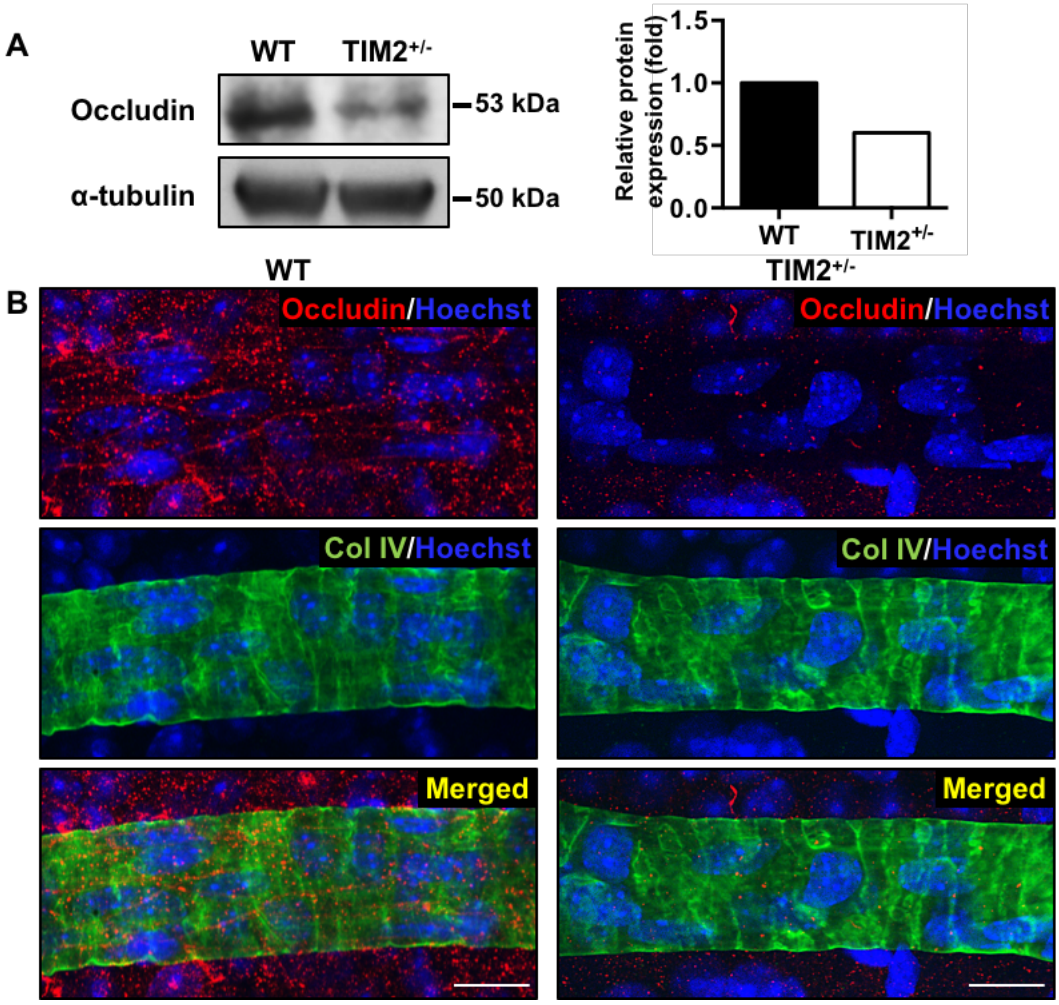

Figure 57. Analysis of occludin expression in the retina. A. Western blot analysis and quantitative densitometry revealed a decrease of occludin protein expression in a pool of 12 TIM2$^{+/-}$ retinas in comparison to a pool of 12 WT retinas. α-tubulin was used as a loading control. **B.** Confocal microscopy analysis of whole-mount retinas stained with anti-occludin (red) and anti-collagen IV (green) antibodies showed disrupted occludin expression in blood vessels of TIM2$^{+/-}$ mice compared to intact expression in blood vessels of WT mice. Nuclei were counterstained with Hoechst (blue). Col IV, collagen IV; WT, wild-type. Scale bars: WT = 15.97 μm; TIM2$^{+/-}$ = 14.71 μm.

D.5. Effects on transcellular transport

Endothelial caveolae are structures responsible for the transcellular transport across the retinal vascular wall. Transcellular transport dysfunction can also be responsible for increased vascular permeability (Minshall et al., 2003; Klaassen et al., 2013). Plasmalemma vesicle-associated protein (PLVAP) is an endothelial cell-specific protein that is known to be a structural component of caveolae (Schlingemann et al., 1985; Hallmann et al., 1995; Stan et al., 1999; Stan, 2005). PLVAP expression is absent or low in intact BRB and BBB endothelia, correlating with a low number of caveolae. However, in pathological conditions, its expression is highly up-regulated and associated with increased barrier permeability. Therefore, PLVAP is a well-accepted marker for increased transcytosis and its expression is associated with barrier function loss (Vinores, 1995; Schlingemann et al., 1997, 1999; Wisniewska-Kruk et al., 2016; Díaz-Coránguez et al., 2017). In view of the previous result concerning tight junction protein expression accounting for the increased permeability of retinal blood vessels and BRB breakdown, we next investigated the contribution of transcellular transport to BRB permeability and integrity loss by verifying the presence of PLVAP and caveolae in retinal vasculature of TIM2$^{+/-}$ mice.

Western blot analysis with a specific antibody (Wisniewska-Kruk et al., 2014) revealed an increase of PLVAP expression in TIM2$^{+/-}$ retinas compared to WT retinas, demonstrated by a specific band with higher intensity with a molecular weight of 51 kDa band. The quantification by densitometry confirmed PLVAP overexpression (1.67-fold change) in a pool of 12 retinas from TIM2$^{+/-}$ mice relative to a pool of 12 retinas from WT mice (Figure 58). This was paralleled by the presence of more caveolae in endothelial cells of retinal blood vessels of TIM2$^{+/-}$ mice observed by means of TEM (Figure 59).

Our results confirmed the presence of PLVAP and an increased transcellular transport via caveolae in TIM2$^{+/-}$ retinal vasculature, contributing to the vascular permeability and BRB impairment observed.

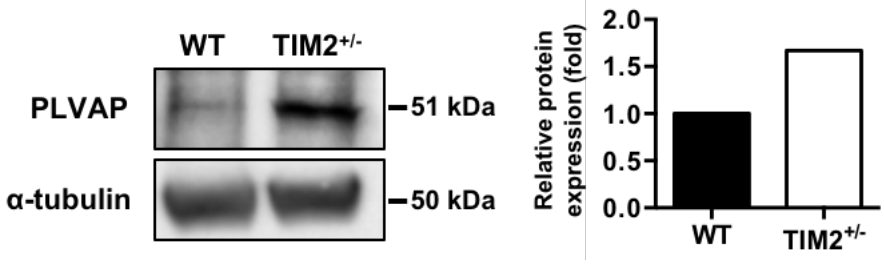

Figure 58. Analysis of PLVAP expression in the retina. Western blot analysis and quantitative densitometry revealed that PLVAP protein expression was increased in a pool of 12 TIM2$^{+/-}$ retinas compared to a pool of 12 WT retinas. α-tubulin was used as a loading control. WT, wild-type.

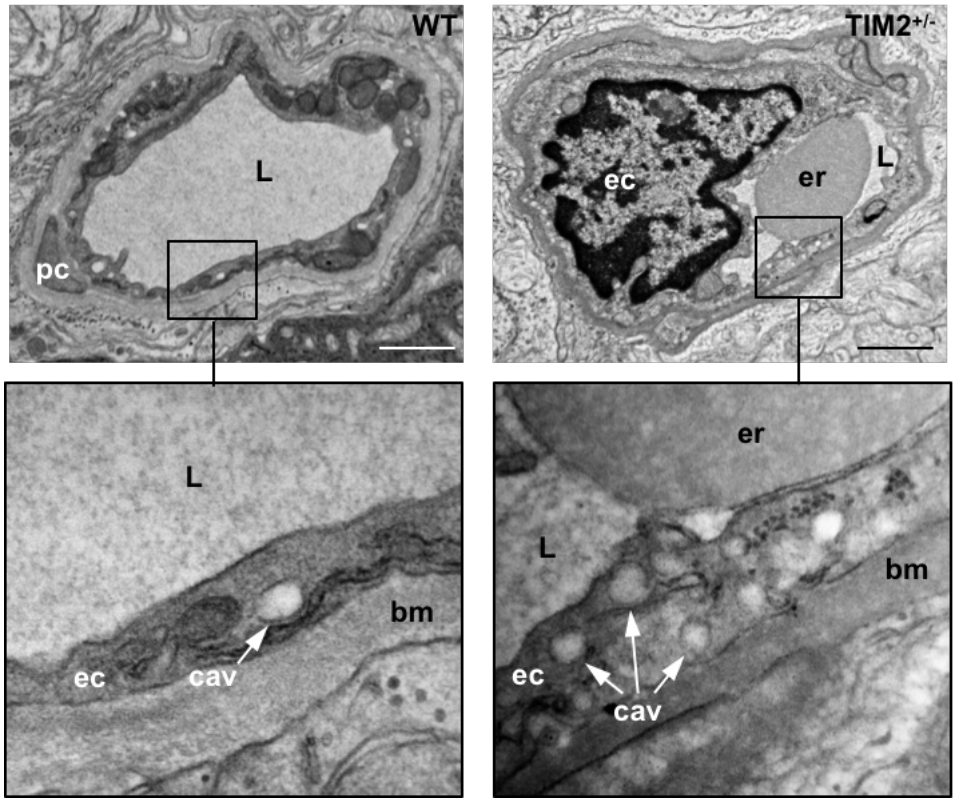

Figure 59. Ultrastructural analysis of caveolae in the retina. Ultrathin sections observed by transmission electron microscopy showed more caveolae in endothelial cells of retinal blood vessels of TIM2$^{+/-}$ mice compared to WT mice. bm, basement membrane; cav, caveolae; ec, endothelial cells; er, erythrocyte; L, lumen; pc, pericyte; WT, wild-type. Scale bars: WT = 0.8 µm; TIM2$^{+/-}$ = 1.05 µm.

D.6. Evaluation of VEGF expression

VEGF, a potent inducer of vasopermeability and angiogenesis, disrupts the endothelial barrier by inducing tight junction phosphorylation and degradation (Antonetti et al., 1999; Argaw et al., 2009; Klaassen et al., 2009; Wisniewska-Kruk et al., 2012) and increasing transcellular transport in endothelial cells mediated by caveolae (Feng et al., 1999; Hofman et al., 2000; Klaassen et al., 2009). PLVAP expression in endothelium is triggered by high levels of VEGF and may therefore be involved in VEGF-induced BRB breakdown (Hofman et al., 2000; Strickland et al., 2005; Wisniewska-Kruk et al., 2012, 2016). Regarding this, we next evaluated VEGF expression in TIM2$^{+/-}$ retinas.

Western blot analysis with a specific antibody (Cheung et al., 2005) revealed an increase of VEGF expression in TIM2$^{+/-}$ retinas compared to WT retinas, demonstrated by an increase in the intensity of the 42 kDa band. Quantitative densitometry confirmed VEGF overexpression (1.60-fold change) in a pool of 12 retinas from TIM2$^{+/-}$ mice relative to a pool of 12 retinas from WT mice (Figure 60).

Our result suggested that the association of iron and ferritin overload with VEGF overexpression could be a possible explanation for the increased vascular permeability and BRB impairment observed in TIM2$^{+/-}$ retinas.

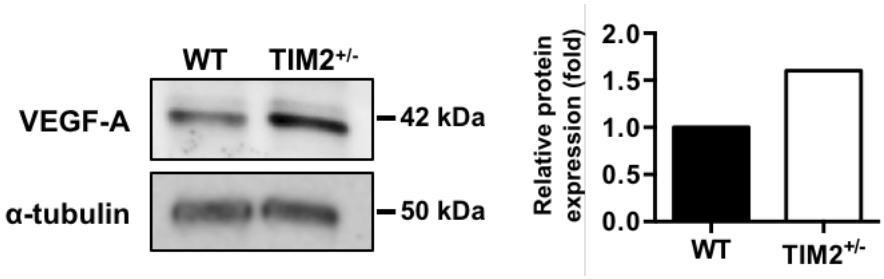

Figure 60. Analysis of VEGF expression in the retina. Western blot analysis and quantitative densitometry revealed an increase of VEGF protein expression, consistent with an increase in the intensity of the 42 kDa band, in a pool of 12 TIM2$^{+/-}$ retinas compared to a pool of 12 WT retinas. α-tubulin was used as a loading control. WT, wild-type.

D.7. Evaluation of glycemia

In diabetes, vision loss is most commonly the result of diabetic retinopathy and diabetic macular edema (Cheung, Mitchell & Wong, 2010). Diabetes result in a persistently elevated blood glucose concentration as a consequence of insufficient insulin release by pancreatic β-cells. Both reduced β-cell mass and impaired β-cell function have been proposed to underlie the defective insulin secretion (Elayat, el-Naggar & Tahir, 1995; Pour, Standop & Batra, 2002; Göke, 2008; Ashcroft & Rorsman, 2012). Hyperglycemia is the strongest risk factor for the development and progression of diabetic retinopathy (Cheung et al., 2010). We next evaluated blood glucose levels to rule out diabetes-associated hyperglycemia as a cause of retinal edema in TIM2$^{+/-}$ mice. Rodents have been considered diabetic when fasting glucose levels exceed 250 mg/dl (Surwit et al., 1988; Svenson et al., 2007; Fajardo et al., 2014).

Two blood samples were collected from 10 WT mice and 10 TIM2$^{+/-}$ mice for blood glucose analysis: the first during *ad libitum* feeding, and, one week later, a second one, after a 12-hour fasting period. No significant statistical differences were found between WT and TIM2$^{+/-}$ mice regarding glycemia in *ad libitum* feeding (143.30 ± 3.14 vs. 136.80 ± 4.53 mg/dl; p=0.1592; n=10) or fasting conditions (69.64 ± 2.44 vs. 63.22 ± 2.44 mg/dl; p=0.1642; n=10) and the cut-off for diabetes was not reached (Figure 61A), suggesting that edema formation was due to causes other than hyperglycemia in TIM2$^{+/-}$ retinas.

The pancreatic islets of Langerhans contain the insulin-producing β-cells and therefore play an important role in glucose metabolism and diabetes. Histological studies of pancreas of diabetic mice demonstrated reduction in size and number of islets as well as cellular atrophy and increased number of vacuoles in islets (Huang et al., 2011; Walvekar et al., 2016; Elkotby et al., 2018).

The analysis of paraffin embedded sections from TIM2$^{+/-}$ pancreas stained with H-E showed typical spherical shaped islets with a large number of β-cells with a normal round shape and distinct round nuclei (Figure 61B). This result suggested that insulin secretion was not affected in TIM2$^{+/-}$ mice, corroborating the normoglycemia obtained in blood glucose analysis.

Altogether, our results demonstrated that TIM2$^{+/-}$ mice were not diabetic, excluding hyperglycemia as the cause of VEGF overexpression and edema formation in TIM2$^{+/-}$ retinas.

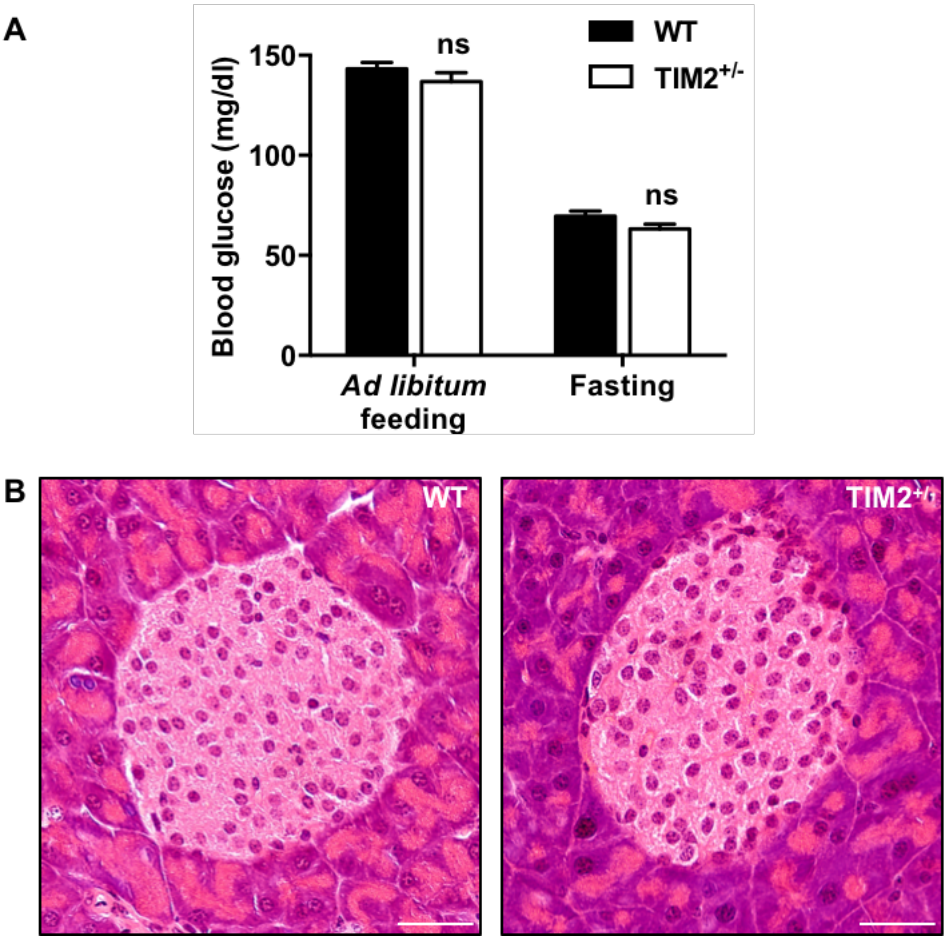

Figure 61. Analysis of blood glucose and pancreatic islets. A. The analysis of blood glucose in *ad libitum* feeding and fasting conditions revealed no significant differences between WT and TIM2$^{+/-}$ mice. **B.** Paraffin embedded sections from WT and TIM2$^{+/-}$ pancreas stained with H-E showed apparent similar morphology of pancreatic islets. ns, not significant; WT, wild-type. Scale bars: WT = 33.83 μm; TIM2$^{+/-}$ = 33.82 μm.

D.8. Evaluation of inflammation

One of the cardinal signs of retinal inflammation is macular edema (Daruich et al., 2018). In response to inflammation, retinal injury, and disease, Müller cells undergo major cellular and molecular changes, known as reactive gliosis (Bringmann et al., 2009; Dinet et al., 2012), whose hallmark is the upregulation of cytoskeletal intermediate filaments, such as GFAP, vimentin, and nestin (Lewis & Fisher, 2003).

In order to assess retinal inflammation through the evaluation of gliosis, paraffin embedded retinal sections of WT and TIM2$^{+/-}$ mice were immunolabeled with a specific anti-GFAP antibody.

Confocal analysis showed no overexpression of GFAP intermediate filaments (Figure 62), excluding the presence of gliosis in TIM2$^{+/-}$ retinas and thereby the involvement of inflammation in the pathogenesis of edema.

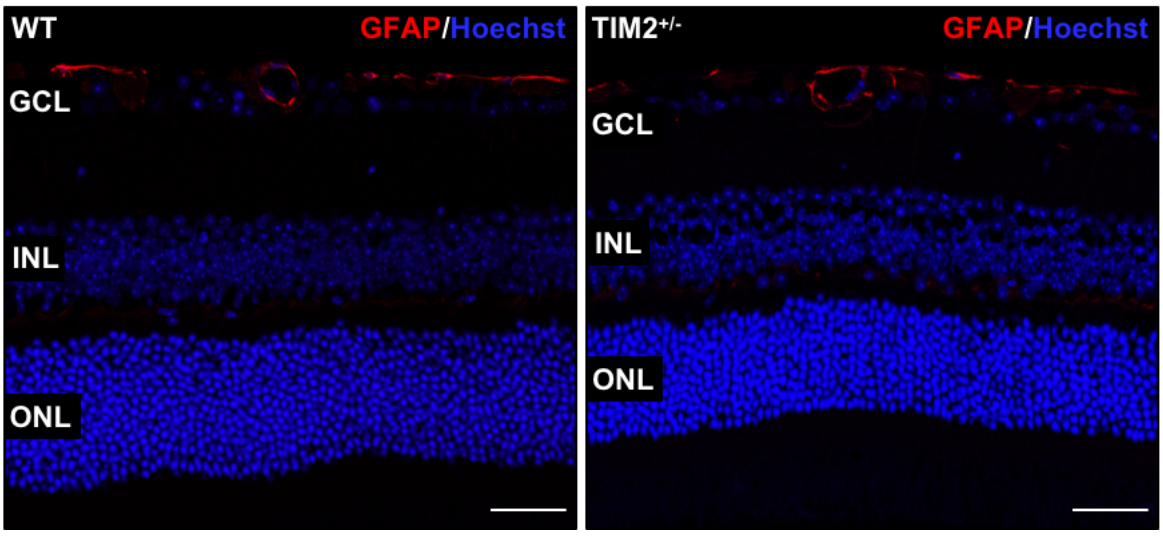

Figure 62. Analysis of gliosis in the retina. Retinal sections immunostained with anti-GFAP antibody (red) showed similar expression between WT and TIM2$^{+/-}$ mice, excluding the presence of gliosis in TIM2$^{+/-}$ mice. Nuclei were counterstained with Hoechst (blue). GCL, ganglion cell layer; INL, inner nuclear layer; ONL, outer nuclear layer; WT, wild-type. Scale bars: WT = 36.9 µm; TIM2$^{+/-}$ = 36.9 µm.

D.9. Evaluation of reactive oxygen species and oxidative stress

Intracellular iron exists in two forms: the highly reactive Fe^{2+} form, that remains free in the cytoplasm, as part of LIP, and Fe^{3+} safely incorporated into ferritin (Richardson & Ponka, 1997; Kohgo et al., 2008; Hentze et al., 2010; Arosio & Levi, 2010). Having found iron and ferritin overload in $TIM2^{+/-}$ retinas, we next determined Fe^{2+} and Fe^{3+} content in this tissue.

Retinal iron measured by a colorimetric assay revealed an increase in Fe^{2+} in a pool of 10 retinas from $TIM2^{+/-}$ mice compared to a pool of 10 retinas from WT mice (1.1334 vs. 1.0759 µg/ml). Fe^{3+} was also increased in the same pool of $TIM2^{+/-}$ retinas in comparison to the pool of WT retinas (0.0804 vs. 0.0276 µg/ml) (Figure 63A). As expected, our results confirmed that both free Fe^{2+} and ferritin-bound Fe^{3+} were increased in $TIM2^{+/-}$ retinas.

Previously we showed that $TIM2^{+/-}$ Müller cells presented iron-loaded ferritin accumulation, with Fe^{3+} stored in its core. We further aimed to investigate free Fe^{2+} cellular distribution.

Fe^{2+} was detected in whole-mount retinas using FeRhoNox-1 fluorescent imaging probe by means of confocal microscopy. Our results revealed a stronger staining in the ganglion cell layer, compatible with the localization of Müller cell processes and endfeet, in retinas from $TIM2^{+/-}$ mice (Figure 63B). This result confirmed a higher content of free Fe^{2+} in the retinas of $TIM2^{+/-}$ mice, predominantly accumulated in Müller cells.

Fe^{2+} participates in the Fenton reaction and, when in excess, generates the overproduction of ROS, triggering oxidative stress, which plays an important role in the pathogenesis of several retinopathies, as diabetic retinopathy (Halliwell & Gutteridge, 1984, 1990; Dröge, 2002; Galaris & Pantopoulos, 2008; Kell, 2009; Gammella et al., 2016; Chaudhary et al., 2018). We next evaluated ROS production in retinas from $TIM2^{+/-}$ mice, regarding the high content of free Fe^{2+}.

Retinal sections stained with DHE, used to detect ROS generation (Zhao et al., 2003; Zielonka et al., 2008), and analyzed by means of confocal microscopy, revealed a stronger staining throughout the entire retinal parenchyma (Figure 64A), consistent with increased generation of ROS in $TIM2^{+/-}$ retinas. Quantitative analysis of DHE fluorescence confirmed a significant increase of fluorescence intensity in retinas from $TIM2^{+/-}$ mice compared with retinas from WT mice (30.29 ± 2.15 vs. 15 ± 1 AU; p=0.0001; n=6) (Figure 64B).

Taken together, our results suggested that elevated levels of oxidative stress in $TIM2^{+/-}$ retinas, promoted by the association of free Fe^{2+} overload with overproduction of ROS, could also be accounting for the increased vascular permeability and BRB impairment observed in $TIM2^{+/-}$ retinas.

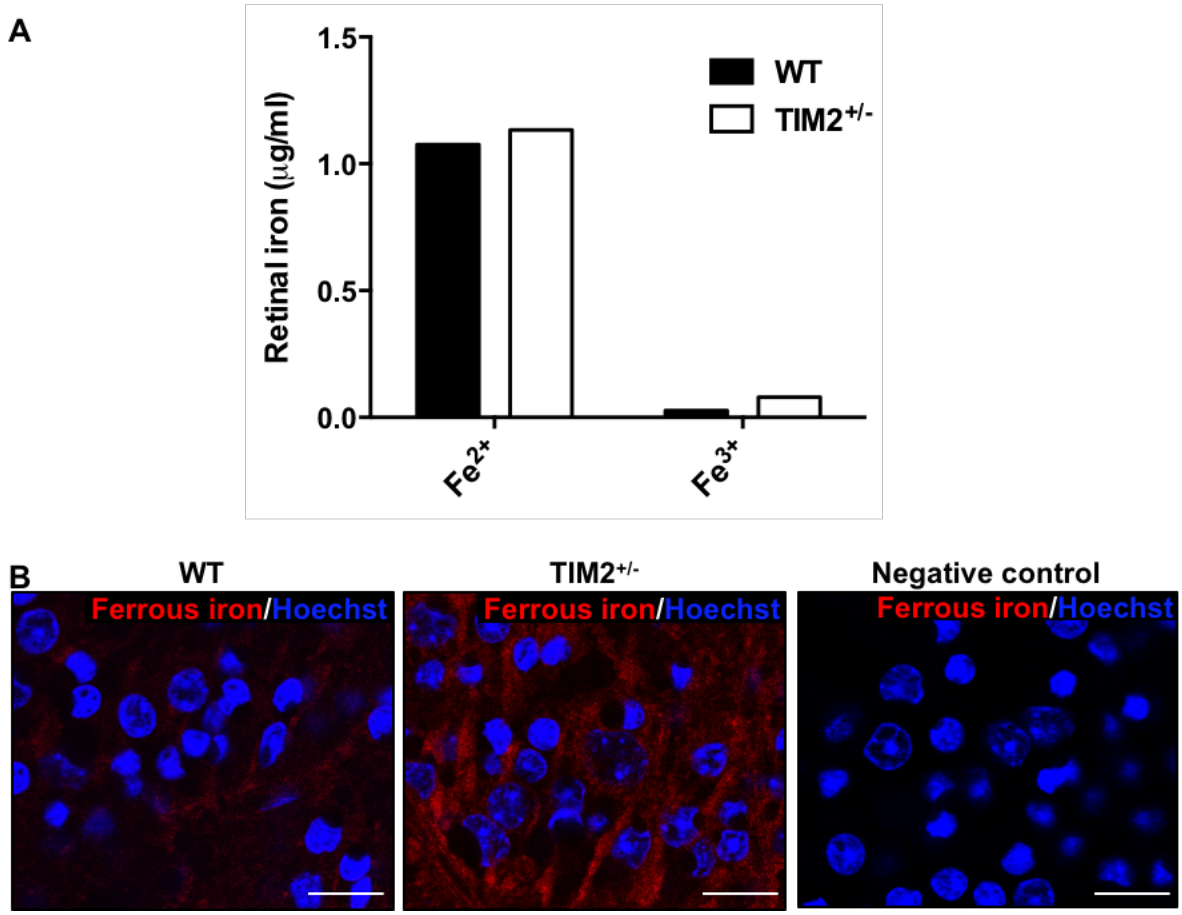

Figure 63. Analysis of Fe^{2+} and Fe^{3+} content in the retina. A. The analysis of retinal iron by a colorimetric assay demonstrated an increase in Fe^{2+} and Fe^{3+} in a pool of 10 retinas from $TIM2^{+/-}$ mice in comparison to a pool of 10 retinas from WT mice. **B.** Detection of Fe^{2+} in whole-mount retinas using FeRhoNox-1 fluorescent imaging probe (red) revealed stronger staining in $TIM2^{+/-}$ retinas compared to WT retinas. Nuclei were counterstained with Hoechst (blue). WT, wild-type. Scale bars: WT = 16.85 µm; $TIM2^{+/-}$ = 17.32 µm; Negative control = 17.63 µm.

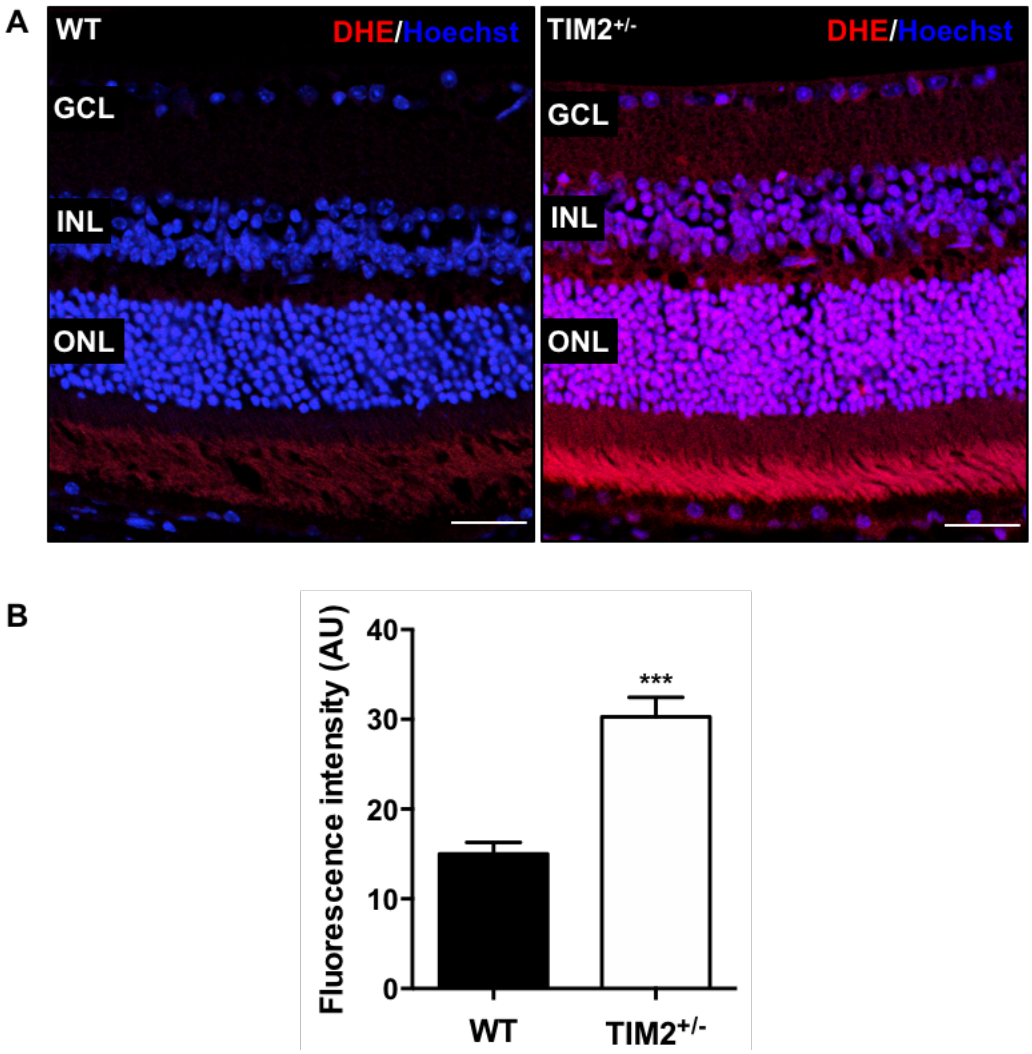

Figure 64. Evaluation of oxidative stress in the retina. Retinal oxidative stress levels were evaluated by the detection of ROS generation by DHE. **A.** Confocal microscopy analysis of retinal sections incubated with DHE from WT and TIM2$^{+/-}$ mice showed stronger labeling of DHE (red) throughout the entire retinal parenchyma in TIM2$^{+/-}$ mice, consistent with increased generation of ROS. Nuclei were counterstained with Hoechst (blue). **B.** Quantitative analysis of DHE fluorescence confirmed a significant increase in fluorescence intensity in TIM2$^{+/-}$ retinas compared with retinas from WT mice. Data are presented as mean ± SEM (n=6). Asterisks indicate statistically significant differences: ***p<0.001. AU, arbitrary units; DHE, dihydroethidium; GCL, ganglion cell layer; INL, inner nuclear layer; ONL, outer nuclear layer; WT, wild-type. Scale bars: WT = 32.7 µm; TIM2$^{+/-}$ = 29.82 µm.

Excess of ROS leads to oxidative DNA damage and lipid peroxidation. Replication protein A (RPA), the eukaryotic single-stranded DNA-binding protein, essential for proper DNA duplication and maintenance, is heavily phosphorylated, specifically on its subunit 2 (RPA2), in response to DNA damage (Iftode, Daniely & Borowiec, 1999; Binz, Sheehan & Wold, 2004). An early event in response to DNA damage is also the phosphorylation of histone H2A variant H2AX (γ-H2AX), particularly when the damage involves induction of double-strand DNA breaks, participating in homologous recombination DNA repair (Rogakou et al., 1998; Jackson, 2002; Xie et al., 2004). 4-hydroxynonenal (4-HNE), a lipid peroxidation product, is upregulated during oxidative stress (Gnana-Prakasam et al., 2008). We further evaluated effects of oxidative stress in the retina by means of western blot and immunohistochemistry analyses.

By means of western blot analysis, we detected an increase in RPA2 and γ-H2AX protein expression in retinas from TIM2$^{+/-}$ mice compared with retinas from WT mice, consistent with higher intensity of 32 and 15 kDa bands observed, respectively. Quantitative densitometry confirmed increased RPA2 (Figure 65A) and γ-H2AX (Figure 65B) protein expression (1.85 and 1.50-fold change, respectively) in a pool of 12 retinas from TIM2$^{+/-}$ mice relative to a pool of 12 retinas from WT mice, demonstrating the presence of DNA damage probably in response to elevated oxidative stress.

Confocal analysis of retinal sections immunostained with anti-4-HNE antibody revealed stronger immunoreactivity in retinas from TIM2$^{+/-}$ mice compared with retinas from WT mice, manly observed in blood vessels, confirming an increase in lipid peroxidation in response to elevated oxidative stress (Figure 65C).

Altogether, these results confirmed elevated oxidative stress levels in TIM2$^{+/-}$ retinas induced by overproduction of ROS, that elicited DNA damage, along with homologous recombination DNA repair. ROS could be involved in disrupting tight junctions, concomitant with the rearrangement of the actin cytoskeleton and redistribution of tight junction protein such as occludin, claudin-5, and ZO-1, with changes in barrier permeability. Contribution of lipid peroxidation to tight junction and BRB loss of integrity was also suggested in TIM2$^{+/-}$ retinas.

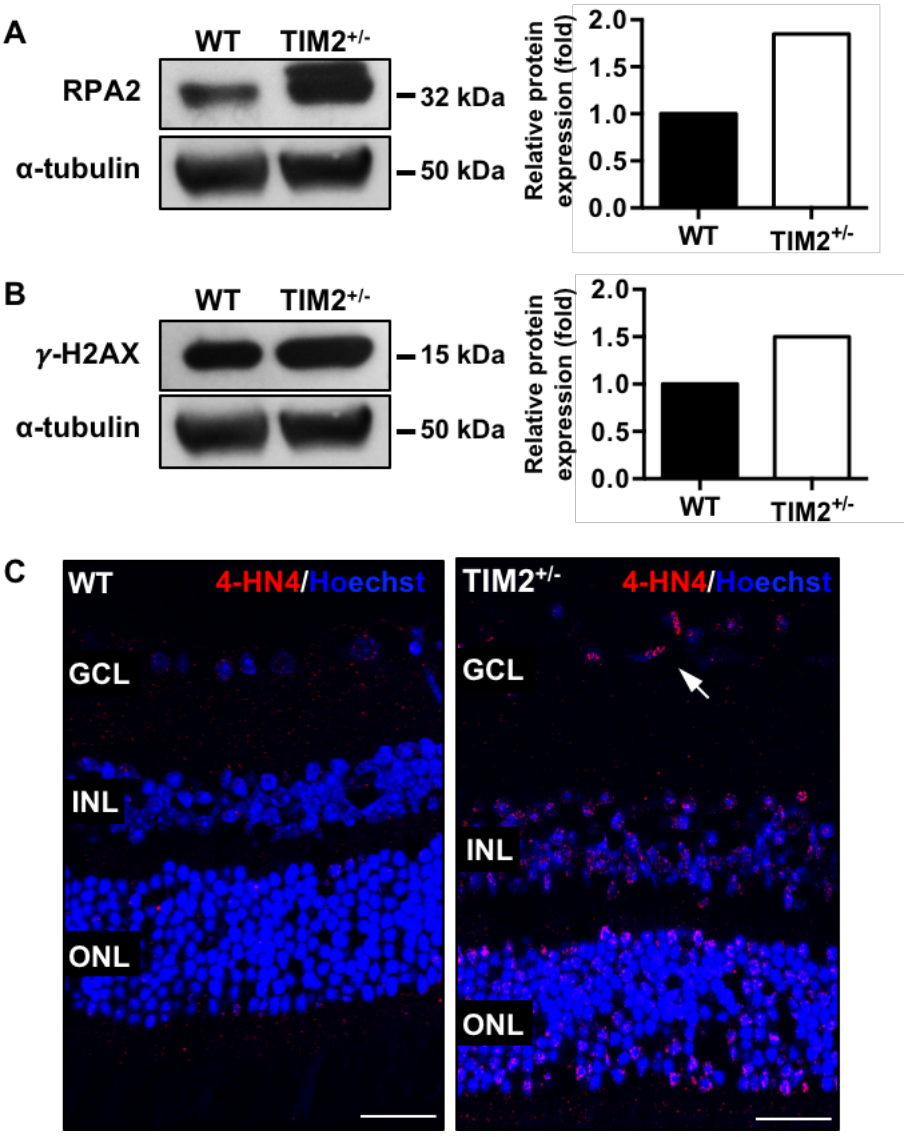

Figure 65. Evaluation of DNA damage and lipid peroxidation in the retina. Western blot analysis and quantitative densitometry revealed an increase in RPA2 (**A**) and γ-H2AX (**B**) protein expression in a pool of 12 TIM2$^{+/-}$ retinas compared to a pool of 12 WT retinas. α-tubulin was used as a loading control. **C.** Immunolabeling against 4-HNE (*red)* showed an increased in the expression of 4-HNE in blood vessels (arrow) of retinas from TIM2$^{+/-}$ mice compared with retinas from WT mice. Nuclei were counterstained with Hoechst (*blue*). GCL, ganglion cell layer; INL, inner nuclear layer; ONL, outer nuclear layer; WT, wild-type. Scale bars: WT = 26.54 μm; TIM2$^{+/-}$ = 26.29 μm.

DISCUSSION

DISCUSSION

Classically, iron import into cells has been known to be mediated by transferrin endocytosis. Fe^{3+} bound to transferrin in the circulation is taken up by high-affinity TfR1 at the cell surface. Ferritin, known for its role in iron storage and detoxification, has also been proposed as an iron carrier protein, likely to undergo endocytosis and be transcytosed across the BRB (Ponka et al., 1998; Fisher et al., 2007). This was paralleled by the identification of new membrane receptors for ferritin: human TIM1 and mouse TIM2 for the H subunit (Chen et al., 2005; Chiou et al., 2018), and Scara5 for the L subunit (Li et al., 2009). Recently, our group described Scara5 in human and mouse retinas for the first time and demonstrated that serum ferritin is transported across the BRB into the retinal parenchyma through L-ferritin binding to Scara5, suggesting the existence of a new pathway for retinal iron delivery and trafficking (Mendes-Jorge et al., 2014). As ferritin is capable of transporting ~ 4,500 iron atoms while transferrin can only bind to two atoms of iron, ferritin can be established as a very efficient iron carrier and source of iron to tissues (Fisher et al., 2007).

TIM2 expression has been described in mouse spleen, liver, kidneys, and brain (Chen et al., 2005; Watanabe et al., 2007; Todorich et al., 2008). Our results revealed for the first time the presence of TIM2 receptors in the mouse retina, giving rise to a new approach in retinal iron metabolism regarding the putative role of TIM2 in this tissue. Furthermore, our results showed that, in the mouse retina, TIM2 is mainly expressed in Müller glial cells.

To our knowledge, no human ortholog for mouse TIM2 has been identified so far. However, it is known that mouse TIM1 and TIM2 share a homology of 66% with each other and 41 and 36%, respectively, with human TIM1. This resulted in a postulation that TIM2 evolved as a gene duplication of mouse TIM1 and that it also shares functional characteristics with human TIM1 because it is found only in rodents and not in primates (McIntire et al., 2001; Kuchroo et al., 2003; Meyers et al., 2005; Rodriguez-Manzanet et al., 2009). Recently, Chiou and colleagues (2018) demonstrated that mouse TIM2 functions, including H-ferritin uptake, are mediated via TIM1 receptor in humans.

Rodent and human oligodendrocytes express TIM2 and TIM1, respectively (Todorich et al., 2008; Chiou et al., 2018). Oligodendrocytes, as well as microglia, astrocytes, and ependymal cells are the major components of neuroglia (Junqueira & Carneiro, 1983). Given the lack of TfR1 in these cells (Hill et al., 1985; Hulet et al., 1999a,b; Han et al., 2003) and their high

requirement of iron for myelin synthesis (Connor & Menzies, 1996), TIM2 and TIM1 provide an alternative pathway for iron import into oligodendrocytes (Todorich et al., 2008; Chiou et al., 2018).

Müller cells, the major component of retinal glia (Bringmann et al., 2006; Goldman, 2014), ensure proper retinal function by performing several functional and supportive roles for the surrounding neurons, including maintaining homeostasis of the neuronal microenvironment, providing nutritional support, and removing metabolic waste (Newman & Reichenbach, 1996; Gardner et al., 2002; Bringmann et al., 2006; Kolb et al., 2011; Kur et al., 2012). Previously, Müller cells have also been proposed to play a major role in the maintenance of retinal iron homeostasis and considered important mediators of retinal iron transport, distribution, and regulation (Baumann et al., 2017). In this regard, Müller cells are critical for the iBRB function, together with endothelial cells, creating a physical barrier to prevent the unregulated flux of iron into the retina (Hollander et al., 1991; Tout et al., 1993; Gardner et al., 2002; Klaassen et al., 2013). Moreover, all proteins involved in iron import, export, and regulation are expressed in Müller cells, whose processes extend almost the entire thickness of the retina and contact all layers of neurons (Gnana-Prakasam et al., 2010; Kolb et al., 2011; Newman, 2013; Vecino et al., 2016; Baumann et al., 2017). TIM2 high expression in Müller cells, together with the involvement of these cells in iron homeostasis, unravels TIM2 as a new important player in retinal iron homeostasis.

Mice can be genetically modified using a number of different approaches, such as gene KO and gene overexpression. Genetically modified models are important tools for studying the function or regulation of a specific gene of interest and for modeling human diseases. KO mouse models are primarily used to understand the role of a specific gene by investigating the effect of gene loss, comparing the KO to a WT with the same genetic background (Capecchi, 1994; Majzoub & Muglia, 1996; Hall, Limaye & Kulkarni, 2009). Thereby, to better understand TIM2 functions in the retina, a KO mouse for this receptor was generated.

Rennert and colleagues (2006) had already generated a TIM2 deficient mouse model on a BALB/c background to study the immune response. However, this model was not suitable for our study in the retina as some mutations can occur in the architecture of retinal layers in BALB/c background (Huber et al., 2009; Santos et al., 2010; Bell et al., 2012). We generated a TIM2 KO mouse model on a C57BL/6 background by disrupting *TIM2* gene function. Although only $TIM2^{+/-}$ mice were obtained, probably due to embryonic lethality in $TIM2^{-/-}$ mice, we were able to decrease TIM2 protein expression in $TIM2^{+/-}$ mice, which was in line with our purpose for this study. Considering that a specific distribution of different retinal cell types is required for proper functioning of the retina (Runkle & Antonetti, 2011), we confirmed the

maintenance of the spatial arrangement of the retinal layers, thus validating TIM2$^{+/-}$ mice as a physiological model.

Due to the involvement of TIM2 in the iron metabolism as a receptor for ferritin, we further investigated the influence of decreasing TIM2 expression. The analysis of the main iron-handling proteins revealed that retinal TIM2 deficiency affected iron metabolism, probably increasing iron import into the retina through ferritin binding to Scara5 that led to the accumulation of iron-loaded ferritin, mainly in Müller cells. Similarly, iron import into the retina mediated by transferrin and TfR1 was also increased. Serum ferritin can also be regarded as an indicator of body iron stores, being upregulated during intracellular iron accumulation (Chaudhary et al., 2018). Consequently, and concomitantly with higher levels of serum ferritin, retinal iron overload was established in TIM2$^{+/-}$ mice.

Cellular iron levels are modulated by an elegant machinery involving IRPs that bind to the IREs on the iron-handling proteins mRNA (Mackenzie et al., 2008; Wang & Pantopoulos, 2011; Anderson et al., 2012). Accordingly, when LIP levels rise, IRPs remain inactive and do not bind to IREs on ferritin mRNA, enhancing ferritin synthesis, or TfR1 mRNA that undergoes degradation by nucleases, leading to a decrease in iron import and an increase in iron storage, reducing intracellular free Fe^{2+} (Rouault, 2006; Wallander, Leibold & Eisenstein, 2006; Muckenthaler, Galy & Hentze, 2008; Anderson et al., 2012). On the other hand, in conditions of iron deficiency, IRPs bind to IREs on mRNAs to prevent mRNA translation and ferritin synthesis and TfR1 mRNA degradation resulting in TfR1 synthesis, leading to an increase in iron import and a decrease in iron storage, incrementing intracellular free Fe^{2+} (Binder et al., 1994; Muckenthaler et al., 2008).

Appropriate LIP levels are critical for homeostasis, as free Fe^{2+} in the LIP is toxic when in excess (Rouault & Cooperman, 2006; He et al., 2007; Mackenzie et al., 2008; Song & Dunaief, 2013). In general, LIP mirrors the cellular iron content and its levels are tightly regulated by stimulating or inhibiting ferritin and TfR1 synthesis (Mackenzie et al., 2008; Wang & Pantopoulos, 2011; Anderson et al., 2012). LIP level dysregulation probably led to the accumulation of ferritin and iron in retinas from TIM2$^{+/-}$ mice. Moreover, to counterbalance the decrease in TIM2 expression, Scara5 expression was upregulated, probably leading to the increase in ferritin import. On the one hand, upregulation of ferritin in iron overload conditions is expected to sequester iron and protect cells against oxidative damage by reducing LIP levels. But chronic overexpression of ferritin rather than be protective may lead to the opposite effect in mice, suggesting that iron sequestered in ferritin shells may eventually become pro-oxidant. Heavily iron-loaded ferritin can create a pool of easily releasable iron. For example, in the brain, prolonged elevation of ferritin levels within dopaminergic midbrain neurons results in their progressive age-related neurodegeneration (Kaur et al., 2007; Kaur, Rajagopalan &

Andersen, 2009). It was demonstrated that Fe^{3+} stored within the ferritin shell can be easily reduced by cytotoxic byproducts of dopamine oxidation within dopaminergic neurons, including superoxide and 6-hydroxydopamine, allowing its release from ferritin as Fe^{2+} (Thomas & Aust, 1986; Monteiro & Winterbourn, 1989; Kienzl et al., 1995; Linert et al., 1996; Double et al., 1998; Comporti, 2002). The present study demonstrates that the retina accumulates ferritin and iron when TIM2 expression is decreased, suggesting that TIM2 has a crucial role in the effective modulation of iron levels. Furthermore, retinal chronic accumulation of ferritin seems to have deleterious effects rather than protective.

The retina is constantly exposed to oxidative stress caused by photo-oxidation, and iron overload within this tissue exacerbates this oxidative stress, leading to deleterious effects. Also, increased iron accumulation is associated with several degenerative diseases, such as diabetic retinopathy (Feng et al., 2007; Ciudin et al., 2010; Chaudhary et al., 2018). Iron overload in $TIM2^{+/-}$ retinas was paralleled with increased vascular permeability and BRB breakdown, which consequently induced edema. The neurosensory retina is protected from potentially harmful molecules in the circulation by the iBRB that regulates the entry of molecules into the inner retina. This barrier is mainly formed by specialized tight junctions sealing the intercellular space between endothelial cells and an array of specific transcellular transport mechanisms and supported by glial cells and pericytes (Cunha-Vaz, 1976; Abbott et al., 2006; Fruttiger, 2007; Klaassen et al., 2013). An intact BRB is essential for proper vision and its breakdown, resulting in retinal vascular leakage and subsequent macular edema, plays an important role in the pathology and vision loss in diabetic retinopathy, age-related macular degeneration, retinal vein occlusion, and uveitis (Klassen et al., 2013). Furthermore, diabetic macular edema, characterized by focal enlargement of the extracellular space and retinal thickening, is the major cause of loss of vision in patients with diabetic retinopathy due to the alteration of the functional cell relationship (Cunha-Vaz, 1976; Coscas, Cunha-Vaz & Soubrane, 2010; Cunha-Vaz et al., 2011; Frey & Antonetti, 2011; Duh et al., 2017; Daruich et al., 2018). Endothelial cells of an intact BRB possess well-developed tight junctions, have few caveolae, which are mainly localized at their abluminal side, and express selective transporters. Dynamic adaptations of endothelial cells and other cell types that constitute the BRB underlie vascular leakage in retinal disease. In this regard, two main cellular mechanisms have been proposed to cause BRB loss: increased paracellular transport due to disrupted interendothelial cell tight junction integrity and increased transendothelial transport mediated by caveolae (Lum & Malik, 1994; Antonetti et al., 1999; Minshall at al., 2003; Abbott et al., 2006; Klaassen et al., 2013; Díaz-Coránguez et al., 2017).

Low levels and disrupted expression of the main endothelial tight junction proteins, ZO-1, claudin-5, and occludin, were found in $TIM2^{+/-}$ retinas, leading to the increased vascular permeability with fluorescein and serum albumin leakage observed in the retinas of these mice.

ZO proteins are considered to be the center of tight junction assembly and organization and also account for claudin molecules polymerization, and increased paracellular flux has been associated with delocalization of ZO-1 from the cell border (Fischer et al., 2002; Harhaj & Antonetti, 2004; Umeda et al., 2006). Occludin and claudins have been reported to be decreased in conditions associated with BRB permeability (Antonetti et al., 1998; Barber & Antonetti, 2003; Nitta et al., 2003). Reduced levels of endothelial tight junction proteins have been associated with retinal vascular permeability in diabetic retinopathy (Antonetti et al., 1998; Barber et al., 2005).

Furthermore, the expression of the transcellular transport-related protein PLVAP was increased in parallel with a higher number of caveolae in TIM2$^{+/-}$ retinas. It has been suggested that PLVAP is necessary for the formation of new caveolae in conditions with increased permeability (Wisniewska-Kruk et al., 2016). PLVAP is an endothelial cell-specific protein that is upregulated in pathologic conditions, such as diabetic retinopathy, and associated with loss of BRB and BBB and increased transcellular transport (Schlingemann et al., 1985, 1997, 1999; Vinores, 1995; Wisniewska-Kruk et al., 2016; Díaz-Coránguez et al., 2017). As PLVAP is one of the structural components of caveolae (Schlingemann et al., 1985; Stan et al., 1999; Stan, 2005), which carry out transendothelial transport, it may contribute to vascular permeability by increasing transcellular endothelial transport.

Our results showed that both paracellular and transcellular transport are altered in retinas from TIM2$^{+/-}$ mice, which lead to increased vascular permeability and BRB loss of integrity. As a result of BRB breakdown, abnormal inflow and accumulation of fluid in the extracellular space induced the formation of edema.

Hyperglycemia, inflammation, hypoxia, VEGF, ROS, and oxidative stress are the main underlying factors contributing to BRB impairment (Klaassen et al., 2013). Though presenting a diabetic macular edema-like phenotype, TIM2$^{+/-}$ mice are not diabetic nor present retinal inflammation indications, therefore excluding the involvement of hyperglycemia and inflammation in BRB breakdown. On the other hand, VEGF overexpression was found in TIM2$^{+/-}$ retinas. VEGF is the most potent and primary endothelial specific angiogenic growth factor, both in physiological and pathological conditions. VEGF signaling is ultimately required for normal vascular development and homeostasis, but it is also actively engaged in tumor progression by promoting growth of tumor vasculature and vasopermeability, disrupting the endothelial barrier by inducing tight junction phosphorylation and degradation (Antonetti et al., 1999; Fischer et al., 2002; Shibuya, 2008; Argaw et al., 2009; Klaassen et al., 2009; Wisniewska-Kruk et al., 2012) and increasing transcellular transport in endothelial cells mediated by caveolae (Feng et al., 1999; Hofman et al., 2000; Klaassen et al., 2009).

Increased retinal VEGF levels are associated with BRB breakdown in diabetic rodents,

primates, and humans (Klaassen et al., 2009; Wisniewska-Kruk et al., 2014, 2016). Hyperglycemia and hypoxia promote VEGF signaling, resulting in diabetic microvascular complications (Crawford et al., 2009; Gupta et al., 2013). There are also potentially important relationships between intracellular iron metabolism and VEGF, as iron seems to be also involved in regulation of VEGF production through its effects on hypoxia inducible factor-1, the most potential stimulator of VEFG production. It is predicted that iron chelation could suppress several angiogenic mediators including VEGF (Harned et al., 2010; Guo et al., 2014). Moreover, Guo and colleagues (2014) showed that high levels of ferritin co-occur with high levels of VEGF, and a strong positive correlation was found between serum ferritin and VEGF in diabetes patients. It has also been reported that retinal iron overload upregulates GPR91 expression in retinas of HFE and hemojuvelin KO mice models of hemochromatosis, a genetic disorder of iron overload, and subsequently stimulates the production of VEGF (Gnana-Prakasam et al., 2011; Arjunan et al., 2016; Chaudhary et al., 2018). In this study, we show that the association of elevated levels of iron and ferritin with VEGF overexpression in normoglycemia conditions may contribute to increased vascular permeability and BRB failure in TIM2$^{+/-}$ retinas.

In addition, high VEGF levels induce PLVAP expression in a VEGF receptor 2 dependent manner (Hofman et al., 2000; Strickland et al., 2005; Wisniewska-Kruk et al., 2012, 2016). VEGF receptor 2 is the key mediator of VEGF signaling in endothelial cells and is localized in caveolae (Witmer et al., 2003; Olsson et al., 2006; Tahir, Park & Thompson, 2009). In healthy patients, with intact BRB, low numbers of caveolae and low VEGF receptor-2 and PLVAP protein expression are found. On the other hand, in diabetic retinopathy conditions, both VEGF receptor 2 and PLVAP are expressed in retinal capillaries with BRB loss (Schlingemann et al., 1999; Witmer et al., 2002, 2004). Besides VEGF receptor 2, caveolae harbor many other receptors involved in vascular permeability (Santibanez et al., 2008).

ROS act as a double-edged sword in the vasculature. On the one hand, ROS are involved in important physiological functions and adaptive cell responses. Transient or low levels of ROS are able to activate signaling pathways that eventually promote regeneration and growth (Dröge, 2002; Maulik & Das, 2002; Trachootham et al., 2008; Ray et al., 2012; Kim & Byzova, 2014). On the other hand, chronically produced or highly concentrated ROS are detrimental for most tissues. Iron overload promotes the Fenton reaction, generating the overproduction of ROS, which triggers oxidative stress. In turn, oxidative stress causes DNA damage, lipid peroxidation, and protein modifications, playing an important role in the pathogenesis of several retinopathies, as diabetic retinopathy (Halliwell & Gutteridge, 1984, 1990; Dröge, 2002; Galaris & Pantopoulos, 2008; Kell, 2009; Ray et al., 2012; Udipi et al., 2012; Gammella et al., 2016; Chaudhary et al., 2018). Conversely, oxidative stress itself influences iron metabolism and iron proteins, thus a vicious cycle of oxidative stress and iron accumulation may be

installed (Deb et al., 2009; Hadziahmetovic et al., 2011b). Regarding this, iron may be mobilized from ferritin by oxidative stress. Severe ROS attack on iron-loaded ferritin could become a further considerable threat when safely stored iron is released rendering LIP uncontrollable due to an impaired iron buffering capacity (Galaris & Pantopoulos, 2008; Bresgen & Eckl, 2015).

Furthermore, ROS and oxidative stress may trigger several signaling pathways, including protein kinase B and C, mitogen-activated protein kinases, phosphoinositide 3-kinase, and Rho, that mediate tight junction disruption and barrier dysfunction. In this sense, increased paracellular permeability may be induced by endothelial cell retraction, disruption or rearrangement of the actin cytoskeleton, and redistribution of tight junction protein such as occludin, claudin-5, and ZO-1 (Abbott, 2000; Gloor et al., 2001; Harhaj & Antonetti, 2004; Pérez et al., 2006; Schreibelt et al., 2007; González-Mariscal, Tapia & Chamorro, 2008; Rao, 2008). In addition, ROS can also stimulate the induction of VEGF expression in various cell types, such as endothelial and smooth muscle cells, and macrophages, whereas VEGF further stimulates ROS production through the activation of NAPDH oxidase in endothelial cells (Chua, Hamdy & Chua, 1998; Ushio-Fukai & Alexander, 2004; Wang et al., 2011). Animal studies have demonstrated that oxidative stress in result of metabolic dysregulation contributes to the development and exacerbation of diabetic retinopathy and retinal iron overload is involved in BRB loss of integrity and accelerates retinal cell loss by enhancing oxidative stress (Feng et al., 2007; Ciudin et al., 2010; Frey & Antonetti, 2011; Chaudhary et al., 2018).
Elevated levels of oxidative stress as well as increased expression of oxidative stress-related DNA damage and lipid peroxidation markers were detected in TIM2$^{+/-}$ retinas, probably due to iron overload triggering the overproduction of ROS, which can also contribute for the increased vascular permeability and BRB impairment observed in these retinas. Furthermore, ROS may also be involved in VEGF overexpression and vice-versa, thus exacerbating BRB disruption.

Additionally, RPA2 and γ-H2AX, the two DNA damage markers used in this study, are involved in the cascade of DNA repair in response to DNA damage. Cells respond to DNA damage by activating a complex molecular mechanism developed to detect and repair DNA damage, the DNA damage response. RPA2, the main eukaryotic single-stranded DNA-binding protein, is essential to nucleotide excision repair and the repair of double-strand breaks by homologous recombination, mediating the coordinated assembly of the DNA repair apparatus at sites of DNA damage through specific interactions with key repair proteins. This is concomitant to RPA2 binding tightly to single-stranded DNA and stimulates DNA repair and replication (Bochkarev et al., 1997; Wold, 1997; Iftode et al., 1999; Binz et al., 2004). γ-H2AX has been considered as a biomarker for the presence of DNA damage, particularly when the damage involves induction of double-strand DNA breaks (Rogakou et al., 1998; Jackson, 2002; Redon et al., 2011; Heylmann & Kaina, 2016). These breaks represent the most severe form of DNA

damage, since they result in chromosomal changes and cell death by apoptosis (Durant et al., 2013; Roos & Kaina, 2013). γ-H2AX play a role in the DNA damage response and is required for the assembly of DNA repair proteins at the sites containing damaged chromatin as well as for activation of checkpoints proteins which arrest the cell cycle progression, participating in homologous recombination DNA repair (Xie et al., 2004; Franco et al., 2006; Kouzarides, 2007; Kinner et al., 2008; Podhorecka, Skladanowski & Bozko, 2010).
Thereby, the activation of the DNA damage response in TIM2$^{+/-}$ retinas suggests an attempt to counterbalance the damage caused by elevated levels of oxidative stress, which may explain no evidence of retinal degeneration.

Furthermore, diabetic retinopathy is commonly accompanied by abnormalities in the morphology of the retinal vasculature, such as vessel tortuosity, which may be an early indication of microvascular damage (Dougherty, Johnson & Wiers, 2010; Sasongko et al., 2011, 2012, 2016). In retinal vessels, tortuosity, a key parameter to evaluate the vascular pattern, is considered as an indicative of the optimality of the state of the retinal microcirculation and level of tissue perfusion (Koh et al., 2010). Increased retinal vessel tortuosity has been related to diabetes-related changes, including disturbed blood flow, tissue hypoxia, endothelial dysfunction, and an increased production of VEGF (Kristinsson, Gottfredsdottir & Stefansson, 1997; Hartnett et al., 2008; Sasongko et al., 2011; Han, 2012). Vessel wall weakening, due to degradation of extracellular matrix components and the lack of support from cells of the vessel wall, lead to tortuosity (Han, 2012; Lee et al., 2012; Martinez & Han, 2012).
Our results showed a normal vascular pattern in TIM2$^{+/-}$ retinas. We hypothesize that this intact retinal vascular morphology, though presenting vascular leakage and VEGF overexpression, is due to the protective role of Scara5 overexpression in TIM2$^{+/-}$ retinas.

Scara5, a type II transmembrane protein, is a member of class A scavenger receptor family, a structurally diverse group of membrane receptors. Scara5 is widely expressed in humans and mice, including testis, bladder, ovary, trachea, adrenal gland, lung, skin, heart, kidney, muscle bundles, and brain (Jiang et al., 2006; Li et al., 2009; Zani et al., 2015). Our group described Scara5 expression in mouse and human retina for the first time (Mendes-Jorge et al., 2014).
The overexpression of Scara5 has been shown to significantly inhibit the expression levels of matrix metalloproteinases 2 and 9 (Wen et al., 2016). Matrix metalloproteinases have proteolytic activity and mediate the degradation or remodeling of the extracellular matrix, in particular matrix metalloproteinases 2 and 9 (Massova et al., 1998; Clark et al., 2008). Increased expression and activity of these extracellular proteinases play a role in early diabetic retinopathy and alteration of the BRB (Bhatt & Addepalli, 2010). As the basement membrane and extracellular matrix are degraded by these matrix metalloproteinases, which can lead to tortuous vessels, Scara5 overexpression may be exerting a protective role by inhibiting matrix

metalloproteinases 2 and 9 expression, accounting for maintenance of the morphologic structure with no tortuosity in TIM2$^{+/-}$ retinas.

Moreover, elevated expression of matrix metalloproteinases in the retina are associated with tight junction disruption not only by basement degradation, but also by cleavage of tight junction proteins (Gurney, Estrada & Rosenberg, 2006; Reijerkerk et al., 2006; Feng et al., 2011). In diabetic animals, matrix metalloproteinases 2, 9, and 14 are upregulated and are associated with BRB permeability changes. The increase of matrix metalloproteinases may be partly due to the direct effect of hyperglycemia, increased VEGF expression, ROS, and advanced glycation end products. Results suggest that elevated expression of matrix metalloproteinases in the retina may facilitate an increase in vascular permeability by a mechanism involving proteolytic degradation of the tight junction protein occludin, followed by disruption of the overall tight junction complex (Giebel et al., 2005). Therefore, this pathway seems to be not involved in tight junction impairment observed in TIM2$^{+/-}$ retinas, considering Scara5 overexpression protective role.

In conclusion, and knowing that iron accumulation has been associated with the progression and exacerbation of diabetic retinopathy, the present study shows that iron overload in normoglycemia conditions is enough to trigger BRB breakdown and edema, two aspects characteristic of diabetic macular edema, thus confirming the role of iron in BRB dysfunction. All things considered, TIM2 may be a crucial key player in iron homeostasis in the mouse retina, modulating cellular iron levels and affecting iron metabolism in this tissue. Thus, this new receptor could be a potential therapeutic target in animal models for the treatment of diabetic macular edema, especially considering the existence of its ortholog, TIM1, in human patients.

CONCLUSIONS

CONCLUSIONS

1. TIM2 is expressed throughout the entire mouse retina, mainly in its internal surface.

2. TIM2 is expressed in Müller cells but not in astrocytes.

3. All retinal neurons except ganglion cells express TIM2, although to a lesser extent than Müller cells.

4. Rods but not cones express TIM2 in their inner segments.

5. None of the cellular components of the vascular wall in retinal blood vessels expresses TIM2.

6. The TIM2 KO model generated targets cells expressing TIM2 and, unlike other models, the general morphology of the retina is maintained.

7. Only $TIM2^{+/-}$ mice are obtained, probably due to embryonic lethality in $TIM2^{-/-}$ mice.

8. As expected, retinas from $TIM2^{+/-}$ mice show a substantial decrease of TIM2 protein expression.

9. Although *H-* and *L-ferritin* subunit mRNA transcript levels are not significantly increased in retinas from $TIM2^{+/-}$ mice, both proteins levels are increased.

10. mRNA and protein expression levels of Scara5, the receptor for L-ferritin are significantly increased in retinas from $TIM2^{+/-}$ mice, suggesting the exogenous origin of ferritin accumulation in retinal cells.

11. The increase of H- and L-ferritin proteins in retinas from $TIM2^{+/-}$ mice is concomitant with a significant elevation of serum ferritin.

12. mRNA and protein expression levels of transferrin and its receptor are significantly increased in retinas from $TIM2^{+/-}$ mice, suggesting both endogenous production and exogenous import.

13. The iron saturation of serum transferrin and serum iron content are not changed in TIM2$^{+/-}$ mice, suggesting that specific retinal iron accumulation is mediated by ferritin accumulation.

14. A high density of ferritin granules loaded with iron is observed by TEM analysis, mainly in the inner cytoplasmic prolongations of TIM2$^{+/-}$ Müller cells. This is consistent with a significant increase of retinal iron content in retinas from TIM2$^{+/-}$ mice measured by mass spectrometry and colorimetric analysis.

15. Although the vascular pattern is not altered, fundus fluorescein angiography revealed focal points of vascular leakage in retinas from TIM2$^{+/-}$ mice.

16. Serum albumin is observed both *in vivo* and *ex vivo* in the retinal parenchyma of TIM2$^{+/-}$ mice after tail vein injection of fluorescein-labelled serum albumin, suggesting a breakdown of the BRB.

17. TEM analysis shows morphological alterations of tight junctions between endothelial cells in retinas from TIM2$^{+/-}$ mice, and this is paralleled with a decrease of the main proteins that constitute tight junctions in the retina, ZO-1, claudin-5, and occludin, suggesting an alteration of the paracellular transport.

18. PLVAP is overexpressed in retinas from TIM2$^{+/-}$ mice and this is paralleled with an increase in caveolae, suggesting an alteration of the transcellular transport.

19. VEGF is overexpressed in TIM2$^{+/-}$ retinas, suggesting an association of iron and ferritin overload with VEGF expression as a possible explanation for tight junction integrity loss and PLVAP expression accounting for increased vascular permeability and BRB impairment.

20. As a consequence of BRB breakdown, perivascular edema is observed in retinas from TIM2$^{+/-}$ mice. The retinal edema is more pronounced in the central part of the retina resembling what happens in diabetic macular edema, although TIM2$^{+/-}$ mice are not diabetic nor presented retinal inflammation indications.

21. Ferrous iron is increased in retinas from TIM2$^{+/-}$ mice leading to oxidative stress, a well-known trigger of BRB breakdown.

22. As a consequence of oxidative stress, DNA damage and lipid peroxidation are observed in retinas from TIM2$^{+/-}$ mice.

23. **1st FINAL CONCLUSION**: TIM2 deficiency leads to retinal iron overload probably mediated by serum ferritin accumulation. The association of iron and ferritin overload with VEGF overexpression and oxidative stress triggered by the overproduction of ROS lead to the breakdown of the BRB, both at the paracellular and transcellular level. Consequently, BRB breakdown leads to edema of the central retina, similarly as occurs during diabetic macular edema, although $TIM2^{+/-}$ mice are not diabetic.

24. **2nd FINAL CONCLUSION**: Altogether, these results point to TIM2 as a new key player in iron homeostasis in the mouse retina and a potential target in animal models for the treatment of diabetic macular edema in human patients, since it has recently been elucidated that iron overload exacerbates diabetic edema.

REFERENCES

REFERENCES

Abbott, N.J. (2000). Inflammatory mediators and modulation of blood-brain barrier permeability. *Cellular and Molecular Neurobiology*, 20(2), 131-147.

Abbott, N.J., Rönnbäck, L. & Hansson, E. (2006). Astrocyte-endothelial interactions at the blood-brain barrier. *Nature Reviews Neuroscience*, 7(1), 41-53.

Abboud, S. & Haile, D.J. (2000). A novel mammalian iron-regulated protein involved in intracellular iron metabolism. *The Journal of Biological Chemistry*, 275(26), 19906-19912.

Absher, M., Woodcock-Mitchell, J., Mitchell, J., Baldor, L., Low, R. & Warshaw, D. (1989). Characterization of vascular smooth muscle cell phenotype in long-term culture. *In Vitro Cellular & Developmental Biology*, 25(2), 183-192.

Aijaz, S., Balda, M.S. & Matter, K. (2006). Tight junctions: molecular architecture and function. *International Review of Cytology*, 248, 261-298.

Aird, W.C. (2007). Phenotypic heterogeneity of the endothelium: I. Structure, function, and mechanisms. *Circulation Research*, 100(2), 158-173.

Aird, W.C. (2012). Endothelial cell heterogeneity. *Cold Spring Harbor Perspectives in Medicine*, 2(1), a006429.

Aisen, P., Enns, C. & Wessling-Resnick, M. (2001). Chemistry and biology of eukaryotic iron metabolism. *The International Journal of Biochemistry & Cell Biology*, 33(10), 940-959.

Alm, A. & Bill, A. (1973) Ocular and optic nerve blood flow at normal and increased intraocular pressures in monkeys (*Macaca irus*): a study with radioactively labelled microspheres including flow determinations in brain and some other tissues. *Experimental Eye Research*, 15(1), 15-29.

Anderson, B. & McIntosh, H.D. (1967). Retinal Circulation. *Annual Review of Medicine*, 18, 15-26.

Anderson, C.P., Shen M., Eisenstein, R.S. & Leibold, E.A. (2012). Mammalian iron metabolism and its control by iron regulatory proteins. *Biochimica et Biophysica Acta*, 1823(9), 1468-1483.

Anderson, R.G. (1993). Caveolae: where incoming and outgoing messengers meet. *Proceedings of the National Academy of Sciences of the United States of America*, 90(23), 10909-10913.

Anderson, R.G. (2008). Transendothelial movement and caveolae. *Nature Biotechnology*, 26(4), 380-381.

Antonetti, D.A., Barber, A.J., Bronson, S.K., Freeman, W.M., Gardner, T.W., Jefferson, L.S., Kester, M., Kimball, S.R., Krady, J.K., LaNoue, K.F., Norbury, C.C., Quinn, P.G., Sandirasegarane, L. & Simpson, I.A. (2006). Diabetic retinopathy: seeing beyond

glucose-induced microvascular disease. *Diabetes*, 55(9), 2401-2411.

Antonetti, D.A., Barber, A.J., Hollinger, L.A., Wolpert, E.B. & Gardner, T.W. (1999). Vascular endothelial growth factor induces rapid phosphorylation of tight junction proteins occludin and zonula occluden 1. A potential mechanism for vascular permeability in diabetic retinopathy and tumors. *The Journal of Biological Chemistry*, 274(33), 23463-23467.

Antonetti, D.A., Barber, A.J., Khin, S., Lieth, E., Tarbell, J.M. & Gardner, T.W. (1998). Vascular permeability in experimental diabetes is associated with reduced endothelial occludin content: vascular endothelial growth factor decreases occludin in retinal endothelial cells. Penn State Retina Research Group. *Diabetes*, 47(12), 1953-1959.

Arden, G.B., Sidman, R.L., Arap, W. & Schlingemann, R.O. (2005). Spare the rod and spoil the eye. *The British Journal of Ophthalmology*, 89(6), 764-769.

Argaw, A.T., Gurfein, B.T., Zhang, Y., Zameer, A. & John, G.R. (2009). VEGF-mediated disruption of endothelial CLN-5 promotes blood-brain barrier breakdown. *Proceedings of the National Academy of Sciences of the United States of America*, 106(6), 1977-1982.

Arjunan, P., Gnanaprakasam, J.P., Ananth, S., Romej, M.A., Rajalakshmi, V.K., Prasad, P.D., Martin, P.M., Gurusamy, M., Thangaraju, M., Bhutia, Y.D. & Ganapathy, V. (2016). Increased retinal expression of the pro-angiogenic receptor GPR91 via BMP6 in a mouse model of juvenile Hemochromatosis. *Investigative Ophthalmology & Visual Science*, 57(4), 1612-1619.

Armulik, A., Genové, G. & Betsholtz, C. (2011). Pericytes: developmental, physiological, and pathological perspectives, problems, and promises. *Developmental Cell*, 21(2), 193-215.

Armulik, A., Genové, G., Mäe, M., Nisancioglu, M.H., Wallgard, E., Niaudet, C., He, L., Norlin, J., Lindblom, P., Strittmatter, K., Johansson, B.R. & Betsholtz, C. (2010). Pericytes regulate the blood-brain barrier. *Nature*, 468(7323), 557-561.

Arosio, P., Ingrassia, R. & Cavadini, P. (2009). Ferritins: A family of molecules for iron storage, antioxidation and more. *Biochimica et Biophysica Acta*, 1790(7), 589-599.

Arosio, P. & Levi, S. (2010). Cytosolic and mitochondrial ferritins in the regulation of cellular iron homeostasis and oxidative damage. *Biochimica et Biophysica Acta*, 1800(8), 783-792.

Arribas, S.M., Daly, C.J., González, M.C. & McGrath, J.C. (2007). Imaging the vascular wall using confocal microscopy. *The Journal of Physiology*, 584(Pt1), 5-9.

Ashcroft, F.M. & Rorsman, P. (2012). Diabetes mellitus and the beta cell: the last ten years. *Cell*, 148(6), 1160-1171.

Ayton, S., Lei, P., Adlard, P.A., Volitakis, I., Cherny, R.A., Bush A.I. & Finkelstein, D.I. (2014). Iron accumulation confers neurotoxicity to a vulnerable population of nigral neurons: implications for Parkinson's disease. *Molecular Neurodegeneration*, 9, 27.

Baker, E. & Morgan, E.H. (1994). Iron transport. In: J. Brock, J.H. Halliday, M.H. Pippard & L.W. Powell (Eds.), *Iron metabolism in health and disease.* (pp. 63-95). Philadelphia: W.B. Saunders.

Balda, M.S. & Matter, K. (1998). Tight junctions. *Journal of Cell Science*, 111(Pt5), 541-547.

Baluk, P., Morikawa, S., Haskell, A., Mancuso, M. & McDonald, D.M. (2003). Abnormalities of basement membrane on blood vessels and endothelial sprouts in tumors. *The American Journal of Pathology*, 163(5), 1801-1815.

Barber, A.J. & Antonetti, D.A. (2003). Mapping the blood vessels with paracellular permeability in the retinas of diabetic rats. *Investigative Ophthalmology & Visual Science*, 44(12), 5410-5416.

Barber, A.J., Antonetti, D.A., Kern, T.S., Reiter, C.E., Soans, R.S., Krady, J.K., Levison, S.W., Gardner, T.W. & Bronson, S.K. (2005). The Ins2Akita mouse as a model of early retinal complications in diabetes. *Investigative Ophthalmology & Visual Science*, 46(6), 2210-2218.

Barber, A.J., Lieth, E., Khin, S.A., Antonetti, D.A., Buchanan, A.G. & Gardner, T.W. (1998). Neural apoptosis in the retina during experimental and human diabetes: early onset and effect of insulin. *Journal of Clinical Investigation*, 102(4), 783-791.

Baumann, B., Sterling, J., Song, Y., Song, D., Fruttiger, M., Gillies, M., Shen, W. & Dunaief, J.L. (2017). Conditional Müller cell ablation leads to retinal iron accumulation. *Investigative Ophthalmology & Visual Science*, 58(10), 4223-4234.

Bell, B.A., Kaul, C., Rayborn, M.E. & Hollyfield, J.G. (2012). Baseline imaging reveals preexisting retinal abnormalities in mice. *Advances in Experimental Medicine Biology*, 723, 459-469.

Berman, E.R. (1991). Retina. In E.R. Berman (Ed.), *Biochemistry of the eye*. (pp. 309-467). New York: Plenum Press.

Bharadwaj, A.S., Appukuttan, B., Wilmarth, P.A., Pan, Y., Stempel, A.J., Chipps, T.J., Benedetti, E.E., Zamora, D.O., Choi, D., David, L.L. & Smith, J.R. (2013). Role of the retinal vascular endothelial cell in ocular disease. *Progress in Retinal and Eye Research*, 32, 102-180.

Bhatt, L.K. & Addepalli, V. (2010). Attenuation of diabetic retinopathy by enhanced inhibition of MMP-2 and MMP-9 using aspirin and minocycline in streptozotocin-diabetic rats. *American Journal of Translational Research*, 2(2), 181-189.

Bill, A., Törnquist, P. & Alm, A. (1980). Permeability of the intraocular blood vessels. *Transactions of the Ophthalmological Societies of the United Kingdom*, 100(3), 332-336.

Binder, R., Horowitz, J.A., Basilion, J.P., Koeller, D.M., Klausner, R.D. & Harford, J.B. (1994). Evidence that the pathway of transferrin receptor mRNA degradation involves an endonucleolytic cleavage within the 3' UTR and does not involve poly(A) tail shortening. *The EMBO Journal*, 13(8), 1969-1980.

Binz, S.K., Sheehan, A.M. & Wold, M.S. (2004). Replication protein A phosphorylation and the cellular response to DNA damage. *DNA Repair*, 3(8-9), 1015-1024.

Bochkarev, A., Pfuetzner, R.A., Edwards, A.M. & Frappier, L. (1997). Structure of the single-stranded-DNA-binding domain of replication protein A bound to DNA. *Nature*, 385(6612), 176-181.

Bradbury, M.W. & Lightman, S.L. (1990). The blood-brain interface. *Eye (London, England)*, 4(Pt2), 249-254).

REFERENCES

Bresgen, N. & Eckl, P.M. (2015). Oxidative stress and the homeodynamics of iron metabolism. *Biomolecules*, 5(2), 808-847.

Bringmann, A., Iandiev, I., Pannicke, T., Wurm, A., Hollborn, M., Wiedemann, P., Osborne, N.N. & Reichenbach, A. (2009). Cellular signaling and factors involved in Müller cell gliosis: neuroprotective and detrimental effects. *Progress in Retinal and Eye Research*, 28(6), 423-451.

Bringmann, A., Pannicke, T., Grosche, J., Francke, M., Wiedemann, P., Skatchkov, S. N., Osborne, N. N. & Reichenbach, A. (2006). Müller cells in the healthy and diseased retina. *Progress in Retinal and Eye Research*, 25(4), 397-424.

Bristow, E.A., Griffiths, P.G., Andrews, R.M., Johnson, M.A. & Turnbull, D.M. (2002). The distribution of mitochondrial activity in relation to optic nerve structure. *Archives of Ophthalmology*, 120(6), 791-796.

Burdo, J.R., Antonetti, D.A., Wolper, E.B. & Connor, J.R. (2003). Mechanisms and regulation of transferrin and iron transport in a model of blood-brain barrier system. *Neuroscience*, 121(4), 883-890.

Burdo, J.R. & Connor, J.R. (2003). Brain iron uptake and homeostatic mechanisms: an overview. *Biometals*, 16(1), 63-75.

Burdo, J.R., Menzies, S.L., Simpson, I.A., Garrick, L.M., Garrick, M.D., Dolan, K.G., Haile, D.J., Beard, J.L. & Connor, J.R. (2001). Distribution of divalent metal transporter 1 and metal transport protein 1 in the normal and Belgrade rat. *Journal of Neuroscience Research*, 66(6), 1198-1207.

Burn, S.F. (2012). Detection of β-galactosidase activity: X-gal staining. *Methods in Molecular Biology*, 886, 241-250.

Cairo, G. & Recalcati, S. (2007). Iron-regulatory proteins: molecular biology and pathophysiological implications. *Expert Review in Molecular Medicine*, 9(33), 1-13.

Campbell, M. & Humphries, P. (2012). The blood-retina barrier: tight junctions and barrier modulation. *Advances in Experimental Medicine and Biology*, 763, 70-84.

Capecchi, M.R. (1994). Targeted gene replacement. *Scientific American*, 270(3), 52-59.

Carlson, B.M. (1999). *Human embryology & development.* (2nd Ed.). Saint Louis: Mosby.

Casanueva, E. & Viteri, F.E. (2003). Iron and oxidative stress in pregnancy. *The Journal of Nutrition*, 133(5 Suppl 2), 1700S-1708S.

Catita, J., López-Luppo, M., Ramos, D., Nacher, V., Navarro, M., Carretero, A., Sánchez-Chardi, A., Mendes-Jorge, L., Rodriguez-Baeza, A. & Ruberte J. (2015). Imaging of cellular aging in human retinal blood vessels. *Experimental Eye Research*, 135, 14-25.

Chasteen, N.D. & Harrison, P.M. (1999). Mineralization in ferritin: an efficient means of iron storage. *Journal of Structural Biology*, 126(3), 182-194.

Chaudhary, K., Promsote, W., Ananth, S., Veeranan-Karmegam, R., Tawfik, A., Arjunan, P., Martin, P., Smith, S.B., Thangaraju, M., Kisselev, O., Ganapathy, V. & Gnana-Prakasam, J.P. (2018). Iron overload accelerates the progression of diabetic retinopathy in association with increased retinal renin expression. *Scientific Reports*, 8(1), 3025.

Chaudhury, C., Kim, J., Mehnaz, S., Wani, M.A., Oberyszyn, T.M., Bronson, C.L., Mohanty, S., Hayton, W.L., Robinson, J.M. & Anderson, C.L. (2006). Accelerated transferrin degradation in HFE-deficient mice is associated with increased transferrin saturation. *The Journal of Nutrition*, 136(12), 2993-2998.

Chen, L., Yang, P. & Kijlstra, A. (2002). Distribution, markers, and functions of retinal microglia. *Ocular Immunology and Inflammation*, 10(1), 27-39.

Chen, T.T., Li, L., Chung, D.H., Allen, C.D., Torti, S.V., Torti, F.M., Cyster, J.G., Chen, C.Y., Brodsky, F.M., Niemi, E.C., Nakamura, M.C., Seaman, W.E. & Daws, M.R. (2005). TIM-2 is expressed on B cells and in liver and kidney and is a receptor for H-ferritin endocytosis. *The Journal of Experimental Medicine*, 202(7), 955-965.

Cheung, A.K., Fung, M.K., Lo, A.C., Lam, T.T., So, K.F., Chung, S.S. & Chung, S.K. (2005). Aldose reductase deficiency prevents diabetes-induced blood-retinal barrier breakdown, apoptosis, and glial reactivation in the retina of db/db mice. *Diabetes*, 54(11), 3119-3125.

Cheung, N., Mitchell, P. & Wong, T.Y. (2010). Diabetic retinopathy. *Lancet*, 376(9735), 124-136.

Chiou, B., Lucassen, E., Sather, M., Kallianpur, A. & Connor J. (2018). Semaphorin4A and H-ferritin utilize Tim-1 on human oligodendrocytes: a novel neuro-immune axis. *Glia*, 66(7), 1317-1330.

Chua, C.C., Hamdy, R.C. & Chua, B.H. (1998). Upregulation of vascular endothelial growth factor by H2O2 in rat heart endothelial cells. *Free Radical Biology & Medicine*, 25(8), 891-897.

Ciudin, A., Hernández, C. & Simó, R. (2010). Iron overload in diabetic retinopathy: a cause or a consequence of impaired mechanisms? *Experimental Diabetes Research*, 2010, 714108.

Clark, I.M., Swingler, T.E., Sampieri, C.L. & Edwards, D.R. (2008). The regulation of matrix metalloproteinases and their inhibitors. *The International Journal of Biochemistry & Cell Biology*, 40(6-7), 1362-1378.

Comporti, M. (2002). Introduction-serial review: iron and cellular redox status. *Free Radical Biology & Medicine*, 32(7), 565-567.

Congdon, N. G., Friedman, D. S. & Lietman, T. (2003). Important causes of visual impairment in the world today. *Journal of the American Medical Association*, 290(15), 2057-2060.

Connor, J.R. & Menzies, S.L. (1996). Relationship of iron to oligodendrocytes and myelination. *Glia*, 17(2), 83-93.

Connor, J.R., Menzies, S.L., St Martin, S.M. & Mufson, E.J. (1992). A histochemical study of iron, transferrin, and ferritin in Alzheimer's diseased brains. *Journal of Neuroscience Research*, 31(1), 75-83.

Cook, C.I. & Yu, B.P. (1998). Iron accumulation in aging: modulation by dietary restriction. *Mechanisms of Ageing and Development*, 102(1), 1-13.

Cook, C.S. & Peiffer, R.L.J. (2001). Clinical basic science. In R.L.J. Peiffer & S.M. Peterson-Jones, *Small animal ophthalmology: a problem-oriented approach*. (3rd Ed.). (pp. 1-12). London: W.B. Saunders.

REFERENCES

Coscas, G., Cunha-Vaz, J. & Soubrane, G. (2010). Macular edema: definition and basic concepts. *Developments in Ophthalmology*, 47, 1-9.

Crawford, T.N., Alfaro, D.V. 3rd, Kerrison, J.B. & Jablon, E.P. (2009). Diabetic retinopathy and angiogenesis. *Current Diabetes Reviews*, 5(1), 8-13.

Cunha-Vaz, J.G. (1976). The blood-retinal barriers. *Documenta Ophthalmologica*. 41(2), 287-327.

Cunha-Vaz, J. (2009). The blood-retinal barrier in retinal disease. *European Ophthalmic Review*, 3(2), 105-108.

Cunha-Vaz, J. (2010). An integrated perspective on diabetic retinopathy in type 2 diabetes: 10.4 Characterization of retinopathy phenotypes. In: J. Cunha-Vaz (Ed.), *Diabetic retinopathy*. (pp. 296-300). Singapore: World Scientific Publishing.

Cunha-Vaz, J., Bernardes, R. & Lobo, C. (2011). Blood-retinal barrier. *European Journal of Ophthalmology*, 21 Suppl 6, S3-9.

Cussimanio, B.L., Booth, A.A., Todd, P., Hudson, B.G. & Khalifah, R.G. (2003). Unusual susceptibility of heme proteins to damage by glucose during non-enzymatic glycation. *Biophysical Chemistry*, 105(2-3), 743-755.

Daruich, A., Matet, A., Moulin, A., Kowalczuk, L., Nicolas, M., Sellam, A., Rothschild, P.R., Omri, S., Gélizé, E., Jonet, L., Delaunay, K., De Kozak, Y., Berdugo, M., Zhao, M., Crisanti, P. & Behar-Cohen, F. (2018). Mechanisms of macular edema: beyond the surface. *Progress in Retinal and Eye Research*, 63, 20-68.

de la Rosa, L.C., Moshage, H. & Nieto, N. (2008). Hepatocyte oxidant stress and alcoholic liver disease. *Revista Española de Enfermedades Digestivas*, 100(3), 156-163.

De Schaepdrijver, L., Simoens, P., Lauwers, H. & De Geest, J.P. (1989). Retinal vascular patterns in domestic animals. *Research in Veterinary Science*, 47(1), 34-42.

Delaey, C. & Van De Voorde, J. (2000). Regulatory mechanisms in the retinal and choroidal circulation. *Ophthalmic Research*, 32(6), 249-256.

Deb, S., Johnson, E.E., Robalinho-Teixeira, R.L. & Wessling-Resnick, M. (2009). Modulation of intracellular iron levels by oxidative stress implicates a novel role for iron in signal transduction. *Biometals*, 22(5), 855-862.

Diamond, J.S. (2017). Inhibitory interneurons in the retina: types, circuitry, and function. *Annual Review of Vision Science*, 3, 1-24.

Díaz-Coránguez, M., Ramos, C. & Antonetti, D.A. (2017). The inner blood-retinal barrier: cellular basis and development. *Vision Research*, 139, 123-137.

Dinet, V., Bruban, J., Chalour, N., Maoui, A., An, N., Jonet, L., Buret, A., Behar-Cohen, F., Klein, C., Tréton, J. & Mascarelli, F. (2012). Distinct effects of inflammation on gliosis, osmohomeostasis, and vascular integrity during amyloid beta-induced retinal degeneration. *Aging Cell*, 11(4), 683-693.

Distler, C. & Dreher Z. (1996). Glia cells of the monkey retina--II. Müller cells. *Vision Research*, 36(16), 2381-2394.

Dougherty, G., Johnson, M.J. & Wiers, M.D. (2010). Measurement of retinal vascular tortuosity and its application to retina pathologies. *Medical & Biological Engineering & Computing*,

48(1), 87-95.

Donovan, A., Brownlie, A., Zhou, Y., Shepard, J., Pratt, S.J., Moynihan, J., Paw, B.H., Drejer, A., Barut, B., Zapata, A., Law, T.C., Brugnara, C., Lux, S.E., Pinkus, G.S., Pinkus, J.L., Kingsley, P.D., Palis, J., Fleming, M.D., Andrews, N.C. & Zon, L.I. (2000). Positional cloning of zebrafish ferroportin1 identifies a conserved vertebrate iron exporter. *Nature*, 403(6771), 776-781.

Double, K.L., Maywald, M., Schmittel, M., Riederer, P. & Gerlach, M. (1998). In vitro studies of ferritin iron release and neurotoxicity. *Journal of Neurochemistry*, 70(6), 2492-2499.

Dreher, Z., Robinson, S.R. & Distler, C. (1992). Müller cells in vascular and avascular retinae: A survey of seven mammals. *The Journal of Comparative Neurology*, 323(1), 59-80.

Dröge, W. (2002). Free radicals in the physiological control of cell function. *Physiological Reviews*, 82(1), 47-95.

Duck, K.A. & Connor, J.R. (2016). Iron uptake and transport across physiological barriers. *Biometals*, 29(4), 573-591.

Durante, M., Bedford, J.S., Chen, D.J., Conrad, S., Cornforth, M.N., Natarajan, A.T., van Gent, D.C. & Obe, G. (2013). From DNA damage to chromosome aberrations: joining the break. *Mutation Research*, 756(1-2), 5-13.

Duh, E.J., Sun, J.K. & Stitt, A.W. (2017). Diabetic retinopathy: current understanding, mechanisms, and treatment strategies. *JCI Insight*, 2(14), e93751.

Dunaief, J.L. (2006). Iron induced oxidative damage as a potential factor in age-related macular degeneration: the Cogan Lecture. *Investigative Ophthalmology & Visual Science*, 47(11), 4660-4664.

Ebnet, K., Suzuki, A., Ohno, S. & Vestweber, D. (1993). Junctional adhesion molecules (JAMs): more molecules with dual functions? *Journal of Cell Science*, 117(Pt1), 19-29.

Ebrey, T. & Koutalos, Y. (2001). Vertebrate photoreceptors. *Progress in Retinal and Eye Research*, 20(1), 49-94.

Eisenberg, E. & Levanon, E.Y. (2013). Human housekeeping genes, revisited. *Trends in Genetics*, 29(10), 569-474.

Elayat, A.A., el-Naggar, M.M. & Tahir, M. (1995). An immunocytochemical and morphometric study of the rat pancreatic islets. *Journal of Anatomy*, 186(Pt3), 629-637.

Elkotby, D., Hassan, A.K., Emad, R. & Bahgat, I. (2018). Histological changes in islets of Langerhans of pancreas in alloxan-induced diabetic rats following egyptian honey bee venom treatments. *International Journal of Pure and Applied Zoology*, 6(1), 1-6.

Enge, M., Bjarnegård, M., Gerhardt, H., Gustafsson, E., Kalén, M., Asker, N., Hammes, H.P., Shani, M., Fässler, R. & Betsholtz, C. (2002). Endothelium-specific platelet-derived growth factor-B ablation mimics diabetic retinopathy. *EMBO Journal*, 21(16), 4307-4316.

Esperança-Pina, J.A. (2000). *Anatomia humana da relação – Parte II*. Lisboa: Lidel, Edições Técnicas, Lda.

Fajardo, R.J., Karim, L., Calley, V.I. & Bouxsein, M.L. (2014). A review of rodent models of type 2 diabetic skeletal fragility. *Journal of Bone and Mineral Research*, 29(5), 1025-

1040.

Fanning, A.S., Mitic, L.L. & Anderson, J.M. (1999). Transmembrane proteins in the tight junction barrier. *Journal of the American Society of Nephrology*, 10(6), 1337-1345

Fardy, C.A. & Silverman, M. (1995). Antioxidants in neonatal lung disease. *Archives of Disease in Childhood Fetal Neonatal*, 73(2), F112-F117.

Farquhar, M.G. & Palade, G.E. (1963). Junctional complexes in various epithelia. *The Journal of Cell Biology*, 17, 375-412.

Federman, J.L. (1982). The fenestrations of the choriocapillaris in the presence of choroidal melanoma. *Transactions of the American Ophthalmological Society*, 80, 498-516.

Feng, S., Cen, J., Huang, Y., Shen, H., Yao, L., Wang, Y. & Chen, Z. (2011). Matrix metalloproteinase-2 and -9 secreted by leukemic cells increase the permeability of blood-brain barrier by disrupting tight junction proteins. *PLoS One*, 6(8), e20599.

Feng, Y., Venema, V.J., Venema, R.C., Tsai, N., Behzadian, M.A. & Caldwell, R.B. (1999). VEGF-induced permeability increase is mediated by caveolae. *Investigative Ophthalmology & Visual Science*, 40(1), 157-167.

Feng, Y., vom Hagen, F., Lin, J. & Hammes, H.P. (2007). Incipient diabetic retinopathy--insights from an experimental model. *Ophthalmologica*, 221(4), 269-274.

Fischer, A.H., Jacobson, K.A., Rose, J. & Zeller, R. (2008). *Hematoxylin and eosin staining of tissue and cell sections.* Cold Spring Harbor Protocol, Retrieved March, 2018, from http://cshprotocols.cshlp.org/content/2008/5/pdb.prot4986.abstract.

Fisher, J., Devraj, K., Ingram, J., Slangle-Webb, B., Madhankumar, A.B., Liu, X., Klinger, M., Simpson, I.A. & Connor, J.R. (2007). Ferritin: a novel mechanism for delivery of iron to the brain and other organs. *American Journal of Physiology - Cell Physiology*, 293(2), C641-C649.

Fischer, S., Wobben, M., Marti, H.H., Renz, D. & Schaper, W. (2002). Hypoxia-induced hypermeability in brain microvessel endothelial cells involves VEGF-mediated changes in the expression of zonula occludens-1. *Microvascular Research*, 63(1), 70-80.

Forrester, J.V., Dick, A.D., McMenamin, P.G. & Lee, W.R (2002). *The eye: basic sciences in practice*. (2nd Ed.). Philadelphia: W.B. Saunders.

Forrester, J.V. & Knott, R.M. (1997). Pathogenesis of diabetic retinopathy. In J.C. Pickup & G Williams (Eds.), *Textbook of diabetes*. (2nd Ed.). (pp. 45.1-45.19). Oxford: Blackwell Science Ltd.

Franco, S., Gostissa, M., Zha, S., Lombard, D.B., Murphy, M.M., Zarrin, A.A., Yan, C., Tepsuporn, S., Morales, J.C., Adams, M.M., Lou, Z., Bassing, C.H., Manis, J.P., Chen, J., Carpenter, P.B. & Alt, F.W. (2006). H2AX prevents DNA breaks from progressing to chromosome breaks and translocations. *Molecular Cell*, 21(2), 201-214.

Frey, P.A. & Reed, G.H. (2012). The ubiquity of iron. *ACS Chemical Biology*, 7(9), 1477-1481.

Frey, T. & Antonetti, D.A. (2011). Alterations to the blood-retinal barrier in diabetes: cytokines and reactive oxygen species. *Antioxidants & Redox Signaling*, 15(5), 1271-1284.

Fruttiger, M. (2007). Development of the retinal vasculature. *Angiogenesis*, 10(2), 77-88.

Funk, R.H. (1997). Blood supply of the retina. *Ophthalmic Research*, 29(5), 320-325.

Furuse, M., Hirase, T., Itoh, M., Nagafuchi, A., Yonemura, S., Tsukita, S. & Tsukita, S. (1993). Occludin: a novel integral membrane protein localizing at tight junctions. *The Journal of Cell Biology*, 123(6Pt2), 1777-1788.

Furuse, M. Sasaki, H., Fujimoto, K. & Tsukita, S. (1998). A single gene product, claudin-1 or -2, reconstitutes tight junction strands and recruits occludin in fibroblasts. *The Journal of Cell Biology*, 143(2), 391-401.

Galaris, D. & Pantopoulos, K. (2008). Oxidative stress and iron homeostasis: mechanistic and health aspects. *Critical Reviews in Clinical Laboratory Sciences*, 45(1), 1-23.

Gammella, E., Recalcati, S. & Cairo, G. (2016). Dual role of ROS as signal and stress agents: iron tips the balance in favor of toxic effects. *Oxidative Medicine and Cellular Longevity*, 2016:8629024.

Ganz, T. & Nemeth, E. (2015). Iron homeostasis in host defence and inflammation. *Nature Reviews Immunology*, 15(8), 500-510.

García-Castiñeiras, S. (2010). Iron, the retina and the lens: a focused review. *Experimental Eye Research*, 90(6), 664-678.

Gardiner, T.A., Stitt, A.W. & Archer, D.B. (1995). Retinal vascular endothelial cell endocytosis increases in early diabetes. *Laboratory Investigation*, 72(4), 439-444.

Gardner, T.W., Antonetti, D.A., Barber, A.J., LaNoue, K.F. & Levison, S.W. (2002). Diabetic retinopathy: more than meets the eye. *Survey of Ophthalmology*, 47 Suppl 2, S253-S262.

Gartner, L.P. & Hiatt, J.L. (2007). *Color textbook of histology.* (3rd Ed.). Philadelphia: Saunders Elsevier.

Geisser, P. & Burckhardt, S. (2011). The pharmacokinetics and pharmacodynamics of iron preparations. *Pharmaceutics*, 3(1), 12-33.

Germer, A., Biedermann, B., Wolburg, H., Schuck, J., Grosche, J., Kuhrt, H., Reichelt, W., Schousboe, A., Paasche, G., Mack, A.F. & Reichenbach, A. (1998). Distribution of mitochondria within Müller cells--I. Correlation with retinal vascularization in different mammalian species. *Journal of Neurocytology*, 27(5), 329-345.

Ghassemifar, R., Lai, C.M. & Rakoczy, P.E. (2006). Regulation of tight junction proteins in cultured retinal pigment epithelial cells and in VEGF overexpressing transgenic mouse retinas. *Advances in Experimental Medicine and Biology*, 572, 179-185.

Giebel, S.J., Menicucci, G., McGuire, P.G. & Das, A. (2005). Matrix metalloproteinases in early diabetic retinopathy and their role in alteration of the blood-retinal barrier. *Laboratory Investigation*, 85(5), 597-607.

Gloor, S.M., Wachtel, M., Bolliger, M.F., Ishihara, H., Landmann, R. & Frei, K. (2001). Molecular and cellular permeability control at the blood-brain barrier. *Brain Research. Brain Research Reviews*, 36(2-3), 258-264.

Gnana-Prakasam, J.P., Ananth, S., Prasad, P.D., Zhang, M., Atherton, S.S., Martin, P.M., Smith, S.B. & Ganapathy, V. (2011). Expression and iron-dependent regulation of succinate receptor GPR91 in retinal pigment epithelium. *Investigative Ophthalmology & Visual Science*, 52(6), 3751-3758.

Gnana-Prakasam, J.P., Martin, P.M., Mysona, B.A., Roon, P., Smith, S.B. & Ganapathy, V. (2008). Hepcidin expression in mouse retina and its regulation via lipopolysaccharide/Toll-like receptor-4 pathway independent of Hfe. *The Biochemical Journal*, 411(1), 79-88.

Gnana-Prakasam, J.P., Martin, P.M., Smith, S.B. & Ganapathy, V. (2010). Expression and function of iron-regulatory proteins in retina. *IUBMB Life*, 62(5), 363-370.

Göke, B. (2008). Islet cell function: alpha and beta cells--partners towards normoglycaemia. *International Journal of Clinical Practice*, 62(159), 2-7.

Goldman, D. (2014). Müller glia cell reprogramming and retina regeneration. *Nature Reviews Neuroscience*, 15(7), 431-442.

Gonçalves, C. & Bairos, V. (2006). *Histologia - texto e imagens*. Coimbra: Imprensa da Universidade de Coimbra.

González-Mariscal, L., Tapia, R. & Chamorro, D. (2008). Crosstalk of tight junction componentes with signaling pathways. *Biochimica et Biophysica Acta*, 1778(3), 729-756.

Goralska, M., Ferrell, J., Harned, J., Lall, M., Nagar, S., Fleisher, L.N. & McGahan, M.C. (2009). Iron metabolism in the eye: a review. *Experimental Eye Research*, 88(2), 204-215.

Gozzelino, R. & Arosio, P. (2016). Iron homeostasis in health and disease. *International Journal of Molecular Science*, 17(1), 130.

Greenough, M.A., Camakaris, J. & Bush, A.I. (2013). Metal dyshomeostasis and oxidative stress in Alzheimer's disease. *Neurochemistry International*, 62(5), 540-555.

Gu, X., Reagan, A., Yen, A., Bhatti, F., Cohen, A.W., Elliott, M.H. (2014). Spatial and temporal localization of caveolin-1 protein in the developing retina. *Advances in Experimental Medicine and Biology*, 801, 15-21.

Gunshin, H., Mackenzie, B., Berger, U.V., Gunshin, Y., Romero, M.F., Boron, W.F., Nussberger, S., Gollan, J.L. & Hediger, M.A. (1997). Cloning and characterization of a mammalian proton-coupled metal–ion transporter. *Nature*, 388(6641), 482-488.

Günzel, D. & Yu, A.S. (2013). Claudins and the modulation of tight junction permeability. *Physiological Reviews*, 93(2), 525-569.

Guo, L., Jiang, F., Tang, Y.T., Si, M.Y. & Jiao, X.Y. (2014). The association of serum vascular endothelial growth factor and ferritin in diabetic microvascular disease. *Diabetes Technology & Therapeutics*, 16(4), 224-234.

Gupta, N., Mansoor, S., Sharma, A., Sapkal, A., Sheth, J., Falatoonzadeh, P., Kuppermann, B.D. & Kenney, M.C. (2013). Diabetic retinopathy and VEGF. *The Open Ophthalmology Journal*, 7, 4-10.

Gurney, K.J., Estrada, E.Y. & Rosenberg, G.A. (2006). Blood-brain barrier disruption by stromelysin-1 facilitates neutrophil infiltration in neuroinflammation. *Neurobiology of Disease,* 23(1), 87-96.

Hadziahmetovic, M., Song, Y., Wolkow, N., Iacovelli, J., Grieco, S., Lee, J., Lyubarsky, A., Pratico, D., Connelly, J., Spino, M., Harris, Z.L. & Dunaief, J.L. (2011a). The oral iron chelator deferiprone protects against iron overload-induced retinal degeneration.

Investigative Ophthalmology & Visual Science, 52(2), 959-968.

Hadziahmetovic, M., Song, Y., Wolkow, N., Iacovelli, J., Kautz, L., Roth, M.P., & Dunaief, J.L. (2011b). Bmp6 regulates retinal iron homeostasis and has altered expression in age-related macular degeneration. *The American Journal of Pathology*, 179(1), 335-348.

Hall, B., Limaye, A. & Kulkarni, A.B. (2009). Overview: generation of gene knockout mice. *Current Protocols in Cell Biology*, Chapter 19, Unit 19.12.1-17.

Halliwell, B. & Gutteridge, J.M. (1984). Oxygen toxicity, oxygen radicals, transition metals and disease. *The Biochemical Journal*, 219(1), 1-14.

Halliwell, B. & Gutteridge, J.M. (1990). Role of free radicals and catalytic metal ions in human disease: an overview. *Methods in Enzymology*, 186, 1-85.

Hallmann, R., Mayer, D.N., Berg, E.L., Broermann, R. & Butcher, E.C. (1995). Novel mouse endothelial cell surface marker is suppressed during differentiation of the blood brain barrier. *Developmental Dynamics*, 202(4), 325-332.

Hamilton, N. (2009). Quantification and its applications in fluorescent microscopy imaging. *Traffic*, 10(8), 951-961.

Hammes, H.P. (2018). Diabetic retinopathy: hyperglycaemia, oxidative stress and beyond. *Diabetologia*, 61(1), 29-38.

Han, H.C. (2012). Twisted blood vessels: symptoms, etiology and biomechanical mechanisms. *Journal of Vascular Research*, 49(3), 185-197.

Han, J., Day, J.R., Connor, J.R. & Beard, J.L. (2003). Gene expression of transferrin and transferrin receptor in brains of control vs. iron-deficient rats. *Nutritional Neuroscience*, 6(1), 1-10.

Han, J., Seaman, W.E., Di, X., Wang, W., Willingham, M., Torti, F.M. & Torti, S.V. (2011). Iron uptake mediated by binding of H-ferritin to the TIM-2 receptor in mouse cells. *PLoS One*, 6(8), e23800.

Harhaj, N.S. & Antonetti, D.A. (2004). Regulation of tight junctions and loss of barrier function in pathophysiology. *The International Journal of Biochemistry & Cell Biology*, 36(7), 1206-1237.

Harned, J., Ferrell, J., Lall, M.M., Fleisher, L.N., Nagar, S., Goralska, M. & McGahan, M.C. (2010). Altered ferritin subunit composition: change in iron metabolism in lens epithelial cells and downstream effects on glutathione levels and VEGF secretion. *Investigative Ophthalmology & Visual Science*, 51(9), 4437-4446.

Harrison, P.M. & Arosio P. (1996). The ferritins: molecular properties, iron storage function and cellular regulation. *Biochimica et Biophysica Acta*, 1275(3), 161-203.

Hartnett, M.E., Martiniuk, D., Byfield, G., Geisen, P., Zeng, G. & Bautch, V.L. (2008). Neutralizing VEGF decreases tortuosity and alters endothelial cell division orientation in arterioles and veins in a rat model of ROP: relevance to plus disease. *Investigative Ophthalmology & Visual Science*, 49(7), 3107-3114.

Harwell, B. (2007). Biochemistry of oxidative stress. *Biochemical Society Transactions*, 35(5), 1147-1150.

Hashimoto, H., Ishikawa, H. & Kusakabe, M. (1999). Preparation of whole mounts and thick

sections for confocal microscopy. *Methods in Enzymology*, 307, 84-107.

Haurigot, V., Villacampa, P., Ribera, A., Llombart, C., Bosch, A., Nacher, V., Ramos, D., Ayuso, E., Segovia, J.C., Bueren, J.A., Ruberte, J. & Bosch, F. (2009). Increased intraocular insulin-like growth factor-I triggers blood-retinal barrier breakdown. *The Journal of Biological Chemistry*, 284(34), 22961-22969.

Haverkamp, S. & Wässle, H. (2000). Immunocytochemical analysis of the mouse retina. *The Journal of Comparative Neurology*, 424(1), 1-23.

Hayden, M.R., Sowers, J.R. & Tyagi, S.C. (2005). The central role of vascular extracellular matrix and basement membrane remodeling in metabolic syndrome and type 2 diabetes: the matrix preloaded. *Cardiovascular Diabetology*, 4:9.

He, X., Hahn, P., Iacovelli, J., Wong, R., King, C., Bhisitkul, R., Massaro-Giordana, M. & Dunaief, J.L. (2007). Iron homeostasis and toxicity in retinal degeneration. *Progress in Retinal and Eye Research*, 26(6), 649-673.

Hentze, M.W., Muckenthaler, M.U., Galy, B. & Camaschella, C. (2010). Two to tango: regulation of mammalian iron metabolism. *Cell*, 142(1), 24-38.

Herman, I.M. & D'Amore, P.A. (1985). Microvascular pericytes contain muscle and nonmuscle actins. *The Journal of Cell Biology*, 101(1), 43-52.

Heylmann, D. & Kaina, B. (2016). The γH2AX DNA damage assay from a drop of blood. *Scientific Reports*, 6, 22682.

Hildebrand, G.D. & Fielder, A.R. (2011). Anatomy and physiology of the retina. In J.D. Reynolds & S.E. Olitsky (Eds.), *Pediatric retina*. (pp. 39-65). Heildelberg: Springer.

Hill, J.M., Ruff, M.R., Weber, R.J. & Pert, C.B. (1985). Transferrin receptors in rat brain: neuropeptide-like pattern and relationship to iron distribution. *Proceedings of the National Academy of Sciences of the United States of America*, 82(13), 4553-4557.

Hofman, P., Blaauwgeers, H.G., Tolentino, M.J., Adamis, A.P., Nunes Cardozo, B.J., Vrensen, G.F. & Schlingemann, R.O. (2000). VEGF-A induced hyperpermeability of blood-retinal barrier endothelium in vivo is predominantly associated with pinocytotic vesicular transport and not with formation of fenestrations. Vascular endothelial growth factor-A. *Current Eye Research*, 21(2), 637-645.

Hofman, P., Hoyng, P., vanderWerf, F., Vrensen, G.F. & Schlingemann, R.O. (2001). Lack of blood-brain barrier properties in microvessels of the prelaminar optic nerve head. *Investigative Ophthalmology & Visual Science*, 42(5), 895-901.

Hogan, M.J., Alvarado, J.A. & Weddell, J.E. (1971). *Histology of the human eye: an atlas and textbook*. Philadelphia: W.B. Saunders Company.

Hollander, H., Makarov, F., Dreher, Z., van Driel, D., Chan-Ling, T.L. & Stone, J. (1991). Structure of the macroglia of the retina: sharing and division of labour between astrocytes and Müller cells. *The Journal of Comparative Neurology*, 313(4), 587-603.

Hosoya, K., Yamamoto, A., Akanuma, S. & Tachikawa, M. (2010). Lipophilicity and transporter influence on blood-retinal barrier permeability: a comparison with blood-brain barrier permeability. *Pharmaceutical Research*, 27(12), 2715-2724.

Huang, H.H., Farmer, K., Windscheffel, J., Yost, K., Power, M., Wright, D.E. & Stehno-Bittel, L. (2011). Exercise increases insulin content and basal secretion in pancreatic islets in

type 1 diabetic mice. *Experimental Diabetes Research*, 2011, 481427.

Huber, G., Beck, S.C., Grimm, C., Sahaboglu-Tekgoz, A., Paquet-Durand, F., Wenzel, A., Humphries, P., Redmond, T.M., Seeliger, M.W. & Fischer, M.D. (2009). Spectral domain optical coherence tomography in mouse models of retinal degeneration. *Investigative Ophthalmology & Visual Science*, 50(12), 5888-5895.

Hughes, S. & Chan-Ling, T. (2004). Characterization of smooth muscle cell and pericyte differentiation in the rat retina in vivo. *Investigative Ophthalmology & Visual Science*, 45(8), 2795-2806.

Hulet, S.W., Hess, E.J., Debinski, W., Arosio, P., Bruce, K., Powers, S. & Connor, J.R. (1999a). Characterization and distribution of ferritin binding sites in the adult mouse brain. *Journal of Neurochemistry*, 72(2), 868-874.

Hulet, S.W., Powers, S. & Connor, J.R. (1999b). Distribution of transferrin and ferritin binding in normal and multiple sclerotic human brains. *Journal of the Neurological Sciences*, 165(1), 48-55.

Hunt, R.C. & Davis, A.A. (1992). Release of iron by human retinal pigment epithelial cells. *Journal of Cellular Physiology*, 152(1), 102-110.

Hunt, R.C., Dewey, A. & Davis, A.A. (1989). Transferrin receptors on the surface of retinal pigment epithelial cells are associated with the cytoskeleton. *Journal of Cell Science*, 92(Pt4), 655-666.

Iancu, T.C. (1983). Iron overload. *Molecular Aspects of Medicine*, 6(1), 1-100.

Iancu, T.C. (1992). Ferritin and hemosiderin in pathological tissues. *Electron Microscopy Reviews*, 5(2), 209-229.

Iancu, T.C. & Manov, I. (2017). Inverted ferritin images: electron microscopy of a natural enhanced biomarker. *JSM Nanotechnology & Nanomedicine*, 5(1), 1048.

Iftode, C., Daniely, Y. & Borowiec, J.A. (1999). Replication protein A (RPA): the eukaryotic SSB. *Critical Reviews in Biochemistry and Molecular Biology*, 34(3), 141-180.

Ishikawa, T. (1963). Fine structure of retinal vessels in man and the macaque monkey. *Investigative Ophthalmology & Visual Science*, 2, 1-15.

Jackson, S.P. (2002). Sensing and repairing DNA double-strand breaks. *Carcinogenesis*, 23(5), 687-696.

Jeon, C., Strettoi, E. & Masland, R.H. (1998). The major cell populations of the mouse retina. *The Journal of Neuroscience*, 18(21), 8936-8946.

Jiang, D., Li, X., Williams, R., Patel, S., Men, L., Wang, Y. & Zhou, F. (2009). Ternary complexes of iron, amyloid-β and nitrilotriacetic acid: binding affinities, redox properties, and relevance to iron-induced oxidative stress in Alzheimer's disease. *Biochemistry*, 48(33), 7939-7947.

Jiang, Y., Oliver, P., Davies, K.E. & Platt N. (2006). Identification and characterization of murine SCARA5, a novel class A scavenger receptor that is expressed by populations of epithelial cells. *The Journal of Biological Chemistry*, 281(17), 11834-11845.

Joshi, V.S. (2012). *Analysis of retinal vessel networks using quantitative descriptors of vascular morphology*. Ph.D. Thesis. Iowa: Department of Biomedical Engineering, University of Iowa.

Junqueira, L.C. & Carneiro, J. (1983). *Histologia básica*. Rio de Janeiro: Guanabara Koogan.

Kaur, C., Foulds, W. & Ling, E. (2008). Blood–retinal barrier in hypoxic ischaemic conditions: basic concepts, clinical features and management. *Progress in Retinal and Eye Research*, 27(6), 622-647.

Kaur, D., Rajagopalan, S. & Andersen, J.K. (2009). Chronic expression of H-ferritin in dopaminergic midbrain neurons results in an age-related expansion of the labile iron pool and subsequent neurodegeneration: implications for Parkinson's disease. *Brain Research*, 1297, 17-22.

Kaur, D., Rajagopalan, S., Chinta, S., Kumar, J., Di Monte, D., Cherny, R.A. & Andersen, J.K. (2007). Chronic ferritin expression within murine dopaminergic midbrain neurons results in a progressive age-related neurodegeneration. *Brain Research*, 1140, 188-194.

Kehrer, J.P. (2000). The Haber-Weiss reaction and mechanisms of toxicity. *Toxicology*, 149(1), 43-50.

Kell, D.B. (2009). Iron behaving badly: inappropriate iron chelation as a major contributor to the aetiology of vascular and other progressive inflammatory and degenerative diseases. *BMC Medical Genomics*, 2, 2.

Kienzl, E., Puchinger, L., Jellinger, K., Linert, W., Stachelberger, H. & Jameson, R.F. (1995). The role of transition metals in the pathogenesis of Parkinson's disease. *Journal of the Neurological Sciences*, 134 Suppl, 69-78.

Kim, B., Abdel-Rahman, M.H., Wang, T., Pouly, S., Mahmoud, A.M. & Cebulla, C.M. (2014). Retinal MMP-12, MMP-13, TIMP-1, and TIMP-2 expression in murine experimental retinal detachment. *Investigative Ophthalmology & Visual Science*, 55(4), 2031-2040.

Kim, Y.W. & Byzova, T.V. (2014). Oxidative stress in angiogenesis and vascular disease. *Blood*, 123(5), 625-631.

Kinner, A., Wu, W., Staudt, C. & Iliakis, G. (2008). Gamma-H2AX in recognition and signaling of DNA double-strand breaks in the context of chromatin. *Nucleic Acids Research*, 36(17), 5678-5694.

Klaassen, I., Hughes, J.M., Vogels, I.M., Schalkwijk, C.G., Van Noorden, C.J. & Schlingemann, RO. (2009). Altered expression of genes related to blood-retina barrier disruption in streptozotocin-induced diabetes. *Experimental Eye Research*, 89(1), 4-15.

Klaassen, I., Van Noorden, C.J. & Schlingemann, R.O. (2013). Molecular basis of the inner blood-retinal barrier and its breakdown in diabetic macular edema and other pathological conditions. *Progress in Retinal and Eye Research*, 34, 19-48.

Knutson, M. D., Oukka, M., Koss, L. M., Aydemir, F. & Wessling-Resnick, M. (2005). Iron release from macrophages after erythrophagocytosis is up-regulated by ferroportin 1 overexpression and down-regulated by hepcidin. *Proceedings of the National Academy of Sciences of the United States of America*, 102(5), 1324-1328.

Koch, P.C. & Hess, M. (2011). Topographic mapping of retinal neurons in the european anchovy by nuclear staining and immunohistochemistry. *Journal of Neuroscience*

Research, 89(8), 1316-1330.

Koh, V., Cheung, C.Y., Zheng, Y., Wong, T.Y., Wong, W. & Aung, T. (2010). Relationship of retinal vascular tortuosity with the neuroretinal rim: the Singapore malay eye study. *Investigative Ophthalmology & Visual Science*, 51(7), 3736-3741.

Kohgo, Y., Ikuta, K., Ohtake, T., Torimoto, Y. & Kalo, J. (2008). Body iron metabolism and pathophysiology of iron overload. *International Journal of Hematology*, 88(1), 7-15.

Kolb, H., Fernandez, E., Nelson, R. & Jones, B. (2011). *Webvision: the organization of the retina and visual system*. University of Utah, Health Sciences Center. Retrieved March 2018, from http://webvision.med.utah.edu/.

Komuro, T., Desaki, J. & Uehara, Y. (1982). Three-dimensional organization of smooth muscle cells in blood vessels of laboratory rodents. *Cell and Tissue Research*, 227(2), 429-437.

Konari, K., Sawada, N., Zhong, Y., Isomura, H., Nakagawa, T. & Mori, M. (1995). Development of the blood-retinal barrier in vitro: formation of tight junctions as revealed by occludin and ZO-1 correlates with the barrier function of chick retinal pigment epithelial cells. *Experimental Eye Research*, 61(1), 99-108.

Koto, T., Takubo, K., Ishida, S., Shinoba, H., Inoue, M., Tsubota, K., Okada, Y. & Ikeda, E. (2007). Hypoxia disrupts the barrier function of neural blood vessels through changes in the expression of claudin-5 in endothelial cells. *The American Journal of Pathology*, 170(4), 1389-1397.

Kouzarides, T. (2007). Chromatin modifications and their function. *Cell*, 128(4), 693-705.

Krause, G., Winkler, L., Mueller, S. L., Haseloff, R. F., Piontek, J. & Blasig, I. E. (2008). Structure and function of claudins. *Biochimica et Biophysica Acta*, 1778(3), 631-645.

Kristinsson, J.K., Gottfredsdottir, M.S. & Stefansson, E. (1997). Retinal vessel dilatation and elongation precedes diabetic macular oedema. *The British Journal of Ophthalmology*, 81(4), 274-278.

Kubista, M., Andrade, J.M., Bengtsson, M., Forootan, A., Jonák, J., Lind, K., Sindelka, R., Sjöback, R., Sjögreen, B., Strömbom, L., Ståhlberg, A. & Zoric, N. (2006). The real-time polymerase chain reaction. *Molecular Aspects of Medicine*, 27(2-3), 95-125.

Kuchroo, V.K., Umetsu, D.T., DeKruyff, R.H. & Freeman, G.J. (2003). The TIM gene family: emerging roles in immunity and disease. *Nature Reviews Immunology*, 3(6), 454-462.

Kumanogoh, A., Marukawa, S., Suzuki, K., Takegahara, N., Watanabe, C., Ch'ng, E., Ishida, I., Fujimura, H., Sakoda, S., Yoshida, K. & Kikutani, H. (2002). Class IV semaphorin Sema4A enhances T-cell activation and interacts with Tim-2. *Nature*, 419(6907), 629-633.

Kur, J., Newman, E.A. & Chan-Ling, T. (2012). Cellular and physiological mechanisms underlying blood flow regulation in the retina and choroid in health and disease. *Progress in Retinal and Eye Research*, 31(5), 377-406.

Kurz, T., Leake, A., von Zglinick, T., & Brunk, U.T. (2004). Relocalized redox-active lysosomal iron is an important mediator of oxidative-stress-induced DNA damage. *The Biochemical Journal*, 378(Pt3), 1039-1045.

Lacolley, P., Regnault, V., Nicoletti, A., Li, Z. & Michel, J.B. (2012). The vascular smooth

muscle cell in arterial pathology: a cell that can take on multiple roles. *Cardiovascular Research*, 95(2), 194-204.

LeBleu, V.S., Macdonald, B. & Kalluri, R. (2007). Structure and function of basement membranes. *Experimental Biology and Medicine (Maywood)*, 232(9), 1121-1129.

Lee, A.Y., Han, B., Lamm, S.D., Fierro, C.A. & Han, H.C. (2012). Effects of elastin degradation and surrounding matrix support on artery stability. *American Journal of Physiology - Heart and Circulatory Physiology*, 302(4), H873-H884.

Levi, S., Santambrogio, P., Cozzi, A., Rovida, E., Corsi, B., Tamborini, E., Spada, S., Albertini, A. & Arosio, P. (1994). The role of the L-chain in ferritin iron incorporation. Studies of homo and heteropolymers. *Journal of Molecular Biology*, 238(5), 649-654.

Levi, S., Yewdall, S.J., Harrison, P.M., Santambrogio, P., Cozzi, A, Rovida, E., Albertini, A. & Arosio, P. (1992). Evidence of H- and L-chains have co-operative roles in the iron-uptake mechanism of human ferritin. *The Biochemical Journal*, 288(Pt2), 591-596.

LeVine, S.M. & Macklin, W.B. (1990). Iron-enriched oligodendrocytes: a reexamination of their spatial distribution. *Journal of Neuroscience Research*, 26(4), 508-512.

Lewis, G.P. & Fisher, S.K. (2003). Up-regulation of glial fibrillary acidic protein in response to retinal injury: its potential role in glial remodeling and a comparison to vimentin expression. *International Review of Cytology*, 230, 263-290.

Lhermitte, J., Kraus, W.M. & McAlpine, D. (1924). Original papers: on the occurrence of abnormal deposits of iron in the brain in parkinsonism with special reference to its localisation. *The Journal of Neurology and Psychopathology*, 5(19), 195-208.

Li, J.Y, Paragas, N., Ned, R.M., Qiu, A., Viltard, M., Leete, T., Drexler, I.R., Chen, X., Sanna-Cherchi, S., Mohammed, F., Williams, D., Lin, C.S., Schmidt-Ott, K.M., Andrews, N.C. & Barasch, J. (2009). Scara5 is a ferritin receptor mediating non-transferrin iron delivery. *Developmental Cell*, 16(1), 35-46.

Linert, W., Herlinger, E., Jameson, R.F., Kienzl, E., Jellinger, K. & Youdim, M.B. (1996). Dopamine, 6-hydroxydopamine, iron, and dioxygen--their mutual interactions and possible implication in the development of Parkinson's disease. *Biochimica et Biophysica Acta*, 1316(3), 160-168.

Lisanti, M.P., Scherer, P.E., Vidugiriene, J., Tang, Z., Hermanowski-Vosatka, A., Tu, Y.H., Cook, R.F. & Sargiacomo, M. (1994). Characterization of caveolin-rich membrane domains isolated from an endothelial-rich source: implications for human disease. *The Journal of Cell Biology*, 126(1), 111-126.

Loh, A., Hadziahmetovic, M. & Dunaief, J.L. (2009). Iron homeostasis and eye disease. *Biochimica et Biophysica Acta*, 1970(7), 637-649.

Lum, H. & Malik, A.B. (1994). Regulation of vascular endothelial barrier function. *American Journal of Physiology*, 267(3Pt1), L223-L241.

Mackenzie, EL., Iwasaki, K. & Tsuji, Y. (2008). Intracellular iron transport and storage: from molecular mechanisms to health implications. *Antioxidants & Redox Signaling*, 10(6), 998-1016.

Madsen-Bouterse, S.A. & Kowluru, R.A. (2008). Oxidative stress and diabetic retinopathy: pathophysiological mechanisms and treatment perspectives. *Reviews in Endocrine and Metabolic Disorders*, 9(4), 315-327.

Mahmood, T. & Yang, P.C. (2012). Western blot: technique, theory, and trouble shooting. *North American Journal of Medical Sciences*, 4(9), 429-434.

Majzoub, J.A. & Muglia, L.J. (1996). Knockout mice. *The New England Journal of Medicine*, 334(14), 904-907.

Martin-Padura, I., Lostaglio, S., Schneemann, M., Williams, L., Romano, M., Fruscella, P., Panzeri, C., Stoppacciaro, A., Ruco, L., Villa, A., Simmons, D. & Dejana, E. (1998). Junctional adhesion molecule, a novel member of the immunoglobulin superfamily that distributes at intercellular junctions and modulates monocyte transmigration. *The Journal of Cell Biology*, 142(1), 117-127.

Martinez-Lemus, L.A. (2012). The dynamic structure of arterioles. *Basic & Clinical Pharmacology & Toxicology*, 110(1), 5-11.

Martinez, R. & Han, H.C. (2012). The effect of collagenase on the critical buckling pressure of arteries. *Molecular & Cellular Biomechanics*, 9(1), 55-75.

Masland, R.H. (2011). Cell populations of the retina: the Proctor lecture. *Investigative Ophthalmology & Visual Science*, 52(7), 4581-4591.

Massova, I., Kotra, L.P., Fridman, R. & Mobashery, S. (1998). Matrix metalloproteinases: structures, evolution, and diversification. *FASEB Journal*, 12(12), 1075-1095.

Massover, W.H. & Cowley, J.M. (1973). The ultrastructure of ferritin macromolecules. The lattice structure of the core crystallites. *Proceedings of the National Academy of Sciences of the United States of America*, 70(12), 3847-3851.

Maulik, N. & Das, D.K. (2002). Redox signaling in vascular angiogenesis. *Free Radical Biology & Medicine*, 33(8), 1047-1060.

Maureen, A., McCall, N. & Gregg, R.G. (2008). Neurotransmission in the mouse retina. In L.M. Chalupa & R.W. Williams (Eds.), *Eye, retina, and visual system of the mouse.* (pp. 175-188). London: Mit Press.

McCall, M.A. & Gregg, R.G. (2008a). Comparisons of structural and functional abnormalities in mouse b-wave mutants. *The Journal of Physiology*, 586(18), 4385-4392.

McCall, M.A. & Gregg, R.G. (2008b). Neurotransmission in the mouse retina (chapter 14). In L.M. Chalupa & R.W. Williams (Eds.), *Eye, retina, and visual system of the mouse*. (pp. 175-188). London: Mit Press.

McIntire, J.J., Umetsu, D.T. & DeKruyff, R.H. (2004). TIM-1, a novel allergy and asthma susceptibility gene. *Springer Seminars in Immunopathology*, 25(3-4), 335-348.

McIntire, J.J., Umetsu, S.E., Akbari, O., Potter, M., Kuchroo, V.K., Barsh, G.S., Freeman, G.J., Umetsu, D.T. & DeKruyff, R.H. (2001). Identification of Tapr (an airway hyperreactivity regulatory locus) and the linked Tim gene family. *Nature Immunology*, 2(12), 1109-1116.

McKie, A.T., Marciani, P., Rolfs, A., Brennan, K., Wehr, K., Barrow, D., Miret, S., Bomford, A., Peters, T.J., Farzaneh, F., Hediger, M.A., Hentze, M.W. & Simpson, R.J. (2000). A novel duodenal iron-regulated transporter, IREG1, implicated in the basolateral transfer of iron to the circulation. *Molecular Cell*, 5(2), 299-309.

McLenachan, S., Magno, A.L., Ramos, D., Catita, J., McMenamin, P.G., Chen, F.K., Rakoczy, E.P. & Ruberte, J. (2015). Angiography reveals novel features of the retinal vasculature

in healthy and diabetic mice. *Experimental Eye Research*, 138, 6-21.

McMenamin, P.G. (2000). Optimal methods for preparation and immunostaining of iris, ciliary body, and choroidal wholemounts. *Investigative Ophthalmology & Visual Science*, 41(10), 3043-3048.

Mehlhase, J., Sandig, G., Pantopoulos, K. & Grune T. (2005). Oxidation-induced ferritin turnover in microglial cells: role of proteasome. *Free Radical Biology & Medicine*, 38(2), 276-285.

Mendes-Jorge, L., Ramos, D., Valença, A., López-Luppo, M., Pires, V.M.R., Catita, J., Nacher, V., Navarro, M., Carretero, A., Rodriguez-Baesa, A. & Ruberte, J. (2014). L-ferritin binding to Scara5: a new iron traffic pathway potentially implicated in retinopathy. *PLoS One*, 9(9), e106974.

Meneghini, R. (1997). Iron homeostasis, oxidative stress, and DNA damage. *Free Radical Biology & Medicine*, 23(5), 783-792.

Metz, A. (1868). *The Anatomy and Histology of the Human Eye.* Philadelphia: Office of the Medical and Surgical Reporter.

Meyers, J.H., Sabatos, C.A., Chakravarti, S. & Kuchroo, V.K. (2005). The TIM gene family regulates autoimmune and allergic diseases. *Trends in Molecular Medicine*, 11(8), 362-369.

Michiels, C. (2003). Endothelial cell functions. *Journal of Cellular Physiology*, 196(3), 430-443.

Miller, D.D. & Berner L.A. (1989). Is solubility in vitro a reliable predictor of iron bioavailability? *Biological Trace Element Research*, 19(1-2), 11-24.

Milovanova, T., Chatterjee, S., Hawkins, B.J., Hong, N., Sorokina, E.M., Debolt, K., Moore, J.S., Madesh, M., Fisher, A.B. (2008). Caveolae are an essential component of the pathway for endothelial cell signaling associated with abrupt reduction of shear stress. *Biochimica et Biophysica Acta*, 1783(10), 1866-1875.

Minshall, R.D. & Malik, A.B. (2006). Transport across the endothelium: regulation of endothelial permeability. *Handbook of Experimental Pharmacology*, 176(Pt1), 107-144.

Minshall, R.D., Sessa, W.C., Stan, R.V., Anderson, R.G. & Malik, A.B. (2003). Caveolin regulation of endothelial function. *American Journal of Physiology - Lung Cellular and Molecular Physiology*, 285(6), L1179-L1183.

Mizutani, M., Gerhardinger, C. & Lorenzi, M. (1998). Müller cell changes in human diabetic retinopathy. *Diabetes*, 47(3), 445-449.

Mohsenin, A., Mohsenin, V. & Adelman, R.A. (2013). Retinal vascular tortuosity in obstructive sleep apnea. *Clinical Ophthalmology*, 7, 787-792.

Moiseyev, G., Chen, Y., Takahashi, Y., Wu, B.X. & Ma, J.X. (2005). RPE65 is the isomerohydrolase in the retinoid visual cycle. *Proceedings of the National Academy of Sciences of the United States of America*, 102(35), 12413-12418.

Monteiro, H.P. & Winterbourn, C.C. (1989). 6-Hydroxydopamine releases iron from ferritin and promotes ferritin-dependent lipid peroxidation. *Biochemical Pharmacology*, 38(23), 4177-4182.

Morcos, Y., Hosie, M.J., Bauer, H.C. & Chan-Ling, T. (2001). Immunolocalization of occludin and claudin-1 to tight junctions in intact CNS vessels of mammalian retina. *Journal of Neurocytology*, 30(2), 107-123.

Morita, K., Furuse, M., Fujimoto, K. & Tsukita, S. (1999). Claudin multigene family encoding four-transmembrane domain protein components of tight junction strands. *Proceedings of the National Academy of Sciences of the United States of America*, 96(2), 511-516.

Morona, R., Moreno, N., Lopez, J.M., Muñoz, M., Domínguez, L. & González, A. (2008). Calbindin-D28k and calretinin as markers of retinal neurons in the anuran amphibian Rana perezi. *Brain Research Bulletin*, 75(2-4), 379-383.

Morris, C. M., Candy, J. M., Oakley, A. E., Bloxham, C. A. & Edwardson, J. A. (1992). Histochemical distribution of non-haem iron in the human brain. *Acta Anatomica (Basel)*, 144(3), 235-257.

Muckenthaler, M., Gray, N.K. & Hentze, M.W. (1998). IRP-1 binding to ferritin mRNA prevents the recruitment of the small ribosomal subunit by the cap-binding complex eIF4F. *Molecular Cell*, 2(3), 383-388.

Muckenthaler, M.U., Galy, B. & Hentze, M.W. (2008). Systemic iron homeostasis and the iron-responsive element/iron-regulatory protein (IRE/IRP) regulatory network. *Annual Review of Nutrition*, 28, 197-213.

Nadal-Nicolás, F.M., Jiménez-López, M., Sobrado-Calvo, P., Nieto-López, L., Cánovas-Martinez, I. (2009). Brn3a as a marker of retinal ganglion cells: qualitative and quantitative time course studies in naive and optic nerve-injured retinas. *Investigative Ophthalmology & Visual Science*, 50(8), 3860-3868.

Nascimento, S., Suarez, E.R. & Pinhal M.A.S. (2010). Tecnologia de PCR e RT-PCR em tempo real e suas aplicações na área médica. *Revista Brasileira de Medicina – Especial oncologia*, 67, 7-19.

Nehls, V. & Drenckhahn, D. (1991). Heterogeneity of microvascular pericytes for smooth muscle type alpha-actin. *The Journal of Cell Biology*, 113(1), 147-154.

Nemeth, E., Tuttle, M.S., Powelson, J., Vaughn, M.B., Donovan, A., Ward, D.M., Ganz, T., Kaplan, J. (2004). Hepcidin regulates cellular iron efflux by binding to ferroportin and inducing its internalization. *Science*, 306(5704), 2090-2093.

Newman, E.A. (2003). New roles for astrocytes: regulation of synaptic transmission. *Trends in Neurosciences*, 26(10), 536-542.

Newman, E. & Reichenbach, A. (1996). The Müller cell: a functional element of the retina. *Trends Neurosciences*, 19(8), 307-312.

Nitta, T., Hata, M., Gotoh, S., Seo, Y., Sasaki, H., Hashimoto, N., Furuse, M. & Tsukita, S. (2003). Size-selective loosening of the blood-brain barrier in claudin-5-deficient mice. *The Journal of Cell Biology*, 161(3), 653-660.

Ntziachristos, V. (2006). Fluorescence molecular imaging. *Annual Review of Biomedical Engineering*, 8, 1-33.

Ohtoshi, A., Wang, S.W., Maeda, H., Saszik, S.M., Frishmanl, J., Klein, W.H. & Behringer, R.R. (2004). Regulation of retinal cone bipolar cell differentiation and photopic vision by the CVC homeobox gene Vsx1. *Current Biology*, 14(6), 530-536.

Olsson, A.K., Dimberg, A., Kreuger, J. & Claesson-Welsh, L. (2006). VEGF receptor signaling – in control of vascular function. *Nature Reviews Molecular Cell Biology*, 7(5), 359-371.

Osaki, S., Johnson, D.A. & Frieden, E. (1966). The possible significance of the ferrous oxidase activity of ceruloplasmin in normal human serum. *The Journal of Biological Chemistry*, 241(12), 2746-2751.

Outten, F.W. & Theil, E.C. (2009). Iron-based redox switches in biology. *Antioxidants & Redox Signaling*, 11(5), 1029-1046.

Owens, G.K., Kumar, M.S. & Wamhoff, B.R. (2004). Molecular regulation of vascular smooth muscle cell differentiation in development and disease. *Physiological Reviews*, 84(3), 767-801.

Palade, G.E. (1953). Fine structure of blood capillaries. *Journal of Applied Physics*, 24, 1424.

Pappenheimer, J.R., Renkin, E.M. & Borrero, L.M. (1951). Filtration, diffusion and molecular sieving through peripheral capillary membranes; a contribution to the pore theory of capillary permeability. *American Journal of Physiology*, 167(1), 13-46.

Paques, M., Simonutti, M., Roux, M.J., Picaud, S., Levavasseur, E., Bellman, C. & Sahel, J.A. (2006). High resolution fundus imaging by confocal scanning laser ophthalmoscopy in the mouse. *Vision Research*, 46(8-9), 1336-1345.

Paques, M., Tadayoni, R., Sercombe, R., Laurent, P., Genevois, O., Gaudric, A. & Vicaut, E. (2003). Structural and hemodynamic analisys of the mouse retinal microcirculation. *Investigative Ophthalmology & Visual Science*, 44(11), 4960-4967.

Peng, S., Rao, V.S., Adelman, R.A. & Rizzolo, L.J. (2011). Claudin-19 and the barrier properties of the human retinal pigment epithelium. *Investigative Ophthalmology & Visual Science*, 52(3), 1392-1403.

Pérez, L.M., Milkiewicz, P., Ahmed-Choudhury, J., Elias, E., Ochoa, J.E., Sánchez Pozzi, E.J., Coleman, R. & Roma, M.G. (2006). Oxidative stress induces actin-cytoskeletal and tight-junctional alterations in hepatocytes by a Ca2+ -dependent, PKC-mediated mechanism: protective effect of PKA. *Free Radical Biology & Medicine*, 40(11), 2005-2017.

Pfaffl, M.W. (2001). A new mathematical model for relative quantification in real-time RT-PCR. *Nucleic Acids Research*, 29(9), e45.

Pfaffl, M.W., Horgan, G.W. & Dempfle, L. (2002). Relative expression software tool (REST) for group-wise comparison and statistical analysis of relative expression results in real-time PCR. *Nucleic Acids Research*, 30(9), e36.

Pfister, F., Feng, Y., vom Hagen, F., Hoffmann, S., Molema, G., Hillebrands, J.L., Shani, M., Deutsch, U. & Hammes, H.P. (2008). Pericyte migration: a novel mechanism of pericyte loss in experimental diabetic retinopathy. *Diabetes*, 57(9), 2495-2502.

Phillips, B.E., Cancel, L., Tarbell, J.M., Antonetti, D.A. (2008). Occludin independently regulates permeability under hydrostatic pressure and cell division in retinal pigment epithelial cells. *Investigative Ophthalmology & Visual Science*, 49(6), 2568-2576.

Picazo, M.G. & García-Olmo, D.C. (2015). DNA from tissues of young mice is optimal for genotyping. *Electronic Journal of Biotechnology*, 18(2), 83-87.

Podhorecka, M., Skladanowski, A. & Bozko, P. (2010). H2AX phosphorylation: its role in DNA

damage response and cancer therapy. *Journal of Nucleic Acids*, 2010, pii: 920161.

Ponka, P., Beaumont, C. & Richardson, D.R. (1998). Function and regulation of transferrin and ferritin. *Seminars in Hematology*, 35(1), 35-54.

Pöschl, E., Schlötzer-Schrehardt, U., Brachvogel, B., Saito, K., Ninomiya, Y. & Mayer, U. (2004). Collagen IV is essential for basement membrane stability but dispensable for initiation of its assembly during early development. *Development*, 131(7), 1619-1628.

Poss, K. D. & Tonegawa, S. (1997). Heme oxygenase 1 is required for mammalian iron reutilization. *Proceedings of the National Academy of Sciences of the United States of America*, 94(20), 10919-10924.

Pour, P.M., Standop, J. & Batra, S.K. (2002). Are islet cells the gatekeepers of the pancreas? *Pancreatology*, 2(5), 440-448.

Pournaras, C.J., Donati, G., Kapetanios, A.D., Redard, M., Bochatay-Piallat, M.L. & Gabbiani, G. (1998). Myofibroblasts and retinal fibrovascular membranes. *Klinische Monatsblätter für Augenheilkunde*, 212(5), 356-358.

Pournaras, C.J., Rungger-Brändle, E., Riva, C.E., Hardarson, S.H. & Stefansson, E. (2008). Regulation of retinal blood flow in health and disease. *Progress in Retinal and Eye Research*, 27(3), 284-330.

Predescu, D., Vogel, S.M. & Malik, A.B. (2004). Functional and morphological studies of protein transcytosis in continuous endothelia. *American Journal of Physiology - Lung Cellular and Molecular Physiology*, 287(5), L895-L901.

Presnell, J.K. & Schreibman, M.P. (1997). Topics histology - technique, stains and staining. In G.L. Humanso (Ed.), *Animal tissue techniques*. (5th Ed.). London: WH Freeman and Company.

Pröfrock, D. & Prange, A. (2012). Inductively coupled plasma-mass spectrometry (ICP-MS) for quantitative analysis in environmental and life sciences: a review of challenges, solutions, and trends. *Applied Spectroscopy*, 66(8), 843-868.

Puro, D.G. (2012). Retinovascular pathophysiology: new experimental approach/new insights. *Progress in Retinal and Eye Research*, 31(3), 258-270.

Ramos, D., Carretero, A., Navarro, M., Mendes-Jorge, L., Nacher, V., Rodriguez-Baeza, A. & Ruberte, J. (2013). Mimicking microvascular alterations of human diabetic retinopathy: a challenge for the mouse models. *Current Medicinal Chemistry*, 20(26), 3200-3217.

Rao, R. (2008). Oxidative stress-induced disruption of epithelial and endothelial tight junctions. *Frontiers in Bioscience*, 13, 7210-7226.

Ray, P.D., Huang, B.W. & Tsuji, Y. (2012). Reactive oxygen species (ROS) homeostasis and redox regulation in cellular signaling. *Cellular Signaling*, 24(5), 981-990.

Red-Horse, K. & Ferrara, N. (2007). Vascular targeting via caveolae. *Nature Biotechnology*, 25(4), 431-432.

Redon, C.E., Nakamura, A.J., Martin, O.A., Parekh, P.R., Weyemi, U.S. & Bonner, W.M. (2011). Recent developments in the use of gamma-H2AX as a quantitative DNA double-strand break biomarker. *Aging (Albany NY)*, 3(2), 168-174.

Reichenbach, A., Wurm, A., Pannicke, T., Iandiev, I., Wiedemann, P. & Bringmann, A. (2007). Müller cells as players in retinal degeneration and edema. *Graefe's Archive for Clinical and Experimental Ophthalmology*, 245(5), 627-636.

Reijerkerk, A., Kooij, G., van der Pol, S.M., Khazen, S., Dijkstra, C.D. & de Vries, H.E. (2006). Diapedesis of monocytes is associated with MMP-mediated occludin disappearance in brain endothelial cells. *FASEB Journal*, 20(14), 2550-2552.

Rennert, P.D, Ichimura, T., Sizing, I.D., Bailly, V., Li, Z., Rennard, R., McCoon, P., Pablo, L., Miklasz, S., Tarilonte, L. & Bonventre, J.V. (2006). T cell, Ig domain, mucin domain-2 gene-deficient mice reveal a novel mechanism for the regulation of Th2 immune responses and airway inflammation. *The Journal of Immunology*, 177(7), 4311-4321.

Richardson, D.R. & Ponka, P. (1997). The molecular mechanisms of the metabolism and transport of iron in normal and neoplastic cells. *Biochimica et Biophysica Acta*, 1331(1), 1-40.

Robinson, K.M., Janes, M.S., Pehar, M., Monette, J.S., Ross, M.F., Hagen, T.M., Murphy, M.P. & Beckman, J.S. (2006). Selective fluorescent imaging of superoxide in vivo using ethidium-based probes. *Proceedings of the National Academy of Sciences of the United States of America*, 103(41),15038-15043.

Rodriguez-Manzanet, R., DeKruyff, R., Kuchroo, V.K. & Umetsu, D.T. (2009). The costimulatory role of TIM molecules. *Immunological Reviews*, 229(1), 259-270.

Rogakou, E.P., Pilch, D.R., Orr, A.H., Ivanova, V.S. & Bonner, W.M. (1998). DNA double-stranded breaks induce histone H2AX phosphorylation on serine 139. *The Journal of Biological Chemistry*, 273(10), 5858-5868.

Roitt, I., Brostoff, J. & Male, D. (2001). *Immunology*. (6th Ed.). London: Ed. Mosby.

Roos, W.P. & Kaina, B. (2013). DNA damage-induced cell death: from specific DNA lesions to the DNA damage response and apoptosis. *Cancer Letters*, 332(2), 237-248.

Rossant, J. & Tam, P.P.L. (2002). *Mouse development: patterning, morphogenesis, and organogenesis.* San Diego: Academic.

Rothberg, K.G., Ying, Y.S., Kamen, B.A. & Anderson, R.G. (1990). Cholesterol controls the clustering of the glycophospholipid-anchored membrane receptor for 5-methyltetrahydrofolate. *The Journal of Cell Biology*, 111(6Pt2), 2931-2938.

Rouault, T.A. (2006). The role of iron regulatory proteins in mammalian iron homeostasis and disease. *Nature Chemical Biology*, 2(8), 406-414.

Rouault, T. & Cooperman, S. (2006). Brain iron metabolism. *Seminars in Pediatric Neurology*, 13(3), 142-148.

Ruberte, J., Navarro, M., Carretero, A., Ramos, D. & Mendes-Jorge, L. (2016). Eye and related structures (chapter 14). In J. Ruberte, A. Carretero & M. Navarro, *Morphological mouse phenotyping: anatomy, histology and imaging*. (pp. 475-520). Madrid: Editorial Médica Panamericana S.A.

Runkle, E.A. & Antonetti, D.A. (2011). The blood-retinal barrier: structure and functional significance. *Methods in Molecular Biology*, 686, 133-148.

Sabanayagam, C., Yip, W., Ting, D.S.W., Tan, G. & Wong, T.Y. (2016). Ten emerging trends in the epidemiology of diabetic retinopathy. *Ophthalmic Epidemiology*, 23(4), 209-222.

Sagaties, M.J., Raviola, G., Schaeffer, S. & Miller, C. (1987). The structural basis of the inner blood-retina barrier in the eye of Macaca mulatta. *Investigative Ophthalmology & Visual Science*, 28(12), 2000-2014.

Saint-Geniez, M. & D'Amore, P.A. (2004). Development and pathology of the hyaloid, choroidal and retinal vasculature. *The International Journal of Developmental Biology*, 48(8-9), 1045-1058.

Saint-Geniez, M., Maldonado, A.E. & D'Amore, P.A. (2006). VEGF expression and receptor activation in the choroid during development and in the adult. *Investigative Ophthalmology & Visual Science*, 47(7), 3135-3142.

Santibanez, J.F., Blanco, F.J., Garrido-Martin, E.M., Sanz-Rodriguez, F., del Pozo, M.A. & Bernabeu, C. (2008). Caveolin-1 interacts and cooperates with the transforming growth factor-beta type I receptor ALK1 in endothelial caveolae. *Cardiovascular Research*, 77(4), 791-799.

Santos, A.M., Martin-Oliva, D., Ferrer-Martin, R.M., Tassi, M., Calvente, R., Sierra, A., Carrasco, M.C., Marin-Teva, J.L., Navascues, J. & Cuadros, M.A. (2010). Microglial response to light-induced photoreceptor degeneration in the mouse retina. *The Journal of Comparative Neurology*, 518(4), 477-492.

Santos, M.M., de Sousa, M., Rademakers, L.H., Clevers, H., Marx, J.J. & Schilham, M.W. (2000). Iron overload and heart fibrosis in mice deficient for both β2-microglobulin and *Rag1*. *The American Journal of Pathology*, 157(6), 1883-1892.

Sarthy, P.V., Fu, M. & Huang, J. (1991). Developmental expression of the glial fibrillary acidic protein (GFAP) gene in the mouse retina. *Cellular and Molecular Neurobiology*, 11(6), 623-637.

Sasaki, M., Ozawa, Y., Kurihara, T., Kubota, S., Yuki, K., Noda, K., Kobayashi, S., Ishida, S. & Tsubota, K. (2010). Neurodegenerative influence of oxidative stress in the retina of a murine model of diabetes. *Diabetologia*, 53(5), 971-979.

Sasongko, M.B., Wong, T.Y., Donaghue, K.C., Cheung, N., Jenkins, A.J., Benitez-Aguirre, P. & Wang, J.J. (2012). Retinal arteriolar tortuosity is associated with retinopathy and early kidney dysfunction in type 1 diabetes. *American Journal of Ophthalmology*, 153(1), 176-183.

Sasongko, M.B., Wong, T.Y., Nguyen, T.T., Cheung, C.Y., Shaw, J.E., Kawasaki, R., Lamoureux, E.L. & Wang, J.J. (2016). Retinal Vessel Tortuosity and Its Relation to Traditional and Novel Vascular Risk Markers in Persons with Diabetes. *Current Eye Research*, 41(4), 551-557.

Sasongko, M.B., Wong, T.Y., Nguyen, T.T., Cheung, C.Y., Shaw, J.E. & Wang, J.J. (2011). Retinal Vascular Tortuosity in persons with diabetes and diabetic retinopathy. *Diabetologia*, 54(9), 2409-2416.

Schaller, O. (1992). *Illustrated veterinary anatomical nomenclature.* (2nd Ed.). Stuttgart: Enke verlag.

Schichi, H. (1969). Microsomal electron transport system of bovine retinal pigment epithelium. *Experimental Eye Research*, 8(1), 60-68.

Schlingemann, R.O., Dingjan, G.M., Emeis, J.J., Blok, J., Warnaar, S.O. & Ruiter, D.J. (1985). Monoclonal antibody PAL-E specific for endothelium. *Laboratory Investigation*, 52(1), 71-76.

Schlingemann, R.O., Hofman, P., Anderson, L., Troost, D. & van der Gaag, R. (1997). Vascular expression of endothelial antigen PAL-E indicates absence of blood-ocular barriers in the normal eye. *Ophthalmic Research*, 29(3), 130-138.

Schlingemann, R.O., Hofman, P., Vrensen, G.F. & Blaauwgeers, H.G. (1999). Increased expression of endothelial antigen PAL-E in human diabetic retinopathy correlates with microvascular leakage. *Diabetologia*, 42(5), 596-602.

Schreibelt, G., Kooij, G., Reijerkerk, A., van Doorn, R., Gringhuis, S.I., van der Pol, S., Weksler, B.B., Romero, I.A., Couraud, P.O., Piontek, J., Blasig, I.E., Dijkstra, C.D., Ronken, E. & de Vries, H.E. (2007). Reactive oxygen species alter brain endothelial tight junction dynamics via RhoA, PI3 kinase, and PKB signaling. *FASEB Journal*, 21(13), 3666-3676.

Shahidi, M., Ogura, Y., Blair, N.P., Rusin, M.M. & Zeimer, R. (1991). Retinal thickness analysis for quantitative assessment of diabetic macular edema. *Archives of Ophthalmology*, 109(8), 1115-1119.

Shen, X., Bao, W., Yu, W., Liang, R., Nguyen, B. & Liu, Y. (2017). An improved method with high sensitivity and low background in detecting low β-galactosidase expression in mouse embryos. *PLoS One*, 12(5), e0176915.

Shibuya, M. (2008). Vascular endothelial growth factor-dependent and -independent regulation of angiogenesis. *BMB Reports*, 41(4), 278-286.

Shinoda, K., Yamada, K., Matsumoto, C.S., Kimoto, K. & Nakatsuka, K. (2008). Changes in retinal thickness are correlated with alterations of electroretinogram in eyes with central retinal artery occlusion. *Graefe's Archive for Clinical and Experimental Ophthalmology*, 246(7), 949-954.

Sies, H. (1991). Oxidative stress: introduction. In: H. Sies (Ed.), *Oxidative stress: oxidants and antioxidants*. (pp. xv-xxii). London: Academic Press.

Simionescu, N. (1979). The microvascular endothelium. Segmental differentiation transcytosis: selective distribution of anionic sites. In G. Weissman, B. Samuelsson & R. Paoletti, (Eds.), *Advances in inflammation research*. (pp. 61-70). New York: Raven.

Simionescu, M., Gafencu, A. & Antohe, F. (2002). Transcytosis of plasma macromolecules in endothelial cells: a cell biological survey. *Microscopy Research and Technique*, 57(5), 269-288.

Simionescu, M., Popov, D. & Sima A. (2009). Endothelial transcytosis in health and disease. *Cell and Tissue Research*, 335(1), 27-40.

Simionescu, M. & Simionescu, N. (1991). Endothelial transport of macromolecules: transcytosis and endocytosis. A look from cell biology. *Cell Biology Reviews*, 25(1), 1-78.

Simpson, D.A., Feeney, S., Boyle, C. & Stitt, A.W. (2000). Retinal VEGF mRNA measured by SYBR green I fluorescence: a versatile approach to quantitative PCR. *Molecular Vision*, 6, 178-183.

Sims, D.E. (1986). The pericyte--a review. *Tissue and Cell*, 18(2), 153-174.

Sipe, D.M. & Murphy, R.F. (1991). Binding to cellular receptors results in increased iron release from transferrin at mildly acidic pH. *The Journal of Biological Chemistry*, 266(13), 8002-8007.

Smith, H.E. (1950). Correlation of the anatomic factors concerned in the ophthalmoscopic appearance of retinal hemorrhages. *American Journal of Ophthalmology*, 33(3), 453-458.

Smith, R.S. (2002). *Systematic evaluation of the mouse eye – Anatomy, Pathology, and Biomethods*. New York: CRC Press LLC.

Sobotta, J. & Becher, H. (1974). *Atlas de Anatomía Humana. Tomo III: Sistema nervioso central, sistema nervioso autónomo, órganos de los sentidos y piel, vías de conducción periféricas.* Munich: Toray.

Song, D. & Dunaief, J.L. (2013). Retinal iron homeostasis in health and disease. *Frontiers in Aging Neuroscience*, 5, 24.

Sorrentino, F.S., Allkabes, M., Salsini, G., Bonifazzi, C. & Perri, P. (2016). The importance of glial cells in the homeostasis of the retinal microenvironment and their pivotal role in the course of diabetic retinopathy. *Life Sciences*, 162, 54-59.

Stan, R.V. (2005). Structure of caveolae. *Biochimica et Biophysica Acta*, 1746(3), 334-348.

Stan, R.V., Ghitescu, L., Jacobson, B.S. & Palade, G.E. (1999). Isolation, cloning, and localization of rat PV-1, a novel endothelial caveolar protein. *The Journal of Cell Biology*, 145(6), 1189-1198.

Staurenghi, G., Viola, F., Mainster, M.A., Graham, R.D. & Harrington, P.G. (2005). Scanning laser ophthalmoscopy and angiography with a wide-field contact lens system. *Archives of Ophthalmology*, 123(2), 244-252.

Stevenson, B.R., Siliciano, J.D., Mooseker, M.S. & Goodenough, D.A. (1986). Identification of ZO-1: a high molecular weight polypeptide associated with the tight junction (zonula occludens) in a variety of epithelia. *The Journal of Cell Biology*, 103(3), 755-766.

Storch, G.A. (2007). Diagnostic virology. In D.M. Knipe & P.M. Howley (Eds.), *Fields virology–volume 1*. (5th Ed.). (pp. 565-604). Philadelphia: Lippincott Williams & Wilkins.

Strickland, L.A., Jubb, A.M., Hongo, J.A., Zhong, F., Burwick, J., Fu, L., Frantz, G.D. & Koeppen, H. (2005). Plasmalemmal vesicle-associated protein (PLVAP) is expressed by tumour endothelium and is upregulated by vascular endothelial growth factor-A (VEGF). *The Journal of Pathology*, 206(4), 466-475.

Sumpio, B.E., Riley, J.T. & Dardik, A. (2002). Cells in focus: endothelial cell. *The International Journal of Biochemistry & Cell Biology*, 34(12), 1508-1512.

Surwit, R.S., Kuhn, C.M., Cochrane, C., McCubbin, J.A. & Feinglos, M.N. (1988). Diet-induced type II diabetes in C57BL/6J mice. *Diabetes*, 37(9), 1163-1167.

Svenson, K.L., Von Smith, R., Magnani, P.A., Suetin, H.R., Paigen, B., Naggert, J.K., Li, R., Churchill, G.A. & Peters, L.L. (2007). Multiple trait measurements in 43 inbred mouse strains capture the phenotypic diversity characteristic of human populations. *Journal of Applied Physiology*, 102(6), 2369-2378.

Taddei, A., Giampietro, C., Conti, A., Orsenigo, F., Breviario, F., Pirazzoli, V., Potente, M., Daly, C., Dimmeler, S. & Dejana, E. (2008). Endothelial adherens junctions control tight junctions by VE-cadherin-mediated upregulation of claudin-5. *Nature Cell Biology*, 10(8), 923-934.

Tahir, S.A., Park, S. & Thompson, T.C. (2009). Caveolin-1 regulates VEGF-stimulated

angiogenic activities in prostate cancer and endothelial cells. *Cancer Biology & Therapy*, 8(23), 2286-2296.

Tang, D.D. (2008). Intermediate filaments in smooth muscle. *American Journal of Physiology - Cell Physiology*, 294(4), C869-878.

Tang, J. & Kern, T. S. (2011). Inflammation in diabetic retinopathy. *Progress in Retinal and Eye Research*, 30(5), 343-358.

Thomas, C.E. & Aust, S.D. (1986). Release of iron from ferritin by cardiotoxic anthracycline antibiotics. *Archives of Biochemistry and Biophysics*, 248(2), 684-689.

Thorin, E. & Shreeve, S.M. (1998). Heterogeneity of vascular endothelial cells in normal and disease states. *Pharmacology & Therapeutics*, 78(3), 155-166.

Titford, M. (2009). Progress in the development of microscopical techniques for diagnostic pathology. *Journal of Histotechnology*, 32, 9-19.

Toda, R., Kawazu, K., Oyabu, M., Miyazaki, T. & Kiuchi, Y. (2011). Comparison of drug permeabilities across the blood-retinal barrier, blood-aqueous humor barrier, and blood-brain barrier. *Journal of Pharmaceutical Sciences*, 100(9), 3904-3911.

Todorich, B., Zhang, X., Slagle-Webb, B., Seaman, W.E. & Connor, J.R. (2008). Tim-2 is the receptor for H-ferritin on oligodendrocytes. *Journal of Neurochemistry*, 107(6), 1495-1505.

Törnquist, P., Alm, A. & Bill, A. (1990). Permeability of ocular vessels and transport across the blood-retinal-barrier. *Eye (London, England)*, 4(Pt2), 303-309.

Tout, S., Chan-Ling, T., Holländer, H., Stone J. (1993). The role of Müller cells in the formation of the blood-retinal barrier. *Neuroscience*, 55(1), 291-301.

Trachootham, D., Lu, W., Ogasawara, M.A., Rivera-Del Valle, N. & Huang, P. (2008). Redox regulation of cell survival. *Antioxidants and Redox Signaling*, 10(8), 1343-1374.

Tserentsoodol, N., Shin, B.C., Suzuki, T. & Takata, K. (1998). Colocalization of tight junction proteins, occludin and ZO-1, and glucose transporter GLUT1 in cells of the blood-ocular barrier in the mouse eye. *Histochemistry and Cell Biology*, 110(6), 543-551.

Tsukita, S., Furuse, M. & Itoh, M. (2001). Multifunctional strands in tight junctions. *Nature Reviews Molecular Cell Biology*, 2(4), 285-293.

Udipi, S., Ghugre, P. & Gokhale, C. (2012). Iron, oxidative stress and health. In V. Lushchak (Ed.), *Oxidative stress - Molecular mechanisms and biological effects*. (pp. 73-106). InTech open access publisher.

Umeda, K., Ikenouchi, J., Katahira-Tayama, S., Furuse, K., Sasaki, H., Nakayama, M., Matsui, T., Tsukita, S., Furuse, M. & Tsukita, S. (2006). ZO-1 and ZO-2 independently determine where claudins are polymerized in tight-junction strand formation. *Cell*, 126(4), 741-754.

Ushio-Fukai, M. & Alexander, R.W. (2004). Reactive oxygen species as mediators of angiogenesis signaling: role of NAD(P)H oxidase. *Molecular and Cellular Biochemistry*, 264(1-2), 85-97.

Van Itallie, C. M. & Anderson, J. M. (2006). Claudins and epithelial paracellular transport. *Annual Review of Physiology*, 68, 403-429.

Vandesompele, J., De Preter, K., Pattyn, F., Poppe, B., Roy, N.V., Paepe, A. & Speleman, F. (2002). Accurate normalization of real-time quantitative RT-PCR data by geometric averaging of multiple internal control genes. *Genome Biology*, 3(7), research0034.

Vecino, E., Rodriguez, F.D., Ruzafa, N., Pereiro, X. & Sharma, S.C. (2016). Glia-neuron interactions in the mammalian retina. *Progress in Retinal and Eye Research*, 51, 1-40.

Vinores, S.A. (1995). Assessment of blood-retinal barrier integrity. *Histology and Histopathology*, 10(1), 141-154.

Vulpe, C.D., Kuo, Y.M., Murphy, T.L., Cowley, L., Askwith, C., Libina, N., Gitschier, J. & Anderson, G.J. (1999). Hephaestin, a ceruloplasmin homologue implicated in intestinal iron transport, is defective in the sla mouse. *Nature Genetics*, 21(2), 195-199.

Wallander, M.L., Leibold, E.A. & Eisenstein R.S. (2006). Molecular control of vertebrate iron homeostasis by iron regulatory proteins. *Biochimica et Biophysica Acta*, 1763(7), 668-689.

Wallez, Y. & Huber, P. (2008). Endothelial adherens and tight junctions in vascular homeostasis, inflammation and angiogenesis. *Biochimica et Biophysica Acta*, 1778(3), 794-809.

Walvekar, M.V., Potphode, N.D., Desai, S.S. & Deshmukh, V.M. (2016). Histological studies on islets of Langerhans of pancreas in diabetic mice after curcumin administration. *International Journal of Pharmaceutical and Clinical Research*, 8(9), 1314-1318.

Wanek, J., Blair, N.P., Chau, F.Y., Lim, J.I., Leiderman, Y.I. & Shahidi, M. (2016). Alterations in retinal layer thickness and reflectance at different stages of diabetic retinopathy by en face optical coherence tomography. *Investigative Ophthalmology & Visual Science*, 57(9), OCT341-347.

Wang, J. & Pantopoulos, K. (2011). Regulation of cellular iron metabolism. *The Biochemical Journal*, 434(3), 365-381.

Wang, S., Voisin, M., Larbi, K.Y., Dangerfield, J., Scheiermann, C., Tran, M., Maxwell, P.H., Sorokin & L., Nourshargh. S. (2006). Venular basement membranes contain specific matrix protein low expression regions that act as exit points for emigrating neutrophils. *The Journal of Experimental Medicine*, 203(6), 1519-1532.

Wang, Y., Zang, Q.S., Liu, Z., Wu, Q., Maass, D., Dulan, G., Shaul., P.W., Melito, L., Frantz, D.E., Kilgore, J.A., Williams, N.S., Terada, L.S. & Nwariaku, F.E. (2011). Regulation of VEGF-induced endothelial cell migration by mitochondrial reactive oxygen species. *American Journal of Physiology - Cell Physiology*, 301(3), C695–C704.

Wangsa-Wirawan, N.D. & Linsenmeier, R.A. (2003). Retinal oxygen: fundamental and clinical aspects. *Archives of Ophthalmology*, 121(4), 547-557.

Wardman, P. & Candeias, L.P. (1996). Fenton chemistry: an introduction. *Radiation Research*, 145(5), 523-531.

Watanabe, N., Tanaka, M., Suzuki, K., Kumanogoh, A., Kikutani, H. & Miyajima, A. (2007). Tim2 is expressed in mouse fetal hepatocytes and regulates their differentiation. *Hepatology*, 45(5), 1240-1249.

Watson, M.G., McDougall, S.R., Chaplain, M.A., Devlin, A.H. & Mitchell, C.A. (2012). Dynamics of angiogenesis during murine retinal development: a coupled in vivo and in silico study. *Journal of The Royal Society Interface*, 9(74), 2351-2364.

Wen, X., Wang, N., Zhang, F. & Dong, C. (2016). Overexpression of SCARA5 inhibits tumor proliferation and invasion in osteosarcoma via suppression of the FAK signaling pathway. *Molecular Medicine Reports*, 13(3), 2885-2891.

Wessling-Resnick, M. (2010). Iron homeostasis and the inflammatory response. *Annual Review of Nutrition*, 30, 105-122.

Whallon, J.H., Flegler, S.L. & Klomparens, K.L. (1989). Energy-dispersive X-ray microanalysis. *BioScience*, 39(4), 256-259.

Wigglesworth, J. & Baum, H. (1988). Iron-dependent enzymes in the brain. In M.B.H. Youdim (Ed.), *Topics in neurochemistry and neuropharmacology*. (pp. 25-66). London: Taylor and Francis.

Willoughby, C.E., Ponzin, D., Ferrari, S., Lobo, A., Landau, K. & Omidi, Y. (2010). Anatomy and physiology of the human eye: effects of mucopolysaccharidoses disease on structure and function - a review. *Clinical & Experimental Ophthalmology*, 38, 2-11.

Winey, M., Meehl, J.B., O'Toole, E.T. & Giddings, T.H. (2014). Conventional transmission electron microscopy. *Molecular Biology of the Cell*, 25(3), 319-323.

Wise, G.N., Dollery, C.T. & Henkind, P. (1971). *The retinal circulation*. New York: Harper & Row Publishers Inc.

Wisniewska-Kruk, J., Hoeben, K.A., Vogels, I.M., Gaillard, P.J., Van Noorden, C.J., Schlingemann, R.O. & Klaassen, I. (2012). A novel co-culture model of the blood-retinal barrier based on primary retinal endothelial cells, pericytes and astrocytes. *Experimental Eye Research*, 96(1), 181-190.

Wisniewska-Kruk, J., Klaassen, I., Vogels, I.M., Magno, A.L., Lai, C.M., Van Noorden, C.J., Schlingemann, R.O. & Rakoczy, E.P. (2014). Molecular analysis of blood-retinal barrier loss in the Akimba mouse, a model of advanced diabetic retinopathy. *Experimental Eye Research*, 122(1), 123-131.

Wisniewska-Kruk, J., van der Wijk, A.E., van Veen, H.A., Gorgels, T.G., Vogels, I.M., Versteeg, D., Van Noorden, C.J., Schlingemann, R.O. & Klaassen, I. (2016). Plasmalemma vesicle-associated protein has a key role in blood-retinal barrier loss. *The American Journal of Pathology*, 186(4), 1044-1054.

Witmer, A.N., Blaauwgeers, H.G., Weich, H.A., Alitalo, K., Vrensen, G.F. & Schlingemann, R.O. (2002). Altered expression patterns of VEGF receptors in human diabetic retina and in experimental VEGF-induced retinopathy in monkey. *Investigative Ophthalmology & Visual Science*, 43(3), 849-857.

Witmer, A.N., van Blijswijk, B.C., van Noorden, C.J., Vrensen, G.F. & Schlingemann, R.O. (2004). In vivo angiogenic phenotype of endothelial cells and pericytes induced by vascular endothelial growth factor-A. *The Journal of Histochemistry and Cytochemistry*, 52(1), 39-52.

Witmer, A.N., Vrensen, G.F., Van Noorden, C.J. & Schlingemann, R.O. (2003). Vascular endothelial growth factors and angiogenesis in eye disease. *Progress in Retinal and Eye Research*, 22(1), 1-29.

Wold, M.S. (1997). Replication protein A: a heterotrimeric, single-stranded DNA-binding protein required for eukaryotic DNA metabolism. *Annual Review of Biochemistry*, 66, 61-92.

Wolf, G. (2004). The visual cycle of the cone photoreceptors of the retina. *Nutrition Reviews*, 62(7Pt1), 283-286.

Wong, R., Richa, D.C., Hahn, P., Green, W.R. & Dunaief, J.L. (2007). Iron toxicity as a potential factor in AMD. *Retina*, 27(8), 997-1003.

Worth, N.F., Rolfe, B.E., Song, J. & Campbell, G.R. (2001). Vascular smooth muscle cell phenotypic modulation in culture is associated with reorganization of contractile and cytoskeletal proteins. *Cell Motility and the Cytoskeleton*, 49(3), 130-145.

Wynne, B.M., Chiao, C.W. & Webb, R.C. (2009). Vascular smooth muscle cell signaling mechanisms for contraction to angiotensin II and endothelin-1. *Journal of the American Society of Hypertension*, 3(2), 84-95.

Xie, A., Puget, N., Shim, I., Odate, S., Jarzyna, I., Bassing, C.H., Alt, F.W. & Scully, R. (2004). Control of sister chromatid recombination by histone H2AX. *Molecular Cell*, 16(6), 1017-1025.

Xu, J., Knutson, M.D., Carter, C.S. & Leeuwenburgh C. (2008). Iron accumulation with age, oxidative stress and functional decline. *PLoS One*, 3(8), e2865.

Yamada, E. (1955). The fine structure of the gall bladder epithelium of the mouse. *The Journal of Biophysical and Biochemical Cytology*, 1(5), 445-458.

Yao, H., Wang, T., Deng, J., Liu, D., Li, X. & Deng, J. (2014). The development of blood-retinal barrier during the interaction of astrocytes with vascular wall cells. *Neural Regeneration Research*, 9(10), 1047-1054.

Yau, K.W. & Baylor, D.A. (1989). Cyclic GMP-activated conductance of retinal photoreceptor cells. *Annual Review of Neuroscience*, 12, 289-327.

Yefimova, M.G., Jeanny, J.C., Guillonneau, X., Keller, N., Nguyen-Legros, J., Sergeant, C., Guillou, F. & Courtois, Y. (2000). Iron, ferritin, transferrin, and transferrin receptor in the adult rat retina. *Investigative Ophthalmology & Visual Science*, 41(8), 2343-2351.

Youdim, M. (1990). Neuropharmacological and neurobiochemical aspects of iron deficiency. In J. Dobbing (Ed.), *Brain, behavior, and iron in the infant diet*. (pp. 83-106). London: Springer.

Young, R.W. & Bok, D. (1969). Participation of the retinal pigment epithelium in the rod outer segment renewal process. *The Journal of Cell Biology*, 42(2), 392-403.

Yu, P.K., Balaratnasingam, C., Morgan, W.H., Cringle, S.J., McAllister, I.L. & Yu, D.Y. (2010). The structural relationship between the microvasculature, neurons, and glia in the human retina. *Investigative Ophthalmology & Visual Science*, 51(1), 447-458.

Yu, P.K., Yu, D., Alder, V.A., Seydel, U., Su, E. & Cringle, S.J. (1997). Heterogeneous endothelial cell structure along the porcine retinal microvasculature. *Experimental Eye Research*, 65(3), 379-389.

Zani, I.A., Stephen, S.L., Mughal, N.A., Russell, D., Homer-Vanniasinkam, S., Wheatcroft, S.B. & Ponnambalam, S. (2015). Scavenger receptor structure and function in health and disease. *Cells*, 4(2), 178-201.

Zhang, A.S. & Enns, C.A. (2009). Iron homeostasis: recently identified proteins provide insight into novel control mechanisms. *The Journal of Biological Chemistry*, 284(2), 711-715.

Zhang, W.X., Fan, J., Ma, J., Rao, Y.S., Zhang, L. & Yan, Y.E. (2016). Selection of suitable reference genes for quantitative real-time PCR normalization in three types of rat adipose tissue. *International Journal of Molecular Sciences*, 17(6), 968.

Zhang, X., Zeng, H., Bao, S., Wang, N. & Gillies, M.C. (2014). Diabetic macular edema: new concepts in pathophysiology and treatment. *Cell & Bioscience*, 4, 27.

Zhang, Y. & Stone, J. (1997). Role of astrocytes in the control of developing retinal vessels. *Investigative Ophthalmology & Visual Science*, 38(9), 1653-1665.

Zhao, H., Kalivendi, S., Zhang, H., Joseph, J., Nithipatikom, K., Vásquez-Vivar, J. & Kalyanaraman, B. (2003). Superoxide reacts with hydroethidine but forms a fluorescent product that is distinctly different from ethidium: potential implications in intracellular fluorescence detection of superoxide. *Free Radical Biology & Medicine*, 34(11), 1359-1368.

Zielonka, J., Vasquez-Vivar, J. & Kalyanaraman, B. (2008). Detection of 2-hydroxyethidium in cellular systems: a unique marker product of superoxide and hydroethidine. *Nature Protocols*, 3(1), 8-21.

Zlokovic, B.V. (2008). The blood-brain barrier in health and chronic neurodegenerative disorders. *Neuron*, 57(2), 178-201.